THE UNIVERSITY OF HULL

AKEEM KEHINDE OLALEYE, B.Eng., MSc

# MODELLING AND OPERATIONAL ANALYSIS OF COAL-FIRED SUPERCRITICAL POWER PLANT INTEGRATED WITH POST-COMBUSTION CARBON CAPTURE BASED ON CHEMICAL ABSORPTION UNDER UK GRID REQUIREMENT

FACULTY OF SCIENCES AND ENGINEERING

SCHOOL OF ENGINEERING

PhD THESIS

THE UNIVERSITY OF HULL

FACULTY OF SCIENCES AND ENGINEERING

SCHOOL OF ENGINEERING

# MODELLING AND OPERATIONAL ANALYSIS OF COAL-FIRED SUPERCRITICAL POWER PLANT INTEGRATED WITH POST-COMBUSTION CARBON CAPTURE BASED ON CHEMICAL ABSORPTION UNDER UK GRID REQUIREMENT

Being a Thesis submitted for the Degree of Doctor of Philosophy (PhD) in Engineering at the University of Hull

By

AKEEM KEHINDE OLALEYE, B.Eng., MSc

Supervisor: Professor Meihong Wang

September, 2015

# Abstract

Fossil-fuel fired power plants are subjected to stringent operational regime due to the influx of renewable resources and the $CO_2$ emission reduction target. This study is aimed at modelling and analysis of supercritical coal-fired power plant (SCPP) integrated with post-combustion $CO_2$ capture (PCC) and its response electricity grid demand constraints. Current status of dynamic modelling of SCPP integrated with PCC was reviewed to identify the gaps in knowledge. It was observed that no accurate dynamic model of an SCPP integrated with PCC had been reported in open literature. A steady state model of the SCPP integrated with PCC was developed with Aspen Plus®. The model was validated with the reference plant and it was found that the relative error is about 1.6%. The results of the conventional and advanced exergetic analysis showed that the energy/exergy consumption and the efficiency of the integrated system can be improved by recovering the avoidable exergy destruction in the whole system.

Dynamic models of SCPP once-through boiler based on lumped parameter and distributed parameter approaches were compared. The distributed parameter model gave a more accurate prediction of the SCPP boiler dynamics at different load levels. Analysis of the strategies for operating the SCPP under the UK grid requirement as regards to primary frequency response was performed using the validated SCPP model. The results show that using turbine throttling approach, extraction stop or condensate stop individually was not sufficient to meet the grid requirement. A combination of turbine throttling, extraction stop and/or condensate stop can achieve a 10% increase in maximum continuous rating (MCR) of the power plant within 10 seconds to 30 seconds of primary frequency change as required by the UK grid.

The dynamic model of SCPP was integrated with a validated and scaled-up model of PCC. Analysis of the strategies for operating the SCPP integrated with PCC under the UK grid requirement as regards to primary frequency response was undertaken. The results show that the stripper stop mechanism is not sufficient for the 10% MCR required for the primary

response. The results show that the combination of stripper stop mechanism with extraction stop can meet the 10% MCR requirement for integrated plant operating at above 75% of its full capacity. The throttling and stripper stop configuration only barely meets the demand at full load capacity. The condensate stop combination with the stripper stop mechanism on the other hand could not meet the frequency response requirement at any load level.

Keywords: Dynamic modelling, once-through boiler, supercritical coal-fired power plant, Post-combustion $CO_2$ capture, UK Grid Requirement,

# Acknowledgement

My profound gratitude goes to the Almighty for His abundant blessing and opportunity accorded me to be able to undertake this PhD programme. I also appreciate the financial sponsorship of the Biomass and Fossil Fuel Research Alliance (BF2RA), UK. I also want to acknowledge the support of Professor Chuanlong Xu of the Thermal Engineering Department at South East University (SEU), Nanjing, China for the power plant visit and the data provided for validated the developed model in this thesis.

My special appreciation goes to my indefatigable supervisor Professor Meihong Wang for his advice, comments and suggestions on making this PhD study a fruitful undertaking; and to all the staffs of the School of Engineering, University of Hull for their invaluable help throughout my study.

My friends and colleagues in the Process and Energy Systems Engineering Group whose priceless friendship and mentorship roles have all contributed towards the success of my study: Dr Eni Oko, Dr Mathew Aneke, Olumide Olumayeigun, Atuman Samaila Joel, Chima Okezue, Xiaobo Luo, Hui Meng  and others too numerous to mention.

# Contents

# List of Figures

# List of Tables

# Nomenclature

| Symbol | Quantity | Unit |
|---|---|---|
| $m$ | mass flow | kg/s |
| $P$ | Density | kg/m$^3$ |
| $H$ | specific enthalpy | J/kg |
| Q | Heat flow | J/s |
| $P$ | Pressure | bar |
| $T$ | Temperature | $^o$C |
| $Torq$ | Torque | J |
| $V$ | Volume | m$^3$ |
| $M$ | Mass | kg |
| H | Enthalpy | J |
| U | Internal energy | J |
| $F$ | friction factor | - |
| $V$ | specific volume | m$^3$/kg |
| $v$ | Velocity | m/s |
| $Cp$ | Specific heat capacity | J/kg K |
| $J$ | Moment of Inertia | Kg m$^2$ |
| $\delta$ | Rotor angle of the generator | $^o$C |
| K | empirical constant | - |
| $U_c$ | heat transfer coefficient | J/s.K |
| $W$ | primary air flow rate | kg/s |
| $X$ | mass fraction | - |
| $N$ | pump speed | rpm |
| $x$ | steam fraction | - |
| $q$ | Heat flux | J/kg K |
| $m_i$ | mass flow per unit length of tube | kg/s |

| | | |
|---|---|---|
| $z$ | tube length | m |
| $\dot{E}_n$ | Exergy of component n | MW |
| $\dot{E}_{F,n}$ | Fuel Exergy of component *n* | MW |
| $\dot{E}_{P,n}$ | Product Exergy of component *n* | MW |
| $\dot{E}_{D,n}$ | Exergy destruction of component *n* | MW |
| $\dot{E}_{D,n}^{un}$ | Unavoidable exergy destruction of *n* | MW |
| $\dot{E}_{D,n}^{av}$ | Avoidable exergy destruction of *n* | MW |
| $\dot{E}_{D,n}^{en}$ | Endogenous exergy destruction of *n* | MW |
| $\dot{E}_{D,n}^{ex}$ | Exogenous exergy destruction of *n* | MW |
| $\dot{E}_{D,n}^{av,ex}$ | Avoidable exogenous exergy destruction of *n* | MW |
| $\dot{E}_{D,n}^{un,ex}$ | Unavoidable exogenous exergy destruction of *n* | MW |
| $\dot{E}_{D,n}^{av,en}$ | Avoidable endogenous exergy destruction of *n* | MW |
| $\dot{E}_{D,n}^{un,en}$ | Unavoidable endogenous exergy destruction of *n* | MW |
| $\Delta E^{*,n}$ | Fuel saving potential | MW |
| $\dot{E}_{P,total}^{R}$ | Total exergy of the products under real conditions | MW |
| $E_{F,total}^{R,n}$ | Total fuel exergy under real | MW |
| $E_{F,total}^{T,n}$ | Total fuel exergy under theoretical condition of component *n* | MW |
| $\Delta T$ | Temperature difference | $^{o}$C |
| $y$ | Exergy loss ratio | - |
| α | Air fuel ratio | - |
| $\eta$ | Boiler efficiency | % |
| $\dot{\varepsilon}$ | Exergetic efficiency | % |
| $\dot{W}$ | work | MW |
| **Subscript** | | |
| $M$ | metal tube | |
| $in$ | Input | |

| | |
|---|---|
| *out* | Output |
| *gm* | gas to metal |
| *ms* | metal to steam |
| *f* | furnace |
| *g* | Gas |
| *s* | Steam |
| *c* | Coal |
| *pf* | pulverised fuel (i.e. coal) |
| *i* | working fluid |
| *ref* | reference |
| *turb* | turbine |
| *bfp* | boiler feed pump |
| *ext* | extracted steam from turbine |

# Abbreviation

| | |
|---|---|
| AIC | Absorber Intercooling |
| BFP | Boiler Feed Pump |
| BMCR | Boiler Maximum Continuous Rating |
| BTU | British Thermal Unit |
| CCS | Carbon capture and storage |
| CERT | Carbon Emission Reduction Target |
| CFB | Circulating Fluidized Bed |
| ECCRIA | European Conference on Coal Research and its Application |
| EXERGYFL | Exergy of material/energy flow stream |
| EXERGYML | Exergy of material stream on molar basis |
| EXERGYMS | Exergy of material stream on mass basis |
| FGD | Flue Gas Desulphurization |
| gPROMS | general Process Modelling Software |
| HHV | High Heating Value |
| HP | High Pressure |
| IAPWS | International Association for the Properties of Water and Steam |
| IGCC | Integrated Gasification Combined cycle |
| IP | Intermediate Pressure |
| LP | Low Pressure |
| MCR | Maximum Continuous Rating |
| MEA | Monoethanolamine |
| MWe | Megawatt Electricity |
| ODE | Ordinary Differential Equation |
| PCC | Post-Combustion $CO_2$ Capture |
| PDAE | Partial Differential and Algebraic Equations |
| PDE | Partial Differential Equation |

| | |
|---|---|
| PSE | Process Systems Enterprise |
| SCPP | Supercritical Coal-fired Power Plant |
| SF | Split-flow |
| UK | United Kingdom |
| VHP | Very High Pressure |
| R | Real |
| U | Unavoidable |
| TH | Theoretical |
| GPDC | Generalized Pressure Drop Correlation |
| SIH | Stripper Inter-heating |
| LVR | Lean Vapour Recompression |
| COALMILL | Coal pulveriser |
| PSH | Primary superheater |
| SSH | Secondary superheater |
| VHP-TURB | Very high pressure turbine |
| ECON | Economiser |
| COND | Condenser |
| BFP-TURB | Boiler feed pump turbine |
| BF-PUMP | Boiler feed pump |
| HP-TURB | High pressure turbine |
| IP-TURB | Intermediate pressure turbine |
| LP-TURB | Low pressure turbine |
| RHT | Reheater |
| AIR-PRHT | Air preheater |
| BURN | Burner |
| DECOMP | Decomposition of coal |
| FWH | Feedwater heaters |
| BGS Filter | Baghouse filter |
| ID-FAN | Induce draft fan |

| | |
|---|---|
| FG-Cooler | Flue gas cooler |
| ABSRBR | Absorber |
| DESRBR | Desorber |
| MHEX | Multiple Heat exchanger |
| RAH | Reversible adiabatic heater |

# Chapter 1 Introduction

## 1.1 Background

The overall world energy demand is projected to increase from 495 quadrillion BTU in 2007 to over 700 quadrillion BTU by 2035 based on expected economic growth in developing nations such as China, India as shown in Figure 1.1(EIA, 2010).

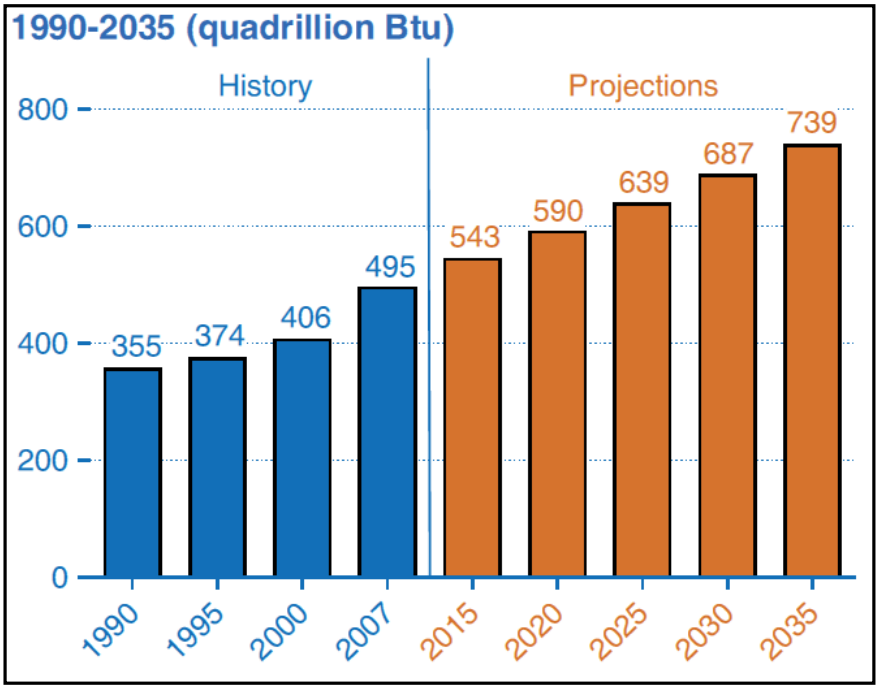


Figure 1.1: Projected world energy demand (EIA, 2010)

Projected energy supply from 2015 to 2035 will be drawn from oil, coal, natural gas, renewable forms of energy, and nuclear energy. Figure 1.2 shows that fossil fuel (oil, coal, and natural gas) will account for over 80% of the world's energy supply (EIA, 2011).

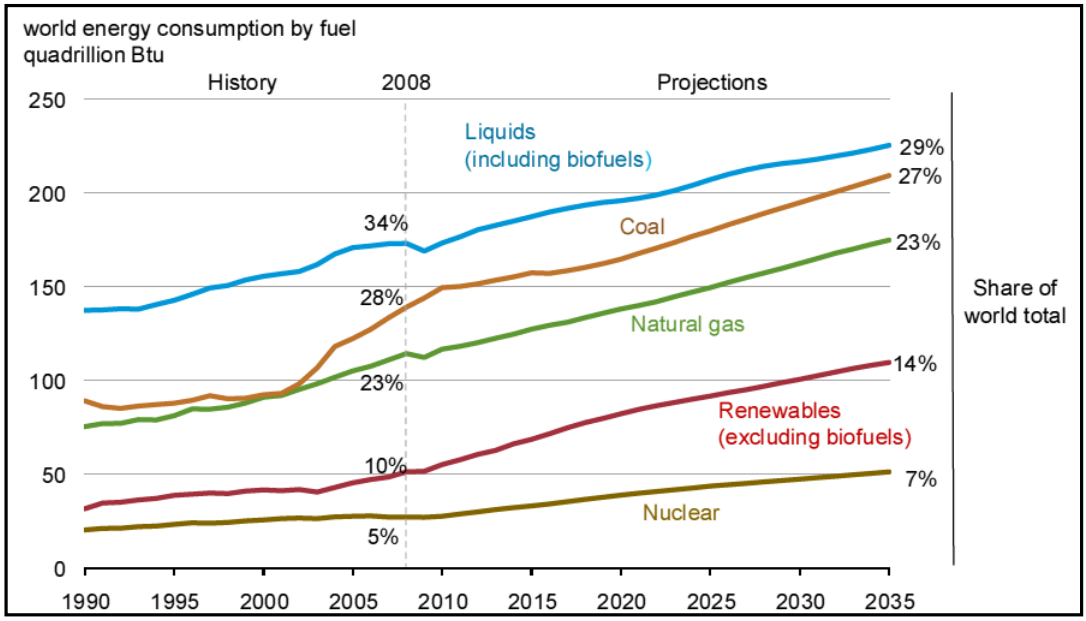


Figure 1.2: Projected world energy supply by fuel types (EIA, 2010)

Combustion of fossil fuel is the major source of $CO_2$ emissions which causes global warming. $CO_2$ is undoubtedly the most common anthropogenic greenhouse gas. World energy related $CO_2$ emission is expected to rise from 29.7 billion metric tons in 2007 to 33.86 and 42.4 billion metric tons in 2020 and 2035 respectively, an increase of 43% over the projected period as shown in Figure 1.3 (EIA, 2010).

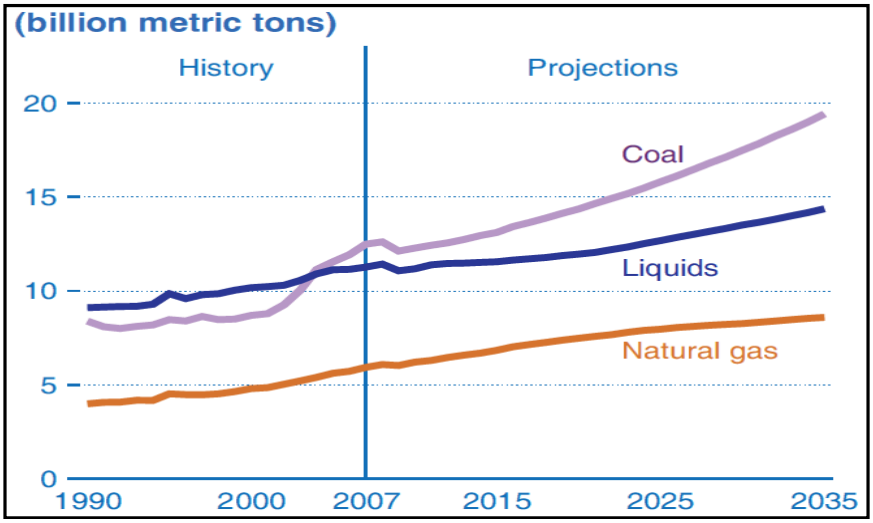

Figure 1.3: World energy related $CO_2$ emissions by fuel (EIA, 2010)

Globally, efforts have been stepped up to limit the emissions of $CO_2$ and the accompanying global warming. Hence, an energy solution driven by the combination of increasing energy consumption and increasing environmental concerns thus requires a consideration of pairing fossil energy conversion systems with economical capture, transportation and safe sequestration schemes for $CO_2$.

### 1.1.1 World fossil fuel outlook

Coal, oil and natural gas are referred to as fossil fuels because they are the remains of plant and animal life preserved in sedimentary rocks. It is commonly believed that coal was formed from plant matter, and oil from aquatic organisms (Spliethoff, 2010). Among the fossil fuel sources, oil is expected to maintain its leading status and its utilization will increase for the projected future. Compared with natural gas and coal, crude oil is relatively easy to be pumped, transported, and processed into high-energy density fuel and chemicals, but the high crude oil prices, limited oil reserves and political instabilities in oil rich regions are expected to decrease the share of liquid fuels in the overall world energy supply from 34% in 2007 to 29% in 2035 as shown in Figure 1.2 (EIA, 2010).

The demand for coal is projected to increase faster than the demand for both crude oil and natural gas because of its relatively low price and abundant supply in some of the largest energy-consuming and developing countries (i.e. China and India).

Table 1.1: World Fossil Fuel Reserve as at the end of 2010 (BP, 2011)

| | Oil ($10^9$ Barrels) | Natural Gas ($10^9$ $m^3$) | Coal ($10^6$tonnes) |
|---|---|---|---|
| North America | 74.3 | 9.9 | 245,088 |
| South& C. America | 239.4 | 7.4 | 12,508 |
| Europe and Eurasia. | 139.7 | 63.1 | 304,604 |
| Middle East | 752.5 | 75.8 | 1,203 |
| Africa | 132.1 | 14.7 | 31,692 |
| Asia Pacific | 45.2 | 16.2 | 265,843 |
| Total | 1383.2 | 187.1 | **860,938** |

Table 1.1: World Fossil Fuel Reserve as at the end of 2010 (BP, 2011) shows a comparison of world fossil fuel reserves by geological regions as at the year ending 2010 from British Petroleum (BP) annual statistical review of world energy. It is expected that the share of the energy supplied by coal will increase from 26% to 29% in the next three decades (2005 – 2035).

### 1.1.2 Electricity generation from coal

Heat coming from coal combustion can be harnessed by using them to produce steam in a boiler. The steam from the boiler is then used to produce a torque in a steam turbine which is transformed to electricity in a generator. . A summary of this process is shown in Figure

1.4. The combustion of coal produces flue gas stream with about 14 vol. % $CO_2$ content (IEA GHG, 2002a).

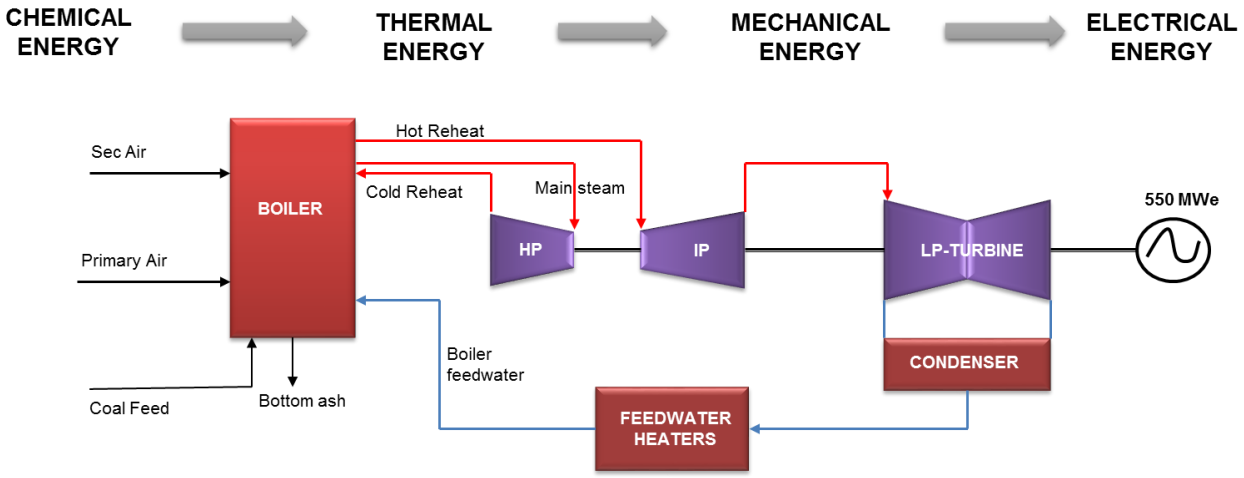


Figure 1.4: Energy transformation in a simple fossil fuel power unit

Coal will continue to occupy the largest share of worldwide electric power generation by a wide margin (EIA, 2010). In 2007, coal-fired power generation accounted for 42% of world electricity supply. In 2035, its share is predicted to increase slightly to 43%. Constant high prices for oil and natural gas make coal-fired power generation more attractive economically, especially in nations that are rich in coal resources, including China and India. World net coal-fired power generation almost doubles over the projection period from 7.9 trillion kWh in 2007 to 15.0 trillion kWh in 2035. The outlook for coal-fired power generation could change considerably by government policies or international agreements to reduce greenhouse gas emissions. (EIA, 2010).

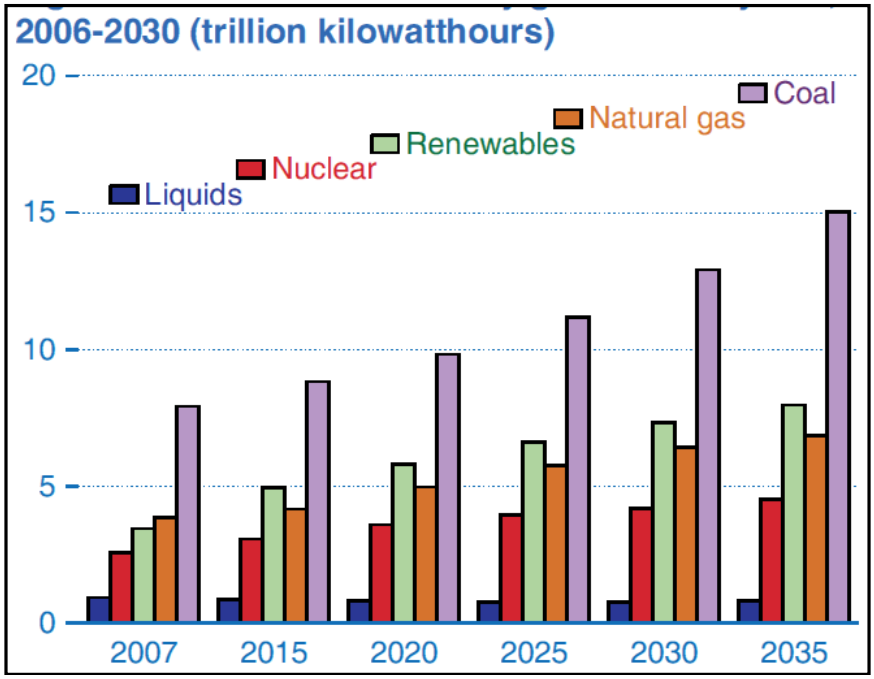

Figure 1.5: World net electricity generation by fuel (EIA, 2010)

High capital cost and safety concerns are major drawbacks for renewable and nuclear power generation which are alternative sources. As a result, coal will remain an important energy source for many years.

According to the UN prediction, the world population will rise from 6.6 billion in 2007 to 8.2 billion by 2030. During this period, electricity demand is projected to rise by 76% (IEA, 2009).

#### *1.1.2.1 UK electricity demand/supply outlook*

In the UK, about 18GW—about a quarter—of power generating capacity is due for decommissioning by 2020. Of this, 8.5GW of coal-fired plants will be decommissioned to meet EU requirements on pollution, and another 2.5GW of oil-fired stations. A further 7GW of nuclear power is scheduled to close by 2020 based on the available lifetimes of the plants. The impact of these closures on UK's electricity generating capacity is shown in Figure 1.6. In the interim, demand for electricity is also projected to increase, which will also have to be met by larger plant capacity. A 20% margin in excess of peak demand which is the present

amount of extra capacity on hand to ensure there are no power cuts when power plants have to be turned off for maintenance and repairs (Nichols and Maxim, 2008).

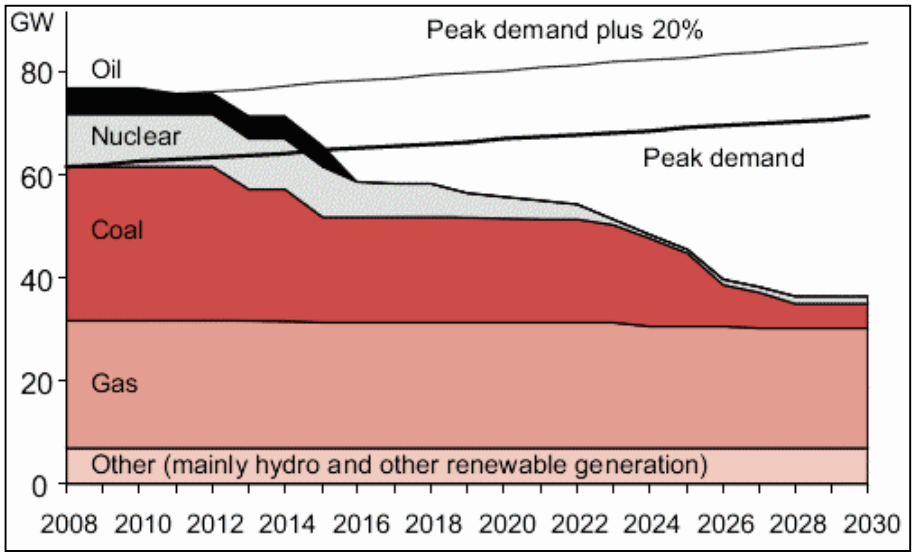


Figure 1.6: Predicted UK electricity demand and generation by fuels (House of Lords, 2008)

If this margin is to be maintained at around 20% then new power stations need to be built in good time to replace these closures and to meet increases in demand. On this basis, the government has estimated that around 20-25 GW of new power stations will be needed by 2020 (House of Lords, 2008). It is predicted that to support the expected gap between generation and demand in the UK market, building new coal-fired power plants will be inevitable.

Despite the environmental issues, coal-fired power plants have clear economic and strategic advantages which include:

- The proven reserves of coal are quite important compared to its alternatives (Table 1.1).
- Coal-based electricity price is considerably low (Figure 1.7) and is likely to stay at a realistic level even on a continuing basis. Certainly, because of the increasing demand

and its lower reserves, the price of natural gas is likely to increase considerably while the price of coal will also increase but at a lower rate.

- Coal offers a relative energy autonomy compared to fuels such as oil or natural gas for regions such as North America, Europe or China.

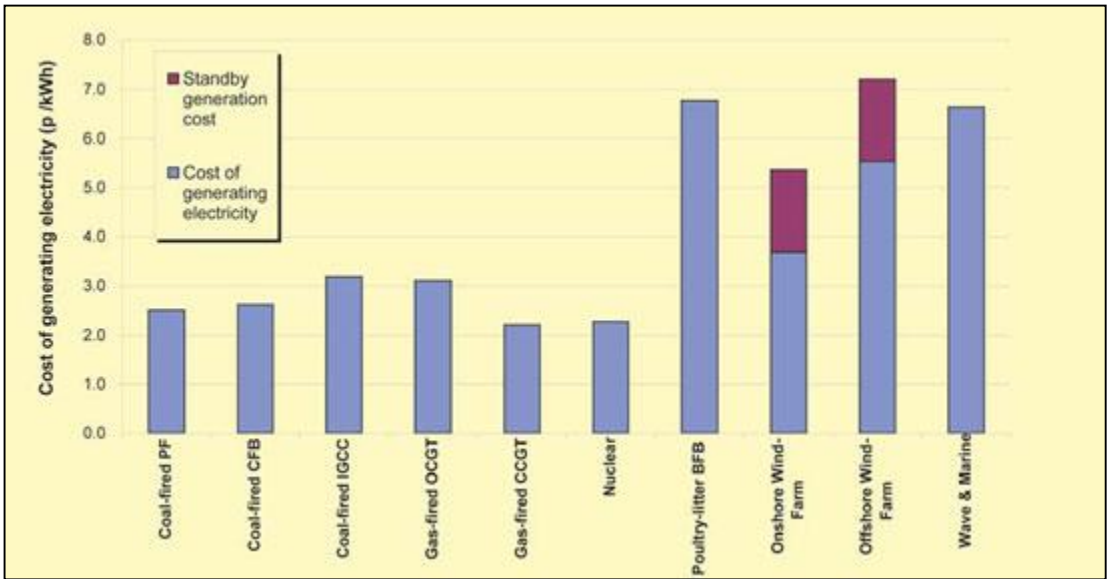

Figure 1.7: Cost (p/kWh) of electricity generation in the UK (PBPower, 2004)

### *1.1.2.2 Coal-fired Power Plant Emission Abatement Strategy*

In the present regime, both national and international governments have formulated abatement strategies to reduce CO2 emissions from coal-fired power plants. This include efficiency improvement and carbon capture and storage (CCS) (Wang *et al*, 2011).

Efficiency improvement involves development of new designs and new strategy for operation. As shown in Figure 1.8, every increment in efficiency results in a proportional reduction in emission.

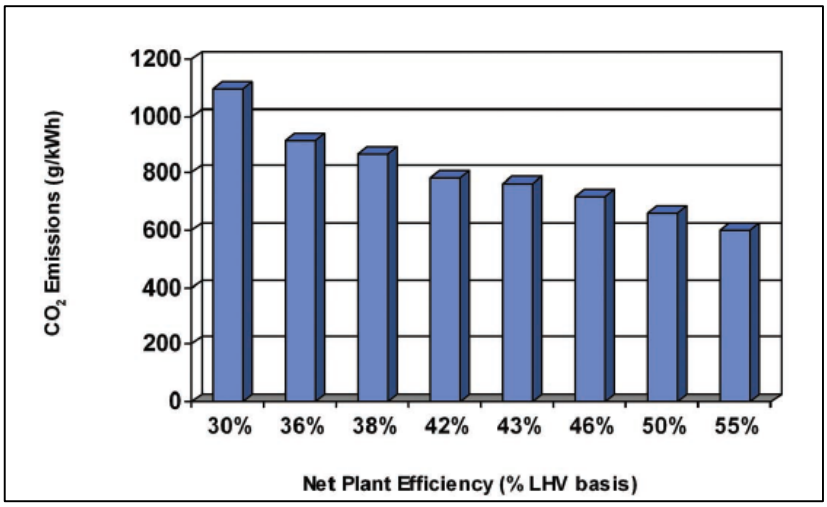

Figure 1.8: Effects of increasing efficiency on $CO_2$ emission (DTI, 2006)

Philibert and Podkanski (2005) also gave useful numeric approximations on the magnitude of the reduction that is achievable in the following quote thus:

"*Coal-fired generating capacity of about 1 TW is installed worldwide. Almost two-thirds of the international coal-fired power plants over 20 years old, average efficiency of 29%, emits almost 4Gt of $CO_2$ per year. If they are replaced after 40 years with modern plants of 45% efficiency, total GHG emissions will be reduced by about 1.4Gt per year*" (Philibert and Podkanski, 2005).

The main technological evolution that can produce high increment in efficiency is the *supercritical pressure technology.*

However, an improvement in efficiency alone is not sufficient to bring down emission levels to an appreciable value.

### 1.1.3 $CO_2$ capture

Anthropogenic activities mainly due to fossil fuel usage, have added to the increase of atmospheric $CO_2$ concentration from the pre-industrial level of 280ppm to the current value

of 380ppm (Caldeira *et al*, 2007). Under the present carbon emission growth rate, the atmospheric $CO_2$ concentration could reach 580 ppm (Fan, 2010).

CO2 capture is a process of capturing CO2 from fossil fuel combustion processes in power plants and industries. It is identified as an important technology for complementing emission cuts in coal-fired power plants through efficiency improvements.

Carbon dioxide levels in flue gases vary depending on the type of fuel used and the excess air level used for optimal combustion conditions. Natural-gas-fired power generation plants are typically combined cycle gas turbines which generate flue gases with low $CO_2$ concentrations, typically 3–4% by volume. Coal for power generation on the other hand, is primarily burnt in pulverized-fuel boilers producing an atmospheric pressure flue gas stream with a $CO_2$ content of up to 14% by volume (IEA GHG, 2002a). From the foregoing discussion, it is clear that a proper $CO_2$ management is therefore imperative. In a fossil fuel-fired power plant, $CO_2$ management is made up of three steps.

### 1.1.4 Power generation and UK grid code requirement

Power generation varies depending on demand with regimes such as peak, intermediate and base load (Figure 1.9). However, it never goes lower than a minimum referred to as *base load*. Base load is the basis of a sound electrical system (Progress Arkansas, 2010).

Peak load generation plants supply electricity at times when power consumption by consumers is highest, i.e. the peak of the curve (see Figure 1.9). Peak regime power plants are designed for high responsiveness to changes in power demand. They have a very short start up time and can vary the quantity of power output within minutes. Also, they operate only 10-15% of the period and are very small compared to base load plants. Hence, peak plants are very costly to operate compared to the quantity of power they generate and cost of fuel used to power them. Nevertheless, because of their size, they are cheaper and easier to construct. They are usually natural gas-fired power plants (Progress Arkansas, 2010).

Intermediate power plants provide the remainder of electricity demand between base load and peak plants, and are also known as “load following” power plants. From a cost and flexibility standpoint, they are larger than peak plants, so construction costs are higher, but they also run more efficiently so the power they produce is cheaper than peak plants. They basically operate within 30-60% of the time with respect to daily, weekly or seasonal demands. They are typically steam turbines with different fuels such as natural gas and renewables (i.e. wind, solar etc.).

Power plants are hence operated constantly to satisfy base load requirements or periodically to meet peak and intermediate load demands. Renewable sources within the grid (i.e. winds, solar) are intermittent, and hence only produce electricity when the wind is blowing and solar only produces power when the sun is shining. They cannot therefore be trusted with constant electricity supply requirement. This irregular service often leads to load swing within the grid. As such, the allowance between on-peak and off-peak loads expands, necessitating that existing power plants (i.e. coal-fired power plants) operate under more flexible and strict regime (Progress Arkansas, 2010).

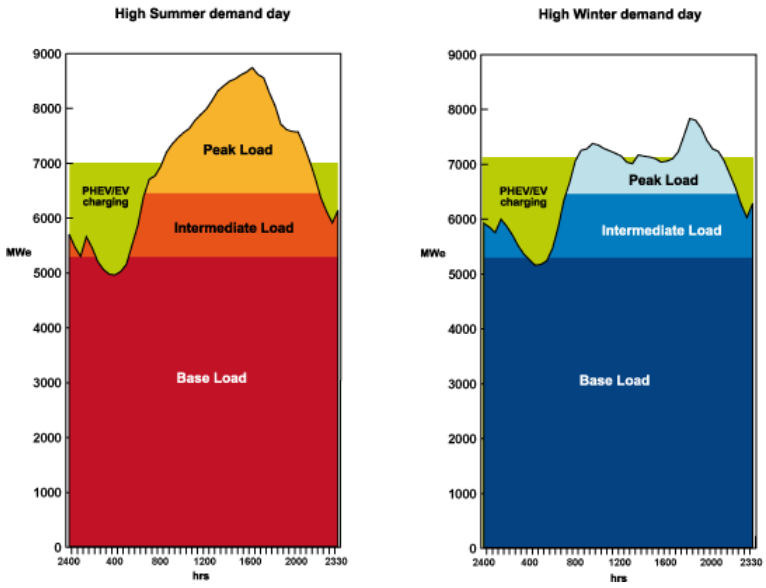


Figure 1.9: Load curves for typical electricity grid (Progress Arkansas, 2010)

Such flexible operation should include less start-up time without reducing the life span of the plant, steady operation during severe load fluctuations among others (Li et al., 2005). In addition to meeting demand continually, power generation companies are also expected to abide by the Grid code requirement. The Grid code is a reliability standards or legislation "*which is designed to permit the development, maintenance and operation of an efficient, coordinated and economical system for the transmission of electricity, to facilitate competition in the generation and supply of electricity and to promote the security and efficiency of the power system as a whole*" (National Grid, 2012). The grid code has strict requirement on power generation companies and they are under obligation to comply with the requirements. Table 1.2 shows a summary of the UK grid code requirements.

For grid system operation, it is required that the power generated is continuously matched to demand. One yardstick for this balance is the *system frequency*. The System frequency *"is a continuously changing variable that is determined and controlled by the careful balance between system demand and total generation" (*Diegel et al., 2006)*.*

#### *1.1.4.1 System frequency stability*

If power generation and power consumption in the grid system are the same under undisturbed generation conditions, the system frequency is exactly equal to the rated frequency (50 Hz for the UK grid). Unforeseen events (i.e. perturbations in the grid system or shutdown of power plants) create an imbalance between electricity generation and consumption, and result in changes in the system frequency *(*Diegel et al., 2006).

In order to achieve the required operation of the transmission system, it is essential to seize the frequency within definite narrow limits. Minor variations from the frequency reference value (50Hz) or absence of any such variations show that there is a balance of generation and power consumption. Faults in the system due to loss of power plants, shutdown of loads, short circuits, etc. result in deviations and gradients of varying magnitudes. These faults can lead to instability of the grid or even in its outage *(*Diegel et al., 2006).

### *1.1.4.2 System frequency response/control*

The response on frequency deviation caused by an event in the grid is handled by the frequency control. This is implemented in time ranges.

*The Primary Response* capability (P) of a generating unit is the minimum increase in active power output between 10 and 30 seconds after the start of the ramp injection (Figure 1.10).

*The Secondary Response* capability (S) is the minimum increase in Active Power output between 30 seconds and 30 minutes (Figure 1.10) after the start of the ramp injection (National Grid, 2012).

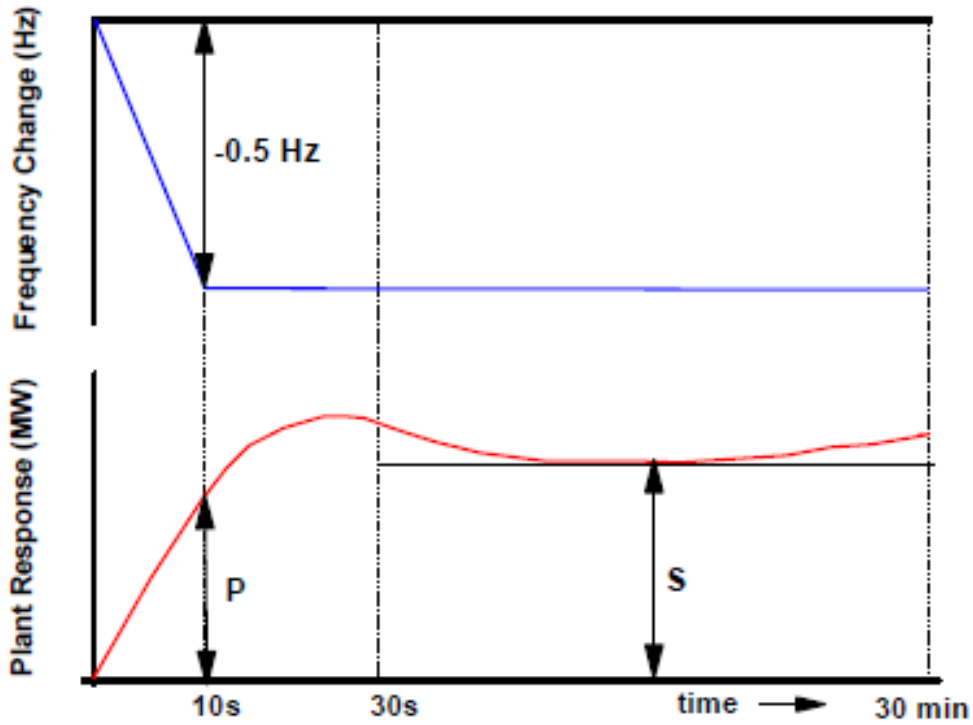


Figure 1.10: Interpretation of primary and secondary response values (National Grid, 2012)

Table 1.2 Summary of the UK Grid Code (E.ON UK, 2010)

| Parameter | UK Requirement |
|---|---|
| Grid Voltage Range (Normal) | 380...420kV (Nominal 400kV) |
| Grid Voltage Range (Abnormal) | 360...440kV (Nominal 400kV) |
| Grid Frequency Range (Normal) | Nominally 50Hz, normally controlled within 49.5...50.5Hz. Shall maintain constant active power between 49.5...50.5Hz |
| Grid Frequency Range (Abnormal) | In range 47.0 ... 47.5Hz, at least 20s operation required.<br>In range 47.5 ... 49.5Hz, continuous operation required (In range 47.5 ... 48.8Hz, at least 5mins operation required for CCGTs)<br>In range 47.0 ... 49.5Hz, Active Power allowed to reduce pro-rata with frequency at a maximum rate of 1% / 0.5Hz frequency fall below 49.5Hz. |
| Grid Frequency Range (Abnormal - high) | In range 50.5 ... 52.0Hz continuous operation required |
| Load Change | Load deviation over 30 minutes must not exceed 2.5% of Registered Capacity. |
| Load Control / Frequency Response | Must be capable of providing Frequency Response of 10% GRC for a +/-0.5Hz change in frequency. Change of active power to be achieved in 10s. Response requirement is reduced when operating at high and low ends of registered capacity. Response to High Frequency must continue at additional 10% GRC reduction per each additional 0.5Hz increase in frequency. |
| Power Factor Range | Power factor cos φ at the generator terminals 0.85 lag (over excited) … 0.95 lead (under excited). This complete range to be achieved at Rated MW, over the complete voltage range of the Grid Entry Point |
| Automatic Voltage Control | Continuously-acting automatic excitation control system to provide constant terminal voltage control of the generator without instability, over the entire operating range. The system shall include a power system stabilizer |
| Transformer Requirements | Not required in the Grid Code, but it is normal practice to specify an on load tap changer. |

*The High Frequency Response* capability (H) of a generating unit is the decrease in Active Power output provided 10 seconds after the start of the ramp injection and sustained thereafter (Figure 1.11).

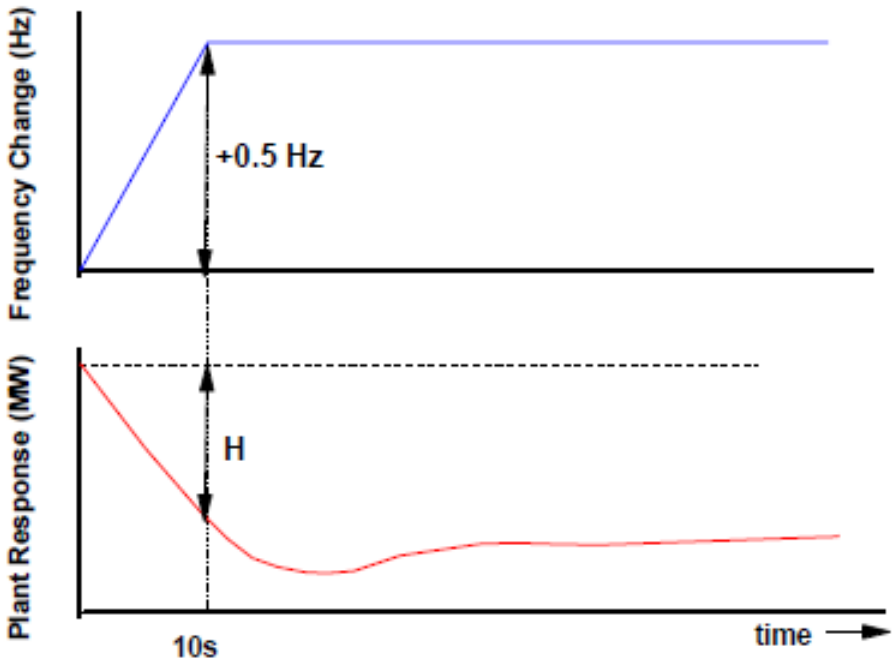


Figure 1.11: Interpretation of high frequency response values (National Grid, 2012)

For coal-fired power plant connection to the electrical transmission network in the UK, the power plant with a CCS process must abide by the requirements of the UK Grid Code, knowing very well that addition of the capture process will introduce extra design, operational, and controllability issues. It will also result in grid code compliance concerns as it will influence with the plant's frequency response capability (E.ON UK, 2010).

It is also expected that the key process variables (i.e., firing rate, furnace pressure, air-fuel ratio, water level in the steam drum (for subcritical), $CO_2$ capture level and overall plant efficiency) be maintained at an optimal value irrespective of variations in load and process

disturbances. To achieve this, it is important to understand how these variables interact during operation. It is also important to understand how the entire plant behaves under varying load conditions so that adequate provisions will be made to accommodate such changes so that they do not interfere with safe and efficient operation of the plant (Åstrom and Bell, 2000). A power plant can only be adjudged efficient and competitive in operation if it responds very fast under such condition without compromising safety and optimal performance with respect to the Grid Code.

## 1.2 Motivations for this research

There is a need to build new electricity generation capacity in the UK to replace existing coal-fired capacity scheduled for decommissioning to meet expected energy generation gap and projected demand. The new capacity is expected to be sustainable and more environmentally friendly. Two technologies can work together to meet this requirement: supercritical coal-fired power plant (SCPP) technology and carbon capture and storage (CCS) technology.

SCPP have low capability to cope with sudden changes in demand within narrow time limits as required by the UK grid code. The extent of their capability to cope with sudden changes in demand under the UK grid code scenario must be investigated and strategies for improving their performance explored before they can be introduced into the grid. This investigation can be performed using SCPP dynamic model. CCS on the other hand is a developing technology with a lot of issues yet to be addressed. One of them being their impact on power plant flexibility. Again, dynamic model of a $CO_2$ capture plant integrated to that of an SCPP can be used to carry out this investigation. Accurate process models of $CO_2$ capture plant integrated to an SCPP do not exist in literature.

## 1.3 Research aims, objectives, novelties and scope of the study

### 1.3.1 Research aims and objectives

This study is aimed at providing insights into the design and operation of a 600 MWe supercritical coal-fired power plant integrated with post-combustion carbon capture under the UK Grid code requirement through modelling and simulation.

The aim is achieved through the following objectives:

- To carry out extensive survey of relevant literatures.
- To develop a simplified flowsheet for SCPP and to develop a steady state simulation of SCPP and PCC in Aspen Plus®.
- To develop a dynamic model in gPROMS® for the whole SCPP and to carry out model validations
- To undertake dynamic process analysis of the SCPP using the model developed in gPROMS®. This is to check whether the SCPP can satisfy the UK Grid requirements.
- To integrate the dynamic model of the SCPP with a dynamic model of PCC.
- To explore whether such an SCPP integrated with PCC can satisfy the UK Grid code requirements.

### 1.3.2 Novelty of the study

Study of the operation of SCPP integrated with PCC under UK grid code requirement is an area of study that has not been investigated by any researchers until date to the best of the author's knowledge. The importance of this study to the UK decarbonisation plans cannot be over-emphasised. The following are the key novel contributions of this study:

- (Conventional and advanced) exergy analysis of SCPP integrated with PCC to reduce the exergy destruction (i.e. energy penalties) in the system.

- Detailed dynamic model for SCPP integrated with dynamic model for PCC using solvents
- Process operational analysis of SCPP under the UK grid code requirement.
- Process analyses of the strategies for improving SCPP operation to satisfy the UK grid code requirement.
- Operational analysis of SCPP integrated with PCC under the UK grid code requirement.
- Process analyses of the strategies for improving the operation of SCPP integrated with PCC to satisfy the UK grid code requirement

### 1.3.3 Scopes of the study

This study includes the modelling and operational analysis of an SCPP integrated with PCC under UK Grid Code requirement. The integrated system includes the coal pulveriser, once-through boiler system, the turbine system, the electric generator system, and the PCC system. The compression and transport of $CO_2$ is not considered in this study.

This study will use a steady state simulation of the SCPP integrated with PCC developed in Aspen Plus® to evaluate potentials for improving the rational efficiency of the system from thermodynamic point of view. The effect of improving the efficiency and reducing the energy penalties associated with the integrated system will be considered through a conventional and advanced exergy analysis of the system. This is very essential in improving the quality of decision making during the design stage of the system.

Aspen Plus® is selected for the steady state simulation because of its easy to use drag and drop unit operation capabilities, and as a first step to developing appropriate model to mimic typical SCPP from literature. Also, the ability of Aspen Plus® to estimate the exergy of individual process streams in each unit operations of the systems using its exergy analysis tool; EXERGYML, makes it the most appropriate tool for the steady state and exergy analysis of SCPP integrated with PCC.

The operation of the SCPP integrated with PCC will also be investigated in the context of UK Grid Code requirement. The requirement in this case refers to the power plant's response to change in system frequency (i.e. primary response) as required by the UK Grid Code. A dynamic model of the SCPP will be developed and integrated with PCC model in gPROMS® The modelling here refers to mathematical modelling based on first principles, not including transfer function models or models in state space.

The economic analysis and the effect of the type of materials selected for the SCPP process operation largely influences the performance and availability of the system. In this thesis, the economic analysis and the impact of materials selected for the SCPP is not considered.

The PCC system to be used in this study does not involve any experimental study, but will use a detailed dynamic model of the PCC system developed and validated with experimental data in another project (Lawal et al., 2010) for the integration with SCPP. The integrated SCPP-PCC system will be analysed for the strategies to satisfy the UK Grid Code requirements.

## 1.4 Methodology

### 1.4.1 Research methodology

There is no commercial SCPP integrated with PCC that is operational in the UK (and around the world). Hence, there are a number of unknowns about the operability of the system under the UK grid code requirements. The research methodology illustrated in Figure 1.12 shows how the research aims and objectives will be realised.

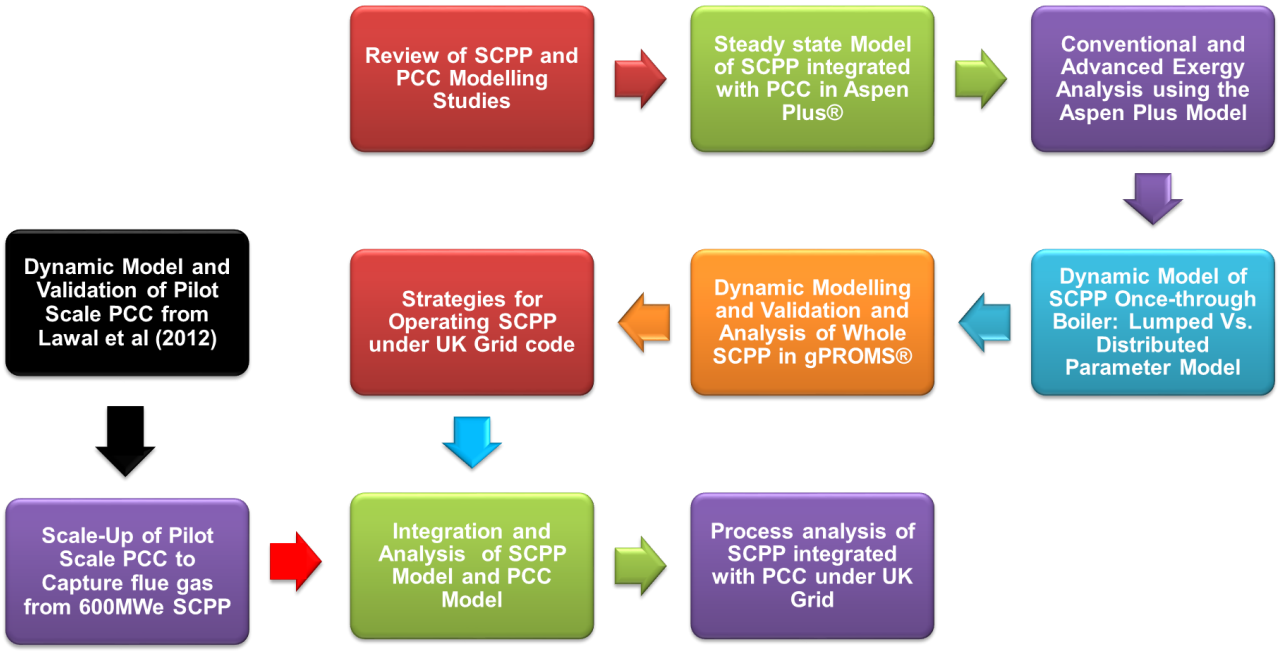


Figure 1.12: Overview of the Research Methodology

### 1.4.2 Modelling tools to be used

The research methodology adopted in this project is through process modelling and analysis of the physics of the power plant and the $CO_2$ Capture using state-of-the-art modelling and simulation tools (i.e. Mathcad®, Aspen Plus® and gPROMS®).

#### *1.4.2.1 Aspen Plus®*

Aspen Plus® is a chemical process flowsheet simulation, optimization and design package. It provides a complete library of steady state models for a number of unit operations in the chemical process industries including petroleum, petrochemical, gas processing, polymer, mineral processing, power generation etc. It also provides a large physical property and rigorous thermodynamic property library.

*1.4.2.2 Mathcad®*

Mathcad® is a mathematical software that performs the function of spreadsheets, word processing, presentation, and programming applications simply cannot do — it combines powerful engineering calculation abilities into a readable form. It also integrates these readable, live calculations with plots, graphs, text, and images into a single, interactive, and professionally presented document.

Presented within an easy-to-use interface, its live mathematical notation, units intelligence, and powerful engineering calculation capabilities allows engineers and design teams to capture and communicate engineering mathematics. Mathcad® is used for solving mathematical problems arising from the analysis of coal combustion in this study

*1.4.2.3 gPROMS®*

General process modelling tool (gPROMS® Model Builder) is used for solving systems of algebraic, differential, and partial differential equations, for construction and execution of custom models within a graphical user environment. Models can be rigorously validated using sophisticated built-in parameter estimation and model-based data analysis facilities capable of handling multiple steady-state and dynamic experiments simultaneously. gPROMS® objects can be used to embed gPROMS® models in MATLAB, Simulink, CAPE-OPEN compliant simulators such as Aspen Plus®, PRO/II and CFD packages like FLUENT. gPROMS® is unique in its ability to solve very large problems including PDE systems and systems involving complex event handling (e.g., complex startup/shutdown procedures, batch process scheduling). Many physical properties package can be used within gPROMS® models namely, Multiflash® and CAPE-OPEN-compliant packages such as Aspen Properties® and SAFT-VR for strongly-associating fluids. These two simulation tools are most widely used in supercritical coal-fired power plant for all the advantages above. However, Aspen Plus® is commonly used for steady state modelling while gPROMS® is more suitable for dynamic modelling and simulation.

## 1.5 Thesis outline

This thesis is organised into eight chapters. The current chapter (*Chapter 1*) is an introduction of the study, its motivation and novel contribution. Other chapters are presented as follows:

In Chapter 2, the review of studies relevant to modelling and process operability analysis of SCPP, PCC and their integration are summarised. In Chapter 3, steady state modelling of SCPP integrated with PCC using chemical absorption process Aspen Plus® software is described. The model was validated with experimental data from a Greenfield SCPP at full load.

In Chapter 4, conventional and advanced exergy analysis of SCPP integrated with PCC is presented in this chapter. The conventional exergy analysis evaluates the amount and location exergy destruction within the whole system. The advanced exergy analysis estimates the sources of the exergy destruction and the potential for reducing it. Seven modifications to the conventional MEA-Based PCC configuration considered for reducing exergy destruction is also presented.

In Chapter 5, dynamic modelling and comparison of the lumped parameter and distributed parameter modelling approaches for SCPP once-through boiler steam generation process was presented. The validation and comparison of the models with reference SCPP once-through boiler at three load levels (50%, 75%, and 87% MCR) was also presented.

In Chapter 6, model of the whole SCPP is presented. The strategies for operating the SCPP under the UK grid requirement as regards to primary frequency response was also described. In Chapter 7, the integration and process analysis of dynamic model of SCPP with dynamic model of PCC is presented. The strategies for operating the SCPP integrated with PCC unit under the UK grid requirement as regards to primary frequency response was also described. The conclusions and recommendations for further studies are presented in Chapter 8.

# Chapter 2 : Literature Review

## 2.1 Coal-fired supercritical power plant technology

### 2.1.1 Coal-fired supercritical power plant and the UK grid code compliance

The steam drum is the key to existing subcritical coal-fired plant delivering the required frequency responses, including primary response. SCPP do not have a steam drum and as a result are unable to offer 10% primary frequency response. A value between 3% and 7% appears possible applying a number of techniques used on supercritical plant throughout the world such as turbine throttling among others (Nichols and Maxim, 2008).

However, the fast load changes can be achieved with a combination of primary measures using the short-term storage behaviour of the power plant: the accumulated steam of the boiler by throttling; the steel mass of the boiler; and by interrupting the bled steam to the feed pre-heating system (condensate stop, feed-water stop). These primary measures are vital for the time lag necessary for the boiler to increase the firing rate (Zindler *et al.,* 2008).

Experience of using SCPP in the way the UK Grid Code recommends is non-existent and there is very little practical experience to draw on. The many measures required have not been tested by operational experience. There is a real risk that relying on several untried techniques in combination could result in a shortfall and non-compliant performance. The techniques proposed can lead to temperature and pressure excursions that will reduce the life of the power plant and without operational experience the effect of this is difficult to predict (Nicholls and Maxim, 2008).

The SCPP integrated with CCS must comply with the UK Grid Code. Knowing very well that addition of the capture process will introduce extra design, operational, and controllability issues. It will also result in grid code compliance concerns as it will interact with the plant's frequency response capability (Nicholls and Maxim, 2008). It is expected that the key process variables such as firing rate, furnace pressure, air-fuel ratio, $CO_2$ capture level and overall plant efficiency be maintained at an optimal value irrespective of variations in load

and process disturbances. To achieve this, it is important to understand how these variables interact during operation. It is also important to understand how the entire plant behaves under varying load conditions so that adequate provisions will be made to accommodate such changes such that they do not interfere with safe and efficient operation of the plant.

### 2.1.2 Economics of the Coal-fired Supercritical Power Plant

Fuel costs represent about two-thirds of the total operating costs of a coal-fired power plant. The main impact of the supercritical plant technology is to increase overall plant efficiency, thereby reducing the fuel consumption per unit of electricity generated (DTI, 2006). A new supercritical boiler/turbine power plant EPC (Energy Performance Certificate) specific price would be around 800 Euros/kWe gross (around £530/kWe). This is not more expensive than a subcritical plant and less expensive than an IGCC for which EPC prices are quoted as US$1250/kWe -US$1440/kWe (approx. £700/kWe - £800/kWe; assuming US$1.8/£) for new plant. Investment costs of existing IGCC plants have been between 1500 and 2000 Euros/kWe (£1000/kWe-£1333/kWe) (DTI, 2006).

### 2.1.3 Material Requirements for Supercritical Power Plants

Supercritical plants differ from their subcritical counterparts in terms of operational characteristics due to the higher steam temperature and pressure, and therefore require more stringent material properties than the subcritical plants. The four key components are high-pressure steam piping and headers, superheater tubing and waterwall tubing (Viswanathan and Bakker 2000). By increasing the temperature and pressure of the working fluid (steam), the level of corrosion and oxidation to which the tubes and the turbine are exposed to is higher. Hence, material requirement is certainly one of the principal challenges facing the supercritical technology (*i.e*. mechanical and metallurgical problems). Most of the problems are due to the use of austenitic steels with low thermal conductivity and high thermal expansion for components operating at high temperatures, resulting in high thermal stresses and fatigue cracking. Any further improvement in the steam conditions at supercritical condition to meet electricity demand will therefore be based on the manufacture

and use of improved steels (DTI, 2006). Intense R&D efforts have been embarked on around the world (i.e. Japan, USA, and Europe) to develop materials suitable for high steam conditions as obtainable in supercritical plants. For example, the EPRI initiated study of development of more economic coal-fired power plant as early as 1978. These studies focused on the development of high-temperature-resistance steels for production of materials capable of operating at inlet steam temperatures of up to $650^0$C.

## 2.2 Modelling of Coal-fired Power Plants

Modelling and simulation, an essential activity in process engineering, is a very useful and economic means of studying complex physical systems. It is a process of developing an operational model of a system and conducting analysis with this model for the sole aim of either analysing the performance of the system or evaluating alternative strategies for the operation of the system. It should have a capability to imitate behaviour of the modelled system to an acceptable level of accuracy. It requires specific skills; accurate description of thermodynamic property of pure components and complex mixtures, accurate models for different types of reactors and unit operations, and techniques for solving large systems of algebraic and/or differential equations (Dimian, 2003). Mathematical modelling provides the comfort of simulating the behaviour of future process plants (i.e. the supercritical coal-fired power plant in the UK) prior to their actual operation. However, mathematical modelling requires clearly defined objectives which often determine the modelling approach to be used. The modelling of pulverized coal-fired power plants has been attempted for different purposes in the past (*i.e.* for control studies, design and optimization, and operational studies).

### 2.2.1 Modelling for plant design and optimization

Power plant design companies use mathematical models to optimize the design of proprietary and off-the-shelf process equipment. Once an accurate mathematical model of a Greenfield power plant has been developed, it becomes possible to optimize the design using numerical optimization techniques (Marto and Nunn, 1981).

### 2.2.2 Modelling for operational studies

Modelling is also performed in order to simulate the dynamics of power plant under normal and emergency operational conditions. Dynamic models are important tools for studying system response to different operational changes. This is often used for analysing the dynamics of the plant over its lifetime for investment decision purposes or for operator training. The complexity of the model depends on the end use of the models.

### 2.2.3 Modelling for Control Studies

Design and implementation of a good control system requires a model of the real world system. The model represents the link between the real system and the design of control system. A good model will help in the understanding of the system to be controlled which is a vital requirement in control system design. For control, simulation and analysis of an SCPP, a mathematical model is required. These models represent the physics of the power plants dynamics. The trend in power plant control is integrated control of the whole plant concerning the boiler-turbine-generator control. However, the integrated control approach will partly depend on accurate depiction of the power plant dynamics (El-Sayad *et al.,* 1989).

## 2.3 Modelling of Coal-fired Supercritical Power Plants (SCPP)

The vast literatures of approaches to modelling SCPP can be divided into two distinct classes. In one group, there are sizeable numbers of studies stressing model accuracy with the objective of developing numerical simulations (e.g. static and dynamic finite element techniques) as a representation of the complex physical phenomena that characterize the energy transformation process in power plants (Kitto and Stultz, 2005). The second major group in SCPP modelling refers to the development of linear (transfer function) models produced around the plants' small signal behaviour. Without doubt, at given operating condition, accurately tuned linear models provide the foundation for building an excellent controller designed around the plant's small signal behaviour (Shoureshi and Paynter, 1983). However, the need for safe and efficient adjustment to highly changing demand cycles, for fast response to unexpected demand changes, and for automated emergency

response, all offer a convincing argument for a large signal (and hence nonlinear) design oriented plant model (Shinohara and Koditschek, 1995).

The dynamic response of SCPP is determined primarily by its “slowest” physics --heat exchange between the furnace and the working fluid, hence, a great deal of literature exist on the modelling of the heat exchange for SCPP components (i.e. boiler, furnace, and superheaters) (Shinohara and Koditschek, 1995). This necessitates the review to adopt a similar approach in presenting the findings so far in this subject area by first reviewing component models, then whole plant model, and whole plant with $CO_2$ capture models.

### 2.3.1 Modelling Supercritical Boiler

The circulating fluidized bed (CFB) supercritical boiler is receiving much interest in terms of improvement. However, majority of existing coal-fired power plants employ pulverized coal-fired (PC) technology. Besides, larger plants built recently have been based on the PC technology (Lundqvist *et al.,* 2003). Hence the focus of this research would be the PC boiler. The conventional PC boiler is the radiant or drum boiler that functions at subcritical steam conditions.

This study, however addresses the once-through boiler operated at supercritical conditions. The pioneering work of Adams et al (1965) marks the landmark in once-through boiler modelling. A simplified dynamic model of a once-through subcritical boiler was presented from first principle. Given that the variables that depict the heat exchanger behaviour of the boiler are continuous functions of time and space variables, a partial differential equation (PDE) will be appropriate. However, a lumped parameter approach was used because PDEs are not directly solvable on analogue computer.

A general heat exchange section/compartment is considered for modelling the dynamics of the entire subcritical boiler furnace-heat exchanger system. The system was divided into fourteen sections. Temperature and other space-dependent variables were considered to have mean values in each section (see Figure 2.1 and Figure 2.2). Several simplifying assumptions were made in modelling the system. The developed model was a linear

approximation of the physical system being considered. But it provides a rational framework that forms the foundation for subsequent boiler model studies by deriving a lumped compartmental model that utilizes the conservation of mass, energy, and momentum. The linear model was obtained by linearization using a method of total differentiation. Dynamic studies were limited to small perturbation around operating point. Consequently, the model will only be useful to study the system in limited operating conditions. Nevertheless, according to the authors, the basic mathematical modelling technique employed was suitable for control studies.

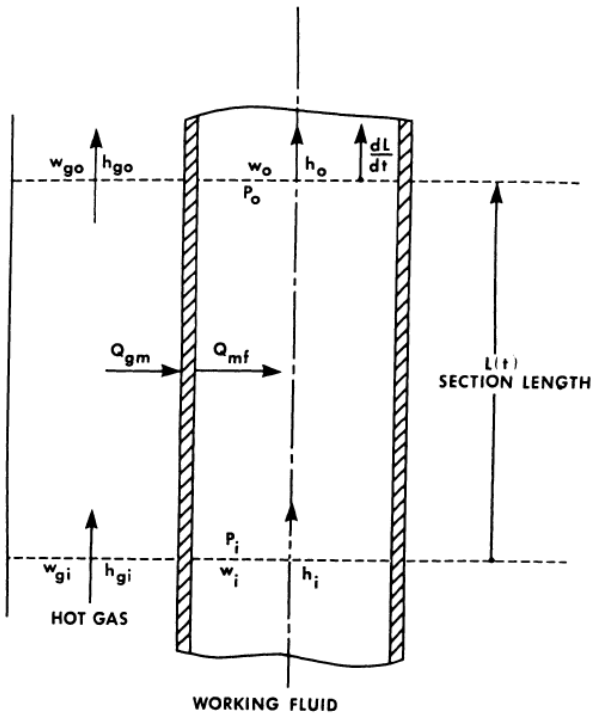


Figure 2.1: General heated section (Adams et al, 1965)

Ray (1980) formulated a nonlinear dynamic model of once-through sub-critical steam generator by extending the concept of time-varying boundaries originally used for analogue simulation of a linearized model of such a steam generator by Adams et al (1965). The boiler is made up of a large number of vertical helically celled tubes. Each tube was considered a counterflow heat exchanger, and was partitioned into three sections; compressed water

(economizer), wet steam (evaporator), and superheated steam (superheater) (see Figure 2.3). The distributed parameter model was simplified to obtain a lumped parameter (transfer function) model through the idea of control volumes. The steam generator considered was of the type used in gas-cooled nuclear power plants. The system transients derived from the model was considered by the authors as useful for designing control systems, and can be used as an element in an overall system performance study of large scale nuclear power plant. However, applying this model to a coal-fired power plant requires the effect of radiation to be included in determining heat transfer from the flames/flue gas to the tube wall.

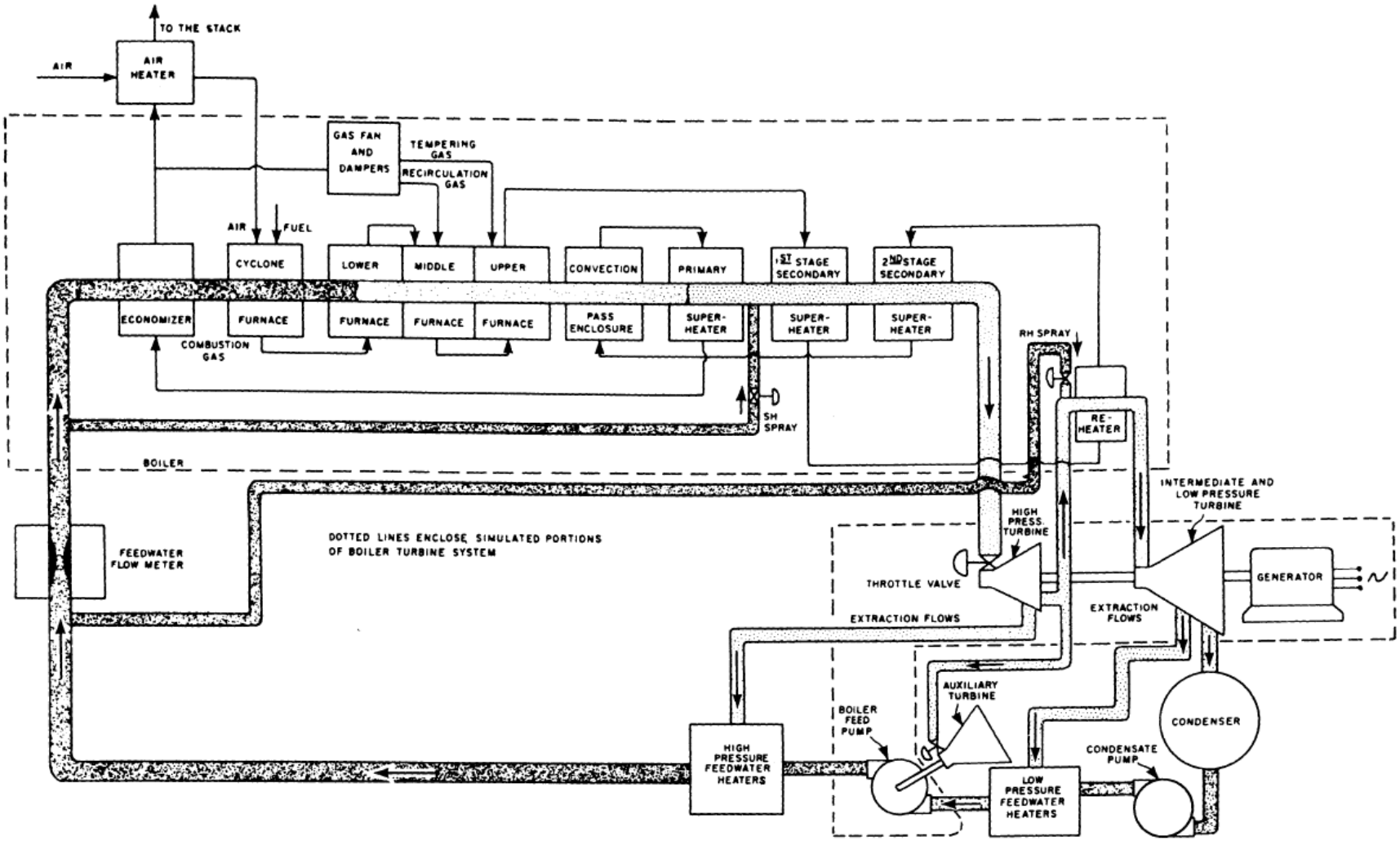


Figure 2.2: Once-through subcritical boiler-turbine system in Adams et al. (1965)

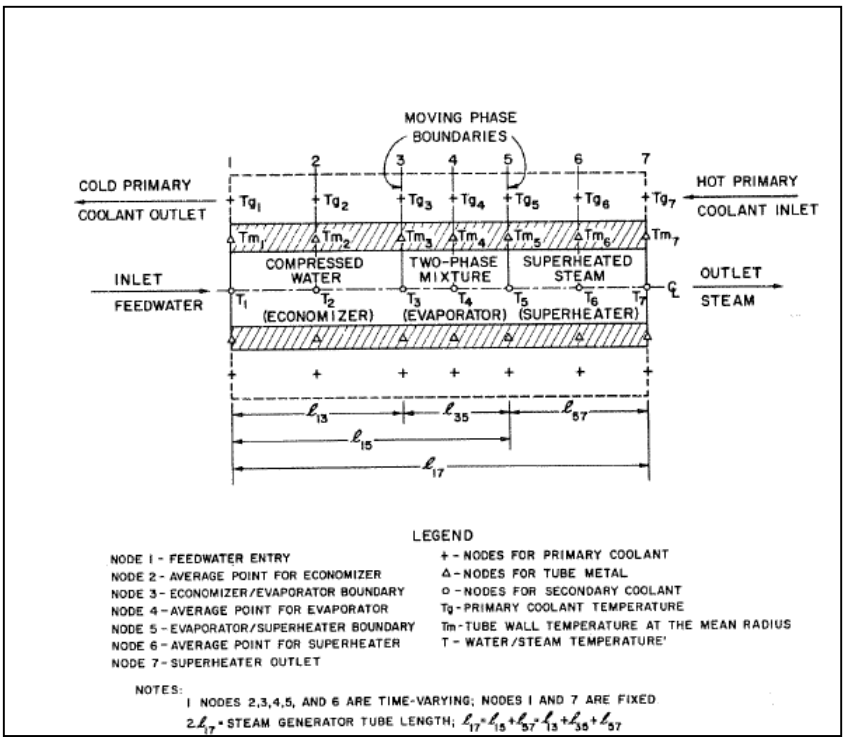


Figure 2.3: Steam generator model solution diagram (Ray, 1980)

Suzuki et al. (1979) constructed nonlinear distributed first principle model of supercritical once-through boiler. The system modelled is a 450MW boiler in operation at Kainan Thermal Power Station of Kansai Elect Co (see Figure 2.4). The model is based on nonlinear PDEs for continuity, enthalpy, and pressure (i.e. the physical conservation principles). The equation of pressure drop, being essentially static was dealt with differently from other fundamental equations, to ensure the accuracy of the dynamic model. This was one of the few distinguishable features of Suzuki et al (1979) model and that developed by Adams et al. (1965) and Ray (1980). Also, in the model Suzuki et al (1979) steam/water velocity was considered as a variable because the change in fluid velocity is responsible for the variations in steam flow and pressure as the position of the governor valve changes, unlike in Ray (1980) where variations in steam/water velocity were assumed negligible The steam/water velocity was considered as a variable. The dynamics of the feedwater flow was included in the model developed in Suzuki et al (1979) unlike Adams et al. (1965) in which the feedwater flow is treated as an independent variable, this is fundamentally not true, as it varies e.g. with the position of the governor valve.

A similar approach used initially by Adams et al (1965) and later by Ray (1980), was adopted in Suzuki et al. (1979) by lumping the thin parallel tubes in actual boiler into a single equivalent tube with same total cross sectional area, and each tube in series represented one section of the boiler (i.e. economizer, primary superheater etc.) as shown in Figure 2.5. The mathematical model developed could not describe the actual behaviour of the plant. The model parameters were adjusted using output error method to ensure better fit with actual plant response. Overall model response was close to actual plant behaviour.

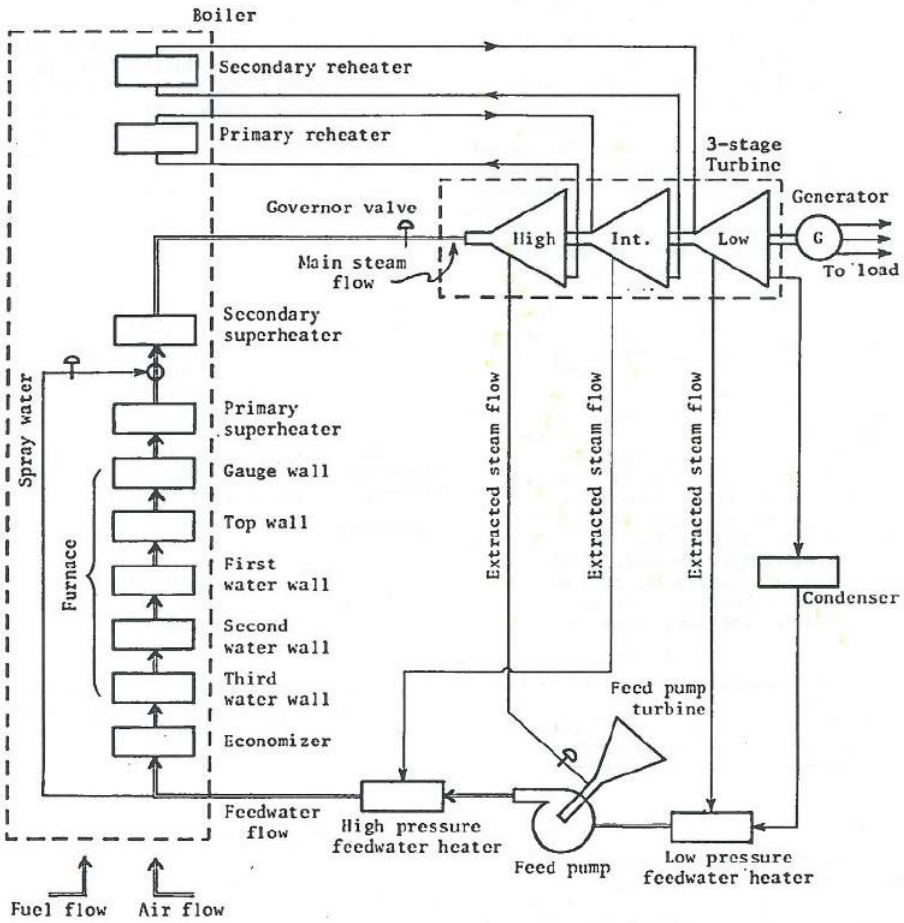


Figure 2.4: Supercritical once-through boiler-turbine system in Suzuki et al (1979)

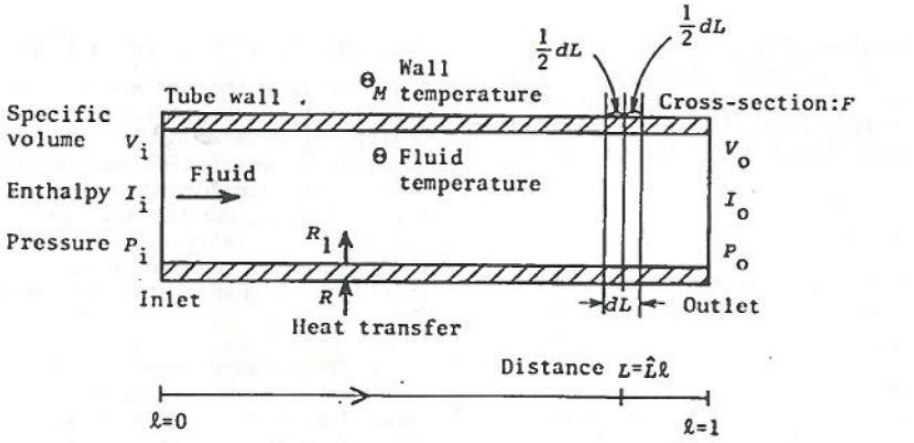


Figure 2.5: a single equivalent tube in one section of boiler in Suzuki et al (1979)

Paranjape (1996) presented a model of a supercritical coal-fired boiler based on first principle for control purposes. The author developed a dynamic simulator of the supercritical unit based on the validated model. Dynamics of steam and flue gas, the dynamics of economizer and feedwater heater were neglected. Simulator response was reportedly in close agreement with plant data. The model was however validated against steady state data and may not reflect actual dynamic behaviour of the plant. A coordinated control system with loops having conventional controller was developed. Nonlinear loops were identified and nonlinear models were developed for control purposes. Coordinated controller having nonlinear models was found to perform better or as good as conventional controller loops.

### 2.3.2 Modelling of Steam Turbine

A steam turbine is a type of steam engine that converts the thermal energy first to kinetic energy by expanding through nozzles or blading, and then to the rotational mechanical energy of a spinning rotor. A turbine stage consists of one set of stationary blades or nozzles and an adjacent set of moving blades or buckets. These stationary and rotating elements act together to allow the steam flow to do work on the rotor. The work is transmitted to the load through the shaft or shafts.

Ray (1980) presented a dynamic model of power plant turbines for controller design. The model approach is deductive and not empirical. Analytical technique used can be applied to other gas and vapour cycle turbines. The model is simplified as it only maps input variables to outputs with many intermediate variables omitted. The steady state model was presented first, and then dynamic model was developed.

Kalnitsky and Kwatny (1981) presented a first principle model of steam turbine. Valve management algorithm is incorporated to enable a good representation of governor valve overlap (allows simulation of turbine valve operation). Stodola equation is used to study effect of HP turbine exhaust pressure on flow. Crossover piping is also modelled. Hence its pressure can be varied (backpressure of IP turbine). The IP turbine flow is represented by Stodola equation. Complex extraction flows are represented approximately at various points in the turbine. The model accurately produced basic heat balance data for loads as low as 3% of rated load conditions. An important limitation of this model is that it can be used only for those models of operation which exhibit “fully developed” flow; it is not intended to predict performance during the initial stages of start-up. This is because the assumptions made during derivation give rise to the need to divide some quantities by flow and densities. At start-up, these entities approach zero, the result becomes meaningless.

Chaibakhsh and Ghaffari (2008) developed a nonlinear first principle model of a supercritical steam turbine based on energy balance, thermodynamic principles, and semi-empirical equations, to characterize the transient dynamics of the steam turbine subsections (HP,IP and LP turbines, reheater and generator). A steam turbine for 440MW power plant with once-through boiler was considered for the modelling. The system dynamics is represented by a number of lumped models for each subsections of the turbine. Model parameters were determined with empirical relations and genetic algorithm (GA). The model was simulated with MATLAB/Simulink. Comparison between the responses of the turbine-generator model with the responses of real system validates the accuracy of the proposed model in steady state and transient conditions. Chaibakhsh and Ghaffari (2008) believed that further model improvements will make the turbine-generator model proper to be used in emergency control system designing.

### 2.3.3 Modelling of other Components

#### *2.3.3.1 Condenser Modelling*

Transient behavior of industrial and power plant condensers has not been examined in detail despite its relevance to start-up, safety and process control of the overall plant. However, few studies are worth mentioning. Ciechanowicz (1968) presented a

mathematical model for the dynamics of a vapour condenser. The condenser was viewed as a cross flow heat exchanger. Two-phase fluid flow (i.e. the primary flow) leaves the turbine and passes through the condenser between the tubes. The one-phase flow in the tube is the secondary flow. Two mathematical model approaches (the 2D model and 1D model) were considered. The results obtained from the 2D model was too complicated despite the simplifying assumptions made. Further simplification of the 2D model was then carried out.

Botsch et al. (1997) developed a model for dynamic behaviour of shell and tube condenser. The model describes the behaviour of an industrial scale (e.g. power station condenser) shell and tube condenser. Derivation of the material and energy balances is presented. The model is able to predict vapour and condensate flow rates, pressure drop and the temperatures of the vapour, condensate, wall and coolant. The condenser is subdivided into increments corresponding to the location of the baffles in the condenser. Each of these baffle spaces is assumed to be fully mixed. The heat and material fluxes between the phases are determined using local transfer coefficients which are calculated for each baffle space. The model also includes the determination of the pressure profile along the apparatus. Results of several simulations are compared with experimental data to achieve a validation of the model. Steady state and the transient behaviour of the condenser were examined. Dynamic behaviour of the system was carried out when the system was subjected to step changes in each of the five key loads that determine the condenser behaviour. These are the pressure, steam flow rate, air flow rate, coolant flow rate, and coolant inlet temperature. Results of the simulations agreed well with the experimental data.

### 2.3.4 Modelling of Whole SCPP

Several once-through boiler-turbine models exist in the literature (Adams et al, 1965; Ray and Bowman, 1976; Shinohara et al, 1996; Chaibakhsh, 2007; Zindler, 2008; and Muhammed et al. 2010). Most are either based on subcritical unit, and/or upon assumptions that are suitable for the full load operating mode, but inadequate for emergency (or part load) mode of operation. However, such assumptions can trigger misleading inferences in developing models that will be able to predict power plant response to frequency transients in the system, which occurs as a result of long term

imbalance between generation and load. This section therefore considers review of supercritical plant model at normal and emergency operations.

Masada and Wormley (1982) developed a lumped parameter dynamic model of a 1400 MW supercritical pressure steam plant for the study of the plant performance under normal and emergency conditions. A systematic study of lumped models for heat exchange, similar to Adams et al (1965) was described, and criteria for determining the accurate number of compartments was further proposed. The dynamic model is developed according to physical conservation principles. Unlike the work of Adams et al. (1965); and Ray (1980) which concerned subcritical plants, the model of Masada and Wormley (1982) is particularly important to this thesis because it treats the supercritical unit at normal and emergency (50-100% load) operation, and also modelled explicitly the condensate and feedwater dynamics of the plant. The model validation confirmed the accuracy of the model in both steady state and transient features with the actual plant. The model provides a valuable tool in understanding the interaction between components and in predicting the system behaviour to various input disturbances.

Shinohara and Koditschek (1996) presented a more simplified and less comprehensive state space model of a supercritical power plant simulated for wide load cycling scenario including start-up and shutdown. The model was developed from a greatly simplified first principle, borrowing a cue from (and further simplifying) the assumptions of previous works (Adams *et al.,* 1965; Ray 1980; and Masada and Wormley, 1982). Fluid properties were assumed to be uniform for individual components at any cross section. Further simplifying assumptions were made departing from earlier work such as considering only two sections in the working fluid path--the furnace and the superheater, assuming that work by the set of turbines (HP/IP/LP) as the work of a single turbine unit. Due to the turbine assumption, the effect of the reheater was considered in the superheater section. The model was fitted to a far more complex and physically accurate simulation model by EPRI. The input-output response was reported close initially. However, large discrepancies between the model and the EPRI simulator were attributed to absence of property value estimates: i.e. the compromise assumptions of constant input enthalpy from economizer and output enthalpy from condenser; and the elimination of the reheat

section means that the throttle valve in the model includes the effect of another throttle valve in the reheater outlet, thereby resulting in large differences in valve opening control response.

Lu (1999) provided a general review of modelling and simulation techniques and describes basic steady state and dynamic models for power plant. A dynamic model for a 677 MWe coal- and gas-fired power plant was built with MATLAB/Simulink. The plant components were built using physical modelling techniques and the whole-plant model was constructed by graphically linking the standard components as in physical processes. The model was constructed from the cause-effect interaction between inputs and outputs at certain boundary conditions. The inputs for the boiler are design parameters (i.e. geometry), operational parameters (i.e. valve positions) and other parameters (i.e. heat transfer coefficients and heat capacity). The outputs are the thermal and mechanical performance parameters. Simulation responses to typical plant disturbances were satisfactory.

Chaibakhsh *et al.* (2007) presented a dynamic model of a 440 MW subcritical once-through boiler-turbine-system using combination of first principle and black box approach. Model parameters were determined with empirical relations. Genetic algorithm (GA) was used to obtain optimal model parameters based on experimental data because it generally requires less knowledge of the complete system model. The boiler system were decomposed into smaller components, analysed and modelled separately (see Figure 2.6). The mathematical models with unknown parameters for subsystems of the once-through boiler were first developed based on the thermodynamics principles and energy balance. Then the related parameters are determined from constructional data such as fuel and water steam specification or by applying genetic algorithm (GA) techniques on the experimental data. In the superheater sections, only the steam phase is presented in these subsystems, and convective heat transfer is the dominating terms in the expression. Non-linear two-phase models were used to describe steam quality in the water walls. Steam quality in evaporator section is adjudged to have a direct effect on the temperature of downstream sections since outflow from the evaporator passes through a separator to extract the steam phase from the mixture.

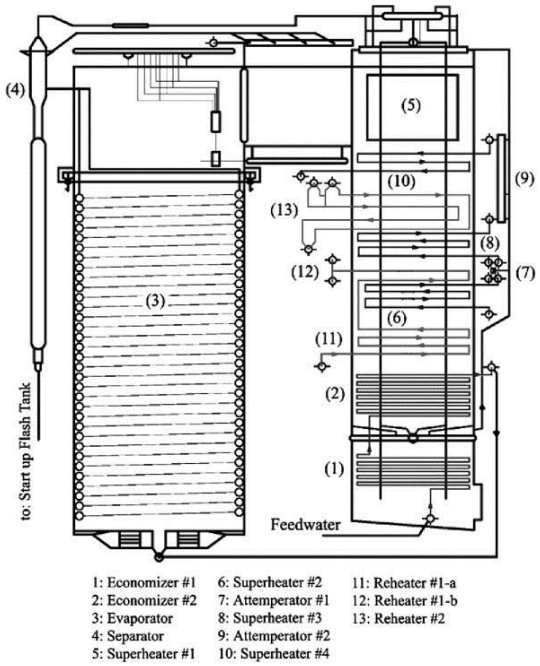

Figure 2.6: Boiler Cross section modelled in Chaibakhsh et al. (2007)

The presented models for turbines were reasonably accurate when it has no frequency control. The comparison between the responses of the corresponding models with the responses of the plant subsystems validates their accuracy in the steady-state and transient conditions.

Zindler *et al.* (2008) simulated the dynamic behaviour of 800 MWe SCPP at fast load changes scenario using a dynamic simulation program Enbipro (Figure 2.7) to examine the plant's ability to fulfil the UK Grid Code requirement. In the UK Grid Code: a linear change of 10% of the power output up to 80% load is the demand, as a reaction of the boiler in case of a frequency drop. This increase in active power output must be released increasingly within 10 seconds with a regeneration time of 20 minutes if the power plant works under part load condition between 55% and 80% of full load. Zindler *et al.* (2008) explains the reason for this extreme condition in the Grid Code thus: "*These extreme requirements are a result of the Great Britain transmission system, because the Great Britain power line works under "isolated operation" conditions. That means, that compared to the mainland of Europe a relatively low number of market participants exist in Great Britain and the individual consumption behaviour of this participants is relatively unpredictable. The requirement diminishes linearly between 80 and 100% load".*

According to Zindler *et al.* (2008), the fast load changes can be achieved with primary measures using the short-term storage behaviour of the power plant: the accumulator steam of the boiler by throttling; the metal mass of the boiler; and the feedwater tank (condensate stop). These primary measures are essential for the time lag required by the boiler to increase the evaporation as a secondary measure based on an increased firing rate. These storages are discharged by opening turbine throttling valve or by condensate stop. Zindler *et al.* (2008) presented the dynamic retention capacity of the boiler related to the thermal storage capacity of the steam mass and the steel mass. Results of the dynamic retention capacity of the boiler after a frequency drop were presented. The result showed that 6% performance improvement was obtained from the analysed primary measures (i.e. valve throttling). Zindler et al. (2008) believed the remaining 4% additional power output to fulfil the grid code must be produced from other primary measures (i.e. condensate stop). However, the simulation was not verified by any measured data at a real power plant.

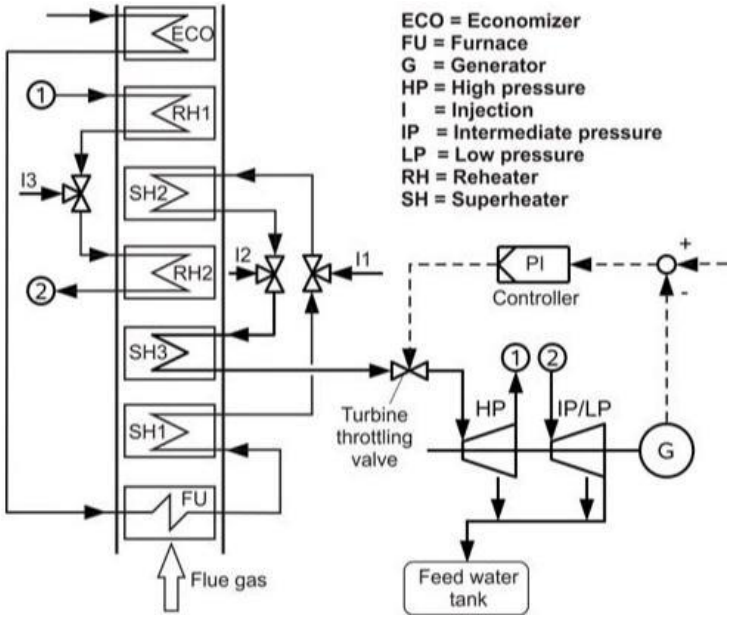


Figure 2.7: The analyzed coal-fired supercritical unit in Zindler *et al.* (2008)

Sanparsertpanich and Aroonwilas (2009) developed a process-based computer model of a pulverized coal-fired power plant (subcritical and supercritical) using the principles of coal combustion chemistry, heat transfer from combustion zone, combined material and energy balances, and thermodynamics of a steam power cycle. Sensitivity analysis was performed on the developed model using rank correlation coefficient and Monte Carlo simulation approaches with the aim of optimizing the design and

operating conditions. The moisture content in coal; the operating pressures at the HP, IP, and LP turbines; the boiler efficiency; the temperatures of preheated air, main steam and reheated steam were identified as the key operating and design parameters influencing the net efficiency of the PC-fired power plants.

Muhammed et al. (2010) developed a mathematical model for 600 MW supercritical coal-fired power plant. A combination of first principle and black box model (using system identification) technique were used. The presented model is similar to that of Chaibakhsh et al. (2007) except that this present study refers to a supercritical power plant, and more simplified approach was adopted. Similar assumptions used in previous work (Adams et al. 965; Ray and Bowman, 1976; Suzuki et al. 1979; Chaibakhsh et al. 2007) for modelling subcritical or supercritical once-through boiler unit were adopted. Genetic algorithm methods were used to obtain optimal model parameters based on experimental data. Identified parameters were verified with different sets of measured plant data. Simulation results show good agreement with measured dynamic response from the power plants.

## 2.4 Status of Post-combustion Carbon Capture (PCC) using solvents

### 2.4.1 Experimental Studies

Experimental study of PCC processes have been widely published in open literature (Wang *et al*., 2011). Experimental studies have been very important for developing correlations used in modelling, and also for validating outcomes of model-based studies. For instance, $CO_2$ reaction kinetics information necessary for PCC modelling has been derived from experimental studies and reported in Aboudheir *et al*. (2003) and Edali *et al*. (2009) among others. Aboudheir *et al*. (2003) developed a thermo-molecular-kinetics model for $CO_2$ reaction with MEA solutions which reported to be better than other published kinetic models. Edali *et al*. (2009) developed kinetic models for $CO_2$ reaction in a mixed solution of MDEA and MEA. Information about thermodynamic and solubility of $CO_2$ in different solvents (MEA, MDEA etc.) obtained through experimental study are reported in Bishnoi and Rochelle (2002) and Inoue *et al*. (2013). Goff and Rochelle (2004) examined the rate of oxidative degradation of MEA under typical operating conditions for PCC.

Some other experimental studies have focused on screening different solvents to determine the solvents that gives best performance in terms of regeneration energy requirement and degradability (Idem *et al*., 2006; Notz *et al*., 2007; Knudsen *et al*., 2009; Mangalapally and Hasse, 2011a; Moser *et al*., 2011). Characteristics of different packing material have equally been assessed to determine their impact on capture performance (Park *et al.*, 2004; Mangalapally and Hasse, 2011). Comparison of different packings and impact of packing height and column was investigated extensively in Dugas (2006). There are 48 experimental tests presented in this study. This was used for model validation by many researchers such as Lawal et al. (2009), Lawal et al. (2010), Lawal et al. (2012), Biliyok et al. (2012). Canepa et al. (2013).

In Faber *et al.* (2011), report on the transient behaviour of the PCC process during step response test was presented. The test was performed at a 1 tonne $CO_2$/hour pilot plant for the amine-based PCC within the EU project CESAR. It was found that the overall system acts like a buffer and tends to accommodate perturbations at the inlet with minor fluctuations downstream. This behaviour is desirable considering the future downstream compression unit.

### 2.4.2 Model Studies

Absorption/desorption of $CO_2$ in PCC with chemical absorption involves simultaneous gas-liquid mass transfer and chemical reactions. When modelling the process from first principle, gas-liquid mass transfer can be described based on the assumption of gas-liquid equilibrium (*i.e.* equilibrium-based approach). In reality, gas-liquid equilibrium is hardly achieved and the approach is therefore not very accurate (Kenig *et al.,* 2001; Peng *et al.*, 2002). More accurate representation of the mass transfer process is obtained using two-film theory (Lawal *et al.,* 2009a) or penetration theory (Tobiesen *et al*., 2007) (*i.e.* rate-based or non-equilibrium approach). Details of two-film and penetration theories are available in literatures such as Treybal (1980).

On the other hand, $CO_2$ reaction kinetics can be represented by assuming that the reactions reach equilibrium instantly (Lawal *et al*., 2010). When the reactions progress very rapidly such as in fast reacting solvents like MEA solvent, this assumption is appropriate (Kenig *et al.,* 2001; Lawal *et al*., 2010). With less reactive solvents (e.g. DEA, MDEA), this assumption is less accurate. More accurate description of the $CO_2$

reaction kinetics can be obtained using actual kinetics model (Zhang *et al.,* 2009). This can be simplified by assuming pseudo first order reaction and introducing an enhancement factor which accounts for the kinetics (Kucka *et al.,* 2003; Kvamsdal *et al*., 2009).

From a combination of the methods for describing mass transfer and reaction kinetics, models of PCC processes with chemical reactions can be classified into different levels of complexities. In literature, five levels of complexity (Figure 2.8) is recognised (Kenig *et al.,* 2001). The level 5 is considered to be the most accurate because it adopts a rate-based approach for describing mass transfer process and actual kinetic model for the chemical reactions. There have been varied PCC models in literature with different level of complexities.

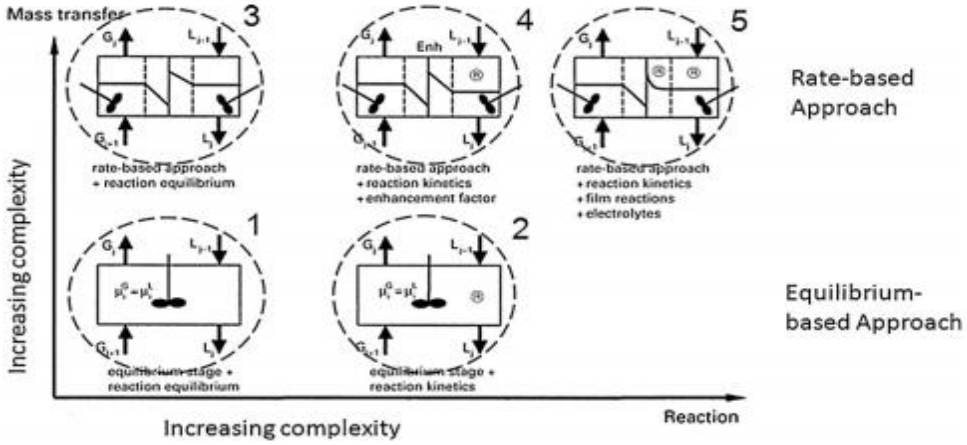


Figure 2.8: Complexity levels of PCC models (Kenig *et al.,* 2001)

Dynamic models involving only the absorber (Kvamsdal and Rochelle, 2008; Lawal *et al.*, 2009a; Kvamsdal *et al.,* 2009; Khan *et al*., 2011; Posch and Haider, 2013) and only the stripper (Lawal *et al.*, 2009b; Ziaii *et al.*, 2009) are available in literature. In these models, rate-based approach has been used to describe gas-liquid mass transfer process except in Posch and Haider (2013) where gas-liquid equilibrium conditions were assumed.

In Lawal *et al.* (2009a), Lawal *et al.* (2009b) and Ziaii *et al.* (2009), the reaction kinetics is approximated by the assumption that the reactions reach equilibrium. This is an

example of level 3 complexity model. As noted earlier, for fast reacting solvents such as MEA, this assumption can be considered fairly reasonable.

On the other hand, in Kvamsdal and Rochelle (2008) and Kvamsdal *et al.* (2009) the reaction kinetics was approximated by an enhancement factor with the reactions assumed to be pseudo first order. In Khan *et al.* (2011), fast second-order kinetics for the $CO_2$–MEA reactions alongside an enhancement factor was used. These models have higher computational requirement and will give better results since the reaction kinetics is represented more accurately (Gáspár and Cormoş, 2011). This is an example of level 4 complexity model. In Posch and Haider (2013), reaction kinetics was obtained using the thermo-molecular reaction scheme presented in Aboudheir *et al.* (2003). This is an example of level 2 complexity model.

Dynamic model of the complete PCC process with chemical absorption including the absorber and stripper is also available (Lawal *et al.*, 2010; Harun *et al*., 2011; Gáspár and Cormoş, 2011; MacDowell *et al*., 2013). Mass transfer process in the models was described using rate-based approach. The reaction kinetics was approximated with equilibrium reactions in Lawal *et al.* (2010) and MacDowell *et al*. (2013) as per level 3 complexity and enhancement factors in Harun *et al*. (2011) and Gáspár and Cormoş (2011) as per level 4 complexity.

Lawal *et al.* (2010) used ElectNRTL for determining thermophysical properties and found that the absorber is more sensitive to L/G ratio than actual solvent flowrate (L) and flue gas flowrate (G). Dynamic validation of the model developed by Lawal *et al*. (2010) is reported by Biliyok *et al*. (2012). Harun *et al*. (2011) showed that performance of the PCC process is affected by load reduction at the absorber inlet as it significantly affects the performance of absorber and stripper.

MacDowell *et al*. (2013) used SAFT-VR EOS for property calculations. The EOS accounts for all of the inter-species interactions in the fluid, including the reactions and therefore avoids for the need for enhancement factors. They found that the position and extent of the mass transfer zone is a function of competing interphase fluxes of $H_2O$ and $CO_2$. Gáspár and Cormoş (2011) used a combination of methods for estimating different thermophysical properties, namely Antoine equation, Lee Kesler, and Wilson –NRF. They conclude from their analysis that reduction of the solvent

temperature at the stripper inlet has strong influence on the behaviour of the whole process.

## 2.5 Modelling of SCPP Integrated with $CO_2$ Capture

A vast number of studies investigated the dynamic response of power plants. Some of these studies were largely based on first principle, black box model, or both. However, the power plant models developed by these authors do not include a $CO_2$ capture plant. On the other hand, steady state models of supercritical power plant integrated with $CO_2$ plant have been reported. Few authors developed a dynamic model of power plant with $CO_2$ capture integrated. This section describes the review of steady state and dynamic model of supercritical plant models with integrated PCC capture plant.

### 2.5.1 Steady State Study

Aroonwilas and Veawab, (2007) developed a steady state, in-house model to compare the performance of different process configurations, different solvents and solvent blend, for a PCC plant integrated with a 500MWe supercritical power plant. Advanced MEA-MDEA blend with split flow configuration was used for $CO_2$ capture unit. Integration of $CO_2$ capture unit into supercritical plant with advanced MEA and split flow configuration achieved lower energy penalty for $CO_2$ capture. It was reported that when a suitable steam pressure was drawn to the $CO_2$ capture unit, it ensured maximum $CO_2$ was avoided. Aroonwilas and Veawab, (2007) also found out that MEA-MDEA required absorber heights of more than three times that of conventional MEA solution to achieve identical $CO_2$ removal target. Higher column height and lower energy requirement however presented a trade-off between capital and operating costs associated with the capture plant.

Lucquiaud *et al.,* (2009) presented a capture ready supercritical coal-fired power plant and post combustion $CO_2$ capture (PCC) plant. The options available for making steam turbines at pulverized-coal (PC) plant suitable for adding PCC was discussed. It was explained that pulverized-coal plants can be made 'capture-ready' for PCC at low cost by using a throttled LP turbine or floating pressure retrofit strategy or a hybrid of both. A hybrid of the two performed better for a wide range of solvent energy requirement. They were able to cope with inevitable uncertainties in future CCS

development. Small penalty in efficiency (about 1%) was observed when retrofit was compared to new built CCS that uses the same solvent as the retrofit. Capture-ready plant retrofitted with PCC using a throttled LP or floating pressure approach $CO_2$ can be reduced to zero to generate additional power.

Sanpasertparnich *et al.,* (2009) presented a steady state model of a Greenfield power plant and an optimized integration of PCC plant. The power plant represented a state-of-the-art hard-coal-fired ultra-supercritical power plant with 600 MWe power output (gross).Two commercial simulation tools were used to ensure an adequate representation of the overall process and a sufficient degree of detail within the sub-process models, two commercial simulation tools EBSILON® Professional (for power plant, $CO_2$ compressor) and Aspen Plus® (for $CO_2$ capture unit) were used. The two tools communicate via a mutual spreadsheet interface (MS Excel). The adaptation of pressure levels in the water-steam-cycle regarding the steam requirements of the PCC plant was evaluated. Particular focus was put on waste heat integration by condensate pre-heating and combustion air pre-heating for minimisation of the overall net efficiency loss. The efficiency potential of the available options as well as the limits of integration, especially with respect to power plant in commercial operation was discussed. EBSILON® Professional was used to develop a steady state model of the overall process including power plant, $CO_2$ compressor and capture plant. The $CO_2$ capture unit was modelled as a black box, where the interface quantities of the black box are determined by a detailed model of the capture process in Aspen Plus® using monoethanolamine (MEA) as solvent.

Zhang et al (2011) presented a steady state model of SCPP with $CO_2$ capture and detail simulation conducted with the model. The reference plant used is a 550MWe SCPP in China. Performance of the supercritical power plant across a wide range of $CO_2$ capture levels/rates (20%-99%) was discussed. Energy consumption for solvent regeneration was reported as the largest source of energy penalty for $CO_2$ capture with MEA. The high cost per $tCO_2$ avoided was the main barrier for CCS deployment. Zhang et al (2011) concluded that choosing a low $CO_2$ capture level/rate other than the proposed >90% might reduce cost per $tCO_2$ avoided. 40% was reported as the cost-optimal $CO_2$ capture ratio for this plant at present due to physical capacity restrain of the MEA.

### 2.5.2 Dynamic Study

Lawal *et al.* (2012) developed, validated, and linked a dynamic model of coal-fired subcritical power plant with a dynamic model of PCC (MEA based) plant. The modelling was constructed with the aid of gPROMS®. The subcritical power plant model was greatly simplified involving only the furnace model, drum, downcomer-riser loop, superheater, reheaters and the steam turbines. The PCC plant was validated from pilot plant scale, and later scaled up to the required capacity suitable for processing flue gas from the 500MWe subcritical power plant. Four case studies were considered to investigate the entire plant performance with and without $CO_2$ capture. The case studies of the two integrated plants revealed that the $CO_2$ capture plant has a slower response compared to the subcritical power plant. The impact of changing absorber packing height on MEA concentrations and load changes was also investigated. It was concluded that an absorber packing height of 27m offered a good trade balance between increasing column costs and reducing boiler heat duty.

## 2.6 Studies Based on Analysis of the SCPP-PCC Model

### 2.6.1 Exergy Analysis

With the widespread progress of SCPP and the ultra-SCPP due to its higher efficiency and lower emission per MWe generated, and the further improvement in its potential through $CO_2$ capture integration, an investigation of efficiency improvement is very important. Exergy analysis will identify the losses associated with this integrated systems, investigate strategies for improvement, and also reduce the penalties due to the capture process.

Exergy analysis of thermal power plants has been investigated by a number of researchers since the early 1980s and has been widely applied to different configurations of thermal power plants (Yang et al, 2013). Some of the researchers have focused on energy and exergy analyses of subcritical, supercritical (SCPP) and ultra-supercritical (Ultra-SCPP) steam power plants [Yang et al, 2013; Senguptal, et al, 2007; Kotas, 1995; Szargut, 2005; Horlock et al, 2000; Dincer and Al-Muslim, 2001; Reddy et al, 2014) while some have extended the analyses to include varying load conditions (Senguptal, et al, 2007; Ameri et al, 2009) and efficient design of power plant components by exergy loss minimization (Siamak et al, 2008). A large number

of studies have also considered combined cycle gas turbine (CCGT) power plants investigating different components exergy losses (Srinivas, 2009; Reddy and Mohamed, 2007; Woudstra et al, 2010). Exergy analysis of standalone (pre-combustion or post-combustion) $CO_2$ capture plants have also been carried out (Geuzebroek et al, 2004; Valenti et al, 2009; Lara et al, 2011) to investigate the effects of exergy destruction on the associated penalties and efficiency reduction. Analysis of $CO_2$ capture plant integrated to a power plant has also been investigated. Most of the integrated SCPP processes have focused mainly on energetic analysis (Aroonwilas et al, 2007; Lucquiaud, 2009; Sanpasertparnich et al, 2010; Zhang et al, 2011; Pfaff et al, 2010; Harkin et al, 2009), while few have included exergy analysis while investigating the improvement of efficiency of power plant with $CO_2$ capture (Dawid et al, 2014; Hagi et al, 2014; Amrollahi et al, 2011).

## 2.7 Summary

Based on this literature review, steady state and dynamic models for SCPP developed so far are based on simplified first principle and/or black box models. Available dynamic models for optimal operation of supercritical power plant on large scale (above 600 MWe) are based on simplified power plant model owing to the end use of the models (e.g. for control studies). Erroneous assumptions, lack of complete plant steady state/dynamic data for model validation, and inadequate information about fluid properties of working fluid at supercritical conditions are few of the reasons for over-simplification of the models.

Steady state modelling of SCPP integrated with PCC has been carried out tremendously by researchers with different commercial software packages and at varying degrees of complexity. Majority of the steady state models have been developed for carrying out energetic and exergetic analyses of the system in order to reduce its energy penalties and improve the efficient design of the process.

Also, from the literatures reviewed for the PCC modelling, it was observed that insufficiency of plant data for detailed dynamic and steady state validations has been a major difficulty in producing a very good reusable models. Based on the model complexity, the most advanced of the studies is based on “model 3”while model 5, which is the most complex and most accurate because it considers both rate-based

mass transfer and actual $CO_2$ reaction kinetics; has not been reported in literature. Also, the huge size (or scale) difference between the pilot plants and the commercial size plants makes it almost impossible to extrapolate the findings from pilot plant to predicting the behaviour of commercial scale units.

Majority of the integrated SCPP with PCC model reviewed are based on steady state for the purpose of performance analysis. Only very few have incorporated the dynamic study of both the SCPP integrated with PCC with chemical absorption. Finally, study on dynamic modelling of SCPP with PCC ability regarding operational study (e.g. under stringent grid requirement) is an area with a wide knowledge gap compared to the plant without CCS. This forms the basis for carrying out this research in addressing the issues raised in the review by providing a state-of-the-art modelling of SCPP integrated with PCC under a stringent grid code (e.g. UK Grid Code) requirement.

# Chapter 3 Steady State Simulation and Validation of SCPP and PCC with solvents

## 3.1 Introduction

Steady state modelling of the SCPP is necessary to evaluate its performance for a variety of conditions such as the energy consumption (or exergy destruction), the impacts of equipment design on overall plant performance and the economic viability of the designs.

### 3.1.1 Benchmark Selection

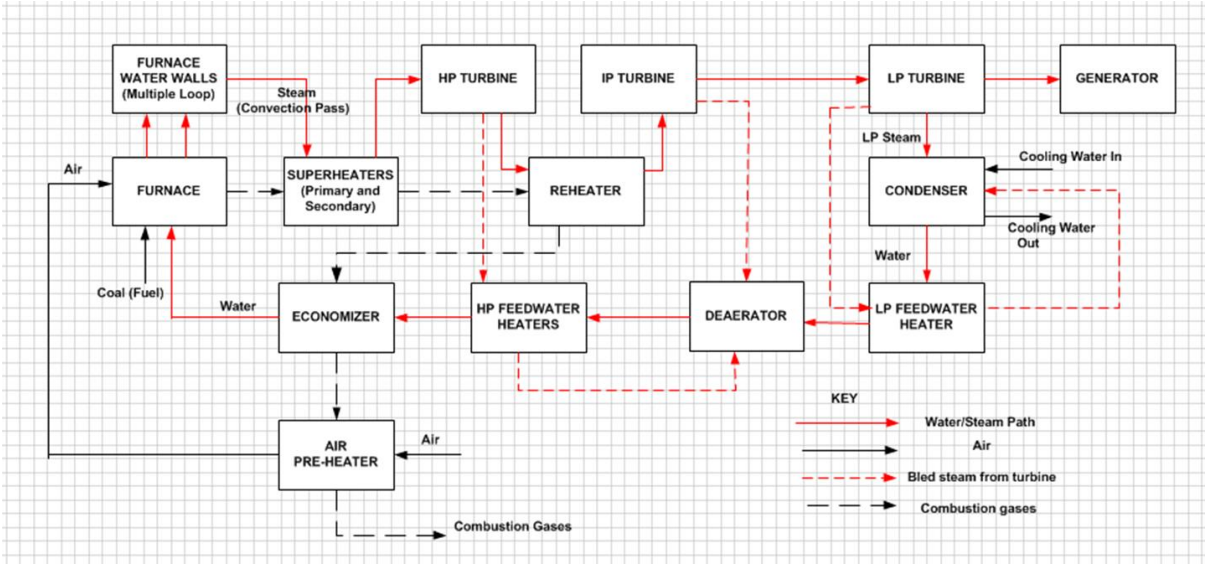


Figure 3.1: A Block Diagram of Simplified SCPP

SCPP is a very complex system with many similar components e.g. feedwater heaters, superheaters, turbines etc. The block flow diagram in Figure 3.1 simplifies actual SCPP design to a form suitable for modelling purpose. Different SCPP designs were compared using different literature sources.

### 3.1.2 Reference SCPP used for this Study

The reference SCPP used in this study is a greenfield power plant of 580 MWe SCPP with flue gas desulphurisation (FGD) and $CO_2$ capture described in Woods *et al* (2007). The steam turbine conditions correspond to 24.1 MPa/593$^{o}$C throttle with 593$^{o}$C at the reheater. Net plant power, after consideration of the auxiliary power load

is 550 $MW_e$. The plant operates with an estimated efficiency of 39.1 % (HHV). The main subsystems of the plant include: coal milling system, coal combustion system, ash handling system, FGD, condensate and feedwater systems. The Aspen Plus® simulation of the integrated system is carried out in eight different hierarchies: (i) the coal mill; (ii) the once- through boiler; (iii) the feedwater heaters and steam extractions; (iv) the steam turbines; (v) the condenser and hotwell; (vi) the flue gas desulfurization; (vii) the air preheating and (viii) the post-combustion $CO_2$ capture. The reference SCPP consists of eight feedwater heaters (including the deaerator); seven were modelled as heat exchangers while the deaerator was modelled as a mixer. The feedwater from the deaerator is pumped into the boiler through a boiler feed pump (turbine driven). Table 3.1 shows the key parameters of the reference SCPP used in this study.

Table 3.1: Key parameters of the Reference SCPP (Woods et al, 2007)

| Description | Value |
|---|---|
| Steam cycle (MPa/$^o$C/$^o$C) | 24.1/593/593 |
| As received coal (kg/hr) | 201,600 |
| Coal Heating Value, HHV (MJ/kg) | 27.113 |
| Condenser pressure (mmHg) | 50.8 |
| Boiler Efficiency (%) | 89.0 |
| Cooling water to condenser ($^o$C) | 16.0 |
| Cooling water from condenser ($^o$C) | 27.0 |
| HP Turbine efficiency (%) | 90.0 |
| IP Turbine efficiency (%) | 92.0 |
| LP Turbine efficiency (%) | 94.0 |
| Generator efficiency (%) | 98.4 |
| Excess air (%) | 20.0 |
| Stack temperature ($^o$C) | 57.0 |
| FGD Efficiency (%) | 98.0 |
| Fabric filter efficiency (%) | 99.8 |
| Ash Distribution, Fly/Bottom ash | 80%/20% |

## 3.2 Steady State Modelling of SCPP

Aspen Plus® V8.0 is used for this steady state simulation study. In order to simulate the SCPP in Aspen Plus®, the necessary parameters needed for setting up the simulation are first determined. Table 3.2 shows the basic parameters settings for the Aspen Plus® simulation.

Table 3.2: Basic parameters for the Aspen Plus® simulation

| Parameter | Parameter Settings |
|---|---|
| Property Databank | Non-Conventional, Combust, Inorganic, Solids, and Pure 27 |
| Stream Class | MIXED, CIPSD, MCINCPSD |
| Property Method | IDEAL |
| Free water Method | STEAM-TA |
| Calculation Algorithm | Sequential Modular (SM) |

Table 3.3: Ultimate Analysis of UKBC as Received (Berry et al, 1998)

| Compositions | Molecular Weight | Ultimate Analysis (wt. %) |
|---|---|---|
| moisture | 18.015 | 12.0 |
| carbon | 12.010 | 60.0 |
| hydrogen | 1.008 | 3.9 |
| nitrogen | 14.006 | 1.3 |
| chlorine | 35.453 | 0.2 |
| sulphur | 32.062 | 1.6 |
| Ash | - | 15.0 |
| oxygen | 15.999 | 6.0 |

Table 3.3 shows details on the ultimate analysis of the coal on a mass basis as received. The Ideal gas equation of state was selected to calculate all thermodynamic properties for the conventional components in the overall process. Also, the HCOALGEN and DCOALIGT models (Aspen, 2013) were used to calculate enthalpy and density for coal and ash (non-conventional components). The type of coal used for this analysis is UK Bituminous coal (UKBC), and it is assumed that the coal is pre-dried before combustion.

Table 3.4 provides details on the proximate analysis of the coal on weight % basis as received respectively. These data are based on the report "Power Generations and the Environment – a UK Perspective" (Berry et al, 1998). These data were used for specifying the coal properties in Aspen Plus®.

Table 3.4: Proximate Analysis of UKBC as Received (Berry et al, 1998)

| Compositions | Proximate Analysis (wt. %) |
|---|---|
| moisture | 12.0 |
| Ash | 6.31 |
| Volatile Matter | 32.17 |
| Sulphur | 0.45 |
| Fixed Carbon | 32.98 |

The steady state simulation of the whole SCPP is carried out in seven different subsystems using the Hierarchy block in Aspen Plus®: (i) The coal Mill Model (ii) The Primary and secondary air-preheating model (iii) The SCPP Once-through Boiler Model (iii) Feedwater Heaters and Steam Extraction model (iv) The Steam Turbine Model (v) Condenser and Hotwell model (vi) The Particulate Removal and Flue gas Desulphurization Model (vii) The $CO_2$ Capture model. The subsystem models were combined under one flowsheet to form the integrated SCPP-PCC system. Figure 3.2 shows a schematic of the whole integrated model developed in this study.

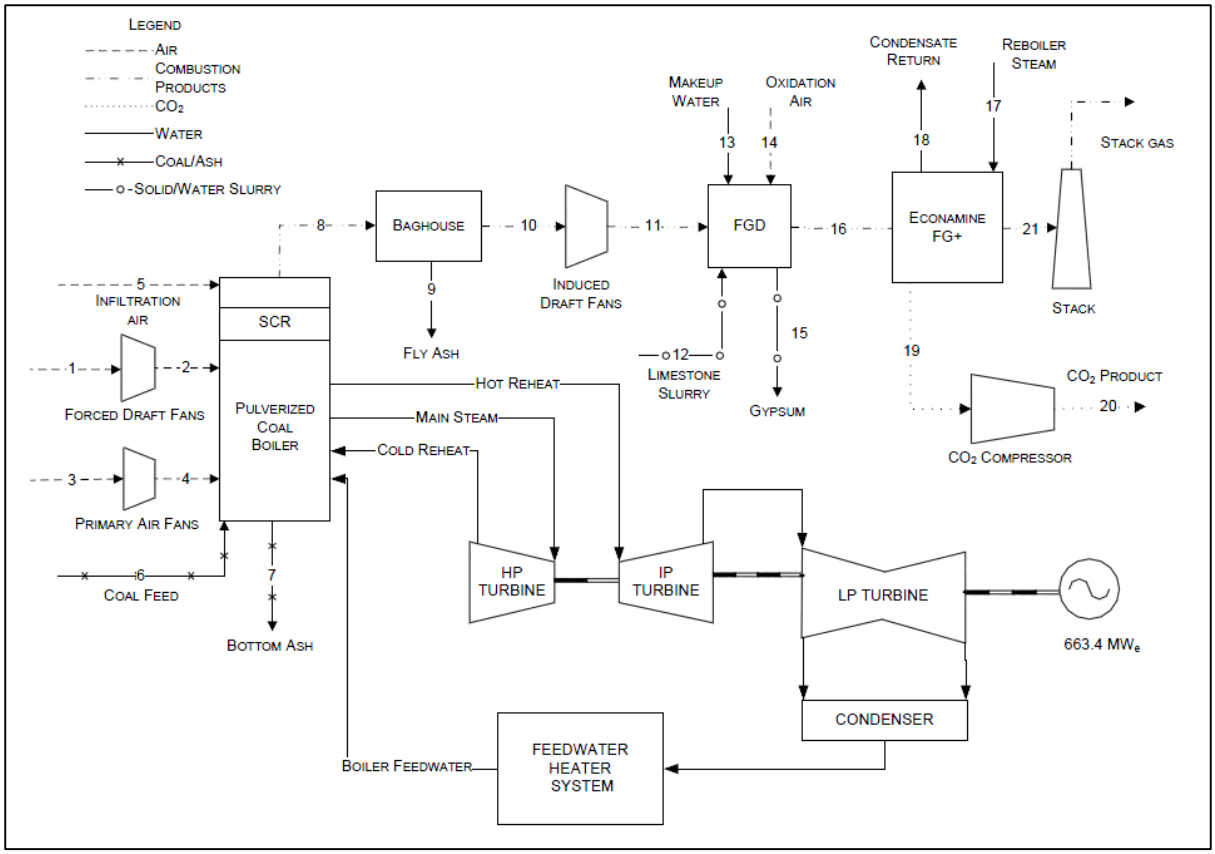


Figure 3.2: Schematic of the reference SCPP-PCC in this study (Wood et al, 2007)

### 3.2.1 Coal Milling Subsystem

The coal milling process reduces the size distribution of the coal by grinding it to a fine powder and thus improves the combustion process in the SCPP boiler by achieving a more uniform distribution of coal in the combustion air. It requires electric power; hence it is modelled to determine the power requirement. During this process, the coal temperature increases in the mill and thus has an effect on the combustion and should be taken into account for an accurate model. In the Aspen Plus® model (Figure 3.3) developed for this simulation; the power requirement for the pulverisers is 12.1 kWh/tonne of coal. For this Process, the material to be crushed was coal and feed flowrate for coal was 201,600 kg/h. The temperature was room temperature (i.e. 25$^{o}$C) and pressure was 1 bar for this process. The size of the particles to be crushed was up to 100 mm with different particle size distribution. The size of screen opening was 10 mm.

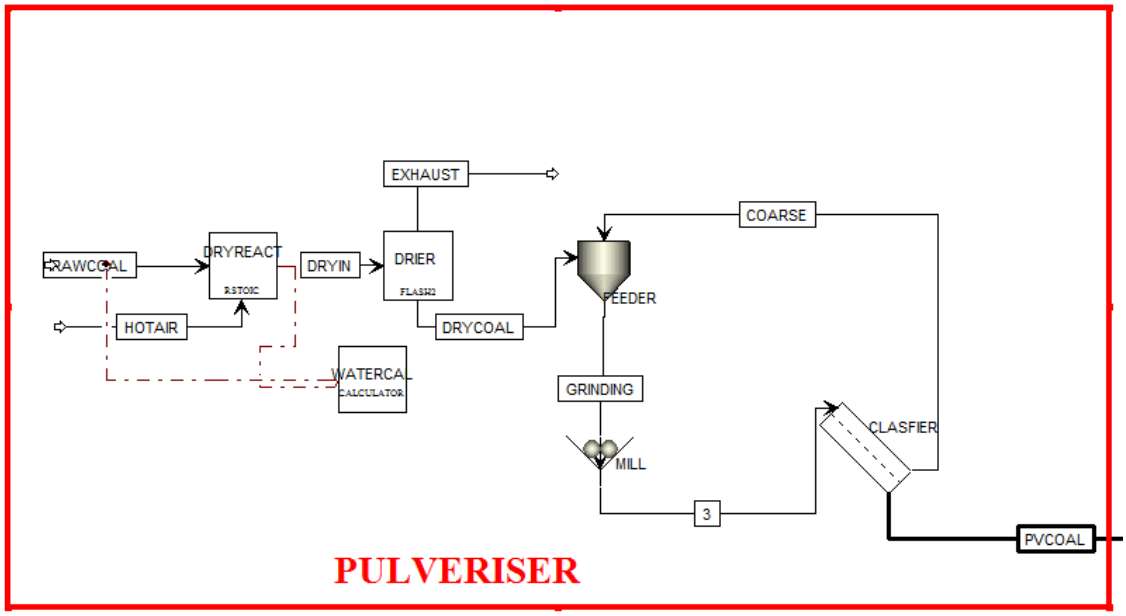


Figure 3.3: Aspen Plus ® Model of Coal Milling System

### 3.2.2 Air Preheating Subsystem

The air preheating subsystem consists of the FD-Fan, steam air heat exchanger (SAH), main preheater, and the primary and secondary air splitter. Steam extracted from the turbine is used to first pre-heat the air in the SAH before entering into the flue gas/air preheater to increase the temperature of the incoming combustion air and thereby improving the efficiency of the boiler. Figure 3.4 shows the aspen plus® simulation of the air preheating system.

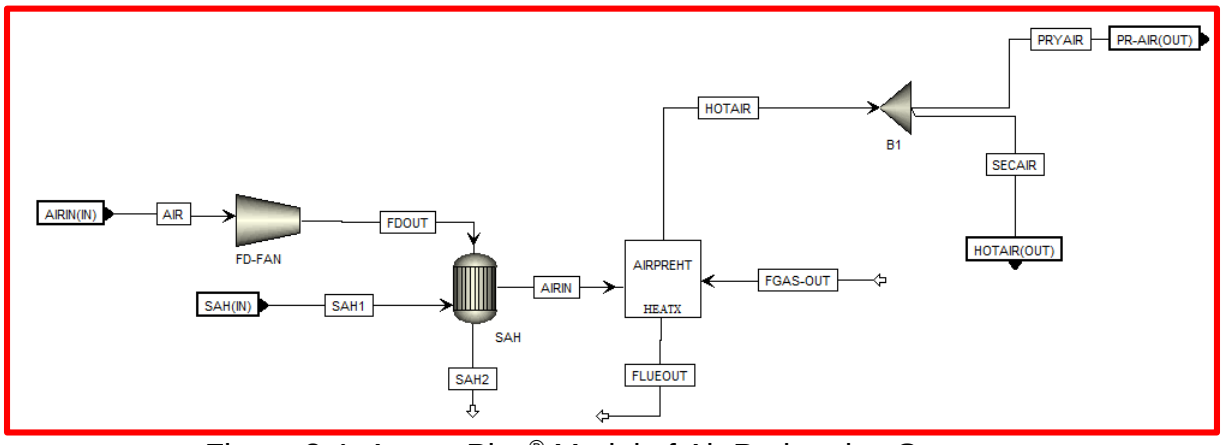


Figure 3.4: Aspen Plus® Model of Air Preheating System

### 3.2.3 Once-through Boiler Subsystem

*3.2.3.1 Air Composition Setup*

For this study, air is assumed to consist of just nitrogen (79 vol %) and oxygen (21% oxygen) at a temperature of 25$^{o}$C and 65% relative humidity (typical UK annual average). The air also contains water vapour which is also accounted for in this study. Detailed calculation of the air compositions used in the combustion process is provided in Appendix B1. From the steam table, the saturation pressure of water at 25$^{o}$C is 0.0316975 bar. Using the air at atmospheric pressure, 0.021 moles of water vapour was obtained in the air per mole of dry air (Appendix B1). The molar composition of the combustion air can then be written in the following form:

$$O_2 + 3.76(N_2) + 0.09996(H_2O) = 4.85996 \text{ mole of air} \qquad (3.1)$$

*3.2.3.2 Combustion Process model setup*

The type of coal used for this analysis is UKBC, and it is assumed that the coal is not pre-dried before combustion and therefore its properties are as-received as shown in Table 3.1 and Table 3.2. The values in the tables were used for specifying the coal properties in Aspen Plus®. The first step is to estimate the stoichiometric combustion of the UKBC, which will then allow the incorporation of the excess air to yield the composition of the flue gas exiting the boiler. Using the data for UKBC in Table 3.2 and Table 3.3, it is possible to determine the molar composition of the coal and to convert it to moles per mole carbon for each component. Based on the calculation (see Appendix B2), the composition of the UKBC on per mole of carbon is expressed as: $C_1\ H_{0.774}\ N_{0.019}\ S_{0.01}\ O_{0.075}\ Cl_{0.001129} + 0.0133(H_2O)$. The chlorine molecule is neglected in the Aspen Plus® simulation, thus the UKBC molecular formula is reduced to $C_1\ H_{0.774}\ N_{0.019}\ S_{0.01}\ O_{0.075} + 0.0133(H_2O)$.

Detailed calculation of the coal combustion process based on (23.1% excess air) is provided in Appendix B2. This gives the stoichiometric equation of the combustion of the UKBC as:

$$C_1\ H_{0.774}\ N_{0.019}\ S_{0.01}\ O_{0.075} + 0.0133H_2O + 1.435(O_2 + 3.76N_2 + 0.09996H_2O)$$
$$\rightarrow 1CO_2 + 0.663H_2O + 0.01SO_2 + 5.407N_2 + 0.1980O_2 \qquad (3.2)$$

*3.2.3.3 Once-through boiler components*

The once-through boiler consists of the pulverized coal conveyed from the pulveriser subsystems, the combustion process in the burners & furnace systems, and the heat exchanger units. The heat exchanger units include the primary superheaters (PSH-1 and PSH-2), the secondary superheaters (SSH-1 and SSH-2), the reheater (RHT), and the economisers (ECON). Figure 3.5 shows the Aspen Plus® model of the once-through boiler. The flue gas from the boiler goes into flue gas desulphurization unit which consists of a fabric filter and desulphurizer for removal of particulates and sulphur respectively.

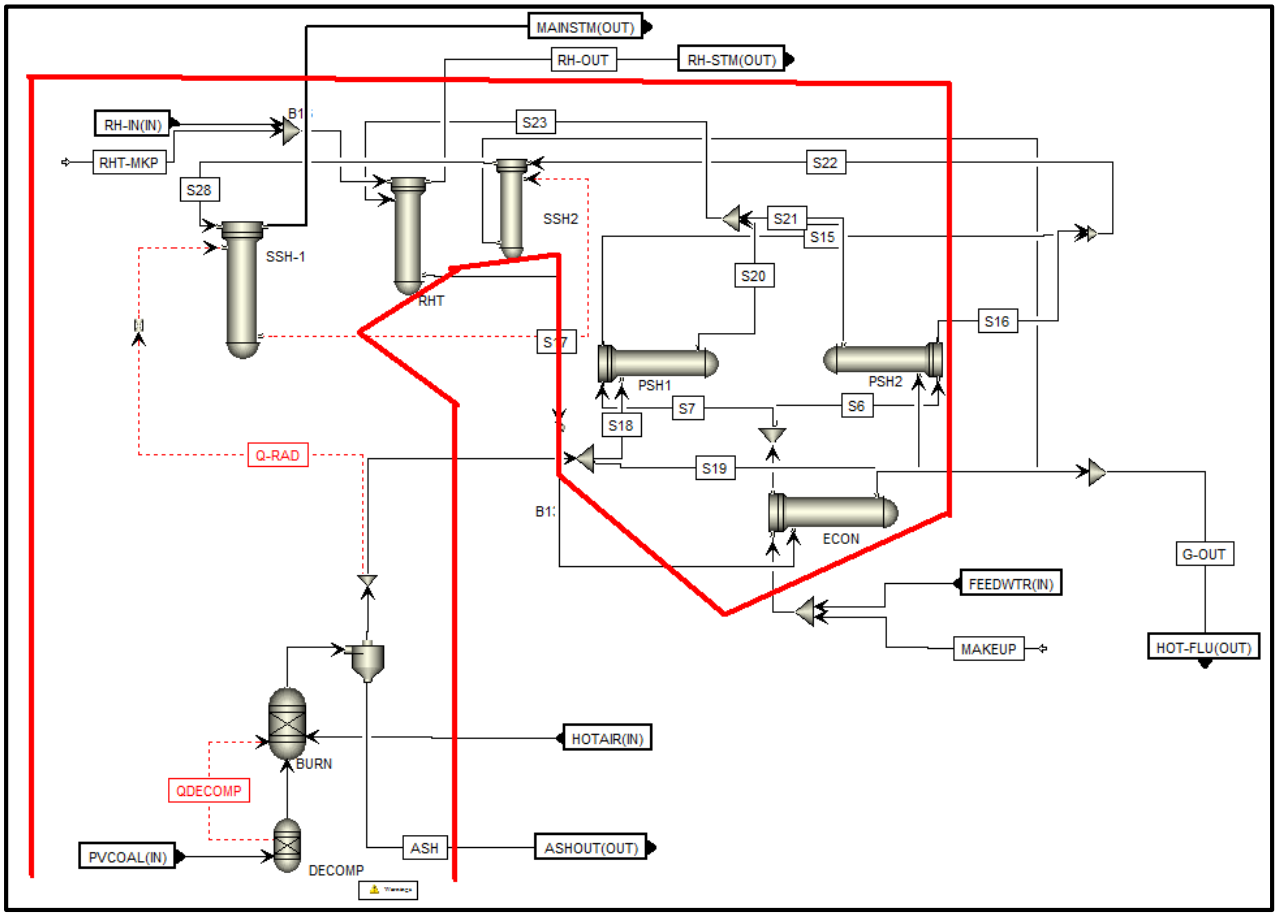


Figure 3.5: Aspen Plus® simulation of Once-through boiler of SCPP

### 3.2.4 Steam Turbine Subsystem

The turbine subsystem of the SCPP is made up of the low-pressure (LP), intermediate-pressure (IP), and the high-pressure (HP) sections. The main steam expands through

stages of the VHP-TURB, HP-TURBs, IP-TURBs, and the LP-TURBs (Figure 3.6) to generate shaft work for electric power. The final exhausted steam at the last stage of the turbine (LP-TURB4) is condensed in a condenser. The turbines also consist of stream extraction ports that connect the extracted steam from the turbines to the feedwater heating train (FWHTRAIN) hierarchy for regenerative feedwater heating; the main steam line from the once-through boiler hierarchy (MAINSTM), and the reheat steam lines (RH-STM and RH-IN).

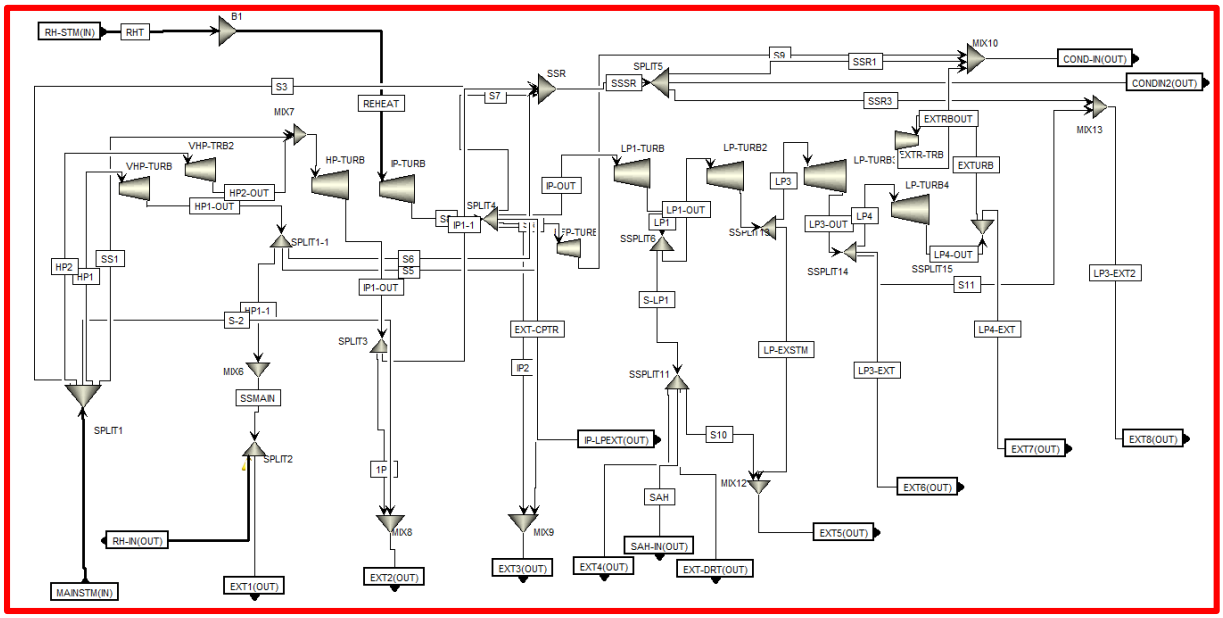


Figure 3.6: Model of the Turbines and Steam Extraction in Aspen Plus®

### 3.2.5 Condensate and Feedwater Heating Subsystem

As part of efficiency improvement in the SCPP, regenerative feedwater heating is done; using steam extracted from the different points on the turbines to heat the feedwater as shown in Figure 3.7. The train consists of four high pressure (FWH5 to FWH8) and four low pressure closed feedwater heat exchangers (FWH1 to FWH4); and one open feedwater heat exchanger (i.e. deaerator). The system also includes an extraction point from the boiler feed pump turbine to meet the power requirement of the feed pump.

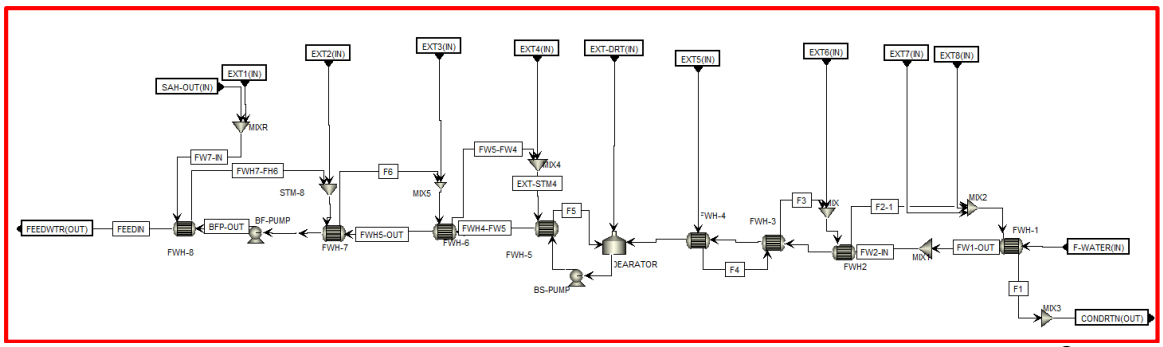


Figure 3.7: Model of the Feedwater Heating Trains in Aspen Plus®

### 3.2.6 Flue Gas Desulphurization System

The flue gas desulphurization (FGD) unit was modelled by a combination of unit operation blocks, which includes a reactor and a separator as shown in Figure 3.8. The overall reactions occurring in the FGD unit are given as follows:

$$CaCO_3\,(s) + SO_2\,(g) + 0.5H_2O \rightarrow 1CO_2 + CaSO_3 \bullet 0.5H_2O + CO_2\,(g) \qquad (3.3)$$

$$CaCO_3\,(s) + SO_2\,(g) + 0.5H_2O + 2H_2O \rightarrow 1CO_2 + CaSO_4 \bullet 2H_2O + CO_2\,(g) \qquad (3.4)$$

The model parameters assumptions for the FGD system can be found in the quality guidelines published by DOE/NETL (NETL, 2014).

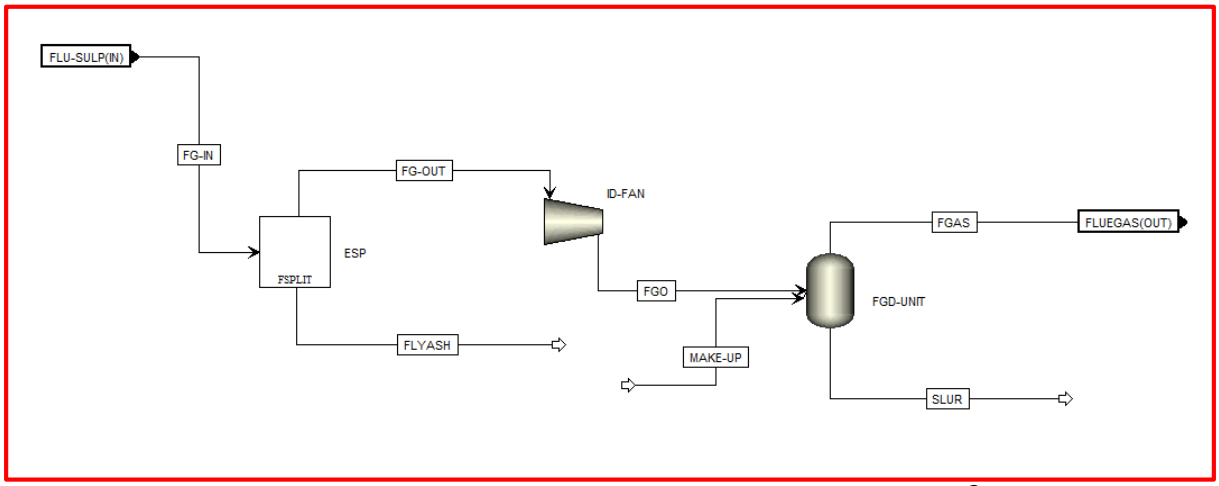


Figure 3.8: Model of the FGD System in Aspen Plus®

## 3.3 Post-Combustion $CO_2$ Capture (PCC) Subsystem

Post-combustion $CO_2$ capture (PCC) is one of the strategic technologies identified to reduce emission of greenhouse gases in existing power plant (Wang et al, 2011). PCC based on chemical absorption of monoethanolamine (MEA) is the most matured and preferred technology for $CO_2$ capture from the flue gases in existing power plant. In this study, data from a $CO_2$ capture pilot facility is used for validation of the model.

### 3.3.1 Chemistry of the MEA-$H_2O$-$CO_2$ System

The solution chemistry for $CO_2$ absorption with MEA includes water dissociation, $CO_2$ hydrolysis, bicarbonate dissociation, carbamate hydrolysis, and MEA protonation (Zhang and Chen, 2013) thus:

$$2H_2O \leftrightarrow H_3O^+ + OH^- \quad (3.5)$$

$$CO_2 + 2H_2O \leftrightarrow HCO_3^- + H_3O^+ \quad (3.6)$$

$$HCO_3^- + H_2O \leftrightarrow HCO_3^{2-} + H_3O^+ \quad (3.7)$$

$$MEACOO^- + H_2O \leftrightarrow MEA + HCO_3^- \quad (3.8)$$

$$MEAH^+ + H_2O \leftrightarrow MEA + H_3O^+ \quad (3.9)$$

In addition to the thermodynamic properties, the kinetics for carbamate formation (3.10 and 3.11) were obtained from Hikita et al (1977), while the reaction for bicarbonate formation (3.12 and 3.13) are obtained from Pinsent et al (1956). Reaction rates are solved by power law expressions in Aspen plus® using the rate expressions and constants obtained from Hikita et al (1977) and Pinsent et al (1956). The equilibrium reactions (3.5 – 3.9) are modelled using data available in Aspen Plus®.

$$MEA + CO_2 + H_2O \rightarrow MEACOO^- + H_3O^+ \quad (3.10)$$

$$MEACOO- + H_3O^+ \rightarrow MEA + CO_2 + H_2O \quad (3.11)$$

$$CO_2 + OH^- \rightarrow HCO_3^- \quad (3.12)$$

$$HCO_3^- \rightarrow CO_2 + OH^- \quad (3.13)$$

### 3.3.2 Modelling of Pilot-Scale PCC

The MEA-based $CO_2$ capture developed in this simulation is based on the pilot plant data from University of Kaiserslautern (Mangalapally and Hasse, 2011). Two series of

experiments were carried out; series A and series B. Series B was selected for this study because the partial pressure of $CO_2$ in the flue gas corresponds to a typical coal-fired power plant (Mangalapally and Hasse, 2011). Table 3.5 shows the main design specifications and geometry of the reference pilot plant.

Table 3.5: Main specifications of the pilot plant (Mangalapally and Hasse, 2011)

| Main Parameter | Data |
|---|---|
| Flue gas source | Natural gas burner |
| $CO_2$ content in the flue gas (vol %) (dry basis) | 3 to 14 |
| Flue gas flow rate (kg/h) | 30 to 100 |
| F-factor in absorber ($Pa^{0.5}$) | 0.6 to 2.1 |
| Solvent flow rate (kg/h) | 20 to 350 |
| Liquid load in absorber ($m^3/(m^2h)$) | 2 to 28.5 |
| Inner diameter absorber and desorber (m) | 0.125 |
| Type of packing in the absorber and desorber | BX 500 |
| Total height of packing in the absorber (m) | 4.25 |
| Total height of packing in the desorber (m) | 2.55 |

Model development of the closed-loop $CO_2$ capture plant based on rate-based modelling approach (Figure 3.9) is presented in this study and validated against the pilot plant data. In this model, the liquid phase non-ideality is accounted for with the electrolyte NRTL property method while the vapour phase uses the Redlich-Kwong equation of state. The transport property model parameters for density, viscosity, surface tension, thermal conductivity, and diffusivity presented in Aspen plus® were examined and updated with literature data. The built-in correlations in Aspen Plus® are used to calculate the performance of packing. For the structured packing of BX 500, the 1985 correlations of Bravo et al. (Fair and Bravo, 1992) are used to predict the mass transfer coefficients and the interfacial area. The 1992 correlation of Bravo et al. (1992) is used to calculate the liquid holdup and the Chilton and Colburn correlation (Taylor and Krishna, 1993) is used to calculate the heat transfer coefficients.

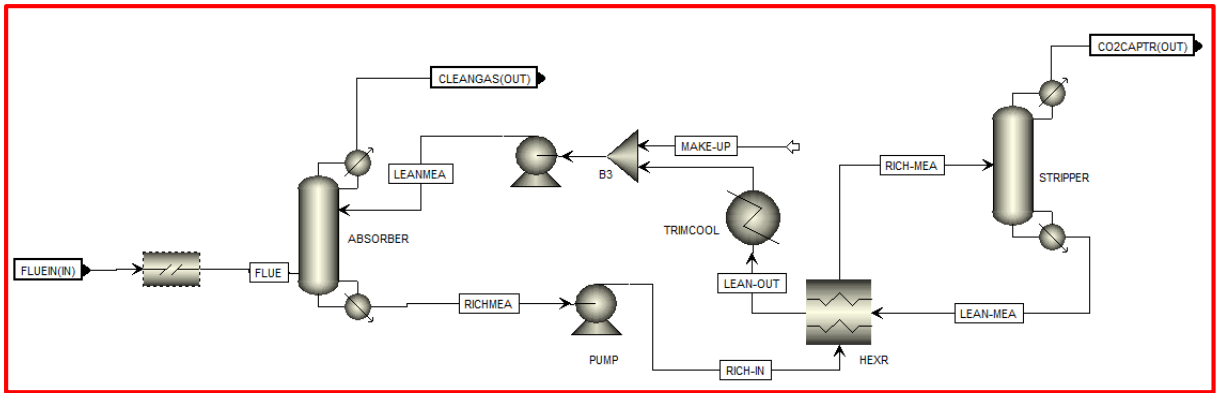


Figure 3.9: Pilot-Scale PCC with Chemical Absorption

### 3.3.3 Scale-Up of PCC Model

In the SCPP, the flue gas leaves the desulphurization unit at a temperature of 57$^{o}$C and is pre-cooled to about 40$^{o}$C in a direct contact cooler before it enters the absorber. The pilot-scale PCC simulation is scaled up to handle the flue gas stream from the 550MWe SCPP. The Aspen plus® model was validated with data from the pilot plant. The validated model was scaled-up using Chemical Engineering design principles as described in Sinnott and Towler (2013). The method employed in determining the column diameter and subsequently the column height for both the absorber and the desorber is the generalized pressure drop correlation (GPDC) principle (Sinnott and Towler, 2013; Lawal et al., 2012). The capture model originally based on pilot plant data was scaled up to process flue gas from a 550MWe SCPP unit. At full load, the flue gas flowrate of the plant is 603.4 kg/s with 21.35 wt. % of $CO_2$. Table 3.6 shows some of the process specifications and preliminary calculation results for the scale-up of the MEA-based PCC plant. The required solvent flow rates are evaluated using the initial estimates based on Table 3.5 to achieve a $CO_2$ capture level of 90 wt. % and purity of the $CO_2$ stream leaving the stripper of 95 wt. %.

Table 3.6 Design Parameters for the Scale-up of the MEA-based PCC unit

| Description | Value |
|---|---|
| Flue gas mass flow rate (kg/s) | 603.4 |
| Flue gas composition ($CO_2$) | 0.2135 |
| Flue gas composition ($N_2$) | 0.7352 |
| Flue gas composition ($H_2O$) | 0.0513 |
| $CO_2$ Capture level (%) | 90.0 |
| Estimated flowrate of $CO_2$ Capture (kg/s) | 128.83 |
| Required MEA flowrate (kg/s) | 828.193 |
| Estimated Lean solvent flow rate (kg/s) | 2717.168 |
| Estimated Rich solvent flow rate (kg/s) | 3040.2 |
| Lean MEA mass fraction (wt. %) | 30.48 |
| Lean MEA $CO_2$ loading (mol $CO_2$/mol MEA) | 0.29 |

Operation of packed columns are limited by (i) flooding, which occurs when a gas flow pressure drop is so high that the liquid is unable to flow downward and it sets the upper capacity limit of the packed column; and (ii) the minimum liquid load, which is the lowest liquid flowrate that gives sufficient mass transfer rate (Lawal et al., 2012). An efficient packed column design is characterised by a good liquid and gas distribution that is achieved by operating at the highest economical pressure drop. The pressure drop per metre packing for absorbers and strippers of 1 to 12 mbar/m of packing height is recommended for the Sulzer BX 500 structured packing; typically away from the flooding line (Sulzer, 2012). 10.5 mbar/m of packing height was used for the design of both the absorber and stripper (Sulzer, 2012).

In this study, the Sulzer BX 500 structured packing is selected because of its higher surface area and low regeneration energy at higher $CO_2$ removal rates when compared with Mellapak 250.Y (Mangalapally and Hasse, 2011). Due to structural limitations, column diameters for the structural packing; Sulzer BX 500 should not exceed 6 m (the largest diameter of the packing supplied to date) (Sulzer, 2012). Hence, to capture the large volumes of flue gases from the SCPP will require more than one absorber, which could in turn improve the turn down ratio of the process (Lawal et al., 2012). Therefore, from the cross-sectional areas determined for both the

absorber and regenerator, a number of parallel units may be needed to meet the capacity requirements. The minimum number of the absorbers and the strippers are determined based on the required column capacities (Lawal et al., 2012). Using one column would result in a diameter of 16.32 m and 13.06 m for the absorber and the stripper respectively, which would be difficult to manage due to structural limitations. Therefore, to process the large volume of flue gas from the SCPP unit, four absorption columns with a diameter of 5.74m and three desorber column of 5.33m diameter are designed for the integrated SCPP process. Table 3.7 shows a summary of the key variables of the scaled-up MEA-based PCC unit integrated with the SCPP process. Detailed calculation steps of the scale-up process is presented in Appendix B3.

Table 3.7: Key Process parameters of the PCC model

| Parameter | Absorber | Desorber |
|---|---|---|
| Calculation type | Rate-based | Rate-based |
| Type of packing | Sulzer BX 500 | Sulzer BX 500 |
| Total Height of Packing (m) | 35.0 | 30.0 |
| Diameter of column (m) | 5.74 | 5.33 |
| Column Number | 4 | 3 |
| No. of Equilibrium stages | 30 | 30 |
| Operating Pressure (bar) | 1.013 | 1.62 |

## 3.4 Model Validation and Analysis

Validating a model developed is necessary in order to verify the accuracy and usability of the model. The model should be able to realistically predict steady state operation of the physical system. In this section, the steady state validation of the Aspen Plus ® SCPP and pilot-scale PCC model is performed.

### 3.4.1 Steady state Validation of SCPP

The SCPP model in Aspen Plus® is validated on a steady state basis. The steady state simulation results were compared with the reference SCPP design data in Wood et al.

(2007) and satisfactory agreement was observed as shown in Table 3.8 and Table 3.9. The thermal efficiency is lower than the design value, in view of the age of the plant.

Table 3.8: Validation of SCPP Simulation based on the Main stream Parameters

| Main Streams | Reference | Aspen plus® | Rel. error (%) | Reference Plant | Aspen Plus® | Rel. error (%) | Reference Plant | Aspen Plus® | Rel. error (%) |
|---|---|---|---|---|---|---|---|---|---|
| *Coal/air/flue gas* | Temperature (°C) | | | Pressure (bar) | | | Mass Flow (kg/s) | | |
| WET COAL | 15.0 | 15.0 | 0.0 | 1.014 | 1.014 | 0.0 | 56.0 | 56.0 | 0.0 |
| 1 | 15.4 | 15.4 | 0.0 | 1.014 | 1.014 | 0.0 | 390.0 | 390.0 | 0.0 |
| 2 | 235.1 | 229.7 | 2.4 | 1.110 | 1.130 | 1.8 | 390.0 | 390.0 | 0.0 |
| 3 | 15.4 | 15.4 | 0.0 | 1.014 | 1.014 | 0.0 | 120.0 | 120.0 | 0.0 |
| 4 | 20.0 | 22.1 | 0.6 | 1.110 | 1.110 | 0.0 | 52.0 | 51.6 | 0.8 |
| 5 | 368.0 | 365.2 | 0.76 | 0.993 | 1.005 | 1.2 | 570.0 | 569.5 | 1.5 |
| 6 | 368.0 | 365.2 | 0.83 | 0.993 | 1.005 | 1.2 | 1.01 | 1.01 | 0.0 |
| 7 | 116.0 | 115.4 | 0.36 | 0.979 | 0.985 | 0.6 | 566.0 | 565.8 | 1.25 |
| 8 | 57.0 | 56.8 | 0.7 | 1.014 | 1.013 | 0.1 | 605.0 | 603.4 | 0.71 |
| *Steam/water* | | | | | | | | | |
| FEEDWTR | 313.0 | 310.8 | 0.7 | 290.0 | 290.0 | 0.0 | 465.0 | 464.2 | 0.2 |
| MAINSTM | 593.0 | 591.5 | 0.3 | 243.0 | 242.6 | 0.2 | 465.0 | 464.2 | 0.2 |
| HOT-RHT | 593.0 | 591.5 | 0.3 | 45.0 | 45.2 | 0.4 | 385.0 | 384.6 | 0.1 |
| COLD-RHT | 352.0 | 356.0 | 1.1 | 49.01 | 51.0 | 4.1 | 385.0 | 384.6 | 0.1 |
| CONDRTN | 44.8 | 45.2 | 0.9 | 0.3 | 0.29 | 1.0 | 60.0 | 60.4 | 0.7 |
| F-WATER | 39.2 | 40.1 | 2.3 | 17.0 | 16.8 | 1.2 | 350.0 | 350.0 | 0.0 |

Table 3.9: SCPP Performance Indicator

| Performance Parameters | Reference Plant | Aspen Plus® | Rel. error (%) |
|---|---|---|---|
| Total power output (MWe) | 580.26 | 585.39 | 0.9 |
| Auxiliary Load (MWe) | 28.28 | 28.42 | 0.5 |
| Gross plant power(MWe) | 551.98 | 556.97 | 0.9 |
| Generator Loss (MW) | 1.83 | 1.83 | - |
| Net Power output (MWe) | 550.15 | 555.14 | 0.9 |
| Unit efficiency, LHV (%) | 39.1 | 39.4 | 0.78 |

### 3.4.2 Steady state Validation of Pilot-Scale PCC

The pilot-scale PCC model was validated with the pilot plant experiment from the University of Kaiserslautern (Mangalapally and Hasse, 2011). The main process parameters of the steady state simulation results were compared with the experimental performance data, and the model shows a reasonable prediction within less than 5% average absolute relative error (Table 3.10). The values of the lean loading, the L/G ratio, and the flue gas flow are values from pilot plant experimental data and are used directly in the simulation.

Table 3.10: Validation of the Pilot-Scale PCC with Chemical Absorption

| Parameter | Experiment | Aspen ® | Rel. error (%) |
|---|---|---|---|
| L/G Ratio | 2.5 | 2.5 | - |
| $CO_2$ Partial pressure in flue gas (mbar) | 102 | 102.0 | - |
| Flue gas flow (kg/hr) | 80.0 | 80.0 | - |
| Lean loading (mol $CO_2$/mol MEA) | 0.205 | 0.205 | - |
| Rich loading (mol $CO_2$/mol MEA) | 0.464 | 0.467 | 0.65 |
| CO2 removal (%) | 90 | 92.17 | 2.41 |
| Rich solvent temperature from absorber ($^oC$) | 48.0 | 50.1 | 4.2 |
| Lean solvent temperature from desorber ($^oC$) | 120.0 | 117.9 | -1.78 |
| Reboiler Duty (MJ/kg $CO_2$) | 4.07 | 4.035 | 0.86 |

## 3.5 Process simulation and Integration of SCPP with PCC

The subsystems (i.e. pulveriser, boiler, turbine, feedwater heaters etc.) are coupled together to fully model the SCPP and integrated with PCC as shown in Figure 3.10. The process of linking the subsystems is done partly. The pulveriser is linked to the boiler, the boiler to the turbine and the feedwater heaters etc. Linking the boiler-turbine models together is the most challenging part, and it's accomplished by using multiple heat exchangers to model the heat transfer that occurs between the flue gas and the main steam and reheat steam in Aspen Plus®. The scaled-up PCC model was also coupled with the whole SCPP system via three ports: steam extraction from HP/IP crossover for solvent regeneration, the flue gas from the FGD to the absorber unit in the PCC simulation, and the condensate return back to the SCPP LP feedwater heater. Figure 3.10 also shows the connection point of the two models.

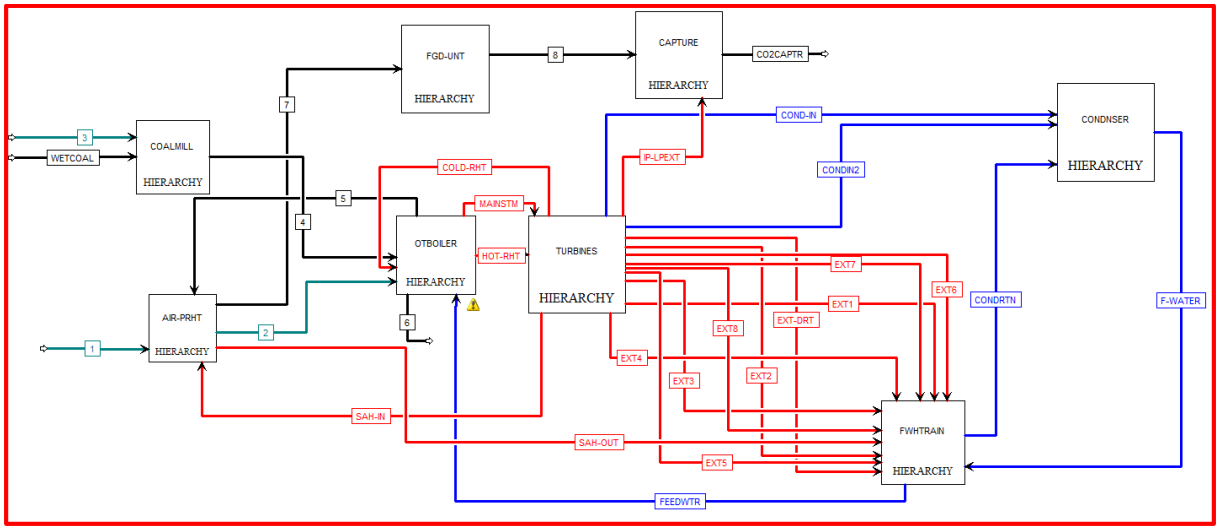


Figure 3.10: Aspen Plus® Model of SCPP Integrated with PCC

### 3.5.1 Performance Analysis of the Integrated Plant

The integrated SCPP-PCC model is used to determine the performance of the entire power plant. The net power produced by the system is calculated from the net power produced by the turbine cycle less the PCC power consumption and the station service power (obtained by summing up the power required for the pulveriser, ID Fan, FD Fan, and other auxiliary equipment in the power plant). Table 3.11 shows a summary of the

key process performance indicators of the integrated SCPP-PCC system with respect to the standalone system.

Table 3.11: Key System Performance Indicators of the Integrated SCPP-PCC Model

| Description | Data | |
|---|---|---|
| *SCPP Performance Summary* | SCPP Standalone | SCPP Integrated with PCC |
| Total (steam turbine) power (MWe) | 580.26 | 482.28 |
| Auxiliary load (MW) | 28.28 | 52.04 |
| Gross plant power (MW) | 551.98 | 430.24 |
| Generator loss (MW) | 1.83 | 1.83 |
| Net power output (MWe) | 550.15 | 428.41 |
| Unit efficiency, HHV (%) | 39.10 | 30.45 |
| *MEA-based PCC Performance Summary* | | |
| Steam extraction (% of IP steam flow) | - | 46.13 |
| Reboiler Duty (MJ/kg $CO_2$) | - | 4.13 |
| Energy penalty (%) | - | 22.13 |
| Efficiency penalty (%) | - | 8.65 |

## 3.6 Summary

This chapter presents steady state simulation of SCPP integrated with PCC in Aspen Plus®. The SCPP model was validated against design data from a Greenfield reference plant. The PCC model was validated at pilot-scale with experimental data. The model was scaled-up and integrated with the SCPP model. The model is made up of subsystems. Each subsystem bases its calculations on inputs from other subsystems, and constants set during the model. There were several stages in the development of the model, and validation checks were performed to ensure realistic results were achieved.

Aspen Plus® was able to match the steady state operating conditions of the reference plant with a relative error of 1.65% in gross power output. It is concluded that the steady state model is fairly accurate when comparing the solutions from the model

with design data from the reference SCPP. The model is verified by comparing the solutions from the model with design data at full load. There is consistency between the model output and the data from the reference plant at full load and that gives confidence on the future use of the model. The importance of this model is to familiarise with the steady state working condition of the SCPP system integrated with PCC, to carry out further analyses and case studies on strategies for minimising energy penalties in the system (i.e. exergy analysis, efficiency etc.), and as a prerequisite to the dynamic model development process.

# Chapter 4 Conventional and advanced exergy analysis of SCPP integrated with $CO_2$ capture

## 4.1 Introduction

In this chapter, the steady state simulation of the SCPP integrated with PCC developed in Chapter 3 will be used for detailed conventional and advanced exergy analyses to evaluate the exergy destructions (i.e. energy consumption) and potential for improvement of the integrated system.

Integrating SCPP with PCC incurs a great deal of energy penalty. Improving the rational efficiency, reducing energy penalty, and the cost of capturing $CO_2$ can be achieved by reducing the irreversibilities in the system. The different types of irreversibilities in the system can be investigated by performing exergy analysis.

The conventional exergy analysis will identify the losses associated with this integrated system; investigate strategies for reducing the penalties due to the capture process. The advanced exergy analyses on the other hand allows for a qualitative understanding of the exergy destruction due to a component's own inefficiency (i.e. endogenous) and/or due to the remaining components' inefficiencies (exogenous) within an integrated system.

## 4.2 Conventional Exergy Analysis of SCPP Integrated with PCC

Exergy defines the maximum possible work potential of a system, a stream of matter and/or heat interaction using the state of the environment as the datum (Kaushik et al, 2011). Conventional exergy analysis identifies the location, magnitude, and sources of thermodynamic inefficiencies in a thermal system.

### 4.2.1 Exergy Analysis of SCPP

#### *4.2.1.1 SCPP System*

The Thermodynamic analysis of any SCPP includes the balance of mass, energy, entropy and exergy. It is important to determine the amount of work potential (or exergy) that can be attained from the SCPP system. Exergy analysis of the SCPP

system is performed using the steady state simulation developed in Chapter 3. Aspen Plus® Version 8.0 and above contains three new property sets; EXERGYMS, EXERGYML (calculated on mass and molar basis respectively), and EXERGYFL (calculated on flow basis) for estimating exergy of material/energy streams, unit operation and utilities. These properties are estimated at a reference temperature and pressure (Kaushik et al, 2011). Detailed calculation methods for physical and chemical exergies of the material flows, work, and heat flows for each SCPP components are estimated using the individual stream flow based on the Aspen Plus® EXERGYFL stream calculations.

The following equations are generally used for evaluation of an individual component and the overall system exergy destruction rate within a component. The exergy balance for the overall SCPP system can be written as (Yang et al, 2013):

$$\dot{E}_{F,total} = \dot{E}_{P,total} + \dot{E}_{D,total} + \dot{E}_{L,total} = \dot{E}_{P,total} + \sum \dot{E}_{D,n} + \dot{E}_{L,total} \qquad (4.1)$$

For a given system (i.e. SCPP), the variables $\dot{E}_{F,total}$, $\dot{E}_{D,total}$, $\dot{E}_{L,total}$, and $\dot{E}_{P,total}$ represent the total exergy of the fuel, the total of exergy destroyed, the total exergy loss, and total exergy of the products respectively.

Whereas for the nth component,

$$\dot{E}_{F,n} = \dot{E}_{P,n} + \dot{E}_{D,n} + \dot{E}_{L,n} \qquad (4.2)$$

The exergy efficiency of the nth component ($\dot{\varepsilon}_n$)

$$\dot{\varepsilon}_n = \dot{E}_{P,n}/\dot{E}_{F,n} = 1 - \dot{E}_{D,n}/\dot{E}_{F,n} \qquad (4.3)$$

and the exergy destruction ratio of the n$^{th}$ component ($y_{D,n}$) is given thus:

$$y_{D,n} = \dot{E}_{D,n}/\dot{E}_{F,total} \qquad (4.4)$$

for the overall SCPP system, the exergy loss ratio ($y_L$) is,

$$y_L = \dot{E}_{L,total}/\dot{E}_{F,total} \qquad (4.5)$$

The chemical exergy of coal is calculated by multiplying its HHV with a constant factor, normally 1.02 (Tsatsaroni and Winhold, 1984). The Aspen Plus® default value for reference environmental temperature and pressure (298.15 K and 1.013 bar respectively) was used throughout the simulation for the base case study. Table 6 shows the computation of the exergy destructions and efficiency for the process equipment in the SCPP subsystems.

### 4.2.2 Exergy Analysis of PCC

Thermodynamic reversibility demands that all process driving forces i.e. temperature, pressure and chemical potential differences be zero at all points and times (Leites et al, 2003). Such a theoretical process results in the production of the maximal amount of useful work (exergy), or in the consumption of the minimal amount of work. Unfortunately, a reversible chemical process operates at an infinitesimal rate, and requires an infinitely large plant (Leites et al., 2003). It has been generally believed that thermodynamic irreversibility in chemical processes/reactions is almost inevitable and leads to large energy consumption and losses (Haywood, 1981). However, some thermodynamic principles based on the second law of thermodynamics such as the so called “counteraction principle”, “driving force method”, “quasi-static method” etc. have been investigated and proven effective for lowering energy consumption more than often predicted (Leites et al., 2003).

In MEA-Based PCC, the greater part of the irreversibility in the absorber (excessive driving force) is in the middle and bottom parts of the column (Leites et al., 2003). Also, analysis of the equilibrium and operating lines of a stripper unit shows that equilibrium can be reached at only one point of a stripper of conventional design (with a single feed of spent absorbent entering the top), even if it were of infinite height (Leites et al., 2003). Thus, the driving force at other points in the desorber can never approach zero, resulting in excessive expenditure of exergy. These led to series of modifications to the conventional flowsheet for MEA-based PCC which has been studied widely in recent years.

This study uses the driving force method to reduce exergy destruction and hence reduce energy consumption in MEA-based PCC process without changing the absorbent. The absorbers and strippers contribute the largest share of total exergy destruction in PCC system. The main sources of exergy destruction in the absorber and stripper include: (i) mass transfer between phases (ii) heat transfer in reboiler and condenser for stripper (iii) heat transfer inside the columns (iv) heat losses through the surfaces (vi) heat of the reaction etc. (Ashrafizadeh et al., 2013).

Several strategies/configurations for reducing exergy destructions from the absorbers and strippers in MEA-based PCC were simulated and analysed. This includes (i) absorber intercooling (AIC), (ii) split flow approach (SF), (iii) absorber inter-cooling with

split flow (AIC+SF), (iv) lean vapour recompression (LVR), (v) absorber intercooling with lean vapour recompression (AIC + LVR) (vi) stripper inter-heating (SIH), and (vii) absorber intercooling with stripper inter-heating (AIC + SIH).

#### *4.2.2.1 Aspen Plus® Setup for Exergy Analysis of PCC*

Aspen plus® exergy estimation property set is used in estimating the exergy of the $CO_2$ capture unit. However, to determine the exergy of reaction systems involving electrolytes (i.e. reaction of MEA and $CO_2$), certain adjustment had to be made to the thermodynamic properties of the ionic species of MEA (i.e. $MEAH^+$ and $MEACOO^-$) supplied by the Aspen Plus property databank. Estimation of the mixing exergy is important to accurately estimate the overall exergy destruction in the $CO_2$ capture system. The Gibbs free energy of formation (DGAQFM) of the ionic species $MEAH^+$ and $MEACOO^-$ which is unavailable in the MEA system databank in Aspen Plus® will have to be estimated. The DGAQFM values used in this study is based on the estimate by Guezebebroek et al. (2004). Guezebebroek et al. (2004) used data generated by Aspen Plus® for a mixture of MEA and $H_2O$ to calculate the DGAQFM. The DGAQFM values of -500.504 kJ/mol and -196.524kJ/mol were obtained for $MEAH^+$ and $MEACOO^-$ respectively.

#### *4.2.2.2 Absorber Inter-cooling (AIC) configuration*

The idea of the AIC modification to the conventional system was to counteract the temperature increase in the solvent stream due to the release of the exothermic heat of reaction generated during the absorption reaction; and thereby reducing the solvent temperature at the absorber bottom. Inter-cooling lowers the absorber temperature which in turn increases the absorption capacity of the solvent (i.e. the rich loading), lowers recirculation and regeneration energy requirement (Amrollahi et al., 2011). The AIC configuration is achieved by extracting a semi-rich solvent from the lower part of the absorber, cool it to 25◦C and recycle back to the absorber column (Figure 4.1). All other components in the PCC system are identical to the base case. Sensitivity analysis was performed on a standalone configuration of AIC to efficiently estimate the flow rate and the location of the side-stream which was withdrawn for intercooling to achieve lower reboiler duty compared to the Base case.

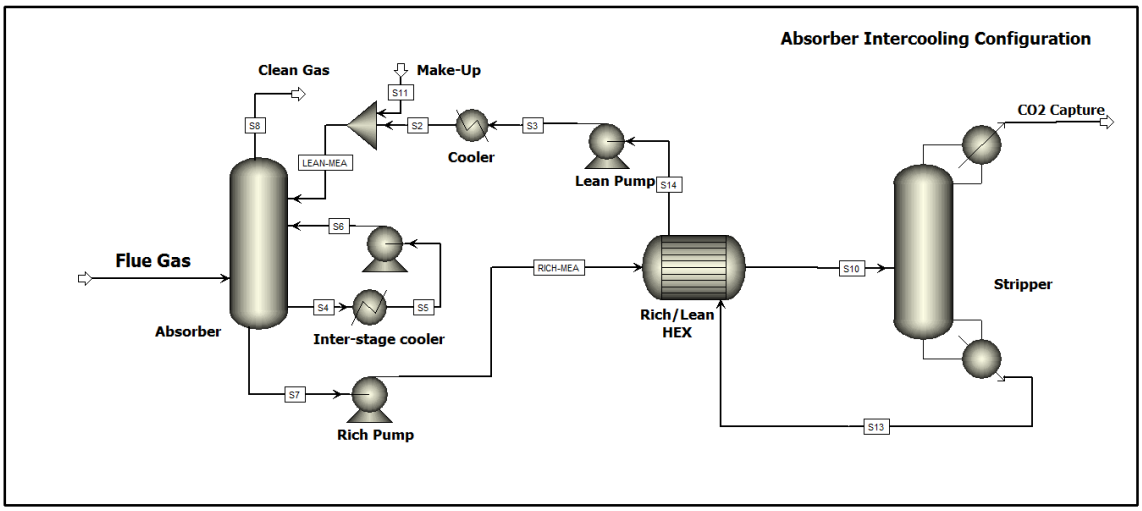


Figure 4.1: Absorber Inter-cooling Configuration (AIC)

*4.2.2.3 Split-flow (SF) configuration*

The split-flow configuration was first suggested by Thompson and King (1987) and later developed by Kohl and Nielsen (1997) as a strategy to reduce steam consumption for solvent regeneration in the stripper. In the SF configuration (Figure 4.2), the rich amine solvent stream to the stripper column is spitted into two, a part is fed to the stripper top without passing through the lean/rich heat exchanger, thereby directly cooling off the stripper top. This results in a reduction in the heat exchanger duty as a result of decrease in the cold-side flow rate. The idea is to approach the theoretical level of adding and removing all flow streams which causes more evenly distribution of driving forces (mass transfer core) through the vapour and liquid phase (Amrollahi et al, 2011). The sensitivity analysis tool in Aspen Plus® was used in standalone SF configuration to determine the split flow fraction that ensures optimal design of the process.

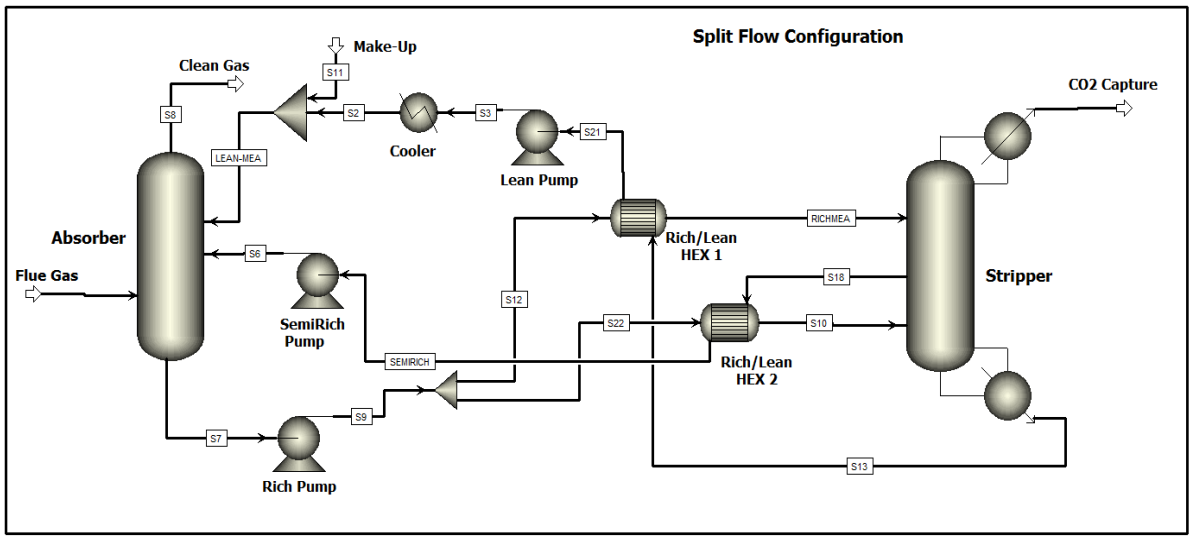


Figure 4.2: Split-flow Configuration (SF)

*4.2.2.4 Absorber Inter-cooling with Split-flow (AIC+SF) configuration*

The (*AIC+SF)* configuration illustrated in Figure 4.3 combines the effect of the AIC and the SF configuration. The sensitivity analysis tool in Aspen Plus® was used in standalone SF and AIC configurations to determine the effective flow-rate of inter-cooled stream, the split flow fraction and the flow rate of semi-rich amine from the stripper that provided the most efficient parameter estimate for the (AIC+SF) configuration.

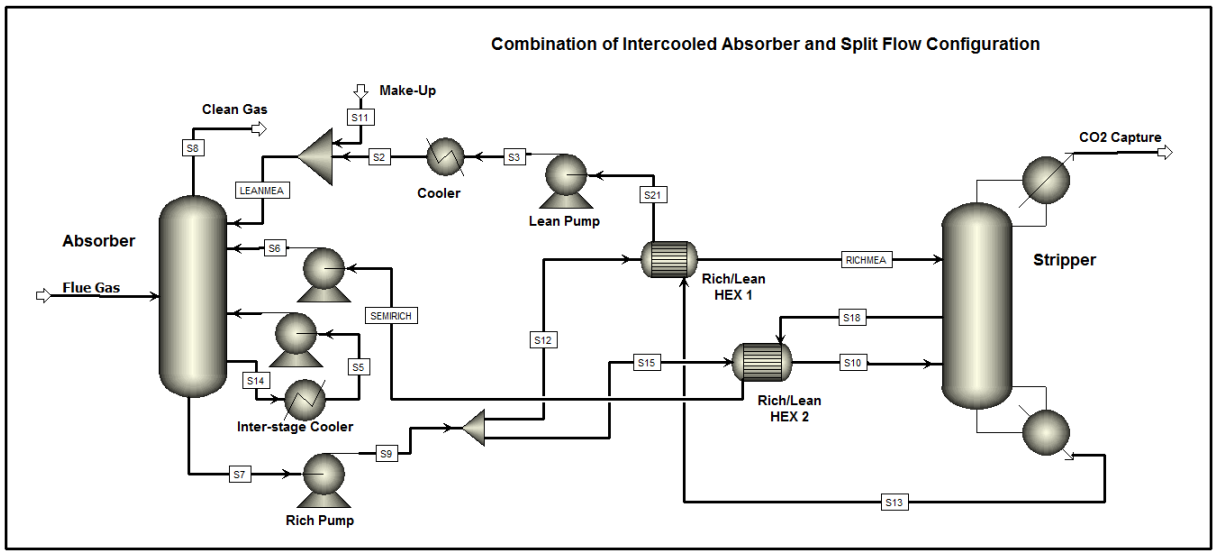


Figure 4.3: Absorber Inter-cooling with Split-flow Configuration (AIC+SF)

*4.2.2.5 Stripper inter-heating (SIH) configuration*

The stripper inter-heating (SIH) configuration shown in Figure 4.4, has the analogous effect of the absorber inter-cooling described in Section 4.2.2.1 on the regeneration process. Stripping $CO_2$ from the aqueous MEA solution is an endothermic process and the inter-heated stripper is a simpler approximation to the more theoretical internal exchange stripper described by Oyenekan and Rochelle (2007), and Van Wagener and Rochelle (2011). In the SIH configuration, a column side stream of semi-lean solvent is heated by heat exchange with the hot lean MEA solution from the bottom of the stripper (Montenegro, 2011). The side stream is then returned to the stripper below its point of withdrawal while the hot lean MEA solvent maintains its conventional path to the rich-lean MEA heat exchanger. Van Wagener and Rochelle (2011) studied the energy performance of conventional and SIH configurations on standalone stripper simulations using MEA and PZ. Their study reveals improvement of up to 7.8% and 4.6% at 0.48 and 0.52 rich loading respectively when compared to a conventional stripper. 10% of improvement was also observed when comparing the SIH configurations between the two solvents.

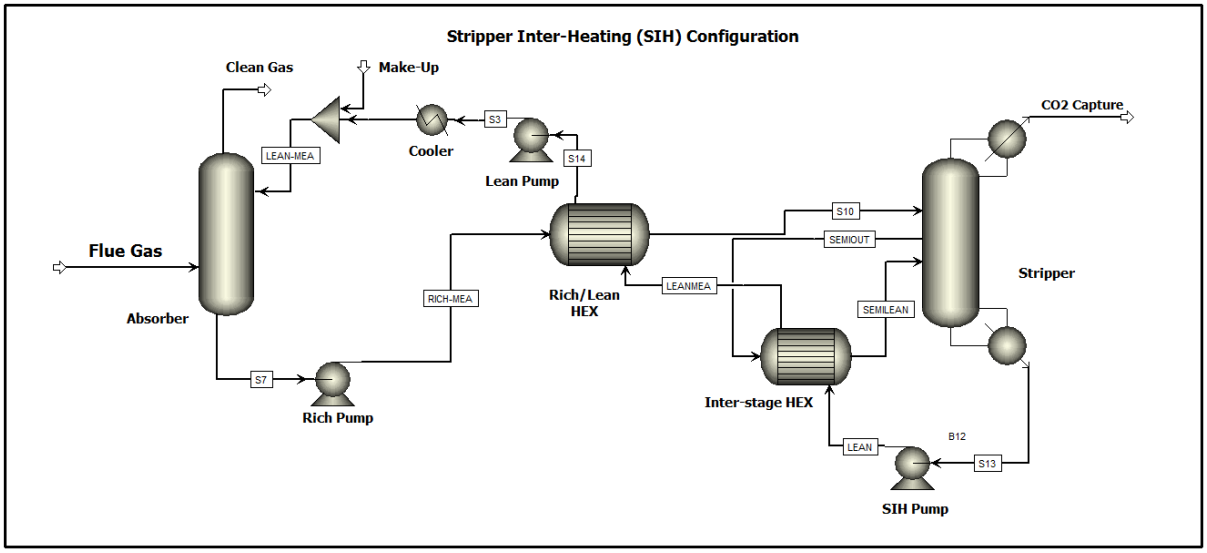


Figure 4.4: Stripper Inter-heating Configuration (SIH)

*4.2.2.6 Stripper inter-heating with absorber inter-cooling (SIH+AIC) configuration*

The (*SIH+AIC)* configuration illustrated in Figure 4.5 combines the effect of the AIC and the SIH configuration. The sensitivity analysis tool in Aspen Plus® was used in standalone SIH configuration to determine the effective flow-rate of the semi-lean MEA from the stripper that provided the most efficient parameter estimate for the (SIH+AIC) configuration.

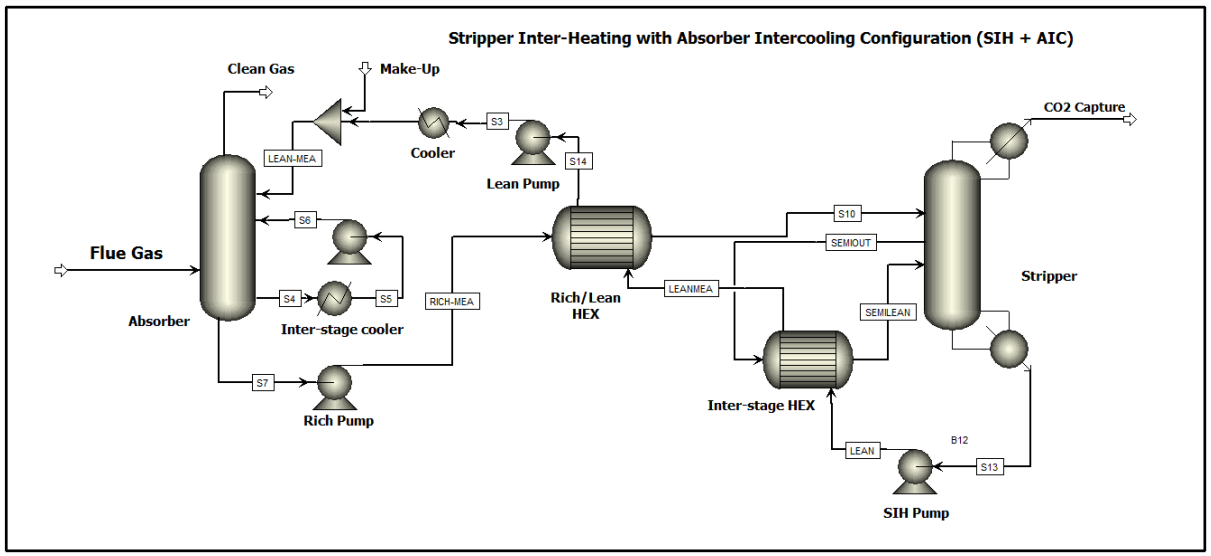


Figure 4.5: Stripper Inter-heating with Absorber Inter-cooling Configuration (SIH+AIC)

*4.2.2.7 Lean vapour recompression (LVR) configuration*

The concept of vapour recompression configuration (Figure 4.6) is to provide steam that is recovered from the stripping process as the heat source to the reboiler (Amrollahi et al, 2013). Jassim and Rochelle (2005) presented the vapour recompression design in which the stripper bottom is used to inter-cool the gaseous stream in a multistage compressor. The idea of the design is to recover the heat of condensation of the overhead water vapour and the heat of compression to re-boil the stripper. The vapour recovered in the flash separator is majorly 90 wt. % water and 10 wt. % $CO_2$. The vapour is compressed and recycled to the stripper where it acts as auxiliary stripping steam and thus leading to lower reboiler duty. Some make-up water is added to the vapour stream to de-superheat it, so as to avoid the vapour temperature exceeding the recommended temperature of 120°C in the column.

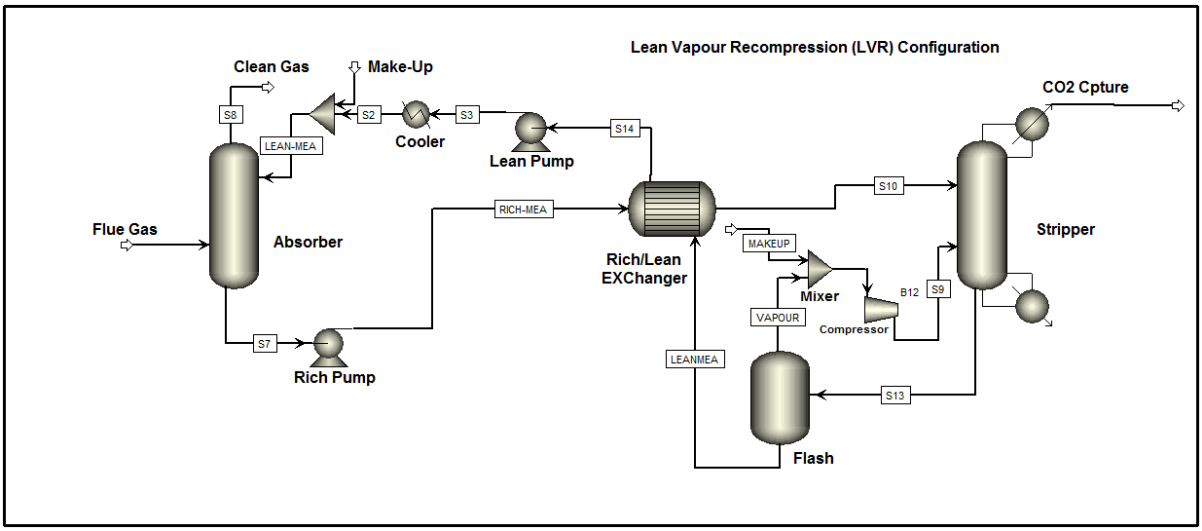


Figure 4.6: Lean vapour recompression Configuration (LVR)

*4.2.2.8 Lean vapour recompression with absorber inter-cooling (LVR+AIC)*

This LVR+AIC configuration combines the effect of AIC and the LVR. The sensitivity analysis tool in Aspen Plus® was used to determine the optimal flow-rate of inter-cooled stream, the lean loading and solvent circulation rate at 90% $CO_2$ capture level. (Figure 4.7) shows the flowsheet of the LVR + AIC simulation in Aspen Plus®.

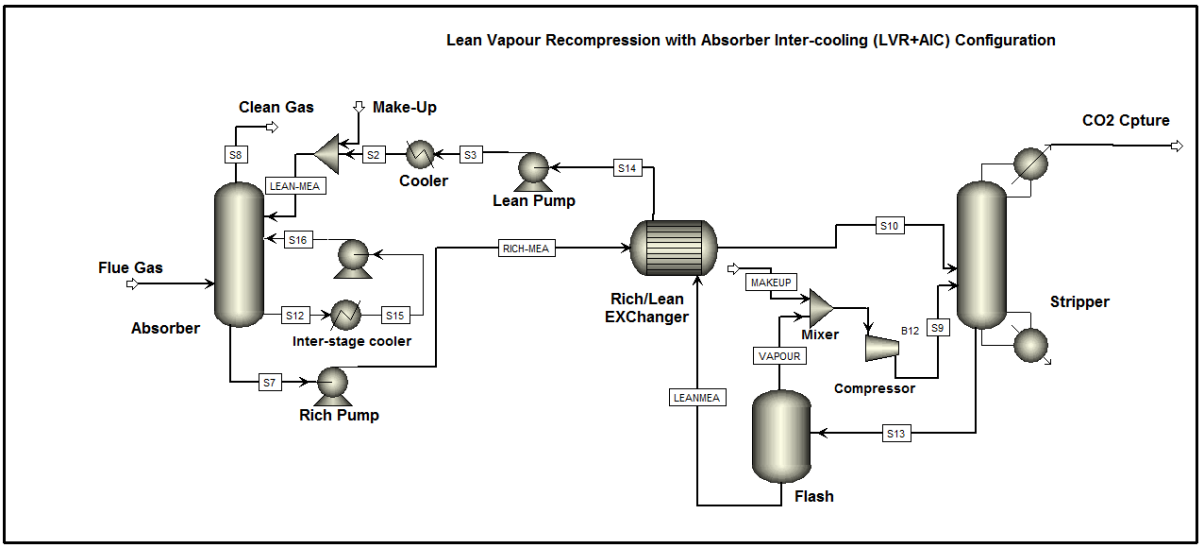


Figure 4.7: Lean vapour recompression with absorber Inter-cooling Configuration (LVR+AIC)

### 4.2.3 Exergy Analysis of SCPP Integrated with PCC

The integrated SCPP-PCC model described in Chapter 3 is used to estimate the exergetic performance of the entire system. The overall exergy destruction, the exergetic efficiency, and the energy penalties in the integrated system are calculated from the exergy properties set described in Section 4.2.1. The exergy flows into and out of each streams in the SCPP-PCC system is first obtained from the Aspen Plus® simulation. The exergy destruction and the exergetic efficiency for each components/subsystems is then computed in Microsoft Excel®. Table 4.1 shows the general equations used for computing the exergy destructions and efficiency for each process equipment in the SCPP and the MEA-based PCC systems. The summary of the results for the exergy destruction, the exergetic efficiency of each components in the SCPP-PCC subsystems, and the exergy destruction ratio for each component as a percentage of the overall system is presented in Table 4.2 . Discussions of the results presented in Table 4.2 are provided in Section 4.4.

Table 4.1: Exergy destruction and efficiency equations for the SCPP-PCC system

| Equipment | Exergy Destruction and Efficiency |
|---|---|
| Mixers | $\dot{E}_D = -\dot{E}_{out} + \sum \dot{E}_{in}$ |
| Splitters | $\dot{E}_D = -\sum \dot{E}_{out} + \dot{E}_{in}$ |
| Pumps, Blowers and Fans (BFP, CFP, ID/FD Fans) | $\dot{W}_{min} = \dot{E}_{out} - \dot{E}_{in} > 0$<br>$\dot{E}_D = \dot{E}_{in} - \dot{E}_{out} + \dot{W}_{real}$<br>$\varepsilon_p = \frac{\dot{E}_{out} - \dot{E}_{in}}{(\dot{E}_{out} - \dot{E}_{in}) + \dot{E}_D} = \frac{-(\dot{E}_{out} - \dot{E}_{in})}{-(\dot{E}_{out} - \dot{E}_{in}) - \dot{E}_D}$ |
| Expanders (HP/IP/LP/BFP Turbines) | $\dot{W}_{max} = -(\dot{E}_{out} - \dot{E}_{in}) > 0$<br>$\dot{E}_D = -(\dot{E}_{out} - \dot{E}_{in}) - \dot{W}_{real}$<br>$\varepsilon_{turb} = \frac{-(\dot{E}_{out} - \dot{E}_{in}) - \dot{E}_D}{-(\dot{E}_{out} - \dot{E}_{in})} = \frac{-(\dot{E}_{out} - \dot{E}_{in}) - \dot{E}_D}{-(\dot{E}_{out} - \dot{E}_{in})}$ |
| Burners, Furnace | $\dot{Q}_{furn} = \dot{h}_{out} - \dot{h}_{in} < 0$<br>$\dot{E}_D = -\dot{E}_{out} + \sum \dot{E}_{in} - (1 - \frac{T_{ref}}{T_{furn}})\lvert\dot{Q}_{furn}\rvert$ |
| Heat exchangers (Superheaters, Economiser, Condenser, Pre-heater) | $\dot{E}_D = -\sum(\dot{E}_{out} - \dot{E}_{in})_{hot} - \sum(\dot{E}_{out} - \dot{E}_{in})_{cold}$<br>$= -\sum \dot{E}_{in} - \sum \dot{E}_{out}$<br>$\varepsilon_{hex} = \frac{-\sum(\dot{E}_{out} - \dot{E}_{in})_{hot} - \dot{E}_D}{-\sum(\dot{E}_{out} - \dot{E}_{in})_{hot}} = \frac{\sum(\dot{E}_{out} - \dot{E}_{in})_{cold}}{-\sum(\dot{E}_{out} - \dot{E}_{in})_{hot}}$ |
| Absorber, Desorber | $\dot{E}_D = -\dot{E}_{out} + \sum \dot{E}_{in}\,;\ \dot{Q}_{react} \geq 0$ |

Table 4.2: Conventional Exergy Analysis of SCPP Integrated with PCC

| Components | $E_{F,n}$(MW) | $E_{P,n}$(MW) | $E_{D,n}$(MW) | $y_{D,n}$(%) | $\varepsilon_n$(%) | Components | $E_{F,n}$(MW) | $E_{P,n}$(MW) | $E_{D,n}$ (MW) | $y_{D,n}$(%) | $\varepsilon_n$(%) |
|---|---|---|---|---|---|---|---|---|---|---|---|
| *Boiler Subsystem* | | | | | | *Feedwater Heating Subsystem* | | | | | |
| COALMILL | 1430.61 | 1425.00 | 5.61 | 0.39 | 99.61 | FWH-1 | 9.96 | 8.04 | 1.92 | 0.13 | 80.72 |
| AIR-PRHT | 81.11 | 61.67 | 19.44 | 1.36 | 76.03 | FWH-2 | 9.92 | 6.57 | 3.35 | 0.23 | 66.23 |
| DECOMP | 1427.01 | 1426.85 | 0.16 | 0.01 | 99.99 | FWH-3 | 4.36 | 3.47 | 0.89 | 0.06 | 79.59 |
| BURN | 1487.97 | 1005.98 | 481.99 | 33.69 | 67.61 | FWH-4 | 16.87 | 12.85 | 4.02 | 0.28 | 76.17 |
| SSH-1 | 109.51 | 83.26 | 26.25 | 1.83 | 76.03 | DEAERATOR | 22.76 | 19.31 | 3.45 | 0.24 | 84.84 |
| RHT | 41.60 | 30.10 | 11.50 | 0.80 | 72.36 | BS-PUMP | 3.50 | 3.12 | 0.38 | 0.03 | 89.14 |
| SSH2 | 93.70 | 72.38 | 21.32 | 1.49 | 77.25 | FWH-5 | 23.18 | 19.83 | 3.35 | 0.23 | 85.55 |
| PSH1 | 54.37 | 45.67 | 8.70 | 0.60 | 84.00 | FWH-6 | 41.69 | 38.27 | 3.42 | 0.24 | 91.80 |
| PSH2 | 64.99 | 52.93 | 12.06 | 0.85 | 81.44 | FWH-7 | 28.79 | 27.08 | 1.71 | 0.12 | 94.06 |
| ECON | 46.58 | 33.90 | 12.68 | 0.89 | 72.78 | FWH-8 | 20.73 | 16.81 | 3.92 | 0.27 | 81.09 |
| *Turbine Subsystem* | | | | | | *FGD Subsystem* | | | | | |
| VHP-TURB | 171.57 | 164.66 | 6.91 | 0.48 | 95.97 | BGS Filter | 41.39 | 40.83 | 0.56 | 0.04 | 98.65 |
| VHP-TRB2 | 40.30 | 38.09 | 2.21 | 0.15 | 94.52 | ID-FAN | 37.91 | 34.43 | 3.48 | 0.24 | 90.82 |
| HP-TURB | 29.91 | 28.53 | 1.38 | 0.10 | 95.39 | Desulphurizer | 42.62 | 36.95 | 5.67 | 0.40 | 86.70 |
| IP-TURB | 76.97 | 72.11 | 4.86 | 0.34 | 93.69 | *MEA-Based PCC Subsystem* | | | | | |
| LP1-TURB | 82.34 | 81.30 | 1.04 | 0.07 | 98.74 | FG-Cooler | 70.19 | 36.82 | 33.37 | 2.33 | 52.46 |
| LP-TURB2 | 56.66 | 55.95 | 0.71 | 0.05 | 98.75 | BLOWER | 50.08 | 20.06 | 30.02 | 2.10 | 40.06 |
| LP-TURB3 | 35.63 | 35.22 | 0.41 | 0.03 | 98.85 | ABSRBR | 96.2 | 41.52 | 54.68 | 3.82 | 44.55 |
| LP-TURB4 | 23.77 | 20.74 | 3.03 | 0.21 | 87.25 | DESRBR | 235.64 | 153.57 | 82.07 | 5.74 | 65.17 |
| BFP-TRB | 20.03 | 15.76 | 4.27 | 0.30 | 78.68 | PUMP | 11.89 | 11.63 | 0.26 | 0.02 | 97.81 |
| COND | 26.99 | 0.35 | 26.64 | 1.86 | 1.30 | T-COOLER | 36.82 | 30.89 | 5.93 | 0.41 | 83.89 |
| BF-PUMP | 17.84 | 15.79 | 2.05 | 0.14 | 88.51 | MHEX | 48.81 | 36.83 | 11.98 | 0.84 | 75.46 |
| | | | | | | Loss (MEA) | | | 5.15 | 0.36 | |

## 4.3 Advanced Exergy Analysis of SCPP Integrated with PCC

Conventional exergy analysis cannot determine the interaction among components or the true potential for the improvement of each component (Wang et al, 2012). However, an advanced exergy analysis evaluates the interaction among components, and the real potential for improving a system component/the overall system (Morosuk et al, 2013). It involves splitting the exergy destruction in system components into endogenous/exogenous and avoidable/unavoidable parts (Wang et al, 2012). It is capable of providing extra information to the conventional analysis for design improvement and operation of the SCPP with $CO_2$ capture systems. Therefore, advanced exergy analysis was applied to reveal the sources (endogenous/exogenous) and the potential for reduction (avoidable/unavoidable) of exergy destruction (Wang et al, 2012).

### 4.3.1 Exogenous and Endogenous Destruction

*Endogenous* exergy destruction ($\dot{E}_{D,n}^{en}$) is the part of exergy destruction within a component obtained when all other components operate in ideal/reversible condition and the component being considered operates with the same efficiency as in the real system (Tsatsaronis and Winhold, 1984; Tsatsaronis and Morosuk, 2008). The *Exogenous* part of the variable ($\dot{E}_{D,n}^{ex}$) is the difference between the value of the variable within the component in the real system and the endogenous part.

Thus;

$$\dot{E}_{D,n} = \dot{E}_{D,n}^{en} + \dot{E}_{D,n}^{ex} \quad (4.6)$$

### 4.3.2 Avoidable and Unavoidable Exergy Destruction

Unavoidable conditions refer to the best unapproachable working conditions associated with the technical and economic limits related to the integrated SCPP-PCC components (Wang et al, 2012). The unavoidable exergy destruction ($\dot{E}_{D,n}^{un}$) (Tsatsaronis et al, 2008) cannot be further reduced or eliminated due to technological limitations such as availability and cost of materials and manufacturing methods. The avoidable part ($\dot{E}_{D,n}^{av}$) is the difference between the total and the unavoidable exergy

destruction. For a component, the avoidable exergy destruction is the part that should be considered during the improvement procedure:

$$\dot{E}_{D,n} = \dot{E}_{D,n}^{un} + \dot{E}_{D,n}^{av} \quad (4.7)$$

### 4.3.3 Avoidable/Unavoidable Endogenous Exergy Destruction

Combining the two splitting options for exergy destruction provides the opportunity to estimate: (i) the avoidable endogenous exergy destruction ($\dot{E}_{D,n}^{av,en}$) which can be reduced by improving the design of the *n*$^{th}$ component of the SCPP system from exergetic view point; (ii) the avoidable exogenous exergy destruction ($\dot{E}_{D,n}^{av,ex}$) that can be reduced by structural improvement of the overall SCPP system; (iii) unavoidable endogenous ($\dot{E}_{D,n}^{un,en}$) part; and (iv) the unavoidable exogenous part ($\dot{E}_{D,n}^{un,ex}$). Figure 4.8 shows the options available for splitting the exergy destruction in the *n*$^{th}$ component of a system.

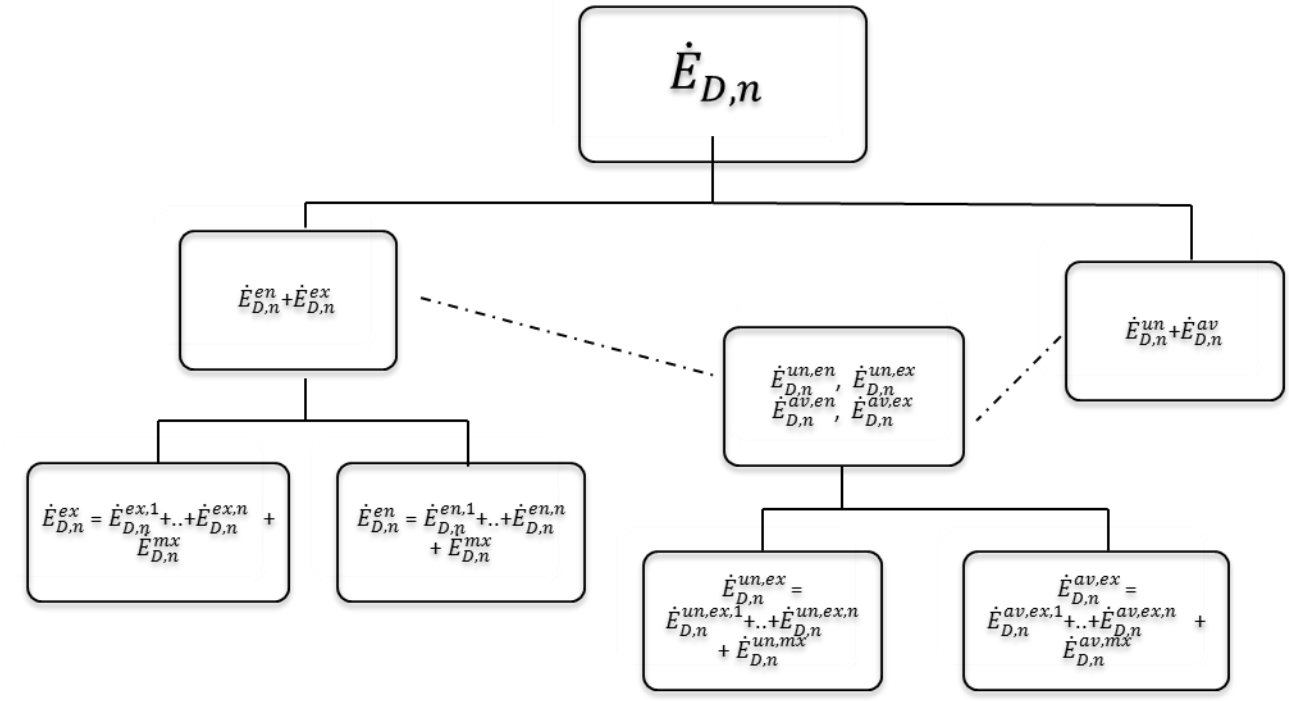


Figure 4.8: Splitting the exergy destruction for advanced exergy analysis. (*Adapted from* Morosuk *et al, 2013)*

These four splitting combinations can be estimated thus (Yang et al, 2013):

$$\dot{E}_{P,n}^{un} = \dot{E}_{P,total}^{R}(\dot{E}_{D,n}/\dot{E}_{P,n})^{un} \quad (4.8)$$

$$\dot{E}_{D,n}^{un,en} = \dot{E}_{P,n}^{en}(\dot{E}_{D,n}/\dot{E}_{P,n})^{un} \quad (4.9)$$

$$\dot{E}_{D,n}^{un,ex} = \dot{E}_{D,n}^{un} - \dot{E}_{D,n}^{un,en} \quad (4.10)$$

$$\dot{E}_{D,n}^{av,en} = \dot{E}_{D,n}^{en} - \dot{E}_{D,n}^{un,en} \quad (4.11)$$

$$\dot{E}_{D,n}^{av,ex} = \dot{E}_{D,n}^{ex} - \dot{E}_{D,n}^{un,ex} \quad (4.12)$$

The ratio $(\dot{E}_{D,n}/\dot{E}_{P,n})^{un}$,$\dot{E}_{P,n}^{en}$, and $\dot{E}_{P,n}^{en}$ are first determined from the unavoidable and theoretical processes.

### 4.3.4 Avoidable/Unavoidable Exogenous Exergy Destruction

Splitting the exogenous exergy destruction within the *n*th component into influences coming from the other components i.e. *m*th components ($\dot{E}_{D,n}^{ex,m}$) shows the effect that the irreversibility within the *m*th component has on the exergy destruction within the *n*th component (Morosuk et al, 2013). The variable, total avoidable exergy destruction ($\dot{E}_{D,n}^{av,total}$) is used to summarise the data obtained from the splitting of the exergy destruction (Morosuk and Tsatsaronis, 2009a). This variable represents the sum of the avoidable endogenous exergy destruction within the *n*th component and the avoidable exogenous exergy destructions within the remaining components (*m*th components) due to the *n*th component (Morosuk et al, 2013). It is used to determine the importance of the *n*th component of any energy system from the perspective of thermodynamics.

$$\dot{E}_{D,n}^{av,total} = \dot{E}_{D,n}^{av,en} - \sum_{\substack{m=1 \\ m\neq n}}^{i} \dot{E}_{D,n}^{av,\ ex,n} \quad (4.13)$$

### 4.3.5 Conditions/Assumptions for splitting Exergy Destruction

#### *4.3.5.1 SCPP Subsystems*

The assumption for theoretical (TH) conditions for different components is: $\dot{E}_D = 0$ or $\dot{E}_D = min$. For turbines, fan and pump, the isentropic efficiency ($\eta_{isent}$) and mechanical efficiency ($\eta_{mech}$) should be 100%. As for single heat exchanger, both pressure drops ($\Delta P$) and minimum temperature difference at the pinch point ($\Delta T_{min}$) should equal zero. The heat exchangers in the boiler subsystem are rather complicated. The theoretical operation of a concurrent heat exchanger may affect its succeeding heat exchangers since the temperature of the steam out of a theoretical

heat exchanger may exceed the allowable temperature of its following component or the temperature of the flue gas entering its successive heat exchanger (Yang et al, 2013). This problem is solved with the use of one reversible adiabatic heater (RAH) added before each heat exchanger (Figure 4.9) and the target of each heater is set to heat the working fluid to a specified temperature (Yang et al, 2013; Morosuk and Tsatsaronis, 2009b). The RAHs are taken offline under real process condition. In this way, the calculation of one heat exchanger starts from computing the heat absorbed by the steam and then the temperature of the flue gas entering the heater can be obtained with the pre-calculated mass flow rate of the flue gas from the heat balance.

For the unavoidable conditions (UN), the best performance characteristics can be derived with investment-efficiency considerations or based on the understanding and practical experience of the designer (Yang et al, 2013). In this study, the unavoidable conditions are selected arbitrarily based on limitations of technology such as the isentropic efficiency ($\eta_{isent}$) of between 96-98%, and mechanical efficiency ($\eta_{mech}$) of 100% for the turbines, fan and pump. For the heat exchanger, the minimum approach temperature difference ($\Delta T_{min}$) was not equated to zero but based on the limitations of technology (Yang et al, 2013; Wang et al, 2012).

For simplification purposes, the combustion process (i.e. DECOMP and BURN units in Figure 3.5 in Chapter 3) is considered as one separate component (FURNACE), SSH-1 & SSH-2, PSH-1 & PSH-2 are also regarded as a single component each (SSH and PSH respectively) because these two concurrent heat exchangers are arranged sequentially along the flue gas as shown in Figure 4.9. The simulations for fuel-savings potentials and advanced exergy analysis are conducted with the help of Aspen Plus® for individual stream exergies and MS-Excel worksheet is used for the computations.

*4.3.5.2 PCC Subsystems*

For splitting the exergy destruction in the PCC system into exogenous and endogenous parts, the assumption for theoretical (TH) conditions for different components is: $\dot{E}_D = 0$ or $\dot{E}_D = min$. For the rich and lean MEA pumps and the flue gas blower, the isentropic efficiency ($\eta_{isent}$) and mechanical efficiency ($\eta_{mech}$) should be 100%. As for the heat exchanger, both pressure drops ($\Delta P$) and minimum temperature difference at the pinch point ($\Delta T_{min}$) should equal zero. For the absorber

and stripper, the calculation of endogenous exergy destruction represents a problem because no ideal condition or theoretical conditions can be defined for the reaction process. In this case, the entire exergy destruction in the absorber and the stripper will be assumed endogenous, with the change in exergy destruction in the other components (their preceding and succeeding components) accounted for in the exergy loss in the entire PCC system.

For the unavoidable conditions (UN), the best performance characteristics is derived based on the understanding and practical experience of the designer. In this study, the unavoidable conditions are selected arbitrarily based on limitations of technology such as the isentropic efficiency ($\eta_{isent}$) of between 96-98%, and mechanical efficiency ($\eta_{mech}$) of 100% for the blower and pumps. For the lean/rich MEA heat exchanger and the Trim-Cooler, the minimum approach temperature difference ($\Delta T_{min}$) should not be equal to zero but based on the limitations of technology. For the absorbers and strippers, since the exergy destruction is due to irreversible processes of heat & mass transfer with the chemical reaction and the mixing, which is directly related to entropy generation, the (UN) is selected based on the lowest technically meaningful value of temperature and concentration that provide the minimal irreversibility (i.e. $\dot{E}_D = min$).

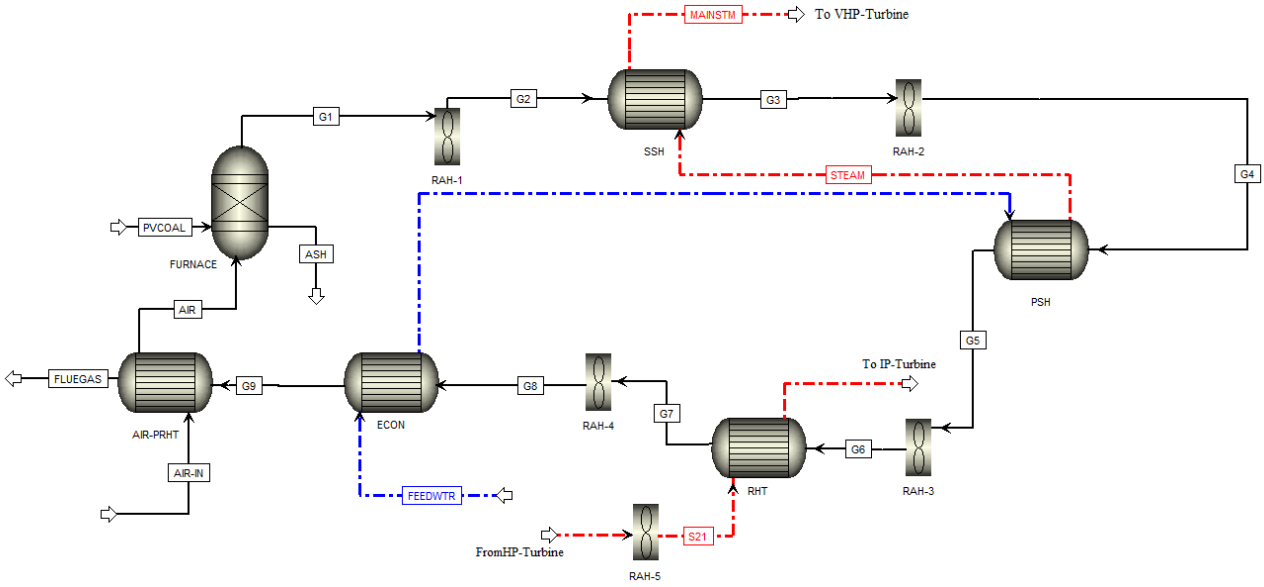


Figure 4.9: Once-through boiler subsystem for advanced exergy analysis

### 4.3.6 Fuel saving potential through individual component improvement

The contribution of irreversibilities in different SCPP components to the fuel consumptions varies significantly due to the relative position of each component to the final product (Yang et al, 2013). The best possible condition of a component can be regarded as the so-called “theoretical” condition within the limits of thermodynamic principles. Hence, the energy-savings potential due to an individual component ($\Delta E^{*,n}_{F,total}$) can be estimated thus (Yang et al, 2013):

$$\Delta E^{*,n}_{F,total} = E^{R,n}_{F,total} - E^{T,n}_{F,total} \qquad (4.14)$$

where $E^{R,n}_{F,total}$ represents the fuel exergy consumption of the overall system when all components are under their “real” process condition, while $E^{T,n}_{F,total}$ represents an hybrid process of the *nth* component, in which only the component of interest operates theoretically while all the other components operates at their real process conditions.

## 4.4 Results and Discussion

### 4.4.1 Conventional Exergy Analysis of SCPP Subsystems

#### *4.4.1.1 Boiler subsystems*

Table 4.2 contains the results obtained from the conventional exergy analysis of the whole SCPP system with $CO_2$ capture. It can be seen from Table 4.2 that the boiler section has the highest exergy destruction with the BURN and DECOMP units where the combustion of fuel take places accounts for the highest irreversibility in the boiler and hence a low exergy efficiency (68%). It accounts for about a third of the total fuel exergy destroyed. Table 4.2 also shows that the thermodynamic inefficiencies of heat exchangers especially the radiant superheaters (SSHs) are generally higher than those of convective heat exchangers in the flue gas duct. While in the convective heat exchangers, the heat release from hot side to cold side is lower than the in the radiation, and the temperature difference for heat transfer is lower. Hence, the exergy efficiencies of the radiant heat exchangers (SSH-1 and SSH-2) are usually lower than 80%. Because the flue gas temperature decreases rapidly in radiation sections, the convection sections always have relatively high efficiency.

*4.4.1.2 Turbine subsystem*

Unlike the once-through boiler, the turbines performed better with exergy efficiency in the range of 95%-99% for HP and IP turbines, while the LP turbines show a decrease in efficiency from the 98% to about 79% from the first stage to the last due to the state of the working fluid being a wet steam (Table 4.2). The low efficiency is mainly due to the losses associated with the wet steam and speed loss of the last stage of the turbine.

*4.4.1.3 Feedwater heating subsystem*

Table 4.2 also shows the exergetic performances of regenerative feedwater heaters improve steadily along the direction of flow of water. Two main factors that determine the exergy performance of feedwater heaters are (i) the increase in temperature of the cold fluid, and (ii) the temperature difference for heat transfer. This is mainly because the higher the cold fluid temperature, the lower the exergy destroyed (i.e. higher exergy efficiency). However, deviations from the main trend are sometimes encountered due to large temperature difference of the condensate section or the high temperature steam extraction after the reheating process.

*4.4.1.4 Location of Exergy Destruction and Losses in SCPP*

Figure 4.10 shows the location and the distribution of exergy destruction and losses (%) associated with the SCPP system without $CO_2$ capture. It is evident from Figure 4.10(a) that the exergy destruction within the once-through boiler subsystem (79%) dominates the overall exergy dissipation, followed by the total exergy losses in the SCPP process (about 9%), and the turbine subsystem (over 7%). Hence, largest energy-savings potential may be present in the boiler subsystem. Figure 4.10(b) shows the spatial distribution of exergy destruction in the boiler subsystem. The boiler combustion zone “BURN” and “DECOMP” units (about 76% and 5% respectively) and the radiant superheaters (about 6%) contributes the largest proportion of exergy destruction, the convective superheaters (0.03% and 4% respectively) and the economiser (2%) have much lower contributions.

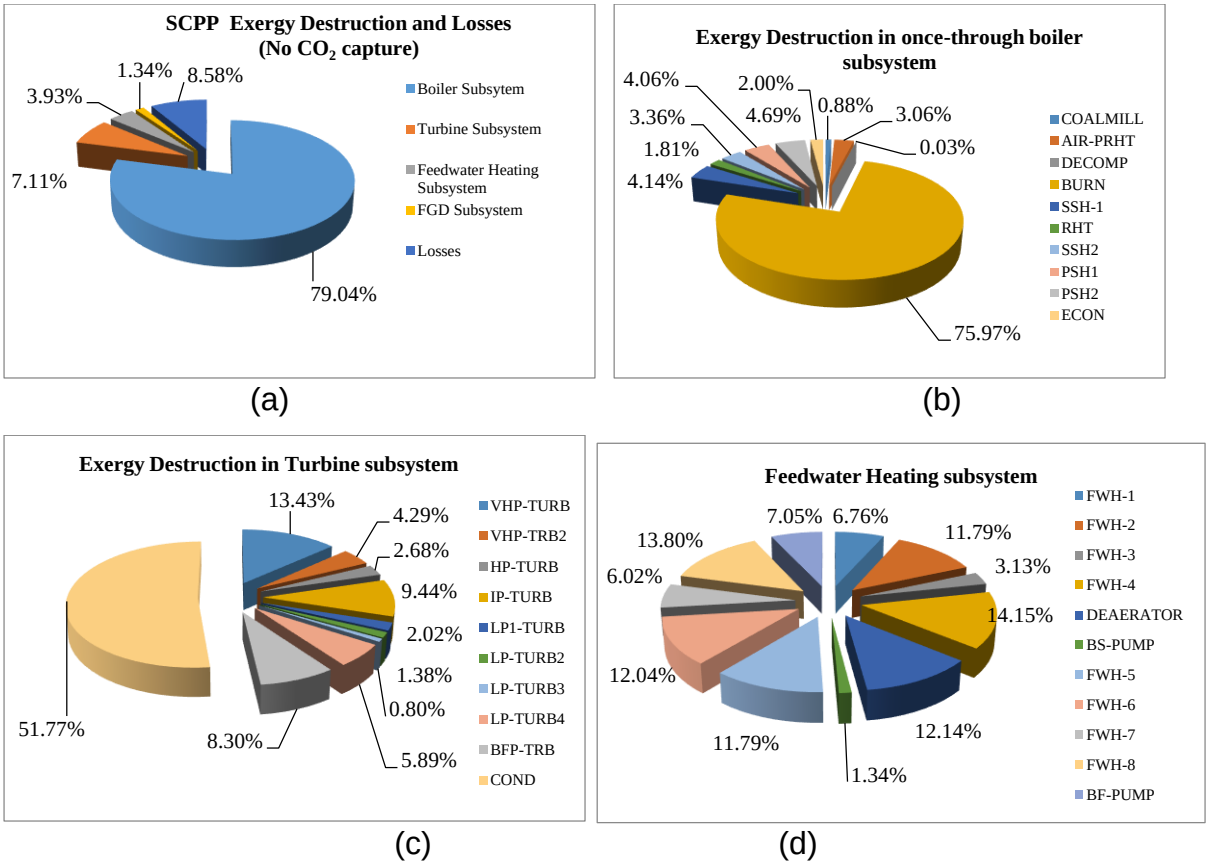


Figure 4.10: Distribution of Exergy losses and Destruction in the SCPP subsystems

However, the effective application of the enormous amount of exergy of waste flue gas should be further investigated for the further reduction of fuel consumption. Figure 4.10(c) shows that the largest proportion (about 52%) of exergy destruction within the turbine subsystem comes from the condenser (i.e. a total of 3.7% destruction in the SCPP accounted for in the condenser); and the turbines stages combined (about 48%) accounts for the remainder (about 3.4% of exergy destroyed in the SCPP system). Figure 4.10(d) illustrates the exergy destruction within the feedwater heaters subsystem. In summary, from conventional exergy analysis of the whole SCPP, around 60% of exergy destroyed was in the furnace.

### 4.4.2 Conventional Exergy Analysis of PCC Subsystems

#### *4.4.2.1 MEA-Based PCC subsystem*

Table 4.2 also shows the exergy destruction and efficiency of the FGD unit and the MEA capture system integrated with SCPP system. Figure 4.11(a) and Figure 4.11(b)

illustrates spatial distribution of the exergy destruction in these systems respectively. The results reveal that the absorber (26%) and the desorber (36%) are the main sources of exergy destruction. The feed cooler (18%) and the blower (16.5%) are also contributing strongly. The total exergy destruction is about 203 MW (1.58 MJ/kg $CO_2$.). Process equipment such as the pump, the blower and the solvent cooler are minor contributors to the exergy destruction. The exergy loss due to the consumption of MEA was included in the overall exergy destruction. Using the chemical exergy of MEA in the liquid phase of 1536 kJ/mol (Geuzebroek et al, 2004), an exergy loss of 5.15MW (0.04 MJ/kg $CO_2$) amounting to about 2.3 % of total exergy destroyed in the $CO_2$ capture subsystem.

Too much of exergy destruction in a single component (e.g. desorber) of a system should be avoided in order to prevent large local driving force which is unfavourable for minimizing exergy destruction (Geuzebroek et al, 2004). This can be achieved by integrating heat and mass transport in the absorber and desorber. However, lower driving force means a larger area for mass transfer and increased capital cost for internals. Dealing with this two opposing factors will require an economic analysis of the trade-offs for optimal design which is beyond the scope of this study. It should be noted that the $CO_2$ compression system is an obvious additional source of exergy loss which is not considered in this study.

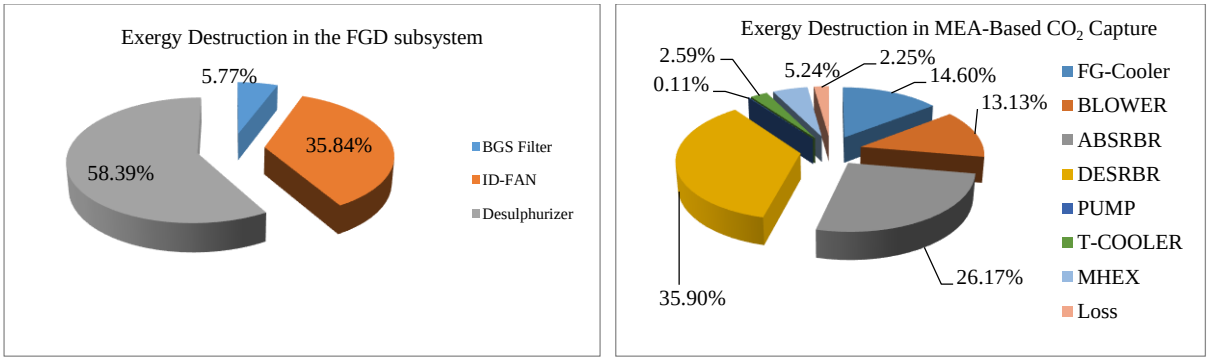


(a) (b)

Figure 4.11: Distribution of Exergy Destruction in (a) FGD and (b) PCC subsystems

*4.4.2.2 Distribution of Exergy Destruction in the Absorber and Stripper*

In the PCC system, a larger part of the exergy destruction is associated with the absorber and stripper columns. The exergy destruction in the columns is largely due to effect of driving forces (i.e. simultaneous heat and mass transfers, heat transfers in the stripper reboiler and condenser, and heat loss through the column metal body) in the columns affect the overall exergy destruction in the system. In this study, the effect of each driving forces to overall column exergy destruction obtained from the Aspen Plus® simulation was estimated using the equations described in Ashrafizadeh et al (2013) as summarised in Table 4.3. Figure 4.12(a) and Figure 4.12(b) shows the spatial distribution of exergy destruction in the stripper and the absorber respectively in relation to the driving forces. The results show that majority of exergy destroyed in the stripper is due to the reboiler (~57%), the condenser (30%) and the mass transfer between phases (8.4%) etc. Exergy destruction due to heat loss to the environment is very negligible (~1.6%) due to adequate insulation of the column. In the absorber, majority of the exergy destruction (about 54%) is due to heat transfer through the exothermic absorption reaction. The mass transfer in the column (i.e. concentration gradient) also accounts for about 43%, while the heat loss accounts for ~2%. This implies that effort to reduce the exergy destruction in the columns should be focused towards principles/strategies that reduces energy consumption in the reboiler (for distillation column), exothermic heat of reaction (for the absorption column), and the mass transfer driving forces in both.

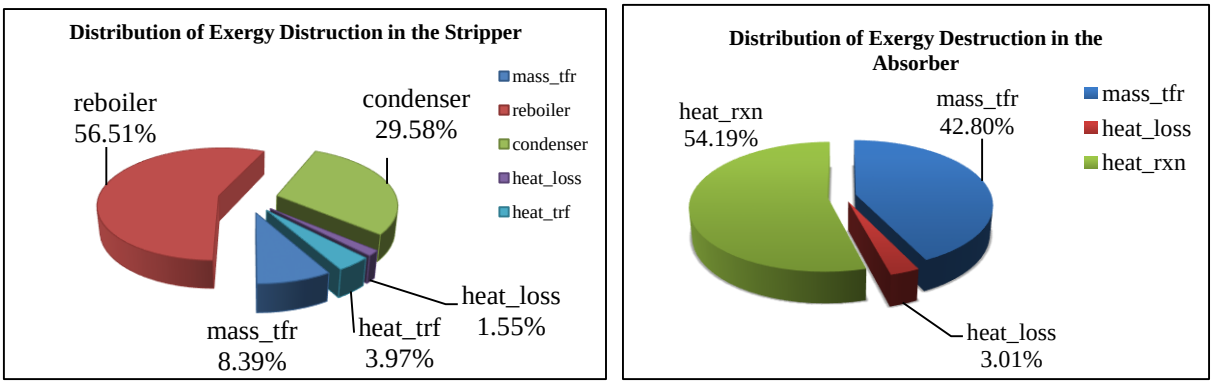


(a) (b)

Figure 4.12: Spatial Distribution of Exergy destruction in the (a) Stripper (b) Absorber

Table 4.3: Equation for Distribution of Exergy Destruction in Absorber and Stripper

| Driving Forces | Stripper (Ashrafizadeh et al, 2013) | Absorber |
|---|---|---|
| Mass transfer due to the mixing liquid and vapour streams | $\dot{E}_{D_{mass\_transfer}} = -\left(\dot{E}_{distillate} + \dot{E}_{bottom}\right) + \dot{E}_{feed}$ $= RT_0[\ln(\prod_{i=1}^{n} \frac{\left(X_{Fi}{}^{niF}\right)}{\left(X_{Di}{}^{niD} * X_{Bi}{}^{niB}\right)})]$ | $\dot{E}_{D_{mass\_trf}} = -\left(\dot{E}_{G} + \dot{E}_{L}\right) + \dot{E}_{Gf} + \dot{E}_{Lf}$ $= RT_0[\ln(\prod_{i=1}^{n} \frac{\left(X_{Gfi}{}^{niGf} * X_{Lfi}{}^{niLf}\right)}{\left(X_{Gasi}{}^{niG} * X_{LQDi}{}^{niL}\right)})]$ |
| Flow Heat transfer through the column | $\dot{E}_{D_{heat.transfer}} = \dot{E}_{\Delta TB} + \dot{E}_{\Delta TD}$ $\dot{E}_{\Delta TB} = \Delta h_{F-B}\left(1 - \frac{T_0}{\overline{T}_{F-B}}\right)$ , $\dot{E}_{\Delta TD} = \Delta h_{F-D}\left(1 - \frac{T_0}{\overline{T}_{F-D}}\right)$ Log mean temperature, $\overline{T}_i = \frac{T_i - T_{feed}}{\ln\frac{T_i}{T_{feed}}}$ | $\dot{E}_{D_{heat.transfer}} = \dot{E}_{\Delta Treaction}$ $\dot{E}_{\Delta T\_reaction} = Q_{Reaction}\left(1 - \frac{T_0}{\overline{T}_L}\right)$ Log mean temperature, $\overline{T}_L = \frac{T_L - T_{Li}}{\ln\frac{T_L}{T_{Li}}}$ |
| Heat transfer in Condenser | $\dot{E}_D = Q_c\left(1 - \frac{T_0}{T_{Distillate}}\right)$ | - |
| Heat transfer in Reboiler | $\dot{E}_D = Q_R\left(1 - \frac{T_0}{T_{Bottom}}\right)$ | - |
| Heat losses through the column wall | $\dot{E}_D = Q_{loss}\left(1 - \frac{T_0}{T_{av}}\right)$ $Q_{loss} = \frac{\Delta T_{overall}}{\sum R_{th}} = \left(\frac{T_i - T_0}{\frac{\ln\frac{r_1}{r_i}}{2k_w\pi L} + \frac{\ln\frac{r_0}{r_1}}{2k_i\pi L} + \frac{1}{2h\pi L}}\right)$ | $\dot{E}_D = Q_{loss}\left(1 - \frac{T_0}{T_{av}}\right)$ $Q_{loss} = \frac{\Delta T_{overall}}{\sum R_{th}} = \left(\frac{T_i - T_0}{\frac{\ln\frac{r_1}{r_i}}{2k_w\pi L} + \frac{\ln\frac{r_0}{r_1}}{2k_i\pi L} + \frac{1}{2h\pi L}}\right)$ |

### 4.4.3 Advanced Exergy Analysis for SCPP Subsystems

*4.4.3.1 Fuel Saving Potential*

Table 4.4 present the fuel-saving potentials ($\Delta E^{*,n}_{F,\,tot}$) of the overall SCPP system. The fuel saving potential was evaluated by improving each component model on standalone basis in Aspen Plus® simulation. The total fuel-saving potential due to improvement in the once-through boiler subsystem (about 61 MW) is very low compared to the turbine system (104 MW). This is because the main steam and the reheat steam flow are determined by the turbine subsystem which in turns implies that the heat absorbed in the boiler is fixed, given its conditions. Hence, at constant air/fuel ratio ($\alpha_{air\_fuel}$) and furnace exit gas temperature there will be only a limited potential to reduce fuel consumption from the boiler subsystem. In this case, only by reducing the pressure drops of working fluid can the fuel consumption be reduced. Table 4.4 also shows that fuel consumption can be reduced by 55 MW from the theoretical operations of the air preheater (AIR-PRHT) and the combustion chamber (FURN). Thus, the promising approaches for reducing fuel consumption from the design perspective of the boiler subsystem would be by reducing the air/fuel ratio ($\alpha_{air\_fuel}$) and the furnace exit gas temperature. For the turbine subsystem, the improvements of the turbines, the feed pumps, feed pump turbines, and the generator are of great significance for reducing fuel consumption, although their exergy destructions under real processes are much smaller than those of the boiler subsystem. The benefits obtained from the turbine subsystem are almost double that of the boiler subsystem. Also, the performance of individual regenerative feedwater heater almost has no influence on fuel consumption in this case, since the pressures of steam extractions remain the same.

*4.4.3.2 Avoidable and Unavoidable Endogenous/Exogenous exergy destruction*

Table 4.4 shows that majority of the exergy destruction within all SCPP components is endogenous as shown in the ($\boldsymbol{E^{en}_{D,n}}$) column. However, the ratio of the exogenous part of the exergy destruction differs considerably from components to components as shown in the ($\boldsymbol{E^{ex}_{D,n}}$) column of Table 4.4. For the boiler subsystem, about 20% of the overall exergy destroyed within it is exogenous as shown in Figure 4.13(b). The results shown in Figure 4.14(b) reveal that about 14% of the exergy destructions in the turbine

subsystem are exogenous. In the regenerative feedwater heating subsystem, about 30% of exergy destroyed within it is exogenous as shown in Figure 4.15(b). The components in the boiler subsystem have large absolute exogenous exergy destruction of about 87MW (Figure 4.13). Hence, their performances are significantly affected by the exergy destructions in the components of the turbine subsystem. The real potential for improving a component is not fully revealed by its total exergy destruction but by its avoidable part (Yang et al, 2013). Table 4.4 also show that a significant part (40–49%) of the exergy destruction within PSH, RHT and AIR-PRT is avoidable. It also shows that due to combustion reactions, most of the exergy destruction (331 MW) within combustion chamber (FURN) is unavoidable in comparison with the avoidable part (30 MW). Also, about 20% of the exergy destruction within SSH (about 17%) and ECON (19%) can be avoided. For the turbine subsystem, about 30–50% of exergy destruction can be avoided as shown in Figure 4.14(a). Figure 4.15(a) also illustrates that the avoidable parts of the exergy destruction in the feedwater heating subsystem is about 24%. Since the work is pure exergy and a slight change of the efficiency of turbine subsystems contributes largely to fuel consumption improvement, more attention should be directed toward the improvement of the efficiencies of turbines, pumps and fans. Most of the avoidable exergy destructions within the heat exchangers in the boiler subsystems (75%), turbine stages (92%) are endogenous as shown in Figure 4.13(c) and Figure 4.14(c) respectively; hence, the improvement measures for these components should be concentrated on the components themselves. The combustion process has an avoidable-exogenous exergy destruction of about 18MW and, thus, its performance improvement should also consider the reductions of exergy destruction of other components. Figure 4.15(c) also reveals that the exogenous exergy destruction contributes over 70% of the avoidable part within the feedwater heating subsystem. Hence, improving feedwater heaters can be more efficiently achieved at the subsystem level. It is important to note that there are no contradictions between the discussions of the fuel-savings potentials in section 4.3.1 and the advanced exergy analysis in section 4.3.2 as pointed out by (Yang et al, 2013). The former focuses on the influence of each component on the overall fuel consumption, while the latter is based on the energy savings potential of the considered component itself.

Table 4.4: Selected results of the Fuel saving potential and advanced exergy analysis of Integrated SCPP-PCC subsystems

| Components | $E^{T,n}_{F,tot}$ | $\Delta E^{*,n}_{F,tot}$ | $E^{T}_{D,n}$ | $E^{R}_{D,n}$ | $E^{un}_{D,n}$ | $E^{av}_{D,n}$ | $E^{en}_{D,n}$ | $E^{ex}_{D,n}$ | $E^{en}_{D,n}$ | | $E^{ex}_{D,n}$ | |
|---|---|---|---|---|---|---|---|---|---|---|---|---|
| | | | | | | | | | $E^{un,en}_{D,n}$ | $E^{av,en}_{D,n}$ | $E^{av,ex}_{D,n}$ | $E^{un,ex}_{D,n}$ |
| *Boiler subsystem* | | | | | | | | | | | | |
| FURN | 1390.37 | 17.35 | 361.50 | 361.50 | 330.95 | 30.55 | 304.45 | 57.05 | 291.66 | 12.79 | 17.76 | 39.29 |
| AIR-PRT | 1371.03 | 36.68 | 6.81 | 18.00 | 9.24 | 8.76 | 16.15 | 1.85 | 8.25 | 7.90 | 0.86 | 0.99 |
| SSH | 1404.17 | 3.55 | 149.67 | 203.17 | 169.59 | 33.58 | 181.59 | 21.58 | 150.54 | 31.05 | 2.53 | 19.05 |
| PSH | 1407.10 | 0.62 | 2.89 | 13.80 | 7.59 | 6.21 | 12.24 | 1.56 | 6.79 | 5.45 | 0.76 | 0.80 |
| RHT | 1404.91 | 2.81 | 4.28 | 24.25 | 14.28 | 9.97 | 21.58 | 2.67 | 12.58 | 9.00 | 0.97 | 1.70 |
| ECON | 1407.50 | 0.22 | 6.20 | 13.42 | 10.74 | 2.68 | 11.64 | 1.78 | 9.30 | 2.34 | 0.34 | 1.44 |
| *Turbine subsystem* | | | | | | | | | | | | |
| VHP-TURB | 1386.47 | 21.25 | 0.00 | 7.11 | 6.18 | 0.93 | 6.46 | 0.65 | 5.61 | 0.85 | 0.08 | 0.57 |
| VHP-TRB2 | 1400.94 | 6.78 | 0.00 | 2.27 | 1.58 | 0.69 | 1.59 | 0.68 | 0.99 | 0.60 | 0.09 | 0.59 |
| HP-TURB | 1401.10 | 6.62 | 0.00 | 1.42 | 0.79 | 0.63 | 1.16 | 0.26 | 0.54 | 0.62 | 0.01 | 0.29 |
| IP-TURB | 1399.30 | 8.42 | 0.00 | 4.81 | 3.24 | 1.57 | 3.18 | 1.63 | 1.73 | 1.45 | 0.12 | 1.51 |
| LP1-TURB | 1401.19 | 6.53 | 0.00 | 1.01 | 0.65 | 0.36 | 0.92 | 0.09 | 0.57 | 0.35 | 0.01 | 0.08 |
| LP-TURB2 | 1402.74 | 4.98 | 0.00 | 0.68 | 0.39 | 0.29 | 0.61 | 0.07 | 0.33 | 0.28 | 0.01 | 0.06 |
| LP-TURB3 | 1402.25 | 5.47 | 0.00 | 0.53 | 0.37 | 0.16 | 0.48 | 0.05 | 0.36 | 0.12 | 0.04 | 0.01 |
| LP-TURB4 | 1382.22 | 25.50 | 0.00 | 3.64 | 1.82 | 1.82 | 3.32 | 0.32 | 1.65 | 1.67 | 0.15 | 0.17 |
| BFP-TRB | 1389.80 | 17.92 | 0.00 | 2.10 | 1.38 | 0.72 | 1.18 | 0.92 | 0.61 | 0.57 | 0.15 | 0.77 |
| COND | 1407.72 | 0.00 | 31.68 | 31.68 | 0.00 | 31.68 | 25.54 | 6.14 | - | - | - | - |
| *Feedwater heating subsystem* | | | | | | | | | | | | |
| FWH-1 | 1407.11 | 0.61 | 1.94 | 2.03 | 1.74 | 0.29 | 1.79 | 0.24 | 1.55 | 0.24 | 0.05 | 0.19 |
| FWH-2 | 1407.13 | 0.59 | 3.26 | 3.41 | 2.93 | 0.48 | 2.48 | 0.93 | 2.40 | 0.08 | 0.40 | 0.53 |
| FWH-3 | 1406.73 | 0.99 | 0.86 | 0.93 | 0.76 | 0.17 | 0.64 | 0.29 | 0.60 | 0.04 | 0.13 | 0.16 |
| FWH-4 | 1405.92 | 1.80 | 4.00 | 4.03 | 3.58 | 0.45 | 2.94 | 1.09 | 2.93 | 0.01 | 0.44 | 0.65 |

| | | | | | | | | | | | | |
|---|---|---|---|---|---|---|---|---|---|---|---|---|
| DEAERATOR | 1406.98 | 0.74 | 3.12 | 2.98 | 2.64 | 0.34 | 1.86 | 1.12 | 1.80 | 0.06 | 0.28 | 0.84 |
| BS-PUMP | 1407.42 | 0.30 | 0.00 | 2.31 | 1.39 | 0.92 | 1.40 | 0.91 | 0.93 | 0.47 | 0.45 | 0.46 |
| FWH-5 | 1406.14 | 1.58 | 2.86 | 2.90 | 2.58 | 0.32 | 2.26 | 0.64 | 2.14 | 0.12 | 0.20 | 0.44 |
| FWH-6 | 1406.65 | 1.07 | 2.18 | 2.45 | 2.14 | 0.31 | 1.62 | 0.83 | 1.59 | 0.03 | 0.28 | 0.55 |
| BF-PUMP | 1402.38 | 5.34 | 0.00 | 2.17 | 1.16 | 1.01 | 1.58 | 0.59 | 0.85 | 0.73 | 0.28 | 0.31 |
| FWH-7 | 1405.92 | 1.80 | 1.64 | 2.19 | 1.89 | 0.30 | 1.66 | 0.53 | 1.59 | 0.07 | 0.23 | 0.30 |
| FWH-8 | 1405.07 | 2.65 | 4.03 | 4.65 | 3.28 | 1.37 | 2.85 | 1.80 | 1.87 | 0.98 | 0.39 | 1.41 |
| *FGD Subsystem* | | | | | | | | | | | | |
| BGS Filter | 1407.25 | 0.47 | 0.38 | 0.62 | 0.41 | 0.21 | 0.56 | 0.06 | 0.48 | 0.08 | 0.13 | -0.07 |
| ID-FAN | 1405.90 | 1.82 | 0.00 | 4.21 | 2.86 | 1.35 | 3.67 | 0.54 | 2.87 | 0.80 | 0.55 | -0.01 |
| Desulphurizer | 1403.98 | 3.74 | 2.86 | 5.81 | 4.63 | 1.18 | 4.43 | 1.38 | 2.96 | 1.47 | -0.29 | 1.67 |
| *Conventional PCC Subsystems* | | | | | | | | | | | | |
| FG-Cooler | 1406.34 | 1.38 | 22.84 | 33.37 | 20.35 | 13.02 | 22.84 | 10.53 | 12.62 | 10.22 | 2.80 | 7.73 |
| BLOWER | 1405.10 | 2.62 | 22.51 | 30.02 | 11.12 | 18.90 | 22.51 | 7.51 | 9.79 | 12.72 | 6.18 | 1.33 |
| ABSRBR | 1394.29 | 13.43 | 59.83 | 59.83 | 43.60 | 16.23 | 50.00 | 9.83 | 37.45 | 12.55 | 3.68 | 6.15 |
| DESRBR | 1385.29 | 22.43 | 82.07 | 82.07 | 68.25 | 13.82 | 75.50 | 6.57 | 61.49 | 14.01 | -0.19 | 6.76 |
| PUMP | 1404.31 | 3.41 | 0.097 | 0.26 | 0.14 | 0.12 | 0.10 | 0.16 | 0.00 | 0.10 | 0.02 | 0.14 |
| T-COOLER | 1406.78 | 0.94 | 0.41 | 5.93 | 5.56 | 0.37 | 0.41 | 5.52 | 0.07 | 0.33 | 0.03 | 5.49 |
| MHEX | 1405.86 | 1.86 | 4.66 | 11.98 | 6.98 | 5.00 | 4.66 | 7.32 | 0.88 | 3.78 | 1.23 | 6.09 |

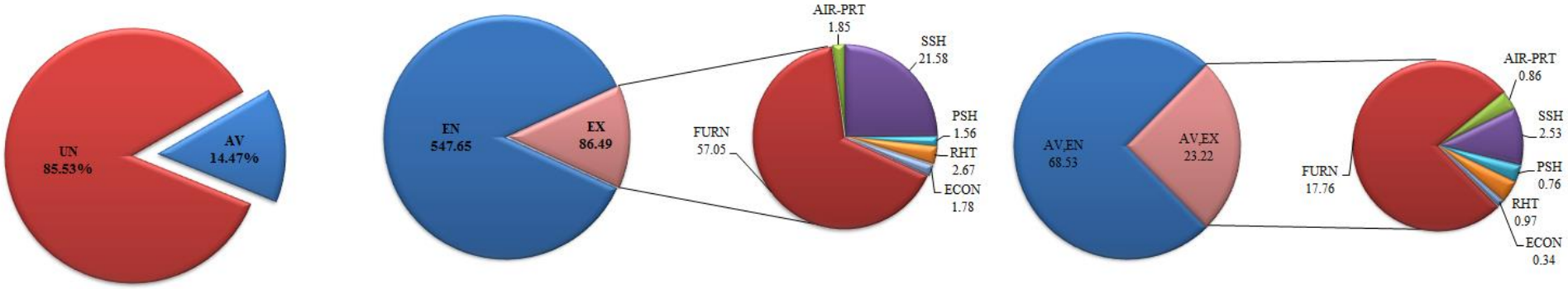


(a) (b) (c)

Figure 4.13: Advanced exergy Analysis of boiler subsystem into (a) AV/UN (b) EN and EX (c) AV, EN and UN, EN

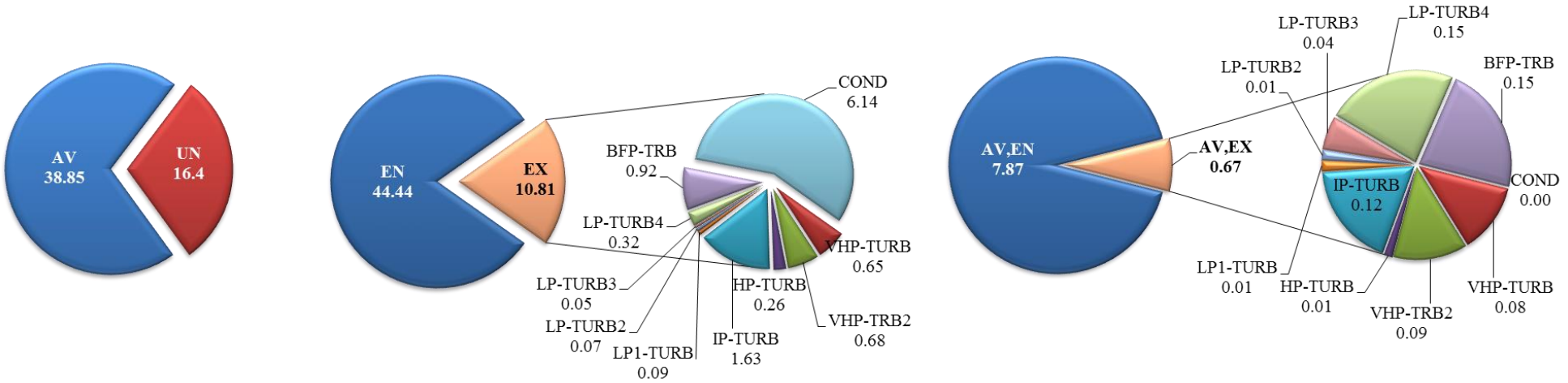


(a) (b) (c)

Figure 4.14: Advanced exergy Analysis of turbine subsystem into (a) AV and UN (b) EN and EX (c) AV-EN and AV-EX

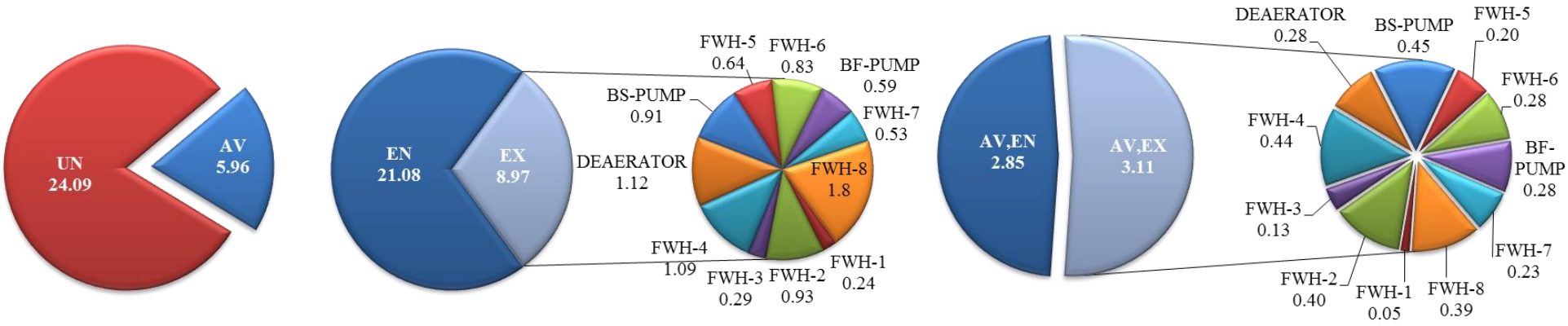


(a) (b) (c)

Figure 4.15: Advanced exergy Analysis of feedwater subsystem into (a) AV and UN (b) EN and EX (c) AV-EN and AV-EX

### 4.4.4 Advanced Exergy Analysis for PCC Subsystems

#### *4.4.4.1 Endogenous and Exogenous Exergy Destruction*

Table 4.4 also shows the distribution of the sources (i.e. endogenous or exogenous) and the potential for improvement (avoidable or unavoidable) for the conventional PCC subsystem. Figure 4.16 reveals that most of the exergy destruction in the components is endogenous (i.e. due to the irreversibilities in the components themselves). The stripper and absorber have largest absolute endogenous exergy destruction of about 75.5MW and 50MW respectively. Hence, their performances will be significantly affected by improving the exergy destructions within the components themselves. However, the potential for improvement is governed by the avoidability or unavoidability of the exergy destroyed.

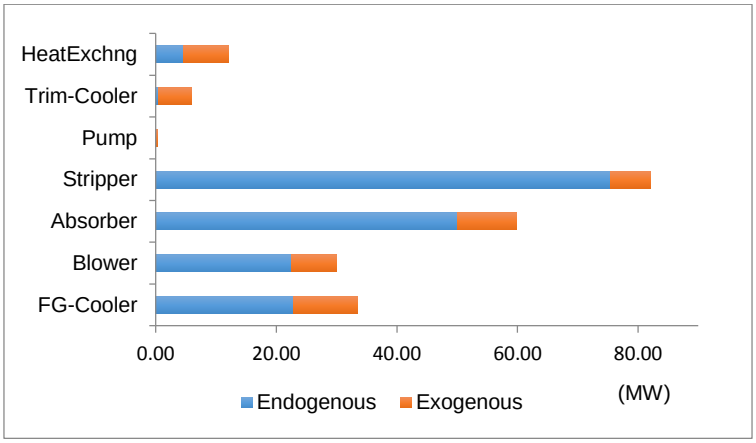


Figure 4.16: endogenous and exogenous exergy destruction of Conventional PCC

#### *4.4.4.2 Avoidable and Unavoidable Exergy Destruction*

Figure 4.17 shows that majority of the exergy destruction within the PCC components is unavoidable. However, the ratio of the avoidable part of the exergy destruction differs considerably from components to components. For the stripper, about 17% (13.83MW) of the overall exergy destroyed within it is avoidable.

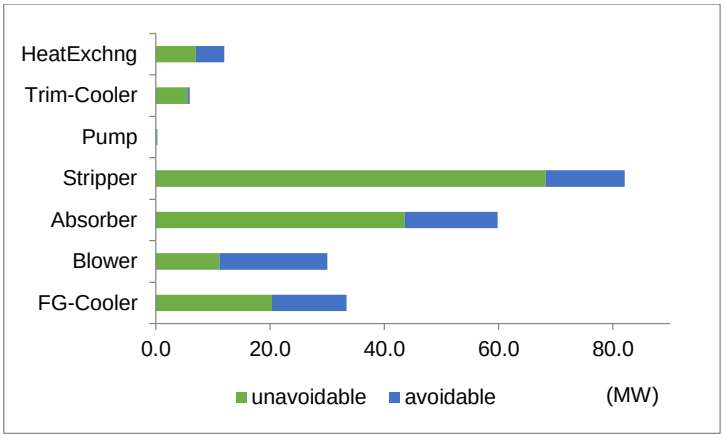


Figure 4.17: avoidable and unavoidable exergy destruction of conventional PCC

The result also reveals that about 27% (16.23MW) of the exergy destructions in the absorber are avoidable. In the heat exchanger, the blower, and the cooler, the avoidable exergy destroyed are 41% (5.01MW), 63% (5.01MW), and 65% (13.02MW) respectively. It is important to know the sources (exo- or endo-) of the avoidable exergies in the components so as to focus attention on reducing the avoidable exergy destruction of a component based on its source.

*4.4.4.3 Avoidable and Unavoidable Endogenous/Exogenous Destruction*

The real potential for improving a component or system is not fully revealed by its total exergy destruction, the sources (exogenous or endogenous), or the potential for improvement (i.e. unavoidable or avoidable) of the destruction alone; but by understanding the source of its avoidable part. As shown in Figure 4.18, in the PCC system, most of the avoidable exergy destructions within stripper (98%), the absorber (77%), the blower (67%), the cooler (78%) and the heat exchangers (65%) respectively are endogenous; hence, the improvement measures for these components should be concentrated on the components themselves.

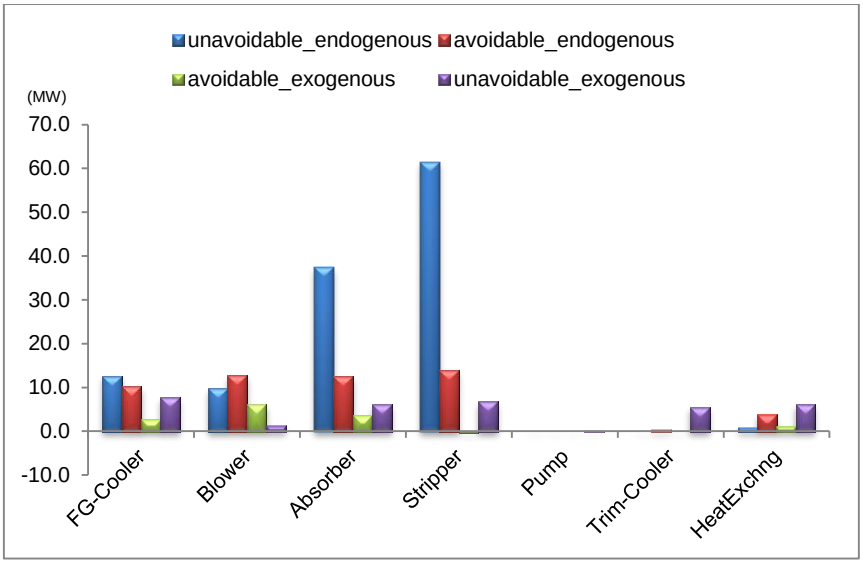


Figure 4.18: un/en, un/ex, av/en, av/ex exergy destruction of Conventional PCC

### 4.4.5 Strategies to Reduce Exergy Destruction in SCPP-PCC Components

Analysis of the energy consumption of the $CO_2$ capture system and the overall exergy destruction in the integrated system necessitated the development of several variations of the conventional $CO_2$ capture. In this study, seven cases were considered as described in section 4.2.2. Case 1: SCPP with AIC, Case 2: SCPP with SF, Case 3: SCPP with (AIC + SF), Case 4: SCPP with SIH, Case 5: SCPP with (SIH + AIC), Case 6: SCPP with LVR, Case 7: SCPP with (LVR+AIC)

#### *4.4.5.1 SCPP-AIC configuration*

Figure 4.19(b) shows the spatial distribution of exergy destruction in the SCPP-AIC subsystems. From Figure 4.19(b), the exergy destruction within the once-through boiler subsystem (~69%) contributes the largest exergy destruction, followed by the PCC system (~22%), and the turbine subsystem (~ 5.6%). The AIC inclusion reduces the local exergy destruction in the PCC by about 2.2% when compared to the conventional case. Table 4.5 also shows a summary of the system energy/exergetic performance. The result shows about 0.2% reduction in overall exergy destruction when compared to the SCPP system with base case $CO_2$ capture. The reboiler duty, energy penalty and the efficiency penalty were decreased by about 3.2%, 0.43% and

0.16% respectively. The exergetic efficiency of the AIC-integrated system was also improved by about 0.5% when compared to the base case.

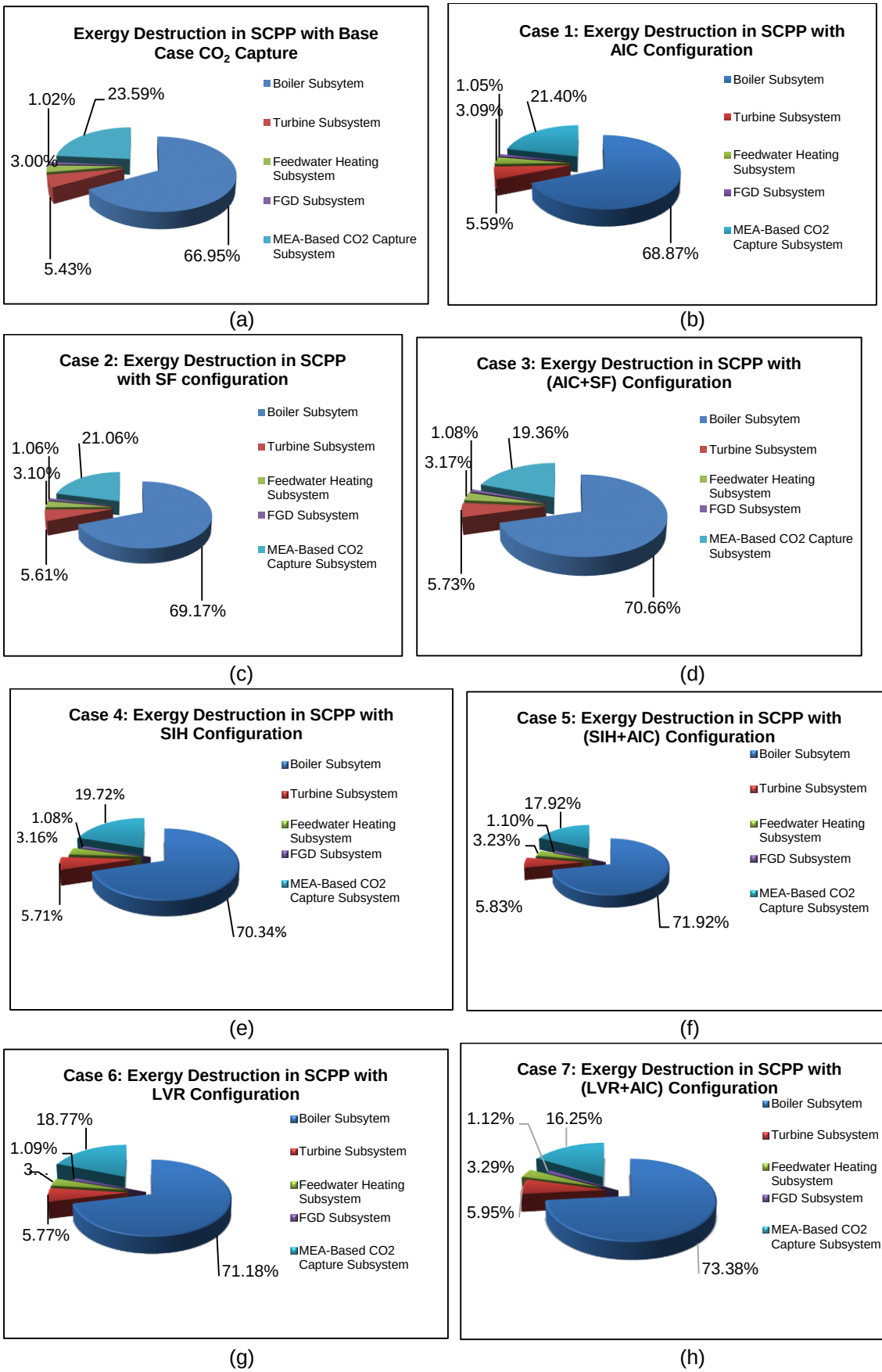


Figure 4.19: Case Studies of Exergy Destruction in SCPP Integrated with PCC

*4.4.5.2 SCPP-SF configuration*

Figure 4.19(c) shows the spatial distribution of exergy destruction in the SCPP-SF subsystems. From Figure 4.19(c), the exergy destruction within the once-through boiler subsystem (~69%) contributes the largest exergy destruction, followed by the PCC system (~21%), and the turbine subsystem (5.6%). The SF inclusion reduces the local exergy destruction in the PCC by about 2.6% when compared to the conventional case. Table 4.5 also shows a summary of the system energy/exergetic performance. The result shows about 0.5% reduction in overall exergy destruction when compared to the SCPP system with base case $CO_2$ capture. The reboiler duty, energy penalty and the efficiency penalty were decreased by about 7%, 1.41% and 0.6% respectively. The exergetic efficiency of the SCPP-SF integrated system was also improved by about 1.1% when compared to the base case.

*4.4.5.3 SCPP-(AIC+SF) Configuration*

The SCPP-(*AIC+SF)* configuration combined the effect of AIC and the SF configuration. Figure 4.19(d) illustrates the spatial distribution of exergy destruction in SCPP-(AIC+SF). The (AIC+SF) inclusion reduces the local exergy destruction in the PCC by about 4.2% when compared to the conventional case. Table 4.5 shows a summary of the system performance. The result shows about 3.1% reduction in overall exergy destruction when compared to the SCPP system with base case $CO_2$ capture. The reboiler duty, energy penalty and the efficiency penalty were decreased by about 11.8%, 2.8% and 1.1% respectively. The exergetic efficiency of the SCPP-(AIC+SF) integrated system was also improved by about 4.5% when compared to the base case.

*4.4.5.4 SCPP-SIH Configuration*

Figure 4.19(e) illustrates the spatial distribution of exergy destruction in SCPP-SIH. The SIH inclusion reduces the local exergy destruction in the PCC by about 3.9% when compared to the conventional case. Table 4.5 shows a summary of the system performance. The result shows about 1.6% reduction in overall exergy destruction when compared to the SCPP system with base case $CO_2$ capture. The reboiler duty, energy penalty and the efficiency penalty were decreased by about 6.8%, 1.8% and

0.7% respectively. The exergetic efficiency of the SCPP-SIH integrated system was also improved by about 2.4% when compared to the base case.

*4.4.5.5 SCPP-(SIH+AIC) Configuration*

Figure 4.19(f) illustrates the spatial distribution of exergy destruction in SCPP-(SIH+AIC). The (SIH+AIC) inclusion reduces the local exergy destruction in the PCC by about 5.7% when compared to the conventional case. Table 4.5 shows a summary of the system performance. The result shows about 3.8% reduction in overall exergy destruction when compared to the SCPP system with base case $CO_2$ capture. The reboiler duty, energy penalty and the efficiency penalty were decreased by about 11.03%, 4.3% and 1.7% respectively. The exergetic efficiency of the SCPP-(SIH+AIC) integrated system was also improved by about 5.7% when compared to the base case.

*4.4.5.6 SCPP-LVR Configuration*

Figure 4.19(g) illustrates the spatial distribution of exergy destruction in SCPP-LVR. The LVR inclusion reduces the local exergy destruction in the PCC by about 4.8% when compared to the conventional case. Table 4.5 shows a summary of the system performance. The result shows about 5.6% reduction in overall exergy destruction when compared to the SCPP system with base case $CO_2$ capture. The reboiler duty, energy penalty and the efficiency penalty were decreased by about 17.5%, 5.3% and 2.1% respectively. The exergetic efficiency of the SCPP-LVR integrated system was also improved by about 6.2% when compared to the base case.

*4.4.5.7 SCPP-(LVR+AIC) Configuration*

Figure 4.19(h) illustrates the spatial distribution of exergy destruction in SCPP-(LVR+AIC). The (LVR+AIC) inclusion reduces the local exergy destruction in the PCC by about 7.3% when compared to the conventional case. Table 4.5 shows a summary of the system performance. The result shows about 6.6% reduction in overall exergy destruction when compared to the SCPP system with base case $CO_2$ capture. The reboiler duty, energy penalty and the efficiency penalty were decreased by about 19.7%, 6.9% and 2.6% respectively. The exergetic efficiency of the SCPP-(LVR+AIC) integrated system was also improved by about 7.3% when compared to the base case.

Table 4.5: System Performance Indicator of the SCPP with the $CO_2$ Capture Scenarios

| Description | Reference SCPP | SCPP + PCC Base Case | Case 1 | Case 2 | Case 3 | Case 4 | Case 5 | Case 6 | Case 7 |
|---|---|---|---|---|---|---|---|---|---|
| *Performance Summary* | | | | | | | | | |
| Total (steam turbine) power (MWe) | 580.26 | 482.28 | 484.52 | 486.42 | 488.58 | 490.04 | 502.80 | 508.39 | 514.21 |
| Auxiliary load (MW) | 28.28 | 52.04 | 51.95 | 48.45 | 42.8 | 49.87 | 49.02 | 49.06 | 47.97 |
| Gross plant power (MW) | 551.98 | 430.24 | 432.57 | 437.97 | 445.78 | 440.17 | 453.78 | 459.33 | 466.24 |
| Generator loss (MW) | 1.83 | 1.83 | 1.83 | 1.83 | 1.83 | 1.83 | 1.83 | 1.83 | 1.83 |
| Net power output (MWe) | 550.15 | 428.41 | 430.74 | 436.14 | 443.95 | 438.34 | 451.95 | 457.50 | 464.41 |
| Unit efficiency, HHV (%) | 39.10 | 30.45 | 30.61 | 31.00 | 31.55 | 31.15 | 32.12 | 32.51 | 33.01 |
| *$CO_2$ Capture Performance Summary* | | | | | | | | | |
| Reboiler Duty (MW) | - | 528.78 | 511.81 | 492.02 | 466.57 | 492.77 | 470.45 | 436.24 | 424.61 |
| Energy penalty (%) | - | 22.13 | 21.70 | 20.72 | 19.30 | 20.32 | 17.85 | 16.84 | 15.25 |
| Efficiency penalty (%) | - | 8.65 | 8.49 | 8.10 | 7.55 | 7.95 | 6.98 | 6.59 | 6.09 |
| *Exergetic Performance Summary* | | | | | | | | | |
| Exergy Destruction, $y_D$ (%) | 52.61 | 46.27 | 46.15 | 45.81 | 43.19 | 44.69 | 42.44 | 40.69 | 39.65 |
| Exergy Losses, $E_L$ (%) | 8.34 | 5.03 | 4.62 | 4.37 | 3.58 | 4.23 | 3.29 | 2.86 | 2.15 |
| Exergetic efficiency, $\varepsilon$ (%) | 39.05 | 48.7 | 49.23 | 49.82 | 53.23 | 51.09 | 54.36 | 54.87 | 56.04 |

## 4.6 Summary

The conventional and advanced exergetic analysis performed in this study allows a consistent and detailed evaluation of energy consumption in the SCPP-PCC integrated system from a thermodynamic point of view. The conventional exergy analysis evaluates the amount and location of exergy destruction within the whole system. The advanced exergetic analysis estimates the sources (endogenous or exogenous) of the exergy destruction in individual component or the whole system and the potential for reducing it (unavoidable or avoidable). The boiler subsystem has the largest exergy destruction but also has a limited influence on fuel-saving potentials of the SCPP system. The turbine subsystem shows very small exergy destruction compared to the boiler subsystem, but more significance in reducing fuel consumption. This study show that a combination of improvement in turbine performance design and reduction of the driving forces responsible for the $CO_2$ capture (without compromising cost) can help improve the rational efficiency of the integrated system. Seven modifications to the conventional MEA-based PCC were considered for reducing exergy destruction: AIC, SF, AIC+SF, SIH, SIH+AIC, LVR, and LVR+AIC. The LVR+AIC configuration shows the most significant reduction in exergy destruction, reboiler energy and efficiency penalties when compared to the conventional case. The results show that the energy/exergy consumption and the efficiency of the integrated system can be improved by recovering the avoidable exergy destruction in the system.

# Chapter 5 Dynamic modelling and simulation of SCPP once-through boiler: Lumped and distributed parameter modelling approaches

## 5.1 Introduction

The dynamics of the SCPP is largely influenced by the dynamics of the once-through boiler. Steam generation is the heart of the once-through supercritical boiler. Once-through boilers operate in both circulation (during start-up, low-load and shut-down operation) and once-through mode (at full load operation).

In once-through mode, the feedwater converts completely to steam somewhere before the evaporator exit (O'Kelly, 2013). The point along the waterwall flow path at which the water phase disappears is referred to as the dry-out point. During start-up, low load, and shutdown, dry-out is not achieved; hence the exit flow will require separation of the two-phase mixture. A vertical water-steam separator is added between the waterwall exit and inlet, with a forced recirculation back to the waterwall inlet (Dong and Tingkuan, 2001). The total flow to the riser is the sum of the feedwater flow from the boiler feed pump (BFP) and the boiler circulation pump (BCP). At least a minimum flow to the evaporator tubes is guaranteed at all times to ensure adequate cooling of the economiser and the boiler tubes. Circulation around the separator loop is maintained up to approximately 35 % load (Dong and Tingkuan, 2001) or at some pre-determined steam pressure (120 – 140 bar) (O'Kelly, 2013).

### 5.1.1 Description of the Reference SCPP Once-through Boiler

The reference SCPP once-through boiler studied is 600MWe installed capacity at 100% boiler maximum continuous rating (BMCR) operated by Ligang Power and located in Jiangsu Province, China. The boiler was designed based on the supercritical boiler technology of Alstom and also combined the coal combustion experience of Shanghai Boiler Limited, consisting of spiral tube coils, supercritical once-through boiler, single furnace, corner tangential firing, Balanced ventilation, Type II open layout, dry bottom and Full steel suspension structure. Fuel/flue gas flows from the

upper of furnace to the bottom of the boiler through divided platen superheaters，rear platen superheater，final reheater and final superheater, and then reach the low temperature reheater and the flue-side of the economizer. Finally, all the flue gas flows into two tri-sectional volume type preheater located at the rear of boiler. Figure 5.1 is a process schematic of the reference SCPP once-through boiler.

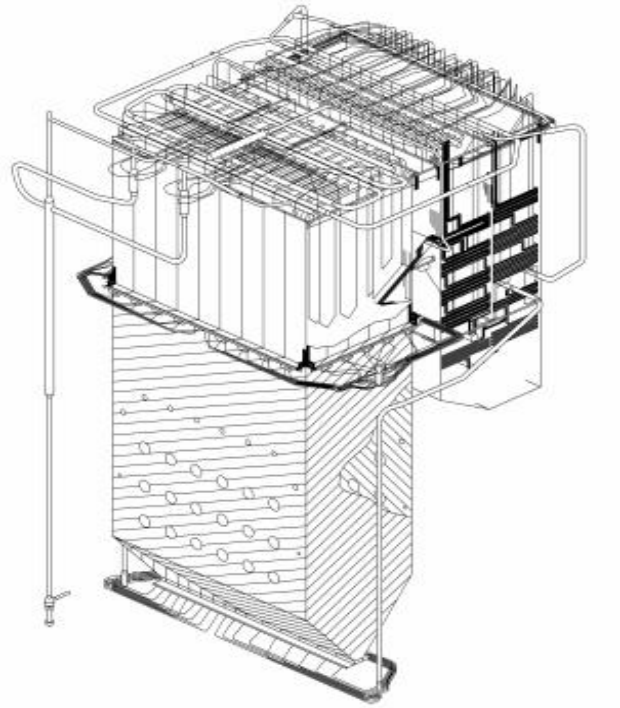

Figure 5.1: Schematic of the reference 600 MWe SCPP boiler Configuration

The boiler feedwater enters inlet collecting header of the economizer then to the economizer tube bank, the intermediate collecting header and the convection pass tubes; it then converges at the outlet collecting header, and then flows into the inlet collecting header of the spiral waterwall tubes. Figure 5.2 shows a schematic diagram of the reference SCPP once-through boiler spiral waterwall evaporation system.

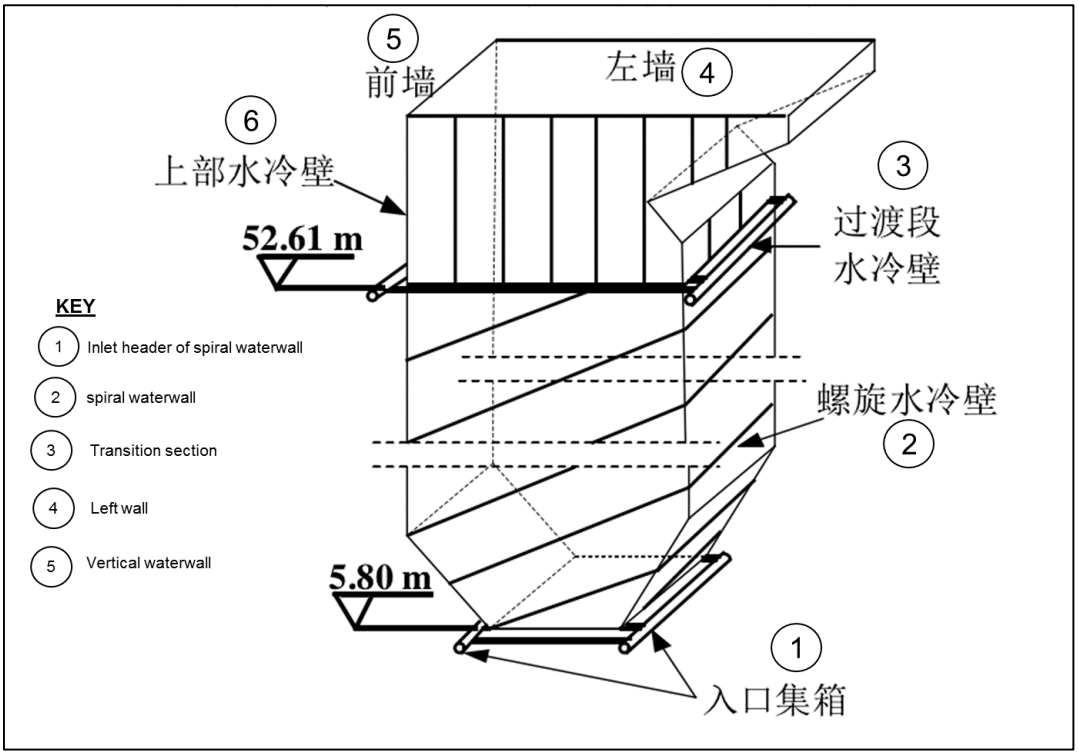


Figure 5.2: Process schematic of typical SCPP boiler evaporation system (Adapted from Lu et al, 2011)

The furnace waterwall is composed of film-type smooth tubes, and are divided into the upper and lower sections. Between the bottoms of the furnace, the dry bottom hopper, and the intermediate collecting header, there are 326 spiral waterwall tubes which are 38.1mm in diameter, 6.35mm pipe thickness, 54mm pitch and 13.95°dip angle. The vertical waterwall tubes are located at the upper section of furnace.

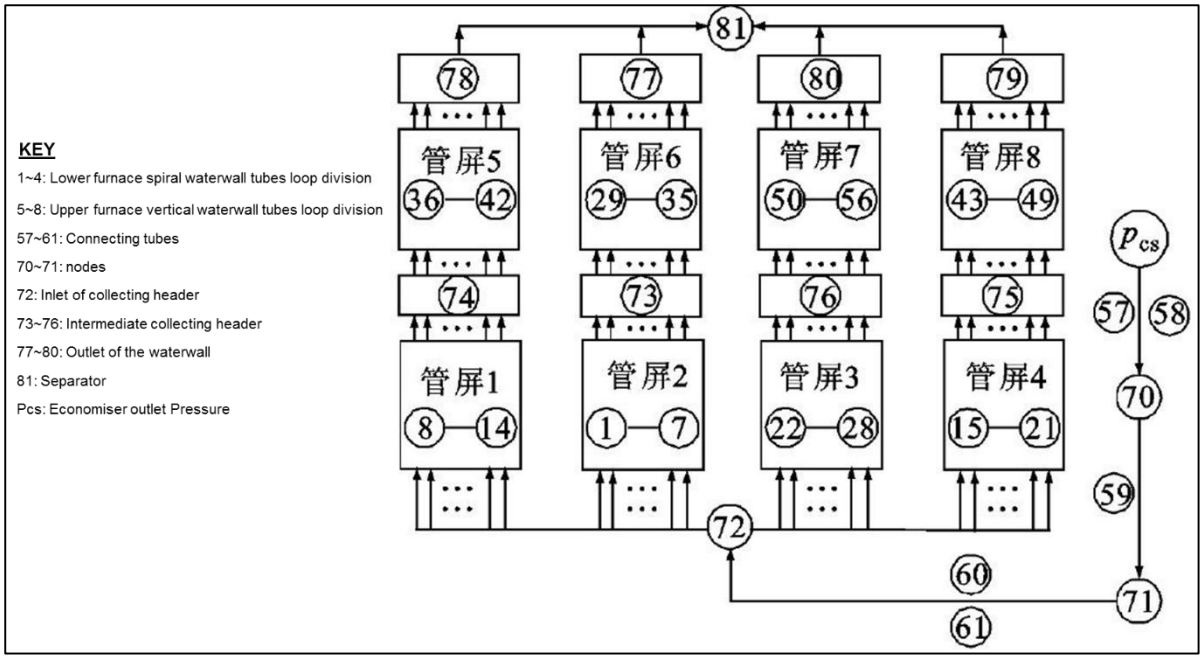


Figure 5.3: Schematics of the flow network of the waterwall in the reference SCPP boiler (Adapted from Lu et al, 2011)

The feedwater enters the four spiral waterwalls tubes on the four sides of the furnace to absorb heat; and then flows to the intermediate collecting header where all the feedwater mix in the transition connecting header. The mixed feedwater flow out through connecting tube in the vertical waterwall tubes. There are 336 vertical waterwalls tubes at the rear of the waterwall and they are divided into 2 parts. The first part are 280 screen falling tubes, the other part is made up of 56 suspension tubes. The feedwater from the four waterwall flows into the outlet collecting header and enters into the steam separator through outlet pipes.

The process schematics of the flow network of the waterwall in the reference SCPP once-through boiler is shown in Figure 5.3. The main parameters of the plant used for model validation were obtained from the reference plant design data (at 100% BMCR) and measurements compiled from weekly performance charts at three load levels: (i) generating at capacity of 520 MWe (87% BMCR); (ii) 450 MWe (75% BMCR); and 300 MWe (50% BMCR). Table 5.1 shows a summary of the main parameters of the evaporator loop.

Table 5.1: Key parameters of the reference SCPP once-through boiler evaporator

| Parameters | (50% BMCR) | (75% BMCR) | (87% BMCR) |
|---|---|---|---|
| LF steam temperature (°C) | 375.47 | 397.9 | 407.8 |
| UF steam temperature (°C) | 381.3 | 409.8 | 417.5 |
| Outlet steam pressure (MPa) | 16.83 | 21.55 | 25.74 |
| Economizer feedwater flow (kg/s) | 262.72 | 393.42 | 465.72 |
| Economizer outlet temperature (°C) | 301.6 | 316.0 | 324.3 |
| Economizer inlet pressure (MPa) | 18.83 | 23.74 | 28.36 |
| Water separator pressure (MPa) | 17.52 | 22.77 | 26.47 |

### 5.1.2 Modelling Treatment and Approaches

The SCPP once-through boiler dynamic model was developed from models of the individual components (i.e. coal milling system, furnace and flue gas-air circuit, the water/steam evaporator circuits, the convectional and radiant superheaters, the deaerator-feedwater system etc.). The equation oriented modelling software gPROMS® is used for the component models. Model equations, parameters, correlations and thermodynamic properties for each of the components were obtained from literature, from live plant design and operational data.

Lumped parameter or distributed parameter modelling approaches have often been applied for accurate modelling of the physical phenomenon in the SCPP at various modes of operation. This chapter presents the SCPP dynamic model and comparison of the lumped parameter and distributed parameter modelling approaches for developing the SCPP boiler dynamic (especially the once-through boiler evaporators at both the circulation mode and once-through mode of operation). It considers: (i) Lumped parameter modelling approach using algebraic equations and ordinary differential equations (ODEs); and (ii) distributed parameter approach using partial differential and algebraic equations (PDAEs).

## 5.2 Lumped Parameter Modelling Approach

The lumped parameter modelling equations are based on physical laws, constitutive relations, and material properties. The general forms of the equations are given thus without considering spatial variation the variables of interest in the SCPP components. In spite of the large number of components and processes to model the SCPP unit,

there are similarities in the modelling equations and assumptions. The general forms of the equations are given thus:

### 5.2.1 General Conservation Principle

*5.2.1.1 Global Mass, Energy and Momentum Balance*

*General Assumption:* Negligible kinetic (small compared to the enthalpy change) and potential energy (due to negligible change in elevation) changes. Considering the control volume shown in Figure 5.4, the general mass, energy and momentum conservation equations can be represented as follows.

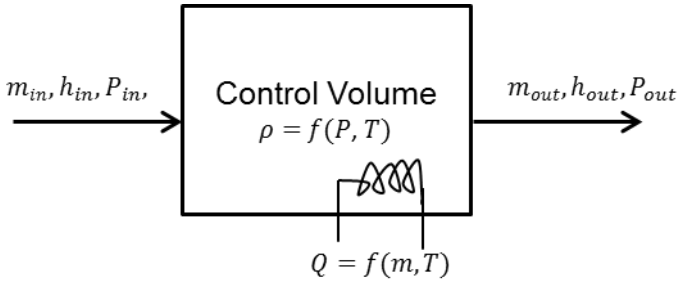


Figure 5.4: General control volume of the Component models

For the global mass balance;

$$m_{in} - m_{out} = V\frac{d\rho}{dt} \qquad (5.1)$$

$m_{in}$ is the mass flowrate of the working fluid into the control volume, $m_{out}$ is the mass flowrate out, $\rho$ is the density of the working fluid, and $V$ is the volume.

But $\rho$ is a function of pressure, $P$, and temperature $T$, as shown in equation (5.2) thus;

$$\rho = f(P,T) \qquad (5.2)$$

Hence,

$$\frac{d(P,T)}{dt} = \frac{\partial\rho}{\partial T} * \frac{dT}{dt} + \frac{\partial\rho}{\partial P} * \frac{dP}{dt} \qquad (5.3)$$

Where:

$$\frac{\partial\rho}{\partial T} = n_i \qquad \frac{\partial\rho}{\partial P} = n_{ii} \qquad (5.4)$$

The global mass balance is thus:

$$m_{in} - m_{out} = V(n_i\frac{dT}{dt} + n_{ii}\frac{dP}{dt}) \qquad (5.5)$$

The global energy balance (along the fluid flow path i.e. steam/water and flue gas) in terms of internal energy can be expressed thus:

$$m_{in}h_{in} - m_{out}h_{out} + Q = \frac{dU}{dt} \qquad (5.6)$$

Internal energy: $U = H - PV$,

and in terms of specific enthalpies: $U = V(\rho h - P)$

Hence, (5.6) becomes:

$$m_{in}h_{in} - m_{out}h_{out} + Q = V\frac{d(\rho h - P)}{dt}$$

$$V\frac{d(\rho h - P)}{dt} = V\frac{d(\rho h)}{dt} - V\frac{dP}{dt}$$

$$= V(h\frac{d\rho}{dt} + \rho\frac{dh}{dt} - \frac{dP}{dt})$$

The global energy balance in the heat exchange surfaces can thus be represented as follows:

$$m_{in}h_{in} - m_{out}h_{out} + Q = V(h\frac{d\rho}{dt} + \rho\frac{dh}{dt} - \frac{dP}{dt}) \qquad (5.7)$$

Where is $h_{in}; h_{out}$ are the specific enthalpy at inlet and outlet respectively

Energy balance on the tube metal;

$$M_m C_p \frac{dT_m}{dt} = Q_{gm} - Q_{ms} \qquad (5.8)$$

Momentum balance; (negligible inertia term)

$$P_{in} - P_{out} = f\frac{m^2}{\rho} \qquad (5.9)$$

*5.2.1.2 Heat transfer processes*

Newton's law for convection and Stefan Boltzmann's law for radiation are the transfer equations describing the heat transfer processes in the SCPP once-through boiler. Heat transfer by radiation is assumed to be the exclusive mode of transfer in the furnace and is represented by the following approximation to the Stefan Boltzmann's law (Ordys et al, 1994).

$$Q_R = \frac{K\sigma V_{Furn} {T^4}_{gas}}{\rho_{gas}} \quad (5.10)$$

The effective gas temperature is obtained from the adiabatic gas temperature thus:

$$T_{gas} = T_{gas.ad} + (1-\beta)T_{g.exit} \quad (5.11)$$

The parameter, $\beta$ accounts for the effect of soot blowing on heat transfer and heat loss to the atmosphere (Lu, 1999). The flue gas temperature at furnace $T_{g.exit}$ is obtained by performing a global energy balance around the furnace. The adiabatic flame temperature $T_{g,ad}$ is obtained from energy balance under adiabatic conditions (*i.e.* no heat loss).

Heat transfer by convection is the exclusive mode of transfer considered for heat transfer from the gas to tube metal body and from the metal tube to the steam (i.e.$Q_{gm}\ and\ Q_{ms}$) and is represented by the Newton's law.

$$Q_C = h_C A(T_{hot} - T_{cold}) \quad (5.12)$$

*5.2.1.3 Heat transfer coefficient at supercritical condition*

The outside (gas side) heat transfer coefficient is given by Colburn's correlation for fully developed gas turbulent flow across the tube banks. The inside (steam side) heat transfer coefficient is given by McAdam's correlation for fully developed fluid flow in the tubes. The outside and inside tube heat transfer coefficients are approximated to be proportional to $m^{0.6}$ and $m^{0.8}$ respectively (Masada, 1979).

Hence,

$$h_C A = U_{kg} {m_g}^{0.6} \quad (5.13)$$

$$Q_{gm} = U_k {m_g}^{0.6}(T_{gas} - T_{metal}) \quad (5.14)$$

$$Q_{gm} = U_{ks} {m_g}^{0.8}(T_{metal} - T_{steam}) \quad (5.15)$$

A detail derivation of the approximations to the heat transfer coefficients equations (5.13), the gas to metal heat transfer equation (5.14), and the metal to steam heat transfer equation (5.15) is presented in Appendix C1.

### 5.2.2 Component Models

*5.2.2.1 Water–Steam Cycle*

The dynamic model equations for the economiser, furnace waterwall (steam side), the convection pass, the primary and secondary superheaters, the platen and divided platen superheaters, the secondary and primary superheaters, the convection pass tubes, the reheaters, and the economiser steam flow side are represented by equations (5.1) to (5.9).

*5.2.2.2 Air–Flue gas Cycle*

The dynamic model equations for the air-flue gas circuit is made up of the flue gas/air flow side of the furnace, the platen superheaters, the divided platen superheaters, the secondary & primary superheaters, the primary and final reheaters, convection pass, the economisers, and the air preheater. All the components are based on the model equations (5.1) to (5.9). The convective transfer equations (5.13) to (5.15) were also included in the convective heat exchangers – the convection pass tubes, the primary superheaters, the primary reheater, the economisers, and the air preheater.

The platen superheaters, the divided platen superheaters, the secondary superheaters, and the final reheaters are all in the radiation zone of the furnace and hence included equation (5.10) and equations (5.11) is used to estimate the flue gas exit temperature from the adiabatic flame temperature computed from the combustion process in the furnace.

*5.2.2.3 Furnace Combustion and Radiation System*

A simplified model can be used to calculate the profiles of flame temperature and heat transfer to the waterwalls from a single flame source to the furnace exit (O'Kelly, 2013). For the lumped parameter model, Heat flux distribution along the heights of the waterwall/riser has been neglected and only the total heat flow rate was considered (Maffezzoni, 1992).This assumption implies uniform surface temperature for the waterwall evaporators. Heat transfer from the furnace flames and flue gas to the waterwalls is mainly due to radiation (Blokh, 1987). Radiation in the furnace relies on furnace properties such as furnace geometry, burner firing system and arrangement,

fuel type, and the operational characteristics of the furnace. Loss of furnace thermal efficiency due to accumulation of slag over time on the waterwalls may reduce the radiation. This was however not accounted for in this study.

The total radiant heat released during combustion is usually distributed between the water walls and the platen superheater. The fractions of the radiant heat absorbed by the waterwalls and the superheaters in the radiant section of the furnace depends on the amount of burners in service and the burner tilt angle (Bhambare *et al., 2007*). The position of the fireball in a furnace relative to a base position is a function of the burners in service and the burner tilt. Hence, the radiant heat absorbed by the superheaters vary with different burner configuration. The burner characteristics is not considered in this lumped parameter model. However, an attenuation factor determined from operating data was used to account for radiant heat distribution between the waterwalls and the radiant superheaters. Table 5.2 shows the properties of coal used for this study.

Table 5.2: Coal Analysis (Lawal *et al.*, 2012).

| Coal Composition | As received basis (wt %) |
|---|---|
| Moisture | 8.00 |
| Ash | 20.00 |
| C | 59.11 |
| H | 3.99 |
| N | 1.00 |
| S | 2.00 |
| O | 5.90 |
| Calorific Values | As received basis (MJ/kg) |
| GCV | 24.51 |
| NCV | 23.33 |

Dynamics of flue gas temperature is described using a global energy balance equation around the furnace as shown in equation (5.16). Mass accumulation is assumed negligible due to the fast dynamics of the flue gas (Lawal *et al.*, 2012). Flue gas re-circulation was also not taken into consideration in this study.

$$V_{furn}\rho_{gas}\frac{dh_{gas}}{dt} = m_{fuel}\left(NCV_{fuel} + h_{fuel}\right) + m_{air}h_{air} - m_{ash}h_{ash} - Q_{rad} \quad (5.16)$$

Where $m_{gas} = m_{air} + m_{fuel} - m_{ash}$ (5.17)

20 % vol. excess air (at 100% MCR) is assumed for the combustion of the pulverised coal in the furnace model. The stoichiometric reactions carbon, hydrogen and sulphur is as shown in the following stoichiometric reactions R5.1, R5.2 and R5.3 below.

$$C(s) + O_2(g) \rightarrow CO_2(g) \quad \text{(R5.1)}$$

$$S(s) + O_2(g) \rightarrow SO_2(g) \quad \text{(R5.2)}$$

$$2H_g(g) + O_2(g) \rightarrow 2H_2O(g) \quad \text{(R5.3)}$$

Nitrogen and other negligible components are assumed as inert. Formation of $NO_X$ was not considered in the furnace reactions. $SO_X$ formation on the other hand is treated as $SO_2$. The assumptions leave no room for unreacted carbon as the excess air assumptions means the reactions proceed to completion. The details of the combustion reactions and flue gas composition is similar to the approach used for the steady state calculation in Mathcad® presented in Appendix B. Total radiant heat energy released in the furnace ($Q_R$) was estimated from Stefan-Boltzmann law of radiation as shown in equation (5.10).

### 5.2.3 Other components

*5.2.3.1 Pulverisers*

The objective of modelling a coal mill is to be able to determine (and possibly control) the quantity of coal being crushed such that adequate amount of pulverised coal is fed to the burners to meet the change in load demands, whilst also maintaining an optimal operation of the mill. Figure 5.55 shows a vertical spindle-type pulveriser used in SCPP once-through boilers.

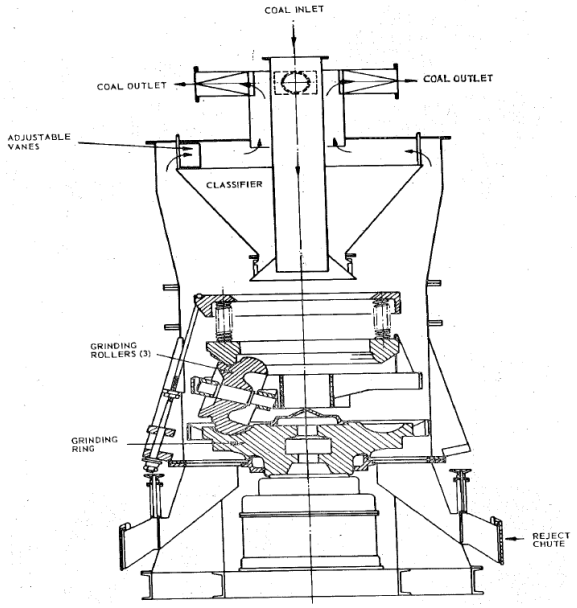


Figure 5.5: A typical Vertical Spindle-type Pulveriser used in SCPP

The basic balance equations describing the dynamic behaviour of the coal mill are: (i) Mass balance equation for the coal, (ii) Energy balance equation for the pulveriser and the pulveriser impeller. Figure 5.6 shows the control volume representation of the pulveriser model and its variables of interest.

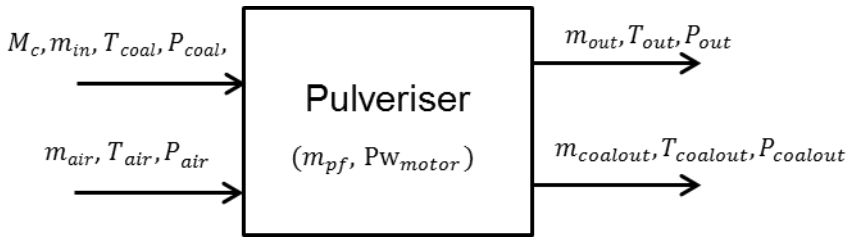


Figure 5.6: Schematics of the Pulveriser model

Hence,

$$\frac{dM_c}{dt} = M_{in} - M_{out} \tag{5.18}$$

$$\frac{dM_c}{dt} = K_{in}I_{in} - K_{out}M_c \tag{5.19}$$

The flow of primary air through the mill is proportional to the feeder stroke $(W_{in} \propto I_{in})$ and the air-coal mixture fills the entire volume representing the deflector and the exhauster.

The mass balance on the fraction of coal ($X_{ci}$) in the volume yields,

$$\frac{dX_{ci}}{dt} = \frac{1}{\rho_c V}\left(K_{out} M_c - m_{pf}\right) \tag{5.20}$$

Where, the flow of coal into the furnace is,

$$m_{pf} = \frac{\rho_c}{\rho_{air}} m_{air} \frac{X_{ci}}{1 - X_{ci}} \tag{5.21}$$

and,

$$m_{air} = m_{air-in} + K_{air} I_{in} \tag{5.22}$$

The rate of change of heat energy in the mill is the difference between the overall energy available in the mill and the energy consumed in the system. The heat energy available and consumed in the system includes the heat input and output in primary air, raw coal, the moisture, the energy gained by the tempering air, energy generated due to the grinding (pulveriser frictional dissipation), heat loss from pulveriser surface, and the power delivered by the roller motor, ($Pw$), for driving the grinding bowl and the exhauster fan at the pulveriser outlet.

$$M_{mill} C_{p.mill} \frac{dT_{mill}}{dt} = \dot{Q}_{in} - \dot{Q}_{out} + \dot{Q}_{gen} - \dot{Q}_{loss} + Pw_{motor} \tag{5.23}$$

*5.2.3.2 Valves/Dampers*

Valves in the steam/water circuit and dampers in the air/flue gas ducts are derived from the orifice equation relating pressure drop to the flowrate thus:

$$\ddot{Q}_{flow} = C_D A \sqrt{2 \frac{\Delta P}{\rho}} \tag{5.24}$$

In the gPROMS® model for the valve and the damper, the relationship between the flowrate and pressure drop is expressed thus:

$$\Delta P = k_{coeff} \frac{m^2}{\rho A^2} \tag{5.25}$$

$k_{coeff}$ = the valve or damper coefficient (1/2$C_D$)

*5.2.3.3 Pumps/Fans*

The SCPP boiler feed pump is usually turbine driven. This is incorporated into the dynamic model. This will enhance the robustness of the model in carrying out full scale dynamic analysis of the whole components when integrated. The dynamic models of the pumps and the fans are described by the pump characteristic equation (head-speed-flow relation), the torque characteristic equation (power-speed-flow relation), and the dynamic coupling (moment of momentum) as described by the following equations:

From the Head-speed–flow relation,

$$\frac{\Delta P}{\rho} = a_o N^2 + a_1 N(\frac{m}{k\rho}) + a_2(\frac{m}{k\rho})^2 \quad (5.26)$$

From Power-speed-flow relation (to compute the fluid torque, Torq)

$$Torq = b_o N^2 + b_1 N(\frac{m}{k\rho}) + a_2(\frac{m}{k\rho})^2 \quad (5.27)$$

Dynamic coupling (angular momentum equation);

$$K\frac{dN}{dt} = Torq_{in} - Torq_{out} \quad (5.28)$$

*5.2.3.4 Steam/Water Separator*

The steam-water separator is an integral part of the once-through boiler especially in the circulation mode of operation. The separator is modelled as a two-phase system. The main governing equations are:

Mass Conservation:

$$\frac{d}{dt}(V_s\rho_s + V_w\rho_w) = \dot{m}_f - \dot{m}_s - \dot{m}_w \quad (5.29)$$

Where: separator volume,

$$V_f = V_s + V_w \quad (5.30)$$

Energy Conservation:

$$\frac{d}{dt}\left(V_s\rho_s h_s + V_w\rho_w h_w + \beta_m M_m c_{pm} T_m\right) = \dot{m}_f h_f - \dot{m}_s h_s - \dot{m}_w h_w \quad (5.31)$$

## 5.3 Distributed Parameter Modelling

The distributed parameter approach is a one-dimensional (1D) model describing the dynamic behaviour of the SCPP once-through boiler. The model includes 1D model of economiser tubes, lower furnace (LF) spiral waterwall tubes, upper furnace vertical waterwall tubes, the convection pass tubes, the superheaters and reheater tubes. Its derivation is based on the 1D mass, momentum, and energy balances for the evaporator waterwall tubes, the economisers, the superheaters, and the reheaters. Other components such as the boiler feed pumps and fans, the feedwater tank, the valves and damper models were developed using lumped parameter modelling approaches.

### 5.3.1 General Mass, Energy and Momentum balance

The general governing equations for a 1D flow through a tube can be expressed thus (O'Kelly, 2013):

*Conservation of mass:*

$$\frac{\partial(\rho A)}{\partial t} = -\frac{\partial \dot{m}}{\partial z} \quad (5.32)$$

$A$ is the cross-sectional area of the tube, $\dot{m}$ is the flow rate of the fluid along tube length, and $z$ is the length of tube in the boiler.

*Conservation of momentum:*

$$\frac{dp}{dz} = -\frac{dp}{dz}\Big|_{loss} - \rho\left(\frac{\partial v}{\partial t} + v\frac{\partial v}{\partial z}\right) - g\rho\sin\beta \quad (5.33)$$

$$where, \quad \frac{dp}{dz}\Big|_{loss} = \frac{1}{2}.\rho v^2 \quad (5.34)$$

*Conservation of energy:*

$$\frac{1}{A}\frac{dq}{dz} = -\frac{\partial p}{\partial z}\Big|_{loss} + \rho\left(\frac{\partial h}{\partial t} + v\frac{\partial h}{\partial z}\right) - \left(\frac{\partial p}{\partial t} + v\frac{\partial p}{\partial z}\right) \quad (5.35)$$

Heat transferred is defined by the supplementary equation:

$$\frac{dq}{dz} = \alpha_{hx} A_{hx} \left(T_f - T_{wall}\right) \quad (5.36)$$

$a_{hx}$ = heat transfer area per unit length.

*The Working fluid equation of state*:

For single-phase (i.e. for sub-cooled water and superheated steam); the temperature, pressure, and flow profile can be obtained from the solution of the conservation equations and the property estimation equations (5.37)

$$\rho = f\left[p(z), T_f(z)\right]; \qquad h = f\left[p(z), T_f(z)\right] \quad (5.37)$$

For two-phase (i.e. for water-steam two-phase mixture at low load/ start-up when the working fluid is below the critical condition); the temperature, pressure, flow profile, and the steam fraction can be obtained from the solution of the conservation equations and the property estimation equations (5.38).

$$\rho = f[p(z), T(z), x(z)]; \; h = f[p(z), T(z), x(z)] \quad (5.38)$$

### 5.3.2 Thermodynamic and Transport Property Relations

The flue gas/air and the feedwater/steam properties were estimated using Multiflash®, a commercial property package embedded in gPROMS®. However, some relations such as ($\partial\rho/\partial T$) and ($\partial\rho/\partial P$) were obtained through regression analysis on the steam table values based on the International Association of the Properties of Water and Steam (IAPWS) industrial formulation IAPWS-IF97. The data were regressed within the range of pressure and temperature anticipated in the reference SCPP design and operational data.

### 5.3.3 Component Models – Distributed Parameter Model

#### *5.3.3.1 Evaporator Loop*

In the evaporator loop model, the general conservation equations (5.32), (5.33), (5.34), and (5.35) were derived for (i) single phase and (ii) two phase flows to reflect the once-through and the circulation modes of operation in the SCPP boiler. The equations were derived in terms of pressure and specific enthalpy (See Appendix D) for ease of thermodynamic property calculations in Multiflash®. The conservation equations applied to the evaporator are therefore summarised as follows:

Mass:

$$\frac{v}{A}\frac{\partial m}{\partial z} - \frac{1}{v}\frac{\partial v}{\partial h}\frac{\partial h}{\partial t} = 0 \qquad (5.39)$$

Momentum:

$$\frac{\partial p}{\partial z} + \frac{1}{A}\frac{\partial m}{\partial t} - \left(\frac{m}{A}\right)^2 \frac{\partial v}{\partial h} = \rho\, g\, \sin\beta + \left.\frac{\partial p}{\partial z}\right|_{loss} \qquad (5.40)$$

Energy:

$$-v\frac{\partial p}{\partial t} + \frac{\partial h}{\partial t} + \frac{m}{A}v\frac{\partial h}{\partial z} = \frac{v}{A}\frac{dq}{dz} \qquad (5.41)$$

Equations (5.39) to (5.41), the heat transfer equations, the transport property relations, and the working fluid equation of states are solved numerically in gPROMS® via appropriate time and space discretisation scheme. Modelling of the two-phase flow process (at circulation and low load operation) in the evaporator requires the use of the two-phase property estimation equations (5.38) and the conservation equations (5.42), (5.43), and (5.44) for the mass, enthalpy and the pressure profiles respectively. These equations accounts for local state of the working fluid in this condition (i.e. wet steam).

*5.3.3.2 Convective Heat Exchangers*

Heat transfer in the once-through boiler is mainly by convection and radiation. Convection heat transfer occurs at between the flue gas and water/steam and the metal tubes in the boiler. Heat transfer between flue gas and the working fluid in the air preheaters, economisers, primary superheaters reheaters and the feedwater heaters etc. The model equations for these heat exchangers is developed from a combination of the conservation equations (5.42), (5.43), and (5.44), convective heat transfer equation, and the heat transfer from the metal body to and from the working fluid inside (steam/water) and outside (air/flue gas) the tube.

*5.3.3.3 Radiative Heat Exchangers*

The platen superheaters, the secondary superheaters, and the final reheaters receive heat directly from the combustion flame in the furnace through radiation. The

modelling equation makes use of the general mass, energy, and momentum balance equations (5.42), (5.43), and (5.44) respectively. The radiation heat transfer is based on Stefan Boltzmann's law for radiation as described in the lumped parameter case.

### 5.3.4 Boundary Conditions at Evaporator Inlet

The inlet boundary conditions $p_o$, $h_o$ and $m_o$ are defined by interfacing systems (O'Kelly, 2013). With these values known, using the profile of the evaporator metal temperature known from the previous time step, solution of this system of equations will give the complete profile of the evaporator fluid conditions at the $(n+1)^{th}$ time step, up to and including the last evaporator cell which defines the discharge conditions at the evaporator outlet. Table 5.3 summarises the identification of riser inlet boundary conditions for each of the two possible plant configurations, circulation loop and once-through.

Table 5.3: Boundary Conditions at the Evaporator Inlet (O'Kelly, 2013)

| Circulation mode | Description |
|---|---|
| Inlet enthalpy $h_o = h_i$ | The circulation pump discharge enthalpy |
| Inlet $m_o$ | flowrate at the evaporator tube inlet header |
| Inlet pressure $p_o = p_i$ | Water separator pressure |
| **Once-through mode** | **Description** |
| Inlet enthalpy $h_o = h_i$ | The enthalpy of the feedwater to the boiler |
| Inlet $m_o$ | The total flow into the tube, calculated as total feedwater into all the evaporator tubes |
| Inlet pressure $p_o = p_i$ | The feedwater pressure at the boiler inlet |

### 5.3.5 Numerical Solution

The distributed parameter model results in a set of partial differential and algebraic equations (PDAEs) describing the mass, momentum and energy balances. The resulting PDAEs were solved by the SRADAU solver in gPROMS®. The axial variables were discretized using the method of centred finite differences (CFDM) on finite elements over a uniform grid. All the simulations were performed at a time step of 0.5s

and spatial steps of 1m. The lumped parameter uses the default gPROMS® solver for handling the ODEs, and the simulation was performed at a time step of 5s.

## 5.4 Modelling the Once-through Boiler Modes of Operation

The model of the SCPP once-through boiler considers both the circulation (i.e. low load/start-up operation) and once-through mode of operation. From modelling perspective, the switch from circulation mode to the once-through mode is implemented once the post dry-out condition is reached. Figure 5.77 shows a schematic diagram of a typical SCPP showing the circulation systems.

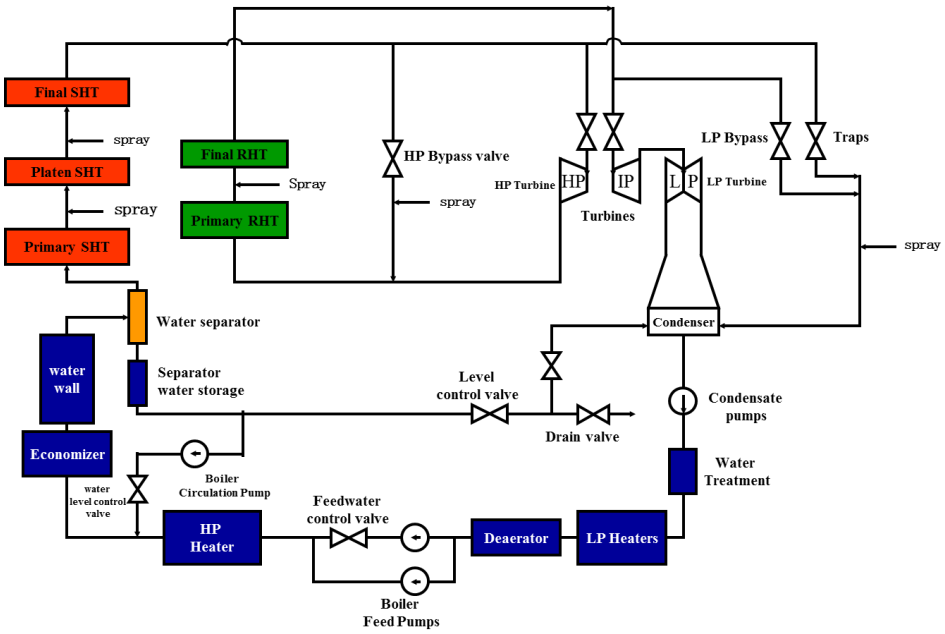


Figure 5.7: The SCPP Boiler Circulation System

The once-through mode of operation is depicted in Figure 5.88. In this mode of operation, there is no need for steam/water separation as the working fluid property is above its critical state.

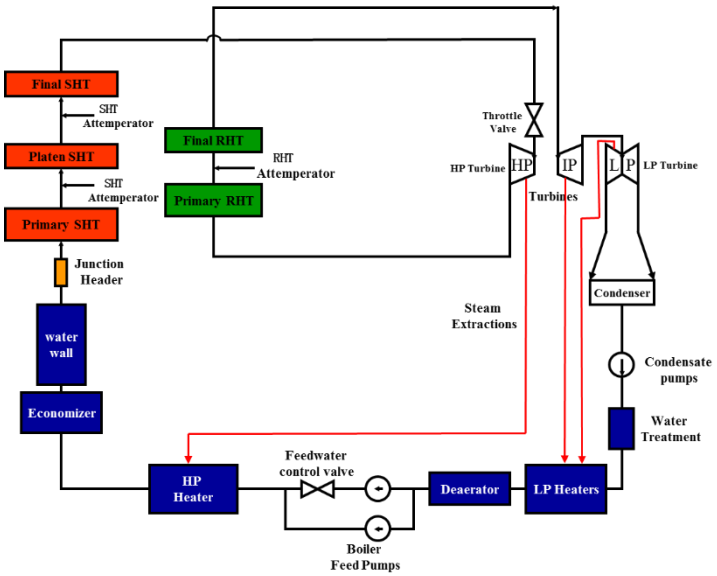


Figure 5.8: The SCPP Once-through System

Table 5.4 also shows the unit responsible for controlling the feedwater, the pressure, and the circulation flow etc. in both the circulation and once-through modes of operation.

Table 5.4: Modes of operation from modelling perspective (O'Kelly, 2013)

| Parameter | Circulation Mode | Once-through |
|---|---|---|
| Pressure | Water separator | Boiler Feed Pump |
| Circulation | Forced | Forced |
| Feedwater | Waterwall | waterwall |
| Waterwall flow | Circulation + feedwater | Feedwater |

### 5.4.2 Circulation Mode of Operation

The circulation (usually at low load or start-up) mode of operation lies within less than 35-40% of full load (Dong and Tingkuan, 2001) or some pre-determined steam pressure around 12-14MPa (O'Kelly, 2013). The model equations consist of the general conservation equations (5.32)-(5.36), the equations of state (5.38) for the working fluid at sub-cooled condition, water-steam two-phase mixture, and superheated steam. Also, an integral part of this mode of operation is the steam-water separation modelled as a two-phase separator (Dong and Tingkuan, 2001).

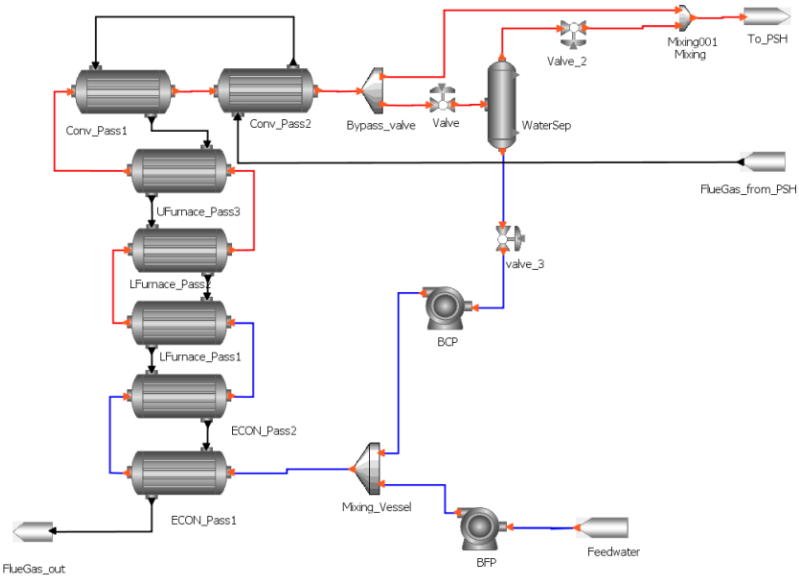


Figure 5.9: Evaporator Circuit of Once-through boiler (Circulation mode)

This mode of operation lies within less than 35-40% of full load (Dong and Tingkuan, 2001) or some pre-determined steam pressure around 12-14MPa (O'Kelly, 2013). Figure 5.99 shows the gPROMS® model topology of the evaporator section of the once-through boiler during circulation mode of operation.

### 5.4.3 Once-through Mode of Operation

In the once-through mode of operation, typically at above 40% of full load, the water separator is dry, hence no two-phase separation is necessary.

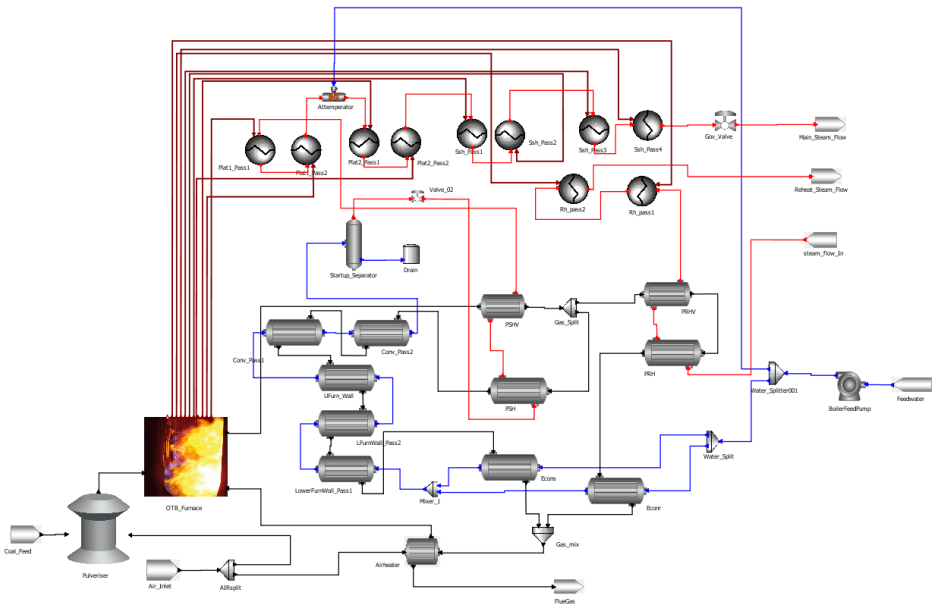

Figure 5.10: Once-through mode of Operation of SCPP once-through boiler

From the model point, the water separator serves as junction header between the evaporators and the superheaters in this mode of operation. The general modelling equations are equations (5.32) – (5.36) and (5.37) for the state equation of steam. Figure 5.1010 shows the gPROMS® model topology for the SCPP once-through mode of operation.

## 5.5 Discussion of Results

### 5.5.1 Steady State Validation

*5.5.1.1 Lumped Parameter Model*

The lumped parameter model of the SCPP boiler components were validated using steady state design data from the reference 600MWe SCPP boiler described in section 5.1 (at 100% MCR). Table 5.5shows a summary of the steady state validation results for some of the key variables of the SCPP component models.

Table 5.5: Steady state validation of the Lumped Parameter

| Parameters | Lumped Model | Reference Plant | Absolute Relative error (%) |
|---|---|---|---|
| Economiser feedwater flow (kg/s) | 516.94 | 523.8 | 1.31 |
| Economiser outlet Temperature ($^oC$) | 317.79 | 325.8 | 2.46 |
| Economiser inlet pressure (MPa) | 29.36 | 29.72 | 1.22 |
| LF spiral waterwall steam Temp ($^oC$) | 413.63 | 418.6 | 1.19 |
| UF vertical waterwall steam Temp ($^oC$) | 422.38 | 431.4 | 2.09 |
| Steam pressure (MPa) | 27.23 | 27.65 | 1.51 |
| Separator pressure (MPa) | 25.07 | 25.48 | 1.62 |

*5.5.1.2 Distributed Parameter Model*

The lumped parameter model of the SCPP boiler components were validated using steady state design data from the reference 600MWe SCPP boiler described in section 5.1 (at 100% MCR). Table 5.6 shows a summary of the steady state validation results for some of the key variables of the SCPP component models.

Table 5.6: Steady state validation of the Distributed Parameter Model

| Parameters | Distributed Model | Reference Plant | Absolute Relative error (%) |
|---|---|---|---|
| Econ feedwater flow (kg/s) | 522.02 | 523.8 | 0.34 |
| Economiser outlet Temperature (°C) | 327.49 | 325.8 | -0.52 |
| Economiser inlet pressure (MPa) | 29.58 | 29.72 | 0.47 |
| LF spiral waterwall steam Temp (°C) | 421.15 | 418.6 | -0.61 |
| UF vertical waterwall steam Temp (°C) | 434.98 | 431.4 | -0.83 |
| Steam pressure (MPa) | 27.54 | 27.65 | 0.39 |
| separator pressure (MPa) | 25.26 | 25.48 | 0.85 |

### 5.5.2 Comparison of the Lumped and the Distributed Parameter Models

The performance of the 1D and the lumped parameter model of the once-through boiler were validated and compared against that of the reference 600 MWe SCPP. The primary interest of the supercritical once-through boiler modes of operation is to accurately predict the temperature profile of the working fluid, the circulation flowrate, the relative fraction of water & steam in the evaporator tubes, and the steam generation rate. Figure 5.1111(a) and Figure 5.1111(b) shows the steam quality of the modelled boiler in the once-through and circulation mode of operation respectively.

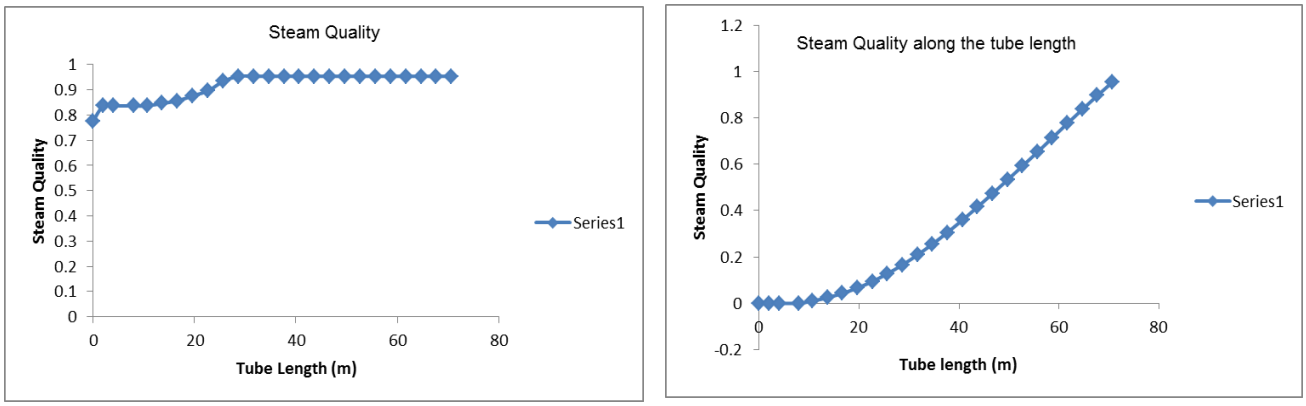


(a) (b)

Figure 5.11: Steam Quality in the SCPP once-through boiler

The models were simulated at 50%, 75%, and 87% BMCR. The model prediction were compared with the plant data for the steam temperature, pressure and total

flowrate of feedwater at the economizer inlet. Table 5.7, Table 5.8, and**Error! eference source not found.**Table 5.9 show the results of the comparison of the model calculated values and the reference plant measurement for the main parameters of the steam generator at 87% BMCR, 75% BMCR and 50% BMCR respectively.

From Table 5.7 (i.e. 87% BMCR), the results show that the distributed model has a relative error of less than 1% for the calculated steam temperature at the lower furnace (LF) and upper furnace (UF) section of the evaporator. The relative error in predicting the steam temperature for the lumped model is however above 2%. The steam pressure prediction also show a relative error of about 3.5% and 7% for the distributed and the lumped model respectively.

Table 5.7: Model Validation at 87% BMCR

| Parameters | Reference Plant (87% BMCR) | Distributed Model | Rel. error (%) | Lumped Model | Rel. error (%) |
|---|---|---|---|---|---|
| Econ feedwater flow (kg/s) | 470.8 | 468.50 | 0.49 | 465.18 | 1.19 |
| Econ outlet Tempe ($^{o}$C) | 324.3 | 322.52 | 0.55 | 318.46 | 1.80 |
| Econ inlet pressure (MPa) | 28.36 | 28.05 | 1.09 | 27.92 | 1.55 |
| LF steam Temp ($^{o}$C) | 407.8 | 406.11 | 0.41 | 398.84 | 2.20 |
| UF steam Temp ($^{o}$C) | 417.5 | 415.92 | 0.38 | 409.03 | 2.03 |
| Steam pressure (MPa) | 25.74 | 24.85 | 3.45 | 23.86 | 7.30 |
| separator pressure (MPa) | 26.47 | 25.17 | 4.91 | 24.19 | 8.61 |

From Table 5.8 (i.e. 75% BMCR), the results show that the distributed model has a relative error of about 0.8% for the calculated steam temperature at the lower (LF) and upper furnace (UF) section of the evaporator. The relative error in predicting the steam temperature for the lumped model is about 2%. The steam pressure prediction also show a relative error of about 3.5% and 7% for the distributed and the lumped model respectively.

Table 5.8: Model Validation at 75% BMCR

| Parameters | Reference Plant (75% BMCR) | Distributed Model | Rel. error (%) | Lumped Model | Rel. error (%) |
|---|---|---|---|---|---|
| Econ feedwater flow (kg/s) | 393.42 | 392.78 | 0.16 | 389.58 | 0.98 |
| Econ outlet Temp ($^oC$) | 316.0 | 314.83 | 0.37 | 374.80 | 313.06 |
| Econ inlet pressure (MPa) | 23.74 | 23.51 | 0.97 | 22.86 | 3.71 |
| LF steam Temp ($^oC$) | 397.9 | 395.03 | 0.72 | 391.15 | 1.70 |
| UF steam Temp ($^oC$) | 409.8 | 406.64 | 0.77 | 401.96 | 1.91 |
| Steam pressure (MPa) | 21.55 | 20.86 | 3.20 | 19.74 | 8.40 |
| separator pressure (MPa) | 22.77 | 21.48 | 5.66 | 20.81 | 8.61 |

From Table 5.9 (i.e. 50% BMCR), the results show that the distributed model has a relative error of about 1.0% for the calculated steam temperature at the lower (LF) and upper furnace (UF) section of the evaporator. The relative error in predicting the steam temperature for the lumped model is about 1.7%. The steam pressure prediction also show a relative error of about 3.2% and 8.4% for the distributed and the lumped model respectively.

Table 5.9: Model Validation at 50% BMCR

| Parameters | Reference Plant (50% BMCR) | Distributed Model | Rel. error (%) | Lumped Model | Rel. error (%) |
|---|---|---|---|---|---|
| Econ feedwater flow (kg/s) | 262.72 | 261.55 | 0.45 | 256.81 | 2.25 |
| Econ outlet Temp ($^oC$) | 301.6 | 300.39 | 0.40 | 298.13 | 1.15 |
| Econ inlet pressure (MPa) | 18.83 | 18.41 | 2.23 | 17.28 | 8.23 |
| LF steam Temp ($^oC$) | 375.47 | 371.86 | 0.96 | 364.17 | 1.68 |
| UF steam Temp ($^oC$) | 381.3 | 377.51 | 0.99 | 375.03 | 1.64 |
| Outlet steam pressure (MPa) | 16.83 | 16.52 | 1.84 | 15.93 | 5.35 |
| separator pressure (MPa) | 17.52 | 17.18 | 1.94 | 16.47 | 5.99 |

The results reflect the accuracy of the distributed model over the lumped parameter approach. The reason for the difference in accuracy is due to the spatial variation of the variables of interest (i.e. temperature, pressure, and flowrate) that was included in the model equation. As shown in Figure 5.122, the heat flux distributions in the furnace waterwall were used in computing the change in temperature across the length of the tube. The lumped parameter model can only predict the dynamics of the steam temperature without consideration of its axial variation along the evaporator tubes.

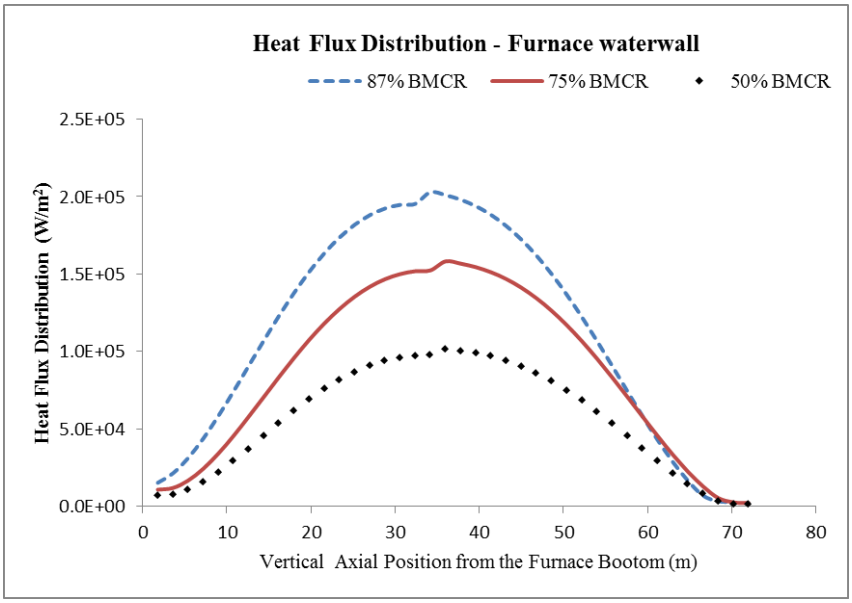


Figure 5.12: Heat Flux Calculation from the 1D Model

Figure 5.133 shows a comparison of simulation results of the lumped and distributed models with the reference plant data, for steam temperature at the upper water wall section of the evaporator at 87% BMCR. It can be seen from the figure that the distributed parameter model shows a more accurate prediction of the reference plant.

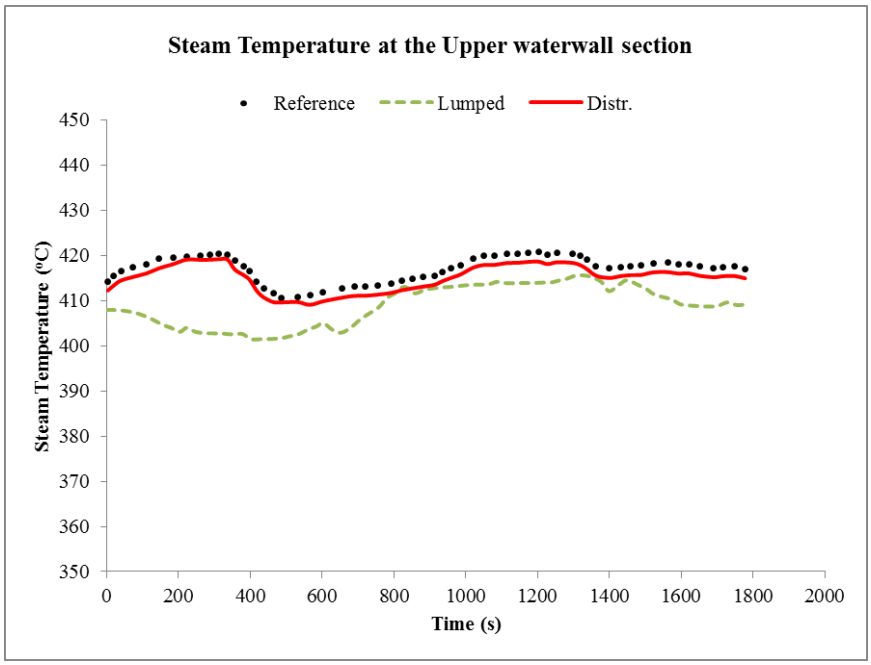


Figure 5.13: Comparison of steam temperature at 87% BMCR

## 5.6 Summary

This chapter presents a dynamic model and comparison of the lumped parameter and distributed parameter modelling approaches for SCPP once-through boiler steam generation process. The models were developed from the mass, momentum, and energy conservation principles. The simulation results show that in the distributed parameter model, the relative errors in predicting the outlet steam temperature and pressure of the evaporator waterwall were less than 1% and 5% respectively at 87% BMCR (boiler maximum continuous rating), 75% BMCR, and 50% BMCR. The lumped parameter model on the other hand, shows average relative error of 2% and 7% for steam temperature and pressures respectively at all the simulated cases. The study shows that a distributed parameter model gives a more accurate prediction of the SCPP boiler dynamics at different load levels and will be more reliable to investigate transient behaviour under very stringent scenarios. The lumped parameter however is also useful for model-based control studies due to its simplicity and reasonable accuracy. The distributed parameter model developed in this chapter will be used in investigating the response of the whole SCPP under varying load and frequency changes.

# Chapter 6 Dynamic Modelling and Operational Analysis of SCPP under UK Grid Requirement

## 6.1 Introduction

This section describes the modelling of the whole SCPP using the 1D model of the once-through boiler developed in Chapter 5, and combining it with the models of the steam turbines, the electric generator, and the feedwater and condensate subsystems developed in this section.

## 6.2 Description of the Reference (600MWe) SCPP

The reference SCPP studied is 600MWe installed capacity at 100% BMCR operated by Ligang Power and located in Jiangsu Province, China. A detailed description of the reference SCPP once-through boiler has already been presented in Chapter 5 of this thesis and is not repeated here. The Ligang power plant is made up of three units of 350 MWe subcritical units (i.e. units #1, #2, and #3) and four units of 600 MWe supercritical units (units #4, #5, #6, and #7). The unit #5 was the reference unit selected as the source of model parameters and validation data. The reference unit #5 is capable of generating 1800 t/h of steam at rated conditions of 24.5 MPa and 537$^{o}$C. The steam is reheated by a single stage reheater to about 540$^{o}$C. The regenerative feedwater heating in both open (i.e. the deaerator) and closed feedwater heaters uses steam extracted from various stages of the HP, IP, and LP turbines. The reference unit has 6 vertical-spindle type pulverisers. The furnace has 24 burners, and burns approximately 201 tonnes of pulverised coal per hour.

This reference SCPP unit is selected for the model development, validation, and analysis for the following reasons: (i) due to its similarity with a typical UK power plant operating under a system frequency of 50 Hz, (ii) absence of any operational SCPP in the UK electricity market.

## 6.3 Dynamic model of the whole SCPP

The dynamic modelling of the whole SCPP is achieved by coupling the 1D model developed for the once-through mode of operation of the boiler, the modelling of the

steam turbines, the condensate and feedwater heating systems, the governing systems, and the electric generator models. The model is based on the 600 MWe SCPP used for the boiler model.

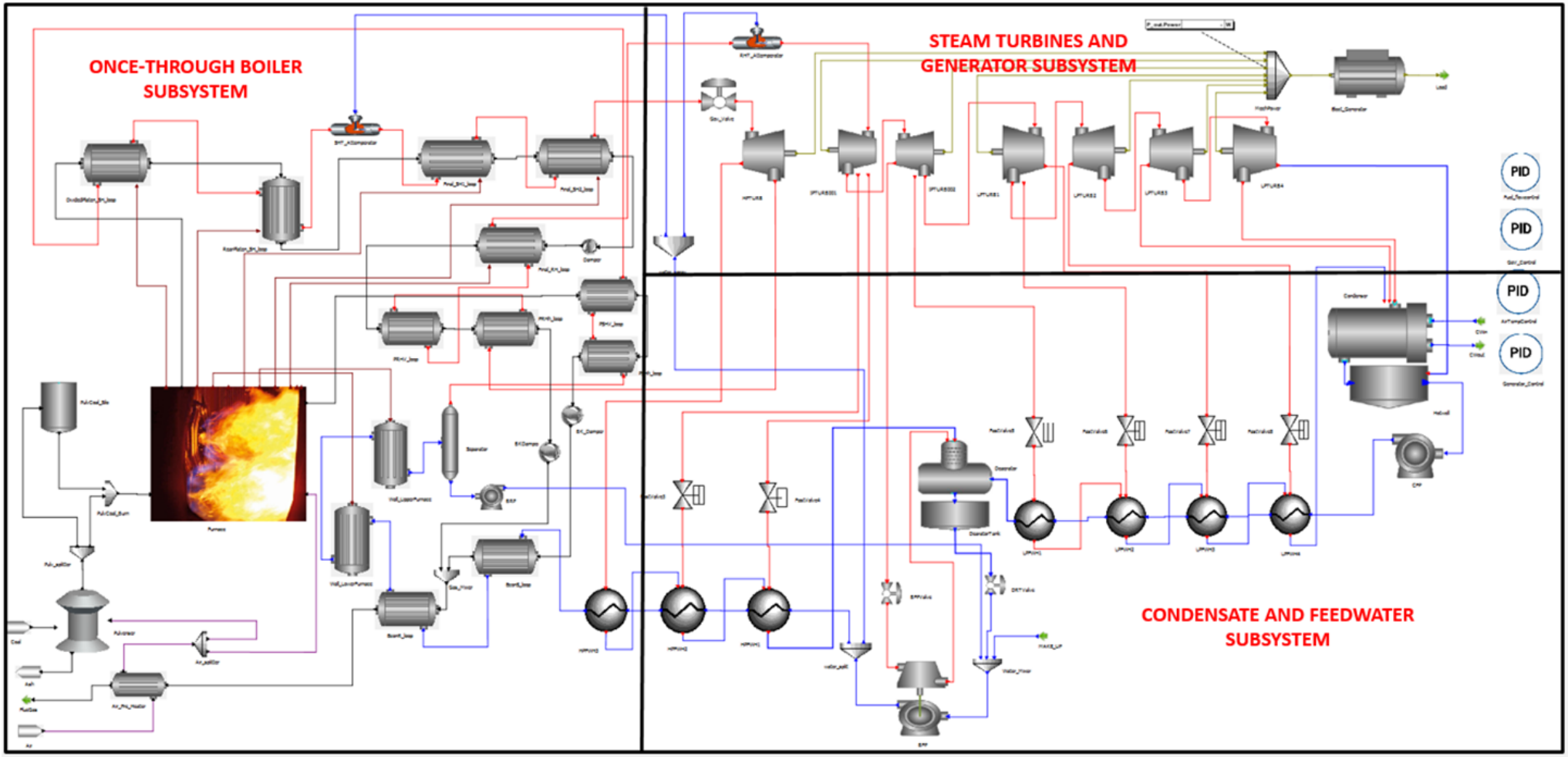


Figure 6.1: Topology of the Whole SCPP Dynamic Model developed in gPROMS®

### 6.3.1 Once-through Boiler Model

One of the intended uses of the SCPP model was to predict the power plant behaviour when operated under a typical UK grid code challenges such as rapid load demand changes and variations in system frequency resulting from imbalance between the power generated and the system load. Hence, detailed representations of the water/ steam and air/flue gas side components and process models developed in chapter 5 of this thesis were included in the whole SCPP boiler-turbine-generator model. Figure 6.1 shows the gPROMS® model topology of the whole SCPP coupled model.

### 6.3.2 Steam Turbines Model

The steam turbine model was obtained using the Stodola ellipse expressed in terms of specific volume shown in Equations (6.1) and (6.2). This form of Stodola ellipse is valid for all cases of compressible fluid compared to the form expressed in terms of temperature which is only valid when the perfect gas law ($Pv = RT$) holds. Considering the rapid response capability of the steam turbine compared to the boiler, steady state models are used for the steam turbine. The HP and IP turbine stages were computed from the inlet steam conditions.

$$\dot{m}_{in} = \frac{K_{trb}}{\sqrt{v_{in}}}\sqrt{\frac{{P_{in}}^2 - {P_{out}}^2}{P_{in}}} \tag{6.1}$$

$$\frac{T_{out}}{T_{in}} = \left(\frac{P_{out}}{P_{in}}\right)^{\left(\frac{\gamma-1}{\gamma}\right)} \tag{6.2}$$

### 6.3.3 Other Component Models

*6.2.3.1 Pulverisers*

The governing equation for the pulveriser model has already been described in section 5.2.3.1 of Chapter 5.

*6.3.3.2 Pumps/Fans*

The general governing equation for the boiler feed pump and the fan models have been presented in section 5.2.3.3 of Chapter 5. Equations (6.3) and (6.4) shows the actual modelling equation used for the turbine-driven boiler feed pump. Due to lack of

actual/design pump curve of the reference SCPP, the constant parameters $K_0, K_1$ and $K_2$ used in this study were adjusted from the values obtained in Masada (1979) to match the actual reference plant data.

The modelling equations are presented thus:

$$0.1047K_{fptrb}\frac{dN_{bfp}}{dt} = Torq_{trb} - Torq_{bfp} \tag{6.3}$$

$$P_{bfp} - (P_{Dtorout} + g\rho Z) = K_0\rho(0.1047N_{bfp})^2 + K_1\dot{m}_{bfp}(0.1047N_{bfp}) + \frac{K_2\dot{m}_{bfp}{}^2}{\rho} \tag{6.4}$$

The constants $K_0, K_1$ and $K_2$ are derived from the pump characteristic equation (Masada, 1979). In this thesis, the original values of the parameters obtained from Masada (1979) were adjusted to match actual data.

*6.3.3.3 Deaerator*

The modelling equations for the deaerator is similar to those used for describing the separator in the once-through boiler model. The deaerator is assumed to be at saturated condition with the control of the water level, the steam and water flowrate into it. From the modelling point, the deaerator is made up of two sections, the de-aerating section (the deaerator head tank) and the storage tank (O'Kelly, 2013). Figure 6.2 shows a process schematics of the deaerator head tank and the storage tank.

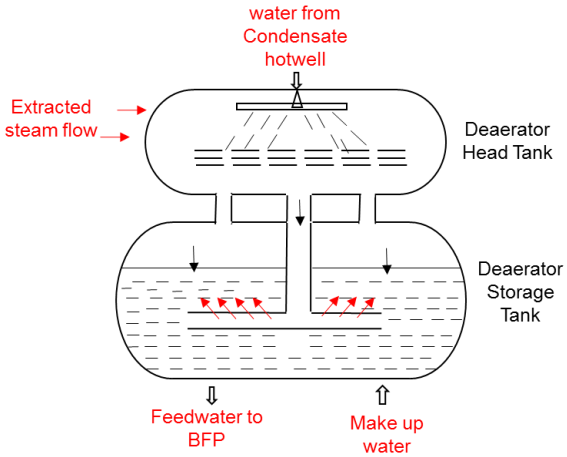


Figure 6.2: Process Schematics of the Deaerator Configuration

The equations describing the phenomenon in the deaerator is represented by the mass and energy conservation equations for water and steam in equilibrium. The main equations in the deaerator are given thus:

$$\frac{dM}{dt} = m_{in} - m_{out} = m_{cond} + m_{stm} - m_{bfp\_out} \tag{6.5}$$

Equation (6.5) can be expressed terms of the steam and water fractions thus:

$$\frac{d}{dt}(\rho_{stm}V_{stm} + \rho_{water}V_{water}) = m_{cond} + m_{stm} - m_{bfp\_out} \tag{6.6}$$

Where, $V_{steam} = V_{tank} - V_{water}$ (6.7)

The energy conservation:

$$\frac{d}{dt}(\rho_{stm}V_{stm}U + \rho_{water}V_{water}U) = m_{cond}H_{cond} + m_{stm}h_{stm} - m_{bfp\_out}h_{bfp} \tag{6.8}$$

*6.3.3.4 Feedwater Heaters*

The feedwater heaters are important for improving the overall efficiency of the SCPP unit. They are design to preheat the boiler feedwater by means of condensing steam extracted ("bled") from a steam turbine (O'Kelly, 2013). The heat transfers in the feedwater heating trains was estimated using the bled steam flow and the drop in enthalpy to saturation condition. The main governing equation in the feedwater heaters are similar to the convective heat exchanger models developed in Chapter 5. The mass conservation equation assumes no accumulation. The energy conservation and the heat transfer equations are presented thus:

$$M_s\frac{dh_s}{dt} = m_{ext}h_{ext} - m_{fout}h_{fout} + m_{fin}h_{fin} - q_s \tag{6.9}$$

Where $M_s = {}^{V_s}/_{v_s}$

$$q_s = A_s\alpha_s\Delta T_{lmtd} \tag{6.10}$$

$$\Delta T_{lmtd} = \frac{\Delta T_2 - \Delta T_1}{\ln\left[\frac{\Delta T_2}{\Delta T_1}\right]}, \quad \Delta T_2 = T_{ext} - T_{fin}, \quad \Delta T_1 = T_{extout} - T_{fwout} \tag{6.11}$$

*6.3.3.5 Condenser and Condensate Hotwell*

A water cooled condenser was selected Performance of condenser as measured by the pressure of steam in the condenser is an important parameter in the optimisation

of economic performance of the plant (O'Kelly, 2013). In this study, only latent heat exchange between the cooling water and the condensing steam is considered in the condenser. Sub-cooling in the condenser is therefore neglected. Steady state conditions were assumed on the steam side. Dynamic conservation equations were applied in the cooling water side. Huge volume of cooling water compared to condensing steam makes this decision sensible. The condensate hotwell was modelled separately as a holding tank using the following mass and energy conservation equations:

Conservation of Mass:

$$\rho A \frac{dl}{dt} = \dot{m}_{in} - \dot{m}_{out} \tag{6.12}$$

The variables $l, A \text{ and } \dot{m}$ are the height of condensate in the hotwell, the cross – sectional area, and the flowrate of condensate in and out of the tank.

Conservation of Energy:

$$\rho A l \frac{dh_{out}}{dt} = \dot{m}_{in} h_{in} - \dot{m}_{out} h_{out} \tag{6.13}$$

*6.3.3.6 Governing System*

The governor systems are the main controllers responsible for frequency regulation of local generation units. The turbine governing method is assumed to be throttle governing and it involves only one governor valve. The valve regulates steam flow to the turbine and consequently the turbine load changes. The key equation in the governor valve model is as follows:

$$m_{in}{}^2 = K_{vf}{}^2 \nu_{in} (P_{in} - P_{out}) \tag{6.14}$$

*6.3.3.7 Electric Generator*

In the electric generator, the mechanical energy gained by the turbine is used to drive the rotor of the generator to a constant speed. The mechanical rotation of the rotor and the coupling magnetic field from the exciter induces the voltage in the winding of the stator (Faraday's Law). When connected to the grid, the current passes through the stator winding. The generator model is coupled to the turbine by the mechanical power and the torque-balance equation to reflect the interaction between the turbine

and the generator dynamics. The main equations in the generator model are as follows:

$$\frac{d\delta}{dt} = \quad 2\pi(f - f_0) \tag{6.15}$$

$$2\pi . J . \frac{df}{dt} = \quad P_{mech} - P_{aux} - P_{elect} - \ 2\pi f D \tag{6.16}$$

$$P_{elect} = p_{factor} . P_{mech} \tag{6.17}$$

Where the variables $\delta, f, f_0, D, P_{mech}, P_{elect}, P_{aux} \ and \ p_{factor}$ are the rotor angle of the generator, the system frequency, the reference frequency, the damping coefficient, the mechanical power from turbine, the electric generator output power, and the power factor respectively.

## 6.4 SCPP Control Loops

The main control modes of operation in power plants are boiler following, turbine following or co-ordinated control (a combination of both boiler and turbine following mode). Depending on whether the power plant place more priority on maintain load-frequency demand at the expense of deviations in steam conditions or vice versa, each control mode of operation has its advantages, and disadvantages. Most SCPP control are based on the co-ordinated control model because it combines the rapid initial response of the boiler following mode and the steady load change and stability advantages of the turbine following mode. Figure 6.3 shows a schematic of the structure of a co-ordinated control of a typical SCPP.

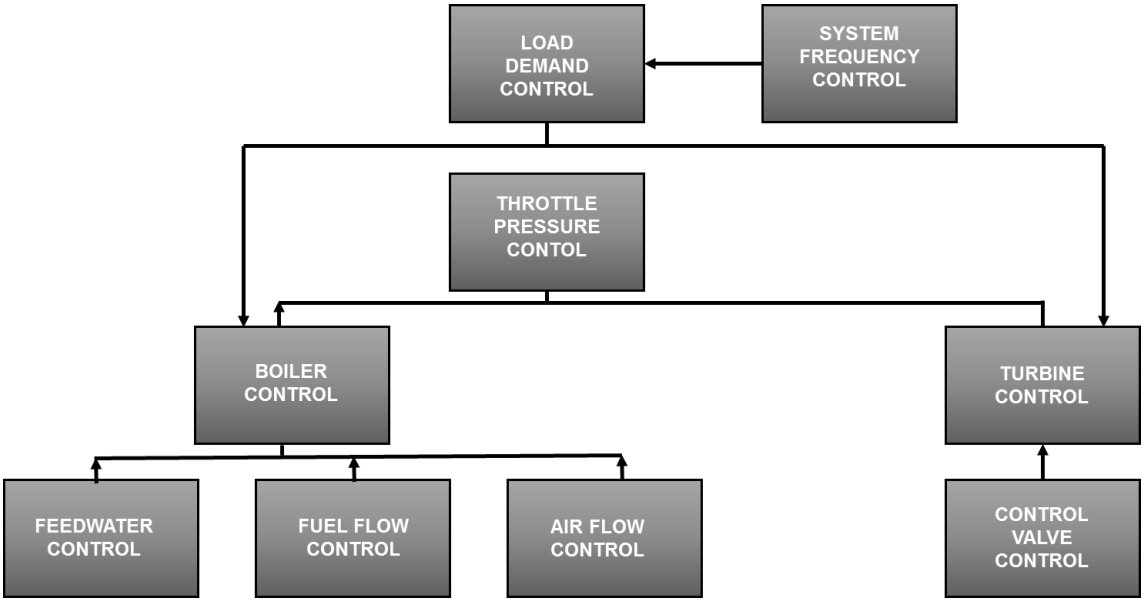


Figure 6.3: Co-ordinated Control System for a SCPP

In this study, the interest was not necessarily to reproduce the actual unit control loops in the reference 600MWe SCPP or to provide detailed design of the controllers. However, basic control loops, namely main steam temperature, reheat steam temperature, power output, and load frequency controls based on the co-ordinated control modes of operation have been included in the model. These control loops are necessary to generate power at the desired rate and level while keeping the steam pressure and temperature at the proper operating conditions, and for load change analysis to be carried out using the model. Default PI controllers in gPROMS Model Builder® were therefore used with their settings manually adjusted to suit the model.

### 6.4.1 Feedwater flow and Heat Input (Fuel/Air)

A proper relationship between the heat input and the feedwater flow is used to control the main steam temperature. Boiler over-or under firing during transience can cause deviation from the set points, and hence the use of water attemperator.

### 6.4.2 Main steam temperature Attemperator

The main steam temperature is controlled using spray water attemperators. This involves mixing the steam in-between the superheater banks with controlled flow of spray water taken from the boiler feed pump discharge to achieve desired temperature. Due to small storage volume of the attemperators, the dynamics are neglected and steady state flow equations are used (Flynn, 1999):

$$\dot{m}_{s,in} + \dot{m}_{att} = \dot{m}_{s,out} \quad (6.18)$$

$$\dot{m}_{s,in} h_{s,in} + \dot{m}_{att} h_{att} = \dot{m}_{s,out} h_{s,out} \quad (6.19)$$

### 6.4.3 Reheat steam temperature Attemperator

The reheat steam temperature is controlled using rear gas pass biasing damper. This involves controlling the flow of flue gas along the divided rear pass between the superheater and the reheater. The dynamics of the rear pass divide are similarly neglected. Consequently, the following steady state flow equations were used:

$$\dot{m}_{gas} = \dot{m}_{spter,gas} + \dot{m}_{rhter,gas} \quad (6.20)$$

$$\dot{m}_{gas} h_{gas} = \dot{m}_{spter,gas} h_{spter,gas} + \dot{m}_{rhter,gas} h_{rhter,gas} \quad (6.21)$$

### 6.4.4 Feedwater Flow and Governing Valve Position

In the SCPP model, the throttle pressure is controlled by proper relationship between the control valve and the boiler feed pump speed (BFP). Given the BFP speed, the governing valve position is set to yield the 24.2 MPa throttle pressure (set point) in the reference SCPP.

### 6.4.5 Deaerator Water Level Control

The Deaerator level control makes adequate feedwater available for the BFP by ensuring the water level remains at a particular level (set point) in the deaerator storage tank.

### 6.4.6 Power output

Control of the power output is needed to simulate changes in load in a manner similar to load changes in the real plant. The target power output is controlled through manipulation of fuel burn rate, the feedwater flow, and the governor valve. The target power plant output is directly controlled by the governor valve; this target also sets the steam pressure which is controlled by the feedwater flow rate.

### 6.4.7 Load–Frequency Control

Most power plant units are under load frequency control from a dispatch control centre (e.g. the National Grid Control Centre, UK). The primary frequency control is assigned

to the turbine control speed governor. When there is change in system frequency, the governor valve moves quickly to provide a short-term response to the frequency change (using the increased valve position and flow, though at reduced pressure).

## 6.5 Steady State Validation of the Whole SCPP

For a model to be considered accurate, it should be able to predict steady state values of variables of interest at different operating levels (or load). The sources of the reference plant data used for this steady state validation was from the plant's heat balance/design data and the operating plant's performance charts at three load levels (50%, 75% and 100% MCR). The data is made up of the thermodynamic and flow profiles (i.e. temperature, pressure, and flowrate) of the water and steam circuits. The data flue gas circuit is only available partially due to measurement difficulty.

For the steady state validation at full load (100% MCR), the model was simulated with the governor valve fully opened and the pulverised fuel flow was 56 kg/s. Key performance variables (i.e. pressure, temperature, and flow) of the SCPP model are then compared with plant measurements taken at the same load level (Table 6.1). Also, the predictions at 75% MCR, and 50% MCR were also compared to plant measurements taken at similar conditions. Table 6.2 and Table 6.3 show a summary of the main parameters of the plant in comparison with the gPROMS® model at these load levels. This comparison is important to determine the model capability and robustness at wide range of load level. The model parameters were kept constant for the different load levels compared. The validation results of the steady state validation show the model predicts the plant measurements with less than 4% average absolute relative error for the three load levels considered. Considering the inherent errors in plant measurements due to measuring devices, the model predictions can be considered acceptable with reasonable accuracy.

Table 6.1: Steady State Validation of SCPP Model at 100% MCR

| Parameter | Plant Data | gPROMS® Model | Relative error (%) |
|---|---|---|---|
| Load (MWe) | 600.0 | 604.44 | -0.32 |
| Main Steam flowrate (kg/s) | 514.0 | 515.78 | 0.37 |
| Reheat Steam Flow (kg/s) | 429.27 | 431.10 | 1.28 |
| Boiler Feed pump flow (kg/s) | 530.1 | 526.8 | 0.63 |
| Total Coal flow (kg/s) | 56.0 | 55.76 | 0.44 |
| Total Air flow (kg/s) | 537.6 | 537.6 | - |
| Main Steam Temperature ($^oC$) | 538.0 | 540.32 | -0.43 |
| Primary Superheater Outlet Temperature ($^oC$) | 475.0 | 478.57 | -0.75 |
| Reheat Outlet Temperature ($^oC$) | 538.0 | 541.60 | -0.67 |
| HP Turbine outlet Temperature ($^oC$) | 293.9 | 290.49 | 1.16 |
| Economiser Outlet Temperature ($^oC$) | 325.8 | 327.11 | -0.40 |
| Feedwater Tank Pressure (MPa) | 0.91 | 0.91 | - |
| Boiler feed pump outlet pressure (MPa) | 30.6 | 29.86 | 2.41 |
| Economiser outlet Pressure (MPa) | 28.85 | 28.67 | 0.62 |
| Primary Superheater Outlet Pressure (MPa) | 26.92 | 27.18 | -0.97 |
| Secondary Superheater Outlet Pressure (MPa) | 25.80 | 25.57 | 0.91 |
| Throttle Pressure (MPa) | 24.2 | 24.74 | -2.23 |
| HP Turbine outlet Pressure (MPa) | 4.43 | 4.58 | -0.59 |
| Make-up water rate (%) | 3.0 | 3.0 | - |

Table 6.2: Steady State Validation of SCPP Model at 75% MCR

| Parameter | Plant Data | gPROMS® Model | Relative error (%) |
|---|---|---|---|
| Load (MWe) | 450.0 | 452.6 | -0.58 |
| Main Steam flowrate (kg/s) | 390.5 | 387.6 | 0.74 |
| Reheat Steam Flow (kg/s) | 327.0 | 324.15 | 0.87 |
| Boiler Feed pump flow (kg/s) | 402.58 | 399.86 | 0.67 |
| Total Coal flow (kg/s) | 46.5 | 46.20 | 0.64 |
| Total Air flow (kg/s) | 446.4 | 449.57 | -0.71 |
| Main Steam Temperature ($^oC$) | 537.8 | 540.65 | -0.53 |
| Primary Superheater Outlet Temperature ($^oC$) | 426.5 | 429.44 | -0.69 |
| Reheat Outlet Temperature ($^oC$) | 533.5 | 539.10 | -1.05 |
| HP Turbine outlet Temperature ($^oC$) | 282.8 | 285.54 | -0.97 |
| Economiser outlet Temperature ($^oC$) | 316.0 | 319.82 | -1.21 |
| Feedwater Tank Pressure (MPa) | 0.65 | 0.602 | -0.38 |
| Boiler feed pump outlet pressure (MPa) | 23.74 | 23.42 | 1.35 |
| Economiser outlet Pressure(MPa) | 23.66 | 23.39 | 1.14 |
| Primary Superheater Outlet Pressure(MPa) | 21.26 | 21.41 | -0.73 |
| Secondary Superheater Outlet Pressure(MPa) | 20.42 | 20.21 | 1.05 |
| Throttle Pressure (MPa) | 19.25 | 19.30 | -0.27 |
| HP Turbine outlet Pressure (MPa) | 3.48 | 3.46 | 0.63 |
| Make-up water rate (%) | 3.0 | 3.0 | - |

Table 6.3: Steady State Validation of SCPP Dynamic Model at 50% MCR

| Parameter | Plant Data | gPROMS® Model | Relative error (%) |
|---|---|---|---|
| Load (MWe) | 300 | 301.47 | -0.49 |
| Main Steam flowrate (kg/s) | 262.5 | 265.03 | -0.96 |
| Reheat Steam Flow (kg/s) | 219.6 | 221.11 | -0.69 |
| Boiler Feed pump flow (kg/s) | 270.2 | 268.85 | 0.50 |
| Total Coal flow (kg/s) | 33.0 | 33.45 | -1.36 |
| Total Air flow (kg/s) | 274.3 | 276.60 | -0.84 |
| Main Steam Temperature ($^oC$) | 537.8 | 539.65 | -0.34 |
| Primary Superheater Outlet Temperature ($^oC$) | 424.2 | 426.47 | -0.54 |
| Reheat Outlet Temperature ($^oC$) | 528.6 | 531.03 | -0.46 |
| HP Turbine outlet Temperature ($^oC$) | 270.5 | 271.68 | -0.44 |
| Economiser outlet Temperature ($^oC$) | 301.6 | 297.84 | 1.24 |
| Feedwater Tank Pressure (MPa) | 0.42 | 0.42 | - |
| Boiler feed pump outlet pressure (MPa) | 18.83 | 18.48 | 1.86 |
| Economiser outlet Pressure(MPa) | 18.75 | 18.41 | 1.79 |
| Primary Superheater Outlet Pressure(MPa) | 17.29 | 17.49 | -1.13 |
| Secondary Superheater Outlet Pressure(MPa) | 16.73 | 16.56 | 1.04 |
| Throttle Pressure (MPa) | 15.93 | 16.22 | -1.84 |
| HP Turbine outlet Pressure (MPa) | 2.34 | 2.32 | 0.78 |
| Make-up water rate (%) | 3.0 | 3.0 | - |

## 6.6 Dynamic Validation and Analysis

Dynamic validation is important for establishing some basis for the capability of the model and to be able to demonstrate capability for predicting plant behaviour over time especially during periods when changes in load (i.e. ramping, step changes) are implemented. The model was validated with actual plant operational data for dynamic conditions obtained at three transient load ramps of the reference plant.

### 6.6.1 Step Change in Load (MWe) Demand

Step changes in load were employed to investigate the capability of the SCPP system variables to reach a new steady state condition from a previous steady state condition. The load (MWe) is determined by the SCPP power output controllers which manipulate the fuel flow, the feedwater flow, and the governing system valve opening to meet the required load demand. The model was initially simulated at 87% MCR (540 MWe) for 3600 seconds, it was then stepped down to 450 MWe and simulated for further 3600 seconds before it was returned back to its initial starting point of 540 MWe and maintained at this load level for a further 3600 seconds.

For this step input change, the model was initially simulated for 540 MWe at fuel flowrate of approximately 56 kg/s; similar to the reference SCPP, the simulation was performed for an hour to allow all the variables the SCPP components reach steady state before the injection of the step changes.

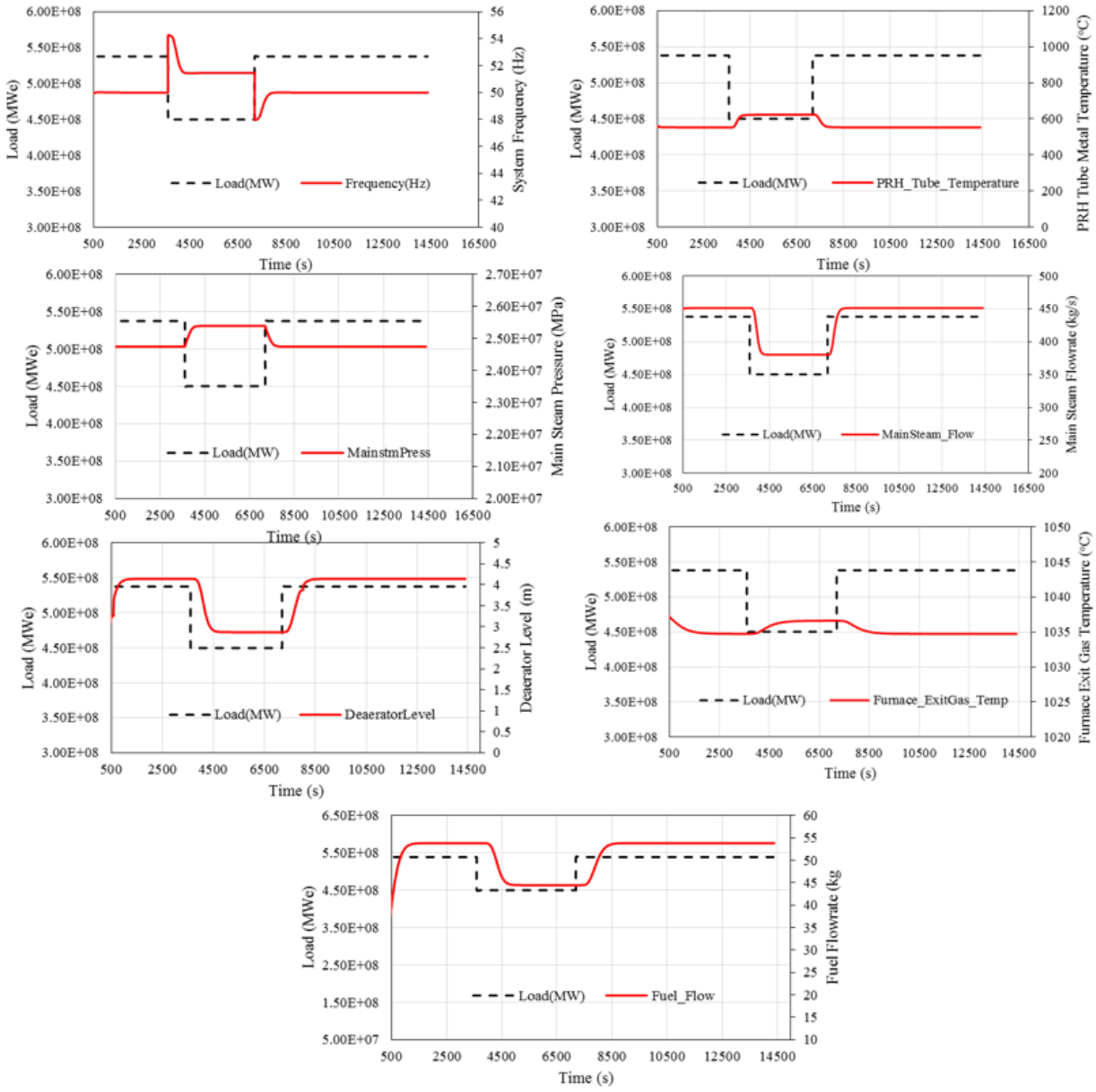


Figure 6.4: Step Input in SCPP Load (MWe) Demand

As the load is stepped down from 540 MWe to 450 MWe, the fuel flow also steps down correspondingly from 56 kg/s and returns to steady state at approximately 45 kg/s and is maintained for about one hour, the load was then step up back to its initial starting point of 540 MWe. The fuel flow also returns back to about 56.3 kg/s as shown in Figure 6.4. On the other hand, stepping down the load from 540 to 450 MWe results in the system frequency increase from 49.99Hz to about 51.8 Hz. This is in line with the relationship between the load and system frequency which maintains the balance between the demand and generation of electricity. It can also observed from Figure 6.4 that the system frequency initially increased suddenly to about 54 Hz when the

step change was initially injected. The trend was also similar when the load was stepped up back to its initial level. The response of the main steam pressure, the main steam flowrate, the deaerator water level, the furnace exit gas temperature, the reheater metal tube temperature were also analysed in the step input change presented here as shown in Figure 6.4. These variables show relatively fast response and reflect expected trends. For instance, as load decreased the deaerator water level decreased. The Furnace exit gas temperature increased as the load is stepped down before stabilising. The set points for the main steam temperature and the reheat temperature were kept constant at 537$^{o}$C throughout the transient analysis. It can be observed from Figure 6.4 that the initial response trend of the SCPP are that as load is stepped down, the temperature increases and vice versa. The increase in the main steam temperature when load is stepped down is as a result of adiabatic compression due to valve closure and the slow response of the pulveriser (Masada, 1979).

### 6.6.2 Ramping

Ramping is a typical practice for effecting load changes in an actual SCPP. This load change approach has been assessed to compare it with the step change and dynamic comparison with the reference plant ramping rate. The load control is similar as in the step change described in section 6.5.1. The same co-ordinate controller settings is used.

To demonstrate the ramp change mechanism, the ramping rate from the reference power plant was used. Three transient cases were considered for ramping change analysis (ramp up and down) and dynamic validation with the reference plant transient. The ramp rate used was estimated from the reference plant load change data. It was determined by estimating the time interval between the initial change in load and the point where the load stabilised. The plant data sample used was chosen at points within which constant load ramps were exhibited in the overall data provided. These are (i) 03 January, 2014 – load ramp from 540 MW to 430 MW at 15 MW/minute, (ii) 03 January, 2014 – load ramp from 460 MW to 355 MW at 12 MW/minute, and (iii) 9 January, 2014 – load ramp from 397 MWe to 537 MWe at 9.5 MW/minute.

*6.6.2.1 Ramping Down Load (MWe) Demand*

For the load ramp down case, the power output was first simulated at 540 MWe (87% MCR, usual normal operating level at the reference plant) for one hour. The load is then ramped down to 430 MWe over an interval of about 7.3 minutes at a rate of 15MW/minute. It is then maintained at this load level for a further one hour. Responses of the fuel flowrate, system frequency, main steam flow, economiser outlet pressure, and the reheat steam flow have been assessed over the course of the change as shown in Figure 6.5. The results are agreeable with expected trends in these variables whenever a ramp change in load change is implemented in SCPP operation.

Unlike the step changes, ramping is achieved over a time range. The results show that ramp changes induce less fluctuation in the process variables on the system frequency than the step change during the course of the change. In actual SCPP, the generally acceptable means of load change is the ramping because it imposes less instability on the system and hence reduces equipment thermal stresses due to sudden load changes.

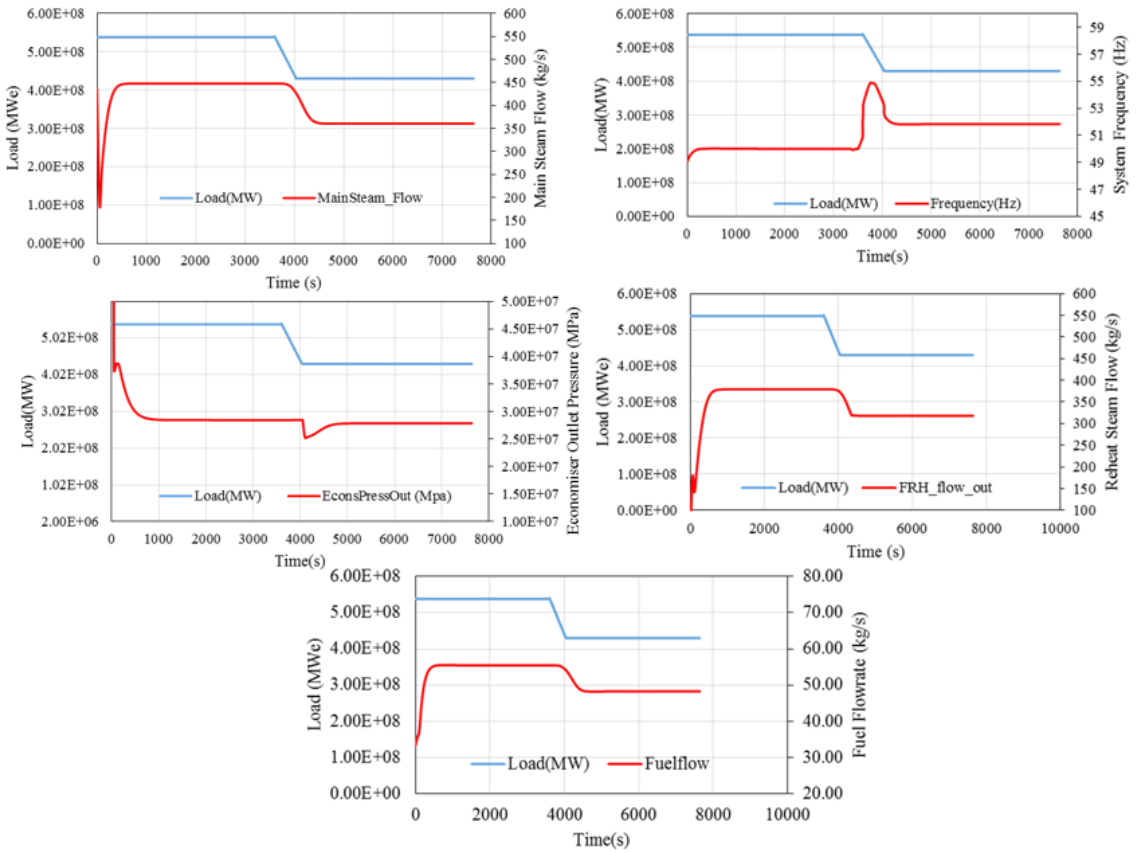


Figure 6.5: Response of SCPP to Ramping Down of Load Demand

*6.6.2.2: Ramping Up of Load (MWe) Demand*

For the load ramp up case, the power output was first simulated at 537 MWe (87% MCR, usual normal operating level at the reference plant) for 30 minutes. The load was initially stepped down to 397 MWe and maintained at this level for another 8 minutes before the start of the ramp injection. The load is then ramped up to 537 MWe over an interval of about 14 minutes at a rate of 9MW/minute. It is then maintained at this load level for a further 30 minutes. Responses of the feedwater flow, main steam and reheat steam flow, main steam temperature, and economiser outlet pressure. The results (Figure 6.6) are agreeable with expected trends in these variables whenever a ramp change in load is implemented in SCPP operation.

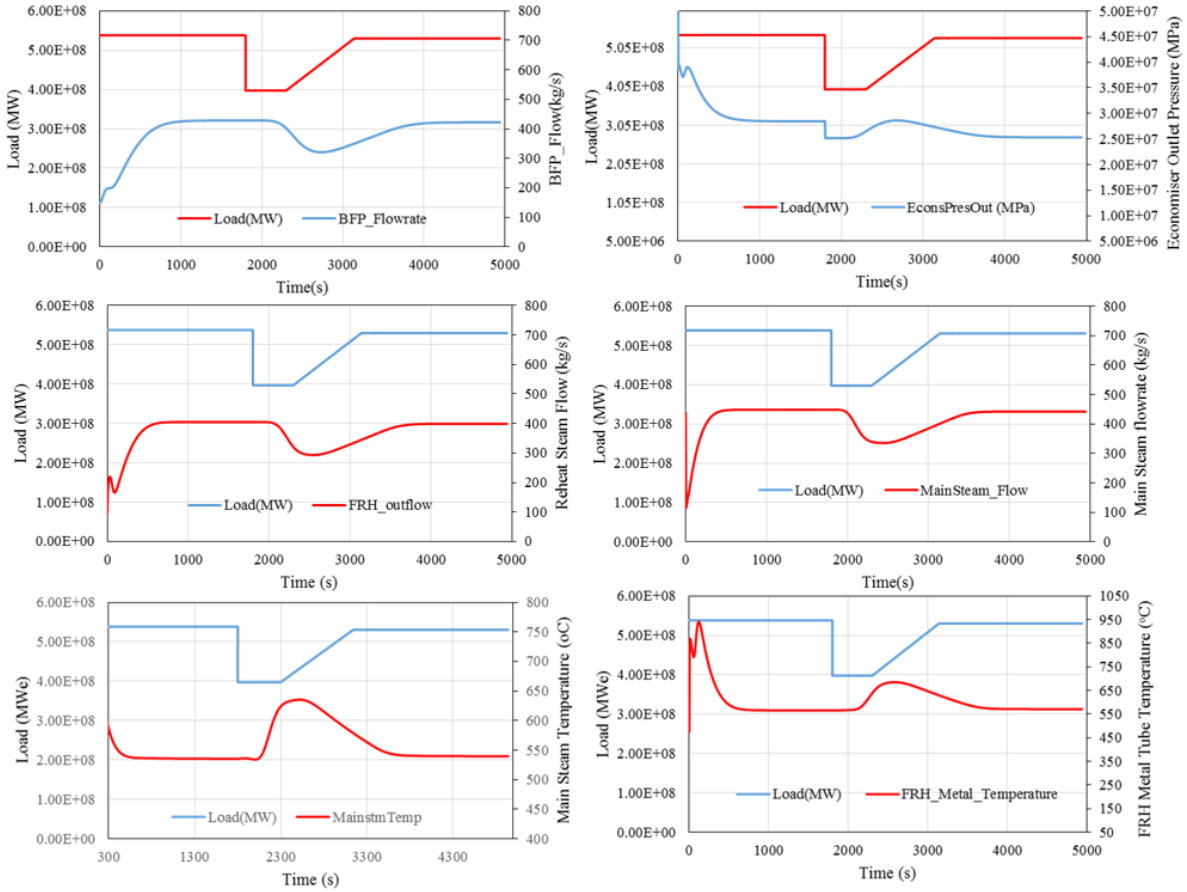


Figure 6.6: Response of SCPP to Ramping Up of Load Demand

*6.6.2.3 Dynamic Validation with Reference SCPP*

In order to compare the dynamic response of the plant with the gPROMS® model prediction, the reference SCPP ramp rate – (i) 03 January, 2014 – load ramp from 540 MW to 430 MW at 15 MW/minute was compared with the gPROMS® model response. The power output was initially simulated for 100 seconds in each case before initiating the load ramp. The load is then ramped accordingly for the three cases. It is then maintained at these load levels for a further 500 seconds. Responses of the main steam flowrate, main steam pressure, and main steam temperatures were compared with the reference plant as shown in Figure 6.7. The results are agreeable with reference plant response characteristics to the ramp change.

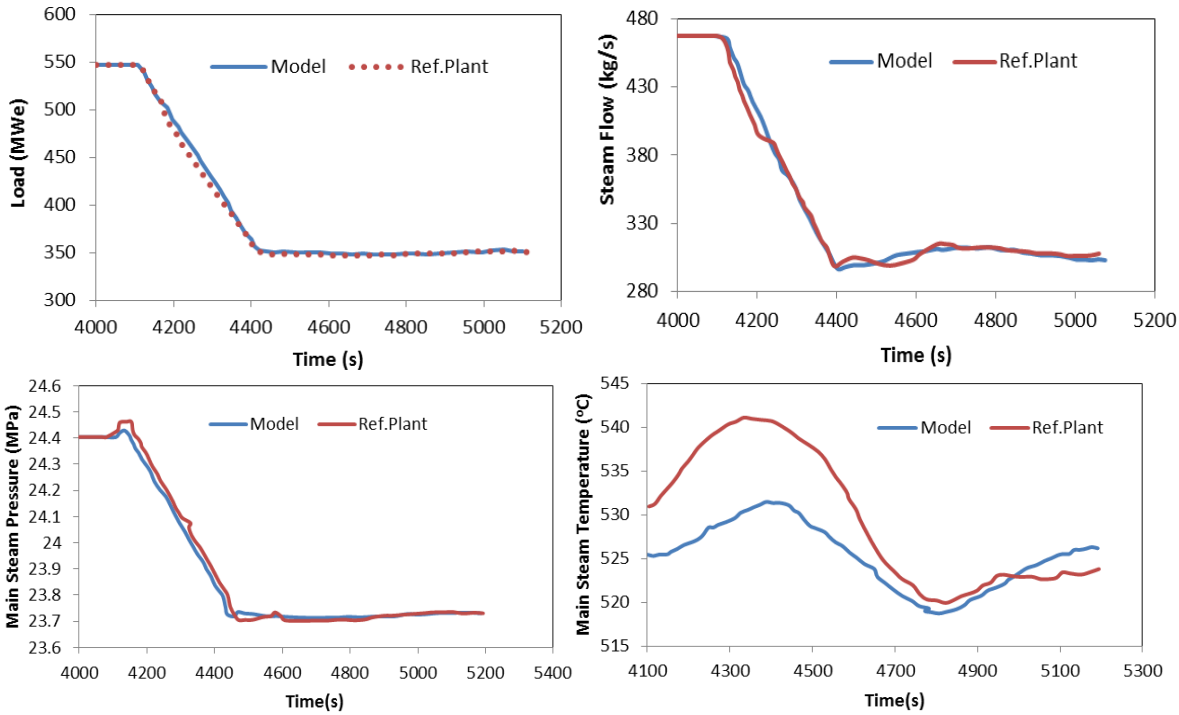


Figure 6.7: Comparison of Ramping of SCPP model with Reference Plant

## 6.7 System Frequency and Load Demand

### 6.7.1 UK Grid Code Requirement and SCPP Operation

Experience of using supercritical coal fired plant in the way the UK Grid Code recommends is non-existent and there is no practical experience to draw on.

The drum is the key to the UK's existing subcritical coal-fired plant delivering the required volume of frequency response, including primary. In the absence of the drum the manufacturers of SCPP appear unable to offer 10% primary frequency response. A value between 3 and 7% appears possible applying a number of techniques used on supercritical plant throughout the world such as using turbine throttling (Nicholls and Maxim, 2008).

The many measures required have not been tested by operational experience. There is a real risk that relying on several untried techniques in combination could result in a shortfall and non-compliant performance. The techniques proposed can lead to temperature and pressure excursions that will reduce the life of the plant and without operational experience the effect of this will be difficult to predict (Nicholls and Maxim, 2008).

However, the fast load changes can be achieved with combination of primary measures using the short-term storage behaviour of the power plant: the accumulated steam of the boiler by throttling; the steel mass of the boiler; and by interrupting the bled steam to the feed pre-heating system (condensate stop, feed-water stop). These primary measures are vital for the time lag necessary for the boiler to increase the firing rate (Zindler *et al.,* 2008).

Also, the supercritical power plant with integrated CCS system must comply with the UK Grid Code; knowing very well that addition of the capture process will introduce extra design, operational, and controllability issues. It will also result in grid code compliance concerns as it will interact with the plant's frequency response capability (Nicholls and Maxim, 2008). It is expected that the key process variables such as firing rate, furnace pressure, air-fuel ratio, $CO_2$ capture efficiency and overall plant efficiency be maintained at an optimal value irrespective of variations in load and process disturbances.

### 6.7.2 Primary and Secondary Frequency

The response on frequency deviation caused by an event in the grid is handled by the frequency control. This is implemented in time ranges. The Primary Response capability (P) of a Generating Unit is the minimum increase in active power output between 10 and 30 seconds after the start of the ramp injection. The Secondary Response capability (S) is the minimum increase in Active Power output between 30

seconds and 30 minutes (Figure 6.8) after the start of the ramp injection (National Grid, 2012).

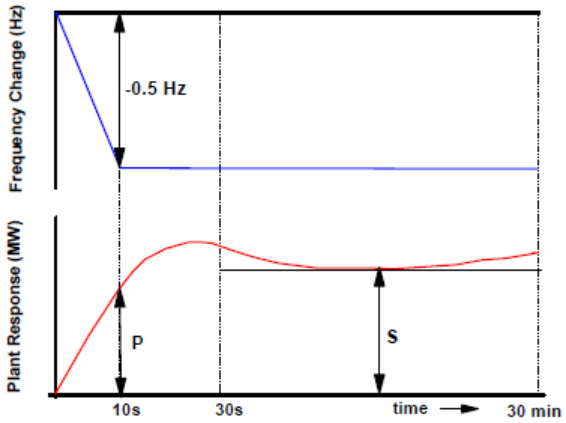


Figure 6.8: Interpretation of primary and secondary response values (National Grid, 2012)

### 6.7.3 High Frequency

*The High Frequency Response* capability (H) of a generating unit is the decrease in active power output provided 10 seconds after the start of the ramp injection and sustained thereafter (Figure 6.9).

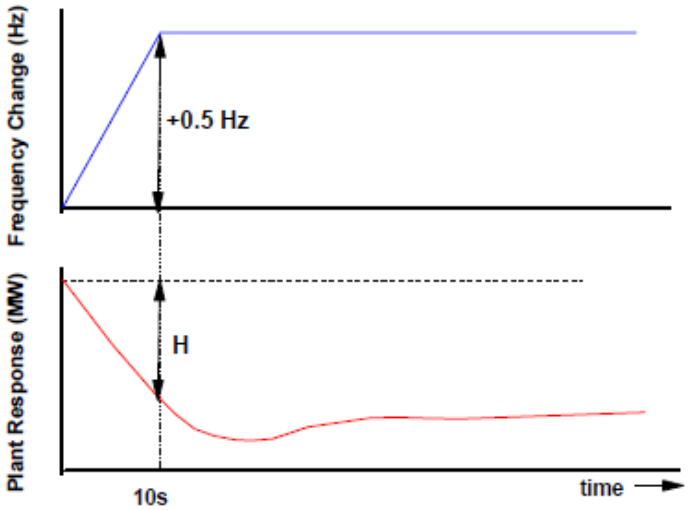


Figure 6.9: Interpretation of high frequency response values (National Grid, 2012)

## 6.8 Strategies for Operating SCPP under UK Grid Code Requirement

### 6.8.1. Introduction

Operating the SCPP in the manner required by the UK grid code will require some major modifications to the plant's operation and control systems especially its response to changes in load, system frequency (i.e. the primary frequency) and emergency situation. This section presents a result of the different strategies proposed to investigate the plant's behaviour under typical UK grid scenario (i.e. during primary frequency change). It considered two conventional approaches used worldwide for SCPP load (i.e. main steam throttling, and Condensate stop), and a novel approach (i.e. steam extraction stop, combination of extraction stops & steam throttling etc.). The strategy also included using an indirect firing system (with the use of pulverised coal silo) to reduce the time required for increasing the firing rate (Mercier and Drenik, 2013).

In using the SCPP dynamic model to simulate the different strategies considered here, certain important modifications were made to the conventional SCPP model to ensure accurate results. These includes:

- Inclusion of models for fast-action valves to replace the conventional control valves as suggested by (Mercier and Drenik, 2013) to ensure rapid response during primary frequency change. The fast action valves were installed on the steam extraction lines in order to analyse the various "extracted steam stop" mechanism without minimal or no delay as a result of slow valve opening.
- Addition of a pulverised coal silo for rapid supply of fuel to aid the firing rate reaction time and overall response time for steam generation
- A system frequency ramp was used throughout the analyses to determine the capability of each strategy to respond to the drop in frequency

#### *6.8.1.1 Fast Action Valve Modelling*

The governing equation for the fast (or quick) action valve model developed for this analysis is similar to the conventional valves in the SCPP but with the substitution of the equation for flow through valve. The equation below describes the main governing equation in the fast action valve:

$$F = C_D f(x) \sqrt{\frac{\Delta P}{\rho}} \quad (6.22)$$

For the fast action valve: $f(x) = \sqrt{x}$ (6.23)

For linear valve however, $f(x) = x$ (6.24)

Where: $x$ is the valve fractional opening (0 to 1),

$f(x)$ is the valve area available for flow

*6.8.1.2 System Frequency Ramp*

In analysing the SCPP response to change in system frequency (i.e. Primary frequency) as required by the UK grid, the system frequency has to serve as the input disturbance into the SCPP model. Since the conventional PI controllers installed in the power plant is based on the coordinated control system mode of operation, the system frequency change signal is sent through its coupling with the to the load; which in turns send the error signals to the boiler control and turbine controls (See Figure 6.3) to control the power generation and the steam conditions respectively. This then balance the power generation with the demand requirement so as to bring the frequency back to normal level (i.e. 50 Hz). In this study, the system frequency ramp of -0.5Hz (as required by UK grid) was injected within 10 to 40 s at a rate of 0.05 Hz per second.

### 6.8.2 Main steam throttling

Opening the main steam throttling valve (Figure 6.10) in the HP steam inlet increases the flow of steam into the HP turbine, and consequently leading to increase in the load.

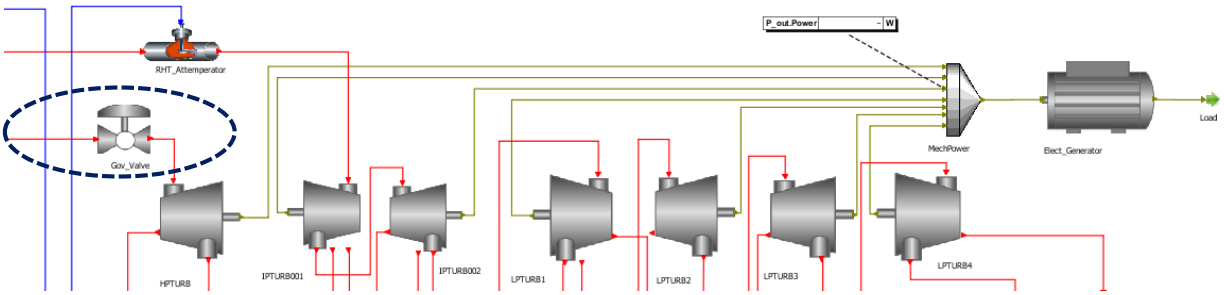


Figure 6.10: Main steam throttling

This method is however not sustainable for meeting primary frequency response within the short time (i.e. 10s) required by the UK grid. From Figure 6.11, it can be observed that the main steam throttling approach only produces about 2.5%, 3.0% and 3.3% increase in load at 50% MCR, 75% MCR, and 87% MCR respectively within the short time before firing rate is increased. However, its contribution within the start of the frequency change when combined with other methods can be useful to meeting overall frequency response requirement.

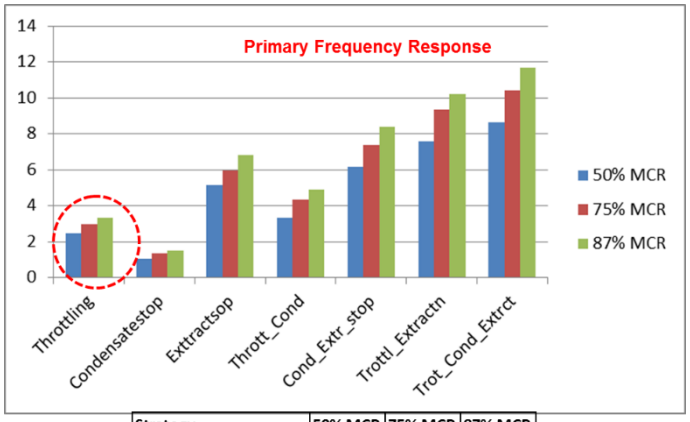


| Strategy | 50% MCR | 75% MCR | 87% MCR |
|---|---|---|---|
| Throttling (%) | 2.45 | 2.96 | 3.31 |
| Throttling(MWe) | 14.7 | 17.8 | 19.86 |

Figure 6.11: Contributions of Main steam throttling

### 6.8.3 Condensate stop (LPT-Extraction)

In this approach, the steam normally extracted from the LP turbine for preheating of the condensate is stopped and allowed to undergo further expansion in the turbine to increase the load during frequency change (Figure 6.12). This process is achievable through the use of fast-acting valves.

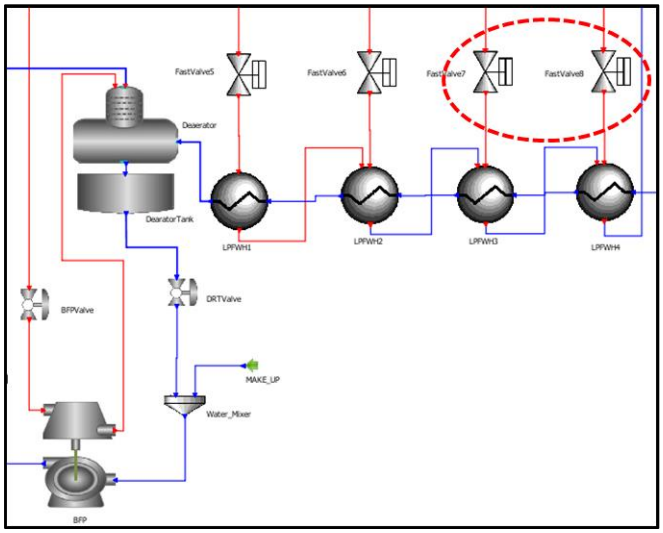


Figure 6.12: Condensate stop

From Figure 6.13, its contribution to the primary frequency response was found to be about 1.1%, 1.4% and 1.5% increase in load at 50% MCR, 75% MCR, and 87% MCR respectively. It is therefore not useful when applied alone.

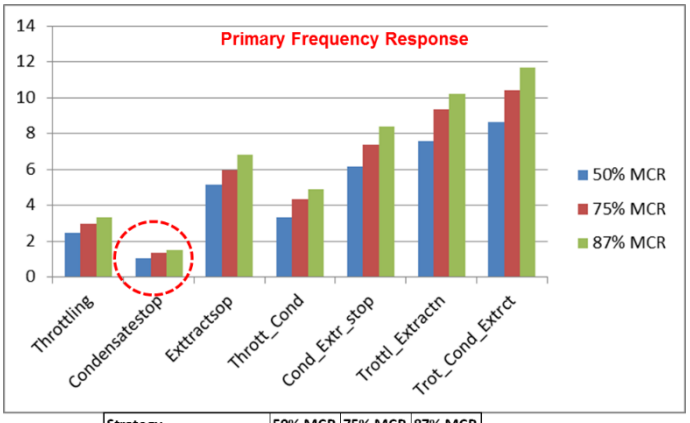


| Strategy | 50% MCR | 75% MCR | 87% MCR |
|---|---|---|---|
| Condensatestop (%) | 1.05 | 1.36 | 1.51 |

Figure 6.13: Contributions of Condensate stop

### 6.8.4 Extraction stop (IP-LPT Extraction)

In this approach, the steam normally extracted from the IP and part of the LP turbines for preheating of the feedwater heaters are stopped (see Figure 6.14) and allowed to undergo further expansion in the turbine to increase the steam flow to the turbine and consequently the load during frequency change.

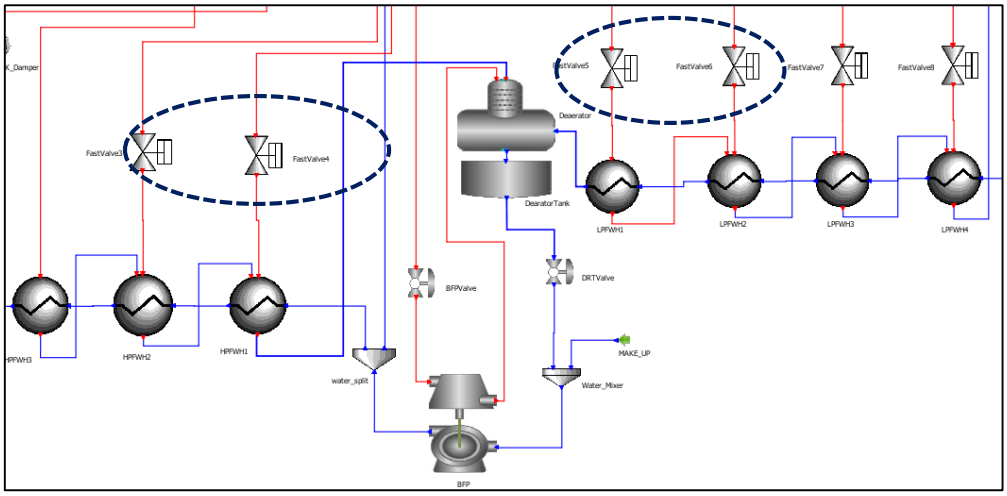


Figure 6.14: Extraction stop

From Figure 6.15, the contribution of the extraction stop to primary frequency response was 6.0%, and 6.8% increase in load at 50%MCR, 75% MCR, and 87% MCR respectively. The results also reveal that the extractions stop alone cannot meet the 10% MCR required by the UK grid for primary frequency response.

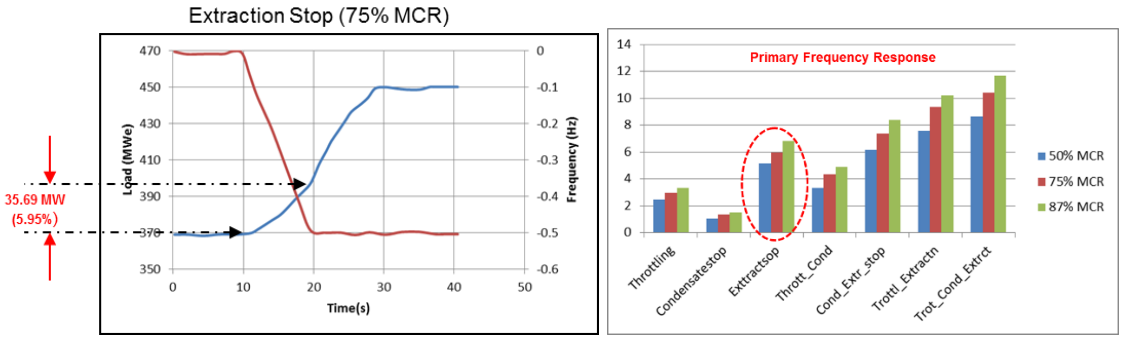


Figure 6.15: Contributions of Extraction stop

### 6.8.5 Combination of Steam throttling and Condensate stop

In this approach, the steam throttling process and the condensate stop mechanism were simulated simultaneously to evaluate their combined effect to meeting the primary frequency response. The results in Figure 6.16 show that only 3.3%, 4.4%, and 5% MCR is achievable at 50%, 75% and 87% MCR operation of the SCPP respectively.

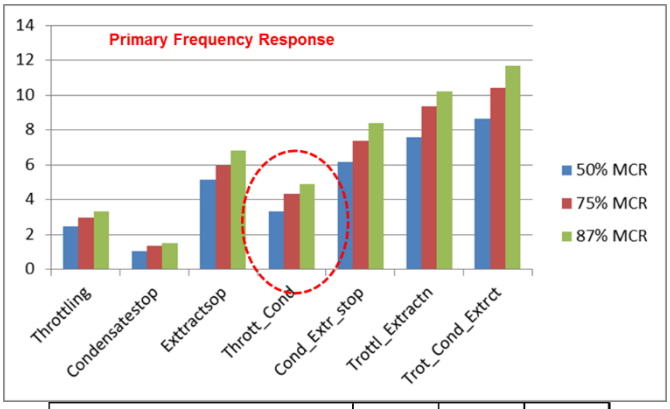


| Strategy | 50% MCR | 75% MCR | 87% MCR |
|---|---|---|---|
| Throttling_Condstop (%) | 3.31 | 4.36 | 4.87 |
| Throttling_Condstop(MWe) | 19.84 | 26.15 | 29.21 |

Figure 6.16: Contributions of Combination Condensate and extraction stops

### 6.8.6 Combination of condensate and extraction stops

The idea of combining the condensate stop and the extraction stop gives room for improvement in the overall amount of MCR recoverable for primary frequency response. Figure 6.17 shows the result of the simulation for the combined approach at the three load levels considered. It can be seen that a considerable improvement is made compared to the combination of steam throttling and the condensate stop. The total additional power generated were 6.2% MCR, 7.4% MCR, and 8.4% MCR at 50%, 75%, and 87% MCR load. It is evident from the results that at higher operating load (e.g. 100% MCR), the combination of extraction and condensate stop could meet the frequency response requirement.

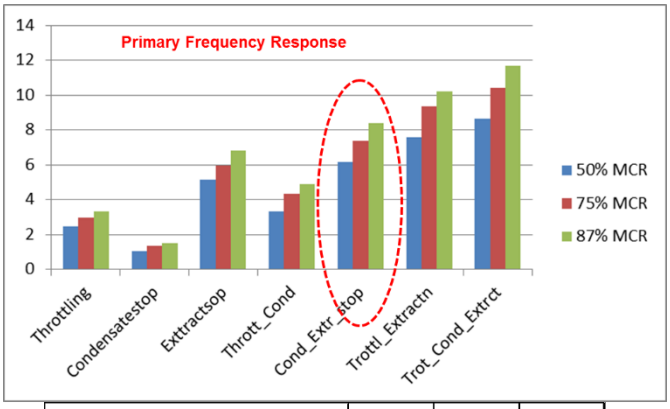


| Strategy | 50% MCR | 75% MCR | 87% MCR |
|---|---|---|---|
| Cond_Extrstop (%) | 6.18 | 7.39 | 8.41 |
| Cond_Extrstop(MWe) | 37.05 | 44.32 | 50.37 |

Figure 6.17: Contributions of Combination Condensate and extraction stops

### 6.8.7 Combination of Steam throttling and extraction stop

This approach tends to combine the fast response of the steam throttling process and the larger amount of power generated from the extraction stop in order to generate high % MCR as a response to primary frequency change. From Figure 6.18, the result shows that a combination of steam throttling and extraction stop can generate extra 7.6% MCR, 9.3% MCR, and 10.6% MCR when operating at 50%, 75%, and 87% MCR load respectively. From the simulation result, it is obvious that a combination of steam throttling and extraction stop can satisfy the primary frequency requirement from above 75% load of operation of the SCPP.

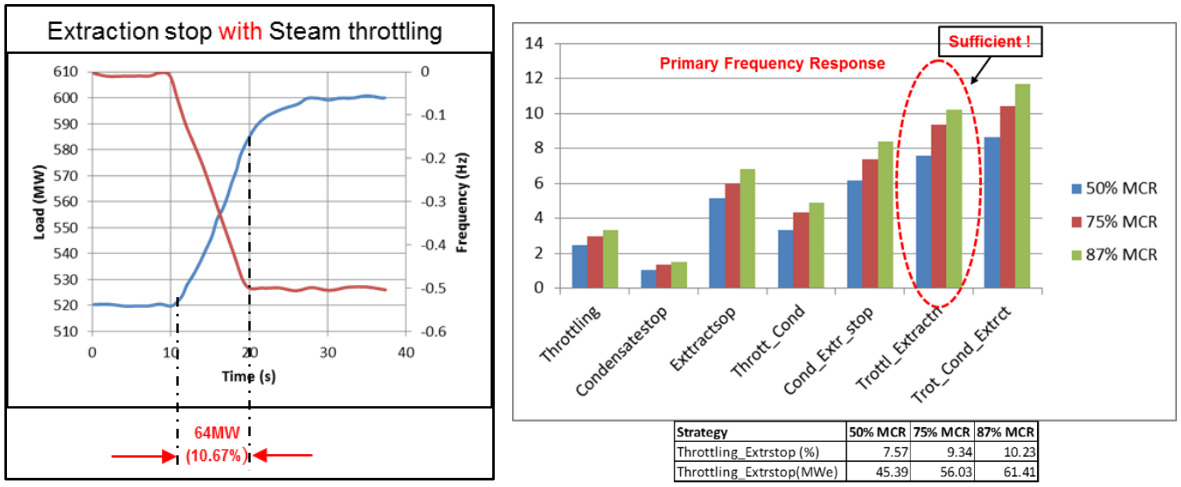


| Strategy | 50% MCR | 75% MCR | 87% MCR |
|---|---|---|---|
| Throttling_Extrstop (%) | 7.57 | 9.34 | 10.23 |
| Throttling_Extrstop(MWe) | 45.39 | 56.03 | 61.41 |

Figure 6.18: Contributions of Combination extraction stop and steam throttling

### 6.8.8 Combination of throttling, condensate and extraction stops

This configurations seeks to utilize all the mechanisms described in this study simultaneously to meet the requirement, although this might not be practical in a real SCPP without advanced co-ordinated control systems in place due to instabilities that could result from stopping condensate, steam extraction, and steam throttling all at the same time. The simulation result shows that 10% MCR is achievable in a SCPP operating at a load level that is as low as 60% of its registered capacity (Figure 6.19).

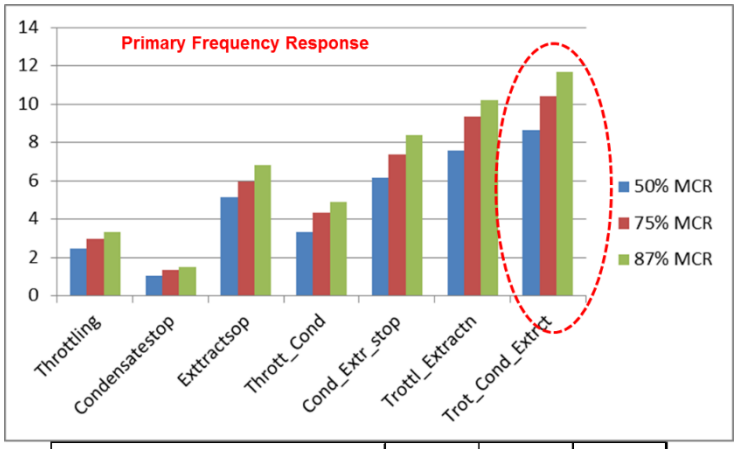


| Strategy | 50% MCR | 75% MCR | 87% MCR |
|---|---|---|---|
| Throttling_Cond_Extrtstop (%) | 8.62 | 10.41 | 11.68 |
| Throttling_Cond_Extrctstop(MWe) | 51.73 | 62.48 | 70.06 |

Figure 6.19: Contributions of Combination of steam throttling, extraction and condensate stops

### 6.8.9 Partial Indirect Firing of Boiler

The use of partial indirect firing is to enable a faster response of firing rate increase by reducing the reaction time in the boiler considerably to allow for a faster response to the secondary frequency change (within 30s of frequency drop and sustained for further 30 minutes). This is achieved through the use of a pulverized coal storage system (Figure 6.20(a)) to ensure pulverized coal of similar particle size is used.

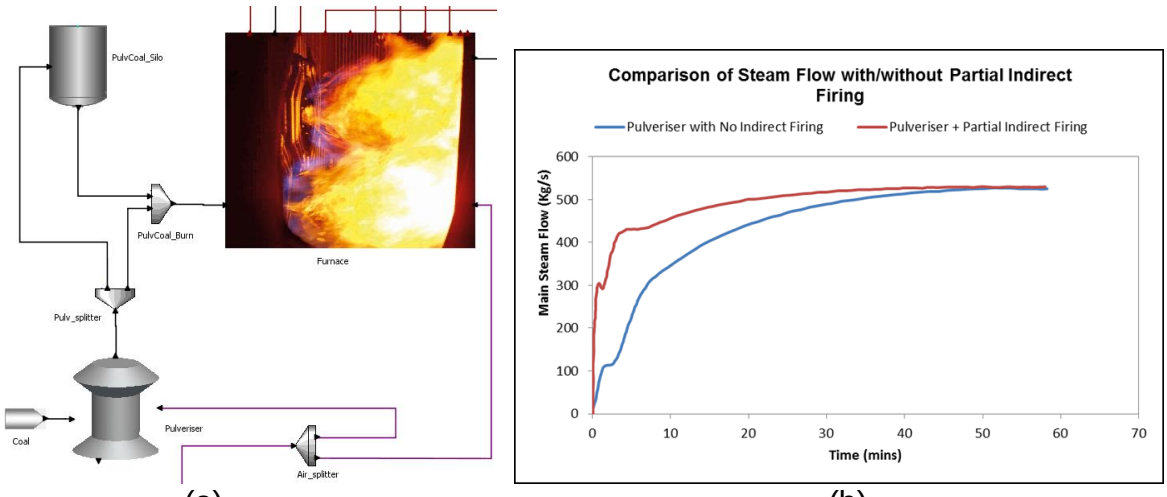


(a) (b)

Figure 6.20: Partial Indirect Firing of SCPP Once-through Boiler

Figure 6.20(b) shows the comparison of the steam generated with conventional pulveriser firing and the firing with a coal storage silo. The result show a rapid response

in steam generation compared to the conventional case. The partial indirect firing approach reduced the reaction time in the firing system considerably.

## 6.9 Summary

This chapter analysed the strategies for operating the SCPP under the UK grid requirement as regards to primary frequency response. The SCPP model was used to simulate the flexibility of the SCPP for rapid load changes and variations in system frequency. The UK grid code stipulates that depending on the operating load as a percentage of the registered capacity (MCR), up to 10% of registered capacity has to be supplied within 10–30s of a 0.5Hz frequency drop occurring over a 10s period. The simulation results show that using turbine throttling approach (about 3.3% MCR), extraction stop (about 6.8% MCR) or condensate stop (about 1% MCR) individually was not sufficient to meet the grid requirement. On the other hand, the study shows that a combination of turbine throttling, extraction stop and/or condensate stop can achieve a 10% increase in generating capacity (MCR) of a SCPP within 10s to 30s of primary frequency change as required by the UK grid while operating at a load level of between 60–100% of its registered capacity.

# Chapter 7 Process analysis of dynamic model of SCPP integrated with dynamic model of PCC

## 7.1 Introduction

Dynamic modelling, scale-up and integration of dynamic model of a pilot-scale PCC with dynamic model of the SCPP is presented in this chapter. A dynamic model of the pilot-scale PCC system was developed in Lawal et al (2012) based on the pilot plant data from the Separations Research Program at the University of Texas at Austin. Based on the insights from the pilot plant model (Figure 7.1), this chapter presents the dynamic modelling and scale-up of the pilot plant model to a commercial-scale PCC that can process flue gas flowrate of about 612 kg/s from the reference (600MWe) SCPP unit. Scale-up calculations of the pilot size PCC process is similar to the approach used for scaling up the steady state model presented in chapter three. This chapter also presents the results and discussion for base case and load change scenarios of the integrated system. The chapter ends with strategies for operating the integrated system under the UK grid code requirements.

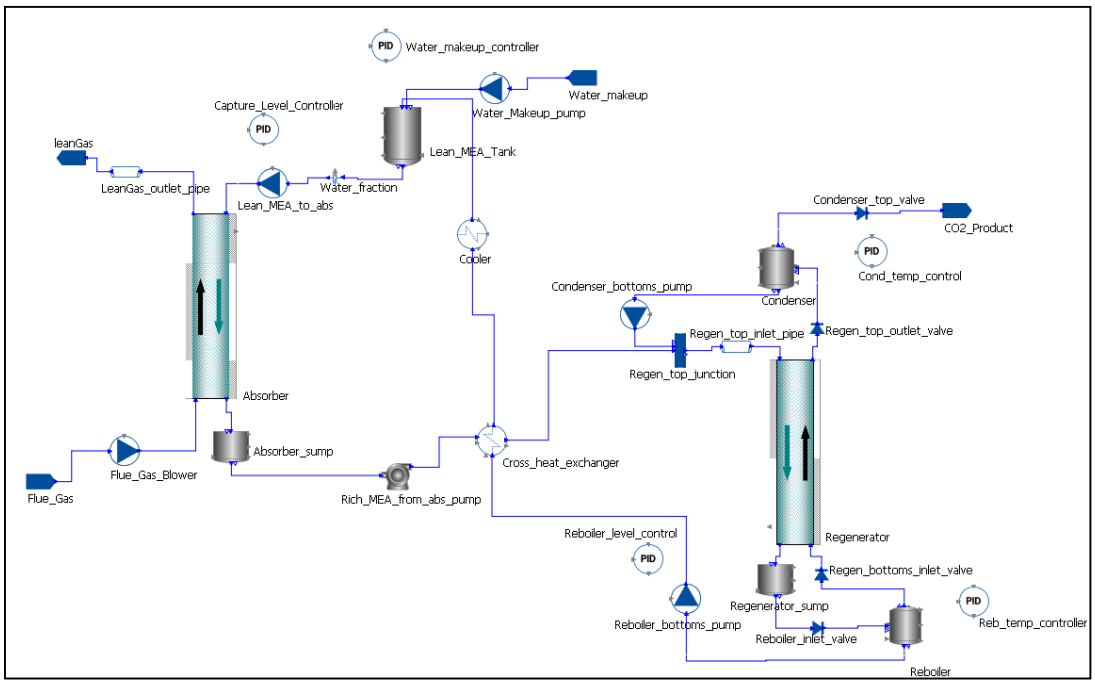


Figure 7.1: Pilot-Scale PCC Dynamic Model Topology (Lawal *et al,* 2012)

## 7.2 Dynamic Modelling and Scale-Up of the PCC system

The dynamic model of the pilot-scale PCC was validated at both steady state and dynamic mode using the pilot plant data (Lawal et al., 2010; Biliyok et al., 2012). The commercial-scale PCC system was designed to capture 90% of the $CO_2$ from the 612 kg/s of the flue gas from the SCPP. This is achieved with a 30 wt. % monoethanol amine solution (MEA). Due to the high number of interacting variables in the PCC system, accurate scale-up procedure is very important to achieve a reliable and realistic plant size.

Based on the aforementioned importance of the scale-up process, the following assumptions were made to achieve a realistic result.

Assumptions:

- The lean solvent loading of 0.29 mol $CO_2$/mol MEA used in the pilot-plant model was also used for this commercial-scale study;
- The rich solvent loading of 0.49 mol $CO_2$/mol MEA was assumed (also similar to the pilot plant study).
- The absorption capacity, i.e. the difference between the rich loading and the lean solvent loading (0.2 in this case) was used to estimate the solvent circulation rate.
- Water wash section was not considered in the absorber
- Make-up water control was included to account for proper balance of water in the system.
- Influence of oxygen on the solvent (MEA) was considered negligible. Oxygen was however included in the nitrogen composition since it was considered as an inert.
- The $SO_X$ and $NO_X$ content in the flue gas was assumed to have been removed in flue gas desulphurization and de-$NO_X$ unit at the upstream of the PCC system.

To simplify the complex scale-up of the pilot plant, the following scale-up steps in Figure 7.22 was used to arrive at the desired commercial-scale PCC configurations. Although this methodology would not result in optimal design for the process

equipment, it would be sufficient for conceptual studies and would minimise the amount of iterative steps needed to develop the scaled-up model.

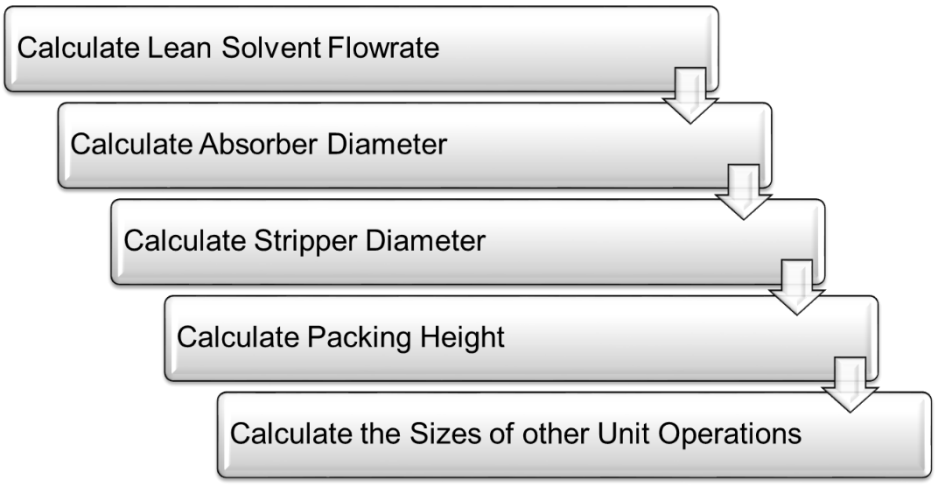


Figure 7.2: Scale-Up Calculation Steps

### 7.2.1 Calculation of Lean Solvent (MEA/$H_2O$) Flowrate

The solvent flowrate is calculated based on the absorption capacity from the pilot plant, the MEA concentration in lean solvent (30.48 wt. % MEA), the flue gas flowrate (612.1 kg/s) and $CO_2$ content (20.54 wt. % $CO_2$) obtained from SCPP dynamic model when simulated at 100% MCR (600 MWe).

Hence,

Molar flowrate of $CO_2$ into the absorber

$$= \frac{(612.1\ kg/s) \times (0.2054)}{(44\,kg/kmol)}$$

$$= 2.8574\,kmol/s$$

Lean solvent flow into the absorber

$$= \frac{(2.8574\ kmol/s) \times (61.08\,kg/kmol)}{(0.2) \times (0.3048)}$$

$$= 2863.02\,kg/s$$

### 7.2.2 Calculation of Absorber Diameter

The absorber diameter is estimated from its cross-sectional area which defines the capacity of the column. The method employed in determining the column cross-sectional area and subsequently the column diameter for both the absorber and the stripper is the generalized pressure drop correlation (GPDC) principle (Sinnot et al,

2005). Operation of packed columns are limited by (i) flooding, which occurs when a gas flow pressure drop is so high that the liquid is unable to flow downward and it sets the upper capacity limit of the packed column (Figure 7.33); and (ii) the minimum liquid load (Figure 7.33), which is the lowest liquid flowrate that gives sufficient mass transfer rate (Lawal et al, 2012).

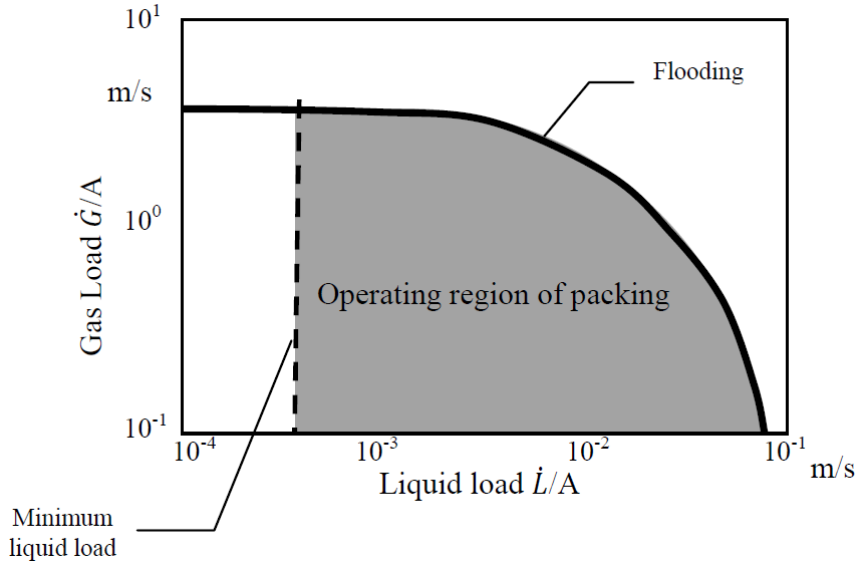


Figure 7.3: Operating region of a packed (Stiltchmai and Fair, 1998)

An efficient packed column design is characterised by a good liquid and gas distribution that is achieved by operating at the highest economical pressure drop (Sinnot et al, 2005). The pressure drop per metre packing for absorbers and strippers of 15 to 50 $mmH_2O/m$ of packing height is recommended for the raschig ring random packing; typically away from the flooding line (Lawal et al, 2012). The GPDC chart shown in Figure 7.44 for packed columns is used. The pressure drop lines in the chart are in $mmH_2O$ per metre of packing. This is within the recommended interval by Sinnot *et al*. (2005) and it can be read off easily. 42 $mmH_2O/m$ of packing height was used for the design of both the absorber and stripper in this thesis.

From Figure 7.44, $F_{LV}$ is the flow parameter which represents the ratio of liquid kinetic energy to vapour kinetic energy (Kister *et al.*, 2007). It can be calculated from equation (7.1) thus:

$$F_{LV} = \frac{L_w^*}{V_w^*}\sqrt{\frac{\rho_V}{\rho_L}} \qquad (7.1)$$

The expression $\frac{L_w^*}{V_w^*}$ is the ratio of liquid to vapour mass flowrate per unit area. The ratio is identical to L/G ratio (*i.e*. liquid to vapour mass flowrate). The L/G ratio is 4.68 for the absorber in this thesis based on estimation in section 7.2.1. The liquid and vapour phase densities (*i.e.* $\rho_L$ and $\rho_V$) were obtained from the pilot scale PCC model simulations as $1066.65\,kg/s$ and $1.3\,kg/m^3$ respectively. Based on the information, the absorber $F_{LV}$ is obtained thus:

$$F_{LV} = 4.68\sqrt{\frac{1.3}{1066.65}} = 0.1634$$

From the GPDC chart in Figure 7.4, the capacity parameter, using the value of $F_{LV} = 0.1634$, at pressure drop of 42 mmH₂O/m of packing, then $K_4 \cong 1.2$.

The percentage flooding is calculated using equation 7.2 (Sinnot *et al*., 2005) thus:

$$\%\,Flooding = \sqrt{\left[\frac{K_4\ at\ design\ pressure\ drop}{K_4\ at\ flooding\ line}\right]} \times 100 \qquad (7.2)$$

The $K_4$ at design pressure drop and at the flooding line (from the GPDC chart) is approximately 1.15 and 2.8 respectively. This gives a percentage flooding of 41.10% which is acceptable (lower than the upper limit for flooding percentage; usually ~80% (Sinnot *et al*. (2005)). The cross-sectional area of the column and hence the diameter is then computed using the $K_4$ value as follows:

$$K_4 = \frac{13.1(V_w^*)^2 F_p \left(\frac{\mu_L}{\rho_L}\right)^{0.1}}{\rho_V(\rho_L - \rho_V)} \qquad (7.3)$$

$$V_w^* = \frac{K_4\,\rho_V(\rho_L - \rho_V)}{13.1F_p\left(\mu_L/{\rho_L}^{0.1}\right)} = \sqrt{\left[\frac{(1.15)(1.3)(1066.65 - 1.3)}{13.1(310)(0.00187/1066.65)^{0.1}}\right]}$$

$$V_w^* = \sqrt{\frac{1592.70}{1078.984}} = 1.2150\,kg/m^2\,s$$

The liquid phase viscosity ($\mu_L = 0.00187\ Pa.s$) is also obtained from the pilot scale PCC model simulations. The packing factor ($F_P = 310\ m^{-1}$) depends on packing type

selected. 38 mm ceramic Raschig rings used for the pilot-scale model is also used in this scale-up study. Vapour mass flowrate per unit area ($V_w^*$) obtained from equation 7.3 is 1.2150 kg/m$^2$s. The cross-sectional area obtained by dividing the flue gas flowrate with $V_w^*$ is 503.70 m$^2$. Diameter obtained from the cross sectional area is 25.32 m. Similar approach was used to estimate the stripper column diameter. The absorber diameter was 25.32m. However, using one column would be difficult to manage due to structural limitations. In Lawal *et al.* (2012), it was suggested that using multiple columns increases operational redundancy and turn-down capability of the PCC plant.

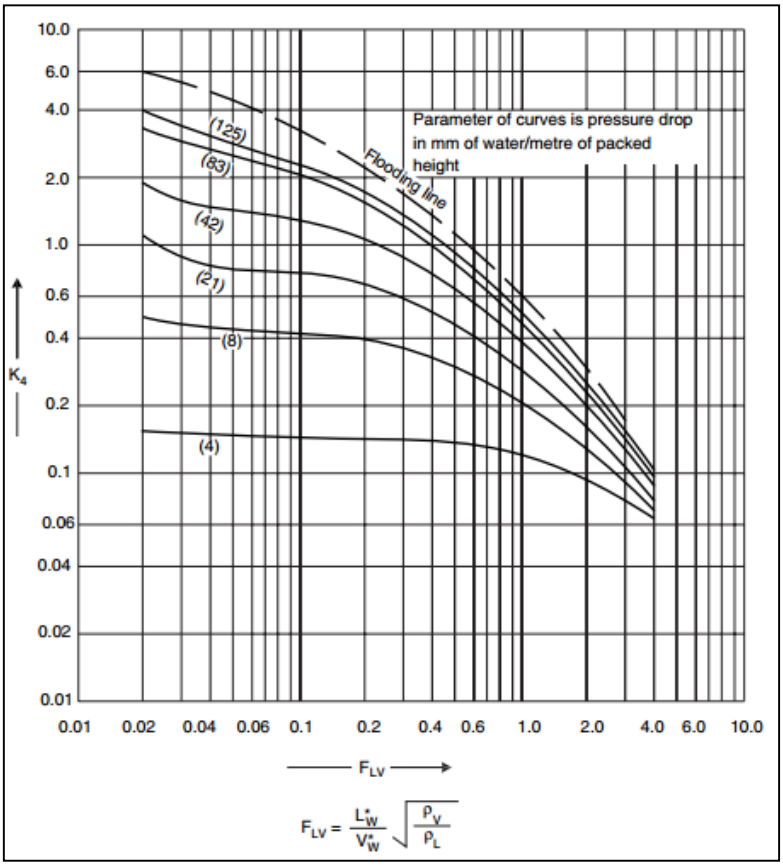


Figure 7.4: Generalised pressure drop correlation (Sinnot *et al*., 2005)

Hence, an estimation of diameter against the number of column was carried out as in Figure 7.5 for both the absorber and stripper columns.

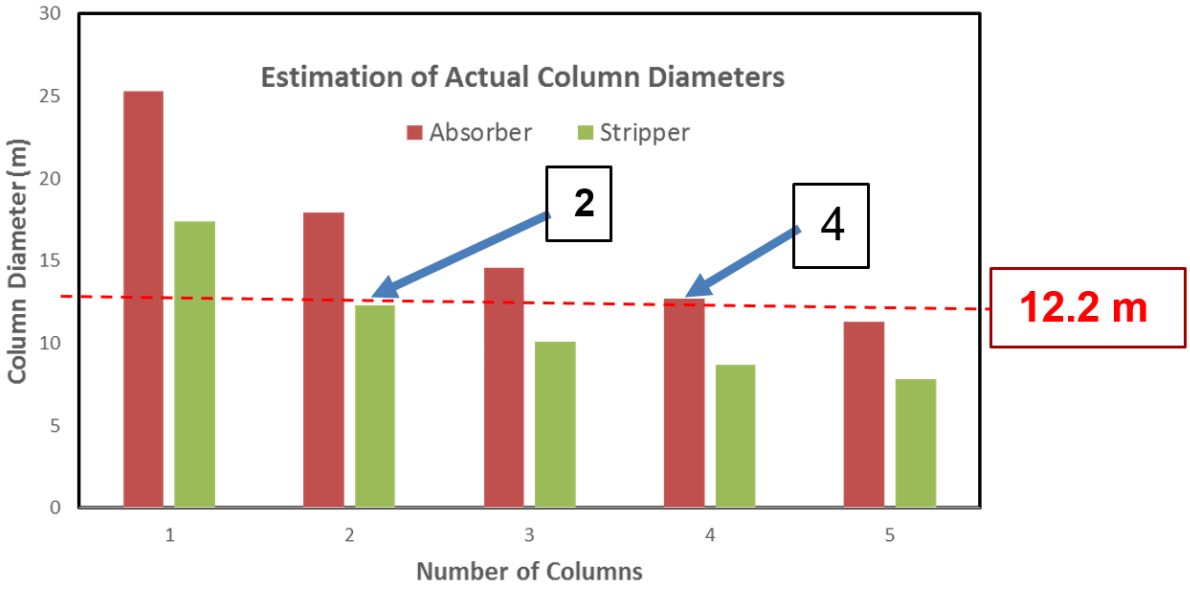


Figure 7.5: Relationship between numbers of Column against Column diameter

Due to numerical instabilities in the complex nature of the rate-based dynamic model of the PCC, it will be difficult to integrate four absorber columns and three stripper with the SCPP dynamic model. Hence, two absorbers of 18 m diameter was used for the integrated model in this thesis.

### 7.2.3 Calculation of Stripper Diameter

From the generalized pressure drop correlation method used in Section 7.2.2, the regenerator diameter was estimated as 17.4 m, thus two 12.3 m diameter column would suffice as shown in Figure 7.5. In the scaled-up model one stripper of 17.4 m diameter was used.

### 7.2.4 Calculation of the Packing height

The packing height of the column was calculated based on a cost-based method as described in Lawal et al (2012). The method involved first using a generic height of 17 m as described in Cifre et al. (2009). Different packing heights are then trialled. The savings in energy corresponding to each trialled packing height was then used to decide the best packing height. Using this approach, it is found that a height of about 27m is ideal for this case (Lawal *et al*., 2012).

### 7.2.5 Sizing of Other Components

Apart from the absorber and stripper, other key components in the PCC process (Figure 7.6) include other unit operations such as Cross heat exchanger, stripper reboiler and condenser, lean MEA cooler, lean solvent (MEA) holding tank, and rich/lean pumps. Rough estimates of the sizes of these unit operations were obtained from Lawal (2010) for the base case integration studies and analysis. However, the components were re-sized for the operational analysis of the SCPP-PCC integrated plant under UK grid code requirement. This was done to accommodate the strategies (i.e. stripper stop, rich solvent storage, extraction/feedwater stop, condensate stop, and the steam throttling approaches) implemented which requires higher capacity and hold-up time (i.e. reboiler and condenser ) , higher pressure (e.g. the stripper column), and larger capacity (e.g. the rich solvent tank) to implement. Table 7.1 shows a summary of the key design parameters of the scaled-up system.

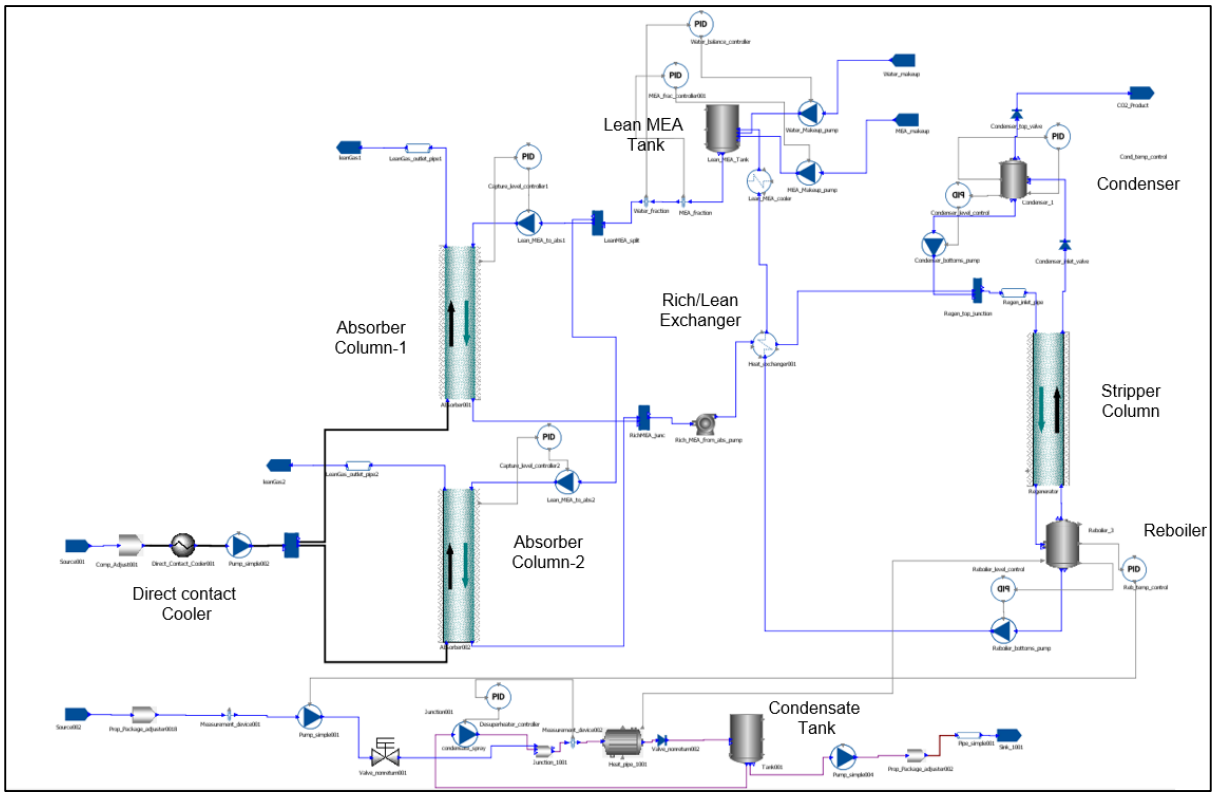


Figure 7.6: gPROMS® Model Topology of the Scaled-Up PCC Unit

Table 7.1: Design Parameters for PCC Scale-Up

| Parameters | Absorber | Stripper |
|---|---|---|
| Type of packing | 38 mm Raschig ring | 38 mm Raschig ring |
| Total Height of Packing (m) | 30.0 | 30.0 |
| Diameter of column (m) | 18.0 | 17.4 |
| Column Number | 2 | 1 |
| $CO_2$ Capture level (%) | 90.0 | - |

## 7.3 Integration of SCPP with PCC based on dynamic Models

### 7.3.1 Introduction

This section describes the integrated plant model – the PCC plant model linked with the 600 MWe SCPP model. The SCPP model and its components are described in detail in Chapter 6. The integration of the two models is discussed briefly. The integrated model is obtained by linking the 600 MWe SCPP and the scaled-up PCC model presented in Section 7.2. The models are linked together via three important connection points. This includes:

- Flue gas stream from the SCPP to the absorber column
- Steam draw-off from the SCPP's IP/LP crossover for solvent regeneration in the stripper (see Figure 7.9)
- Return of spent steam (condensate) from the PCC back to the SCPP low pressure feedwater heater (see Figure 7.9).

The integrated dynamic model is then used for steady state and dynamic analysis. The base case was performed with MEA concentration at 30 wt. % MEA. The steady state analysis of the SCPP with three MEA concentrations is discussed in a case study. A number of dynamic analysis (step change and ramp change) are also presented based on the operation of the integrated plant. Finally the integrated system was simulated for operational issues under a typical UK grid code (i.e. primary frequency change) to determine if the couple system can satisfy the grid requirement. The grid analysis was performed with modifications to the base case system using

different PCC response strategies suggested in literature, and combining the PCC strategies with the SCPP strategies discussed in Chapter six.

### 7.3.2 Linking the PCC model to the SCPP model

*7.3.2.1 Pre-processing of the Flue gas*

The flue gas from the SCPP contains particulates (i.e. fly ash), SOx and NOx. The particulates have the potential to clog the column packings which may result in foaming in the absorber. Particulate matters are removed with the use of electrostatic precipitators or baghouse filters. The flue gas from the SCPP usually at a temperature of 70–80$^{o}$C is not favourable for the absorption process, therefore the temperature is first reduced to about 40$^{o}$C in a direct contact cooler (DCC). In the integrated model, it is assumed that all the particulate matter, the SOx and NOx in the flue gas have been removed upstream of the absorber. Also, the degradation of MEA solvent due to the presence of oxygen is neglected. Hence, oxygen is considered inert and its mass fraction is simply combined to the nitrogen mass. Figure 7.7 shows the block diagram of the link between the pre-processed flue gas and the capture plant's absorber columns.

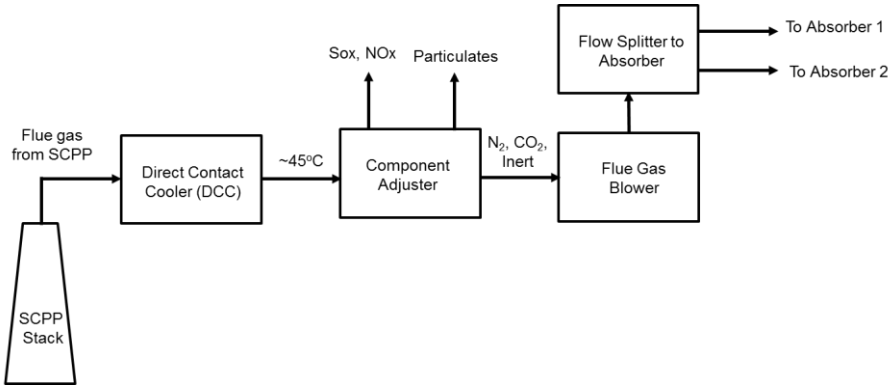


Figure 7.7: The SCPP Flue gas links with the PCC (*Adapted from* Lawal, 2010)

*7.3.2.2 Steam Draw-off from the IP/LP Crossover*

Steam from the IP/LP crossover section of the SCPP is drawn from for solvent regeneration in the PCC stripper section as recommended by Ramezan et al. (2007) and Lucquiaud and Gibbins (2009) etc. Due to the reduced flow through the turbine, the pressure upstream of the LP turbine drops with the draw-off (Figure 7.8). The floating IP/LP crossover pressure configuration was employed in this study because it

accommodates a variable flowrate of steam draw-off, similar to Lawal et al (2012) and recommended by Lucquiaud and Gibbins, 2009; Sanpasertparnich et al., 2010 etc.

A throttling valve between the steam draw-off point and the LP turbine adds an additional pressure drop to raise the crossover pressure by about 1 bar as shown in Figure 7.8. This ensures that the pressure across the IP/LP crossover does not drop below the minimum pressure of 3.0 bar required in the reboiler. To use this configuration, it is assumed that the IP turbine can accommodate the reduced exit pressures encountered with the steam draw-off (Lucquiaud and Gibbins, 2009).

A temperature controller is used to measure the temperature of the lean solvent stream from the reboiler and controls the steam drawn-off for regeneration (Lawal, 2010). A water attemperator/spray is used to reduce the steam temperature to a little above saturation. No loss of total enthalpy was assumed in the process because the additional sensible heat is converted to latent heat of the vaporized spray water. This stream is then delivered to the reboiler where it exchanges heat with the solvent. It is also assumed that all the steam delivered condenses in the reboiler leaving only saturated liquid condensate at the outlet stream. It is assumed that there are no heat losses and all the latent heat of vaporisation is transferred to the reboiler fluid (Lawal, 2010).

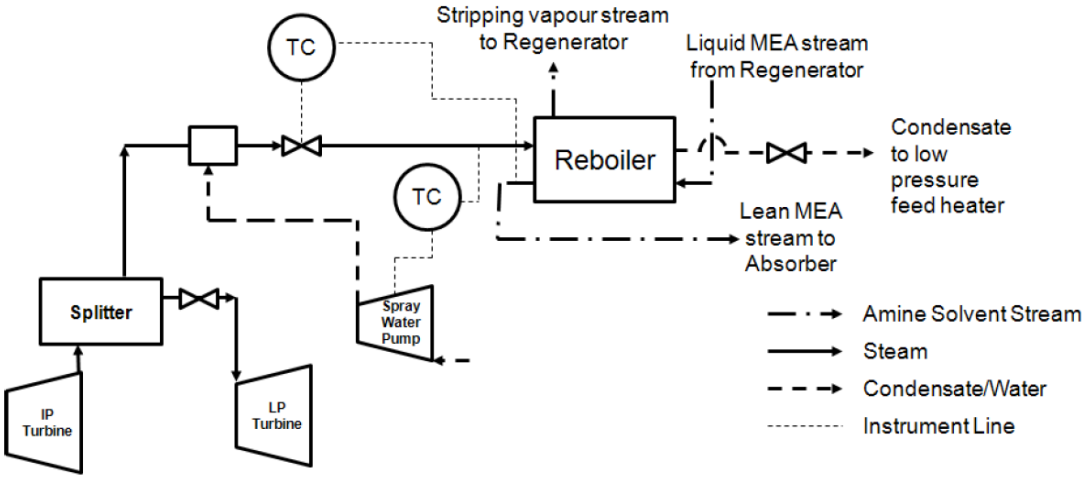


Figure 7.8: Steam Draw-off and Condensate Return (Lawal et al, 2012)

#### *7.3.2.3 Condensate Return to the SCPP Feedwater System*

The condensate is returned to the low pressure feed heater before being sent to the boiler feed pump. Figure 7.8 also shows the two links between the SCPP steam draw-off and the PCC plant condensate return. Part of this stream is used as water spray to reduce the steam temperature to the reboiler (Lawal, 2010).

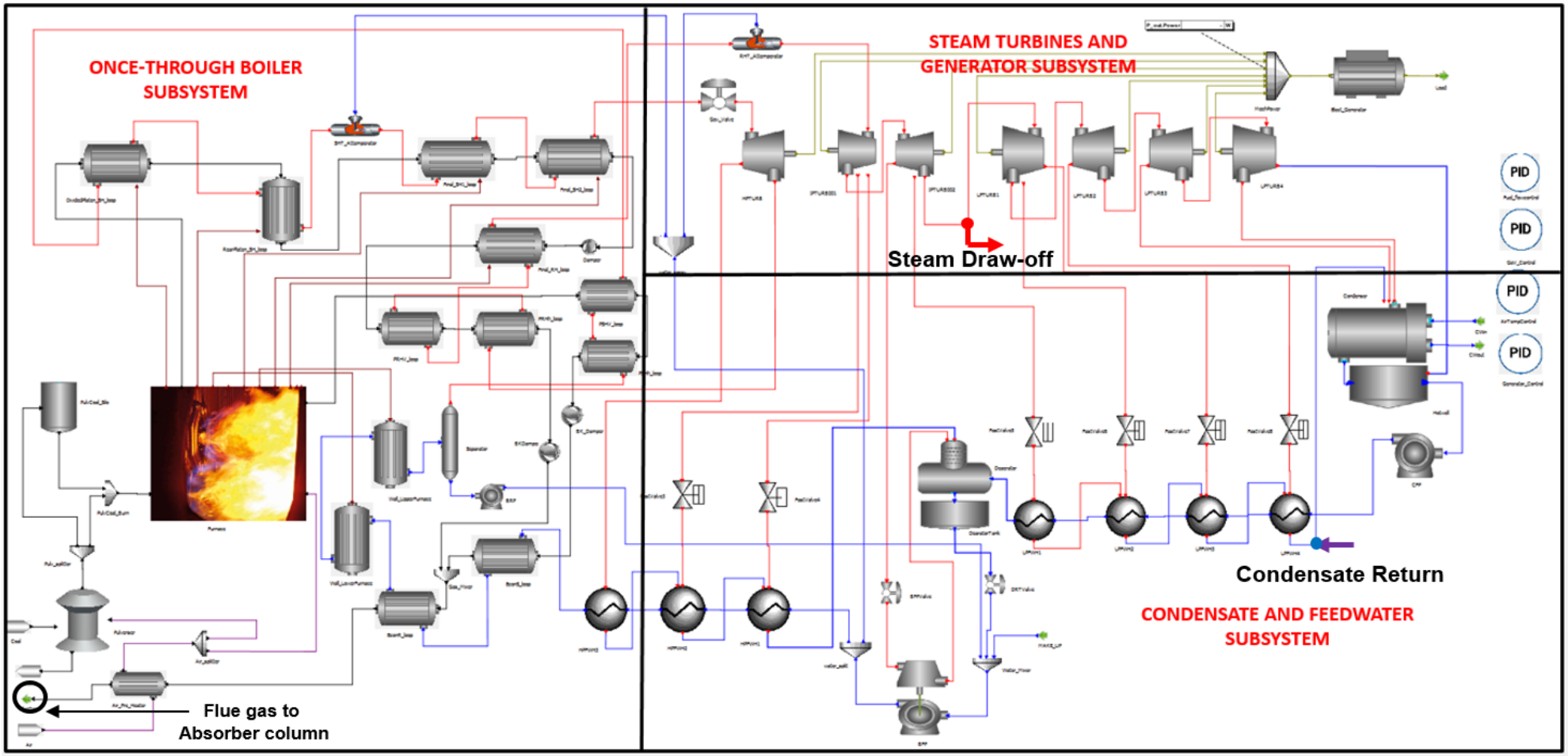


Figure 7.9: SCPP Model Topology showing the three connection points with the Scaled-up PCC Model

### 7.3.3 Integrated SCPP-PCC Dynamic Model

Figure 7.10 shows the SCPP-PCC integrated model topology in gPROMS®. Flue gas from the power plant is passed through the component adjuster that removes the SOx, NOx and includes the $O_2$ composition is merged with the $N_2$ fraction. It is then cooled in the Direct Contact Cooler and then delivered to the two absorber columns through the blower. In each absorber column, the gas is contacted with lean solvent to achieve the target level of $CO_2$ capture (typically 90%). The lean solvent is supplied from the lean amine tank where water and MEA is added to make-up the required solvent concentrations. The Lean solvent MEA chemically absorbs $CO_2$ to form the rich solvent, which is pumped from the absorber bottoms into the lean/rich amine heat exchanger. The regenerated lean solvent from the stripper heats up the rich solvent from the absorber to reduce the reboiler energy consumption. This energy is required to strip $CO_2$ from the solvent giving a $CO_2$ product via the condenser. The regenerated lean solvent is pumped back to the absorber column through the lean/rich heat exchanger, the lean amine cooler and then to the lean MEA tank.

Steam required in the reboiler is drawn from the IP/LP crossover of the SCPP at a controlled flowrate; decided by the reboiler temperature controller. To avoid solvent degradation by the superheated steam drawn-off the IP/LP crossover, part of the condensate returned is sprayed on the steam to reduce its temperature to just above saturation; controlled by the de-superheater control system. Complete condensation of the steam is assumed with the latent heat of vaporisation transferred to the solvent for regeneration in the reboiler. The condensate is returned to the LP feedwater heater in the SCPP.

### 7.3.4 SCPP-PCC Unit Control Systems

As shown in Figure 7.10, conventional proportional integral controllers (PI) is the most common controller in the integrated system. The control system for the SCPP part of the system is similar to the control loops for the standalone SCPP unit (discussed in Chapter 6) with the addition of steam de-superheater controller (DSC) for controlling the temperature of the steam drawn-off for solvent regeneration. The control systems for the PCC unit part of the integrated dynamic is similar to the control systems on the pilot plant simulation in Lawal et al (2010).

The reboiler temperature is controlled by the PI controller–RTC by manipulating the flowrate of steam draw-off from the SCPP. The reboiler liquid levels is controlled by the flowrate of liquid at the outlet stream as shown in Figure 7.10. The condenser temperature is controlled by the PI controller–CTC by manipulating the flowrate of cooling water being supplied. The condenser level (CLC) controller is a proportional only (P). It controls the level in the condenser by manipulating the flowrate of the liquid at the outlet.

The PI controller (Capt.LC) is used to control the capture level in the absorber column as shown in Figure 7.10. The Capt.LC controller controls the $CO_2$ capture level by estimating the quantity of $CO_2$ captured from the flue gas flow at the absorber inlet and manipulating the lean MEA solvent flowrate as shown in Figure 7.10. The addition of an MEA and water make-up streams to the lean MEA tank controls the composition of the lean solvent flow. The PI controllers –WBC and the MEA_frac_controller controls the solvent concentrations by manipulating the corresponding makeup flowrates of MEA and water, as shown in Figure 7.10.

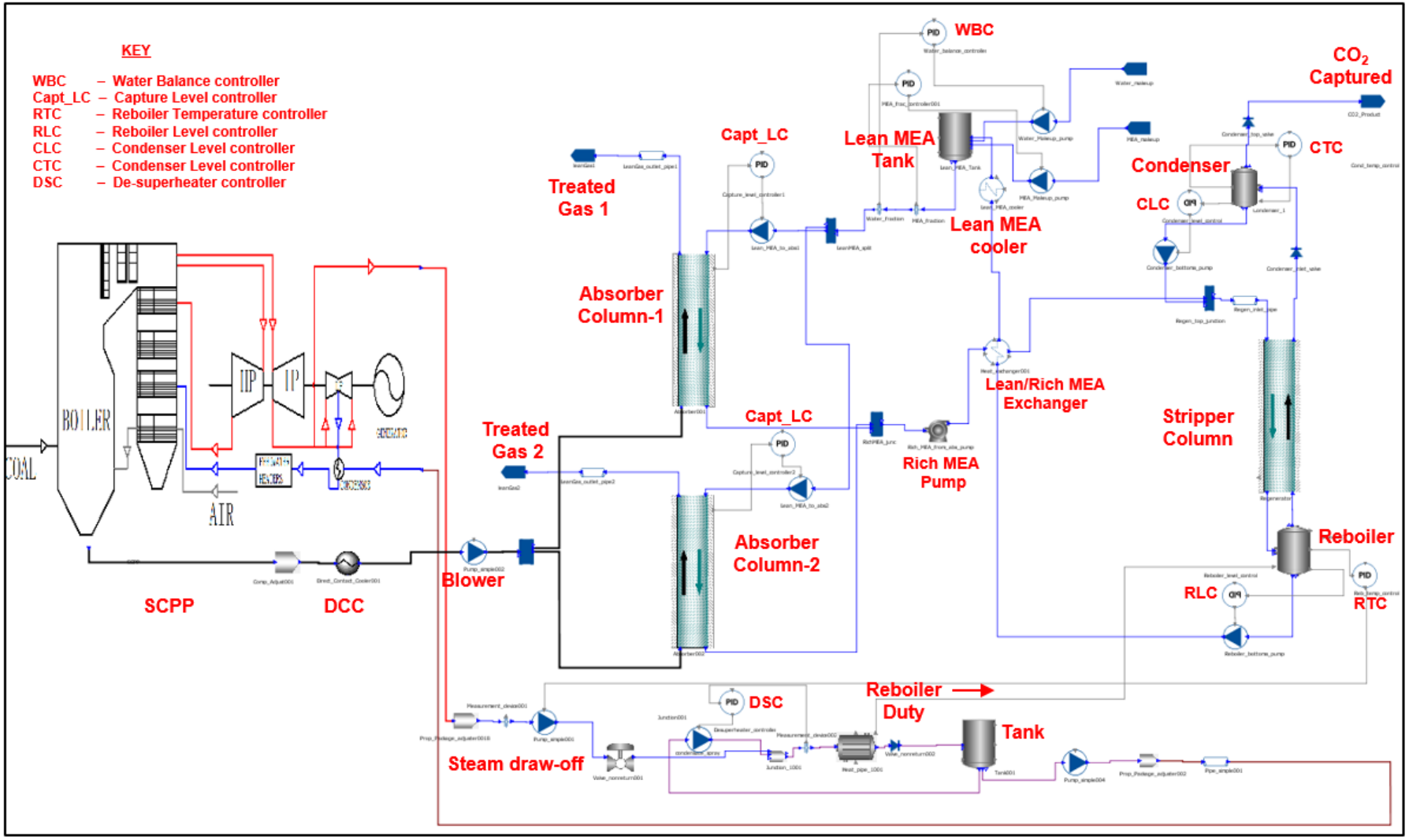


Figure 7.10: gPROMS® Topology of the Integrated SCPP-PCC Mode

## 7.4 Steady State Analysis of the Integrated Model

The performance of the SCPP integrated with the PCC process is investigated in this section. The power requirements for compressing the $CO_2$ leaving the regenerator to a pressure suitable for pipeline transmission to a storage site are not included in this thesis.

### 7.4.1 Base Case Study

The full load SCPP (100% MCR) model developed in section was used to determine base case conditions without the addition of the downstream PCC system. Key variables at the full load condition of SCPP are presented in Table 7.2.

Table 7.2: SCPP at full load (100% MCR) without PCC

| Variables | Value |
|---|---|
| Net power output (MWe) | 600 |
| Efficiency (%) | 40.93 |
| Fuel flow (kg/s) | 56.4 |
| %wt.$CO_2$ in flue gas | 20.54 |
| Flue gas flowrate (kg/s) | 612.03 |

The base case simulation results for the integrated system is simulated with 30 wt. % MEA. The results show that with the addition of the downstream PCC units, there was 24.13% reduction in the net power output of the SCPP to about 455 MWe (at full load) at about 95% $CO_2$ capture level. This reduction was due to the steam drawn-off from the SCPP for the reboiler duty in the stripper. This also leads to a drop in efficiency of the SCPP unit to about 34.62% (about 7% efficiency penalty). At a lower capture level, the energy and efficiency penalty due to the PCC addition is expected to be lower. The energy penalties due to $CO_2$ compression and other auxiliary unit downstream of the PCC was not considered in this thesis. Further reduction in parasitic energy loss is expected if this unit are considered. The power loss due to PCC addition to the SCPP can be improved through reduction of exergy destructions (see Chapter 4), heat integration, and process intensification of the PCC unit (Wang *et al*., 2011).

## 7.5 Dynamic Analysis of the Integrated Model

For the dynamic analysis, ramp test was performed on the integrated model as follows: The SCPP-PCC system was initially simulated for about 240 minutes at 100% MCR load (about 455 MWe net power output) before the injection of the ramp change. The system is then ramp down to 75% MCR (about 340 MWe net power output) at a rate of 9.5MWe/min (similar to the reference SCPP ramp rate) until it reaches a steady state. The steady state level was maintained for a further 120 minutes. The system was ramped up back to 100% MCR at the same ramping rate until it reaches steady state. This steady state level was then maintained for about 480 minutes. Figure 7.11 shows the response of the system to the ramp change.

The results (Figure 7.11) of the ramp test shows expected behaviour as discussed in literature (Lawal et al, 2012). As the power plant load is ramped from 455 MWe to about 340 MWe, the response of the fuel flowrate and subsequently the flue gas flowrate is very fast decreased correspondingly from 56.4 kg/s to about 43 kg/s. The flue gas flowrate changed in like manner. With lower amount of flue gas available in the absorber, a smaller Lean solvent flowrate is required as shown in the ramp test. Hence, the reboiler duty will be lower, resulting in a reduced demand for steam draw-off for solvent regeneration.

The SCPP efficiency shows an initial perturbations at the point of injection of the ramp before flattening out at roughly the same steady state value due to with fluctuations which reflect changes in steam supply to the stripper reboiler. The results also shows that the lean solvent flowrate has the largest deviation to the drop in SCPP load, due to its being sensitive (L/G ratio) to the capture level control. The capture level shows minimal fluctuation before settling at the same set point, but it does not change considerably due to its level control being dependent largely on the solvent circulation rate.

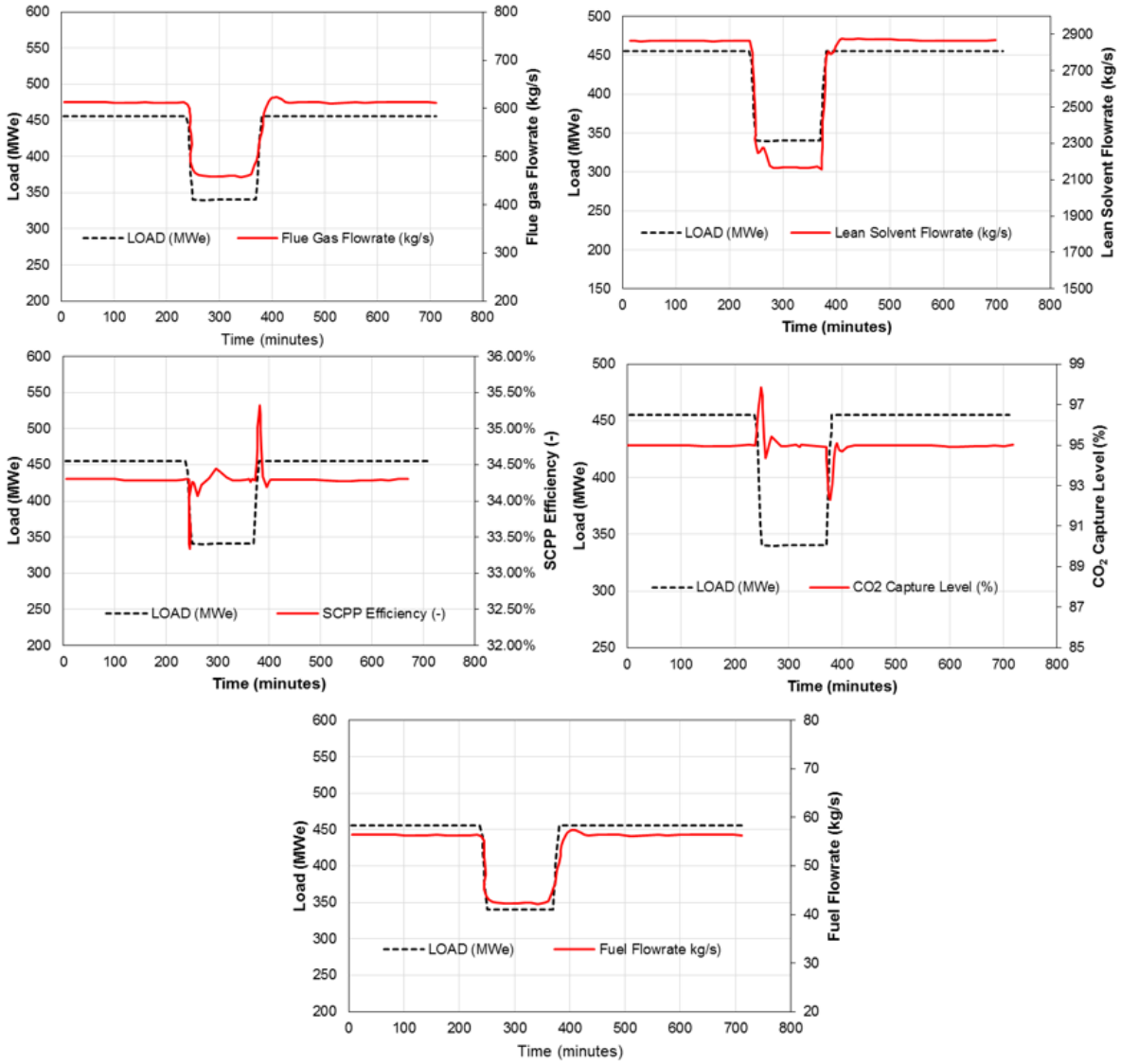


Figure 7.11: Response of the integrated model to Ramp change in Load

## 7.6 Operating SCPP Integrated with PCC under UK Grid Code Requirement

Operating an integrated an SCPP with $CO_2$ Capture ability under the UK grid requirement (especially the primary frequency response) presents its own opportunities and challenges. A very important strategy is the use of the PCC link (i.e. the steam draw-off) with the SCPP as a buffer for meeting the 10% MCR requirement during primary frequency response. In this analysis, the contribution of each methods described is

measured with reference to the power plants registered capacity at full load prior to its integration with the PCC unit.

### 7.6.1 Stripper Stop Mechanism

As suggested by Haines and Davison (2014), a “stripper stop” mechanism whereby the steam normally drawn-off from the IP/LP crossover can be reduced or stopped temporarily and the steam redirected to generate more power during primary frequency response. The SCPP-PCC dynamic model was re-configured to accommodate the “stripper stop” analysis through the use of a fast-action valve between the IP/LP extracted steam and the reboiler temperature controller for fast response. The de-superheater flow controller set point was changed to increase the temperature of the steam inventory in the reboiler during the frequency response period. Lastly, the stripper column pressure set point was increased by +10%. The changes to the reboiler temperature and the stripper column pressure is necessary to provide adequate driving force for the stripper stop mechanism (Haines and Davison, 2014). The integrated model was simulated to determine the contribution of the stripper stop approach to the primary frequency response. The result (Figure 7.12) show that the stripper stop mechanism produces about 4.67% MCR (~28 MWe) and 3.3% MCR (~20 MWe) increase in the SCPP at 75% and 100% load respectively. Other mechanisms i.e. combining stripper stop with condensate/extraction stop is discussed in the following sections.

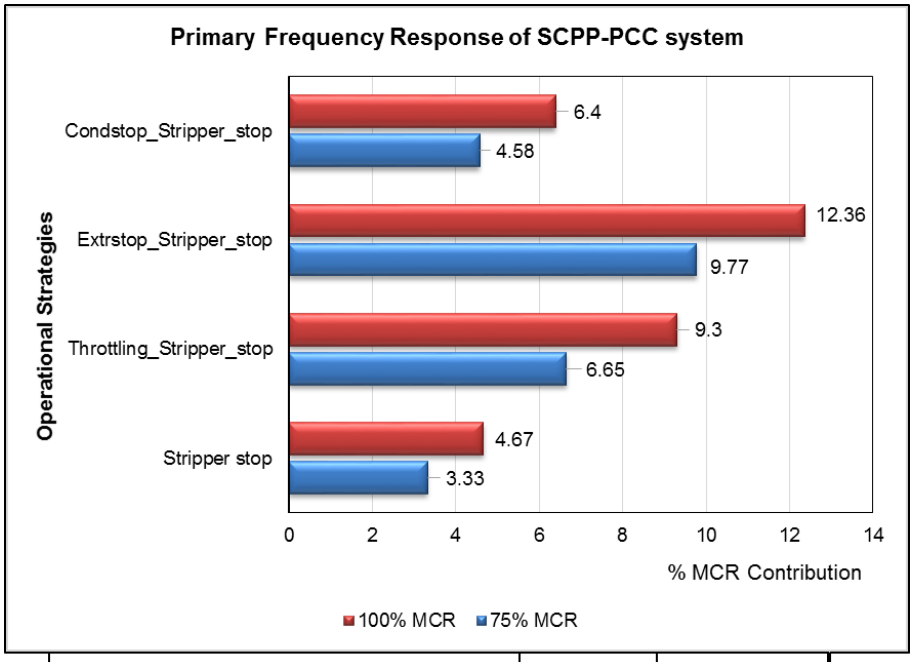


| Strategy | 75% MCR | 100% MCR |
|---|---|---|
| Stripper stop (%) | 3.325 | 4.67 |
| Stripper stop (MWe) | 19.95 | 28 |

Figure 7.12: Contribution of Stripper stop to primary frequency response

### 7.6.2 Combination of Stripper Stop and Condensate stop (LPT-Extraction)

The idea of combining the stripper stop mechanism with the condensate stop of the SCPP is borne out of the need to increase the amount of excess power available for primary frequency control. The simulation was performed based on 0.5 Hz frequency drop over 10 seconds as required by the UK grid. First, the SCPP unit was simulated at full load for one hour, then a ramp in frequency of -0.5Hz was applied at a rate of 0.05 Hz/seconds; then the configuration for the condensate stop discussed in chapter six was implement simultaneously with the stripper stop configuration in section 7.6.1. The result (Figure 7.13) shows that at 100% MCR and 75% load, a combined effect of the stripper stop and the condensate stop only contributed about additional 1.7% MCR and 1.3% MCR to the stripper stop-only approach.

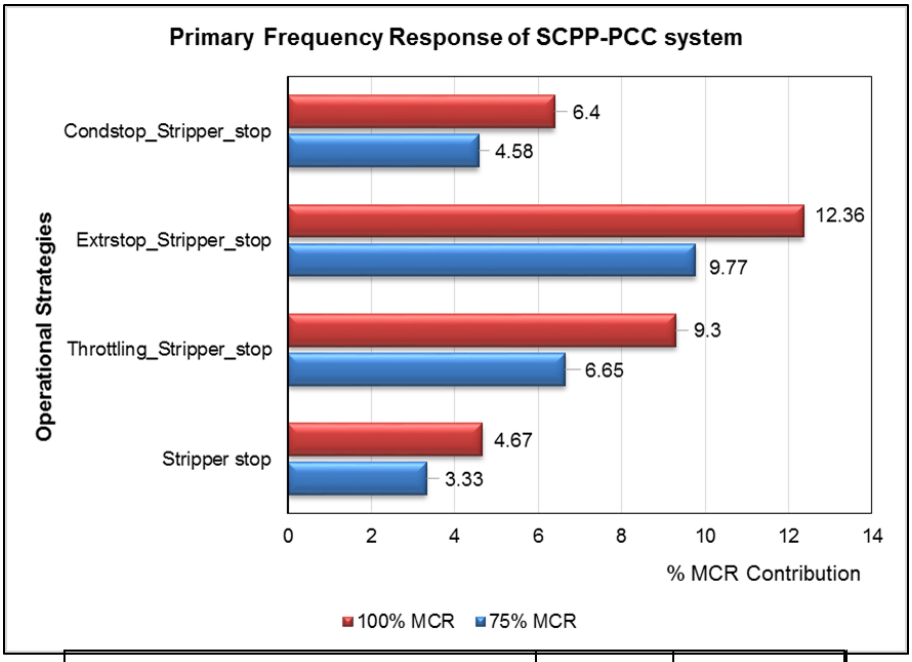


| Strategy | 75% MCR | 100% MCR |
|---|---|---|
| Condstop_Stripper_stop (%) | 4.58 | 6.4 |
| Condstop_Stripper_stop (MWe) | 27.45 | 38.41 |

Figure 7.13: Contribution of Condensate stop and Stripper stop

Combining the condensate stop and stripper stop mechanism as described in this thesis may not be a practicable operation without risking the stability of the system due to the coupling between the condensate return loop and the IP/LP steam extraction. However, implementation of advanced control scheme within this units could ensure smooth operation of this configuration. The additional cost of re-sizing the reboiler sump and the higher pressure operation of the stripper may not be economically justifiable considering the small increment the addition of the condensate stop to the stripper stop contributes to the overall frequency response capability of the plant.

### 7.6.3 Combination of Stripper Stop and Steam Throttling

The stripper stop mechanism with the steam throttling of the SCPP was also used to increase the amount of excess power available for primary frequency control. The simulation was performed based on 0.5 Hz frequency drop over 10 seconds as required by the UK grid. First, the SCPP unit was simulated at full load for one hour, then a ramp

in frequency of -0.5Hz was applied at a rate of 0.05 Hz/seconds; then the configuration for the main steam throttling discussed in chapter six was implemented simultaneously with the stripper stop configuration.

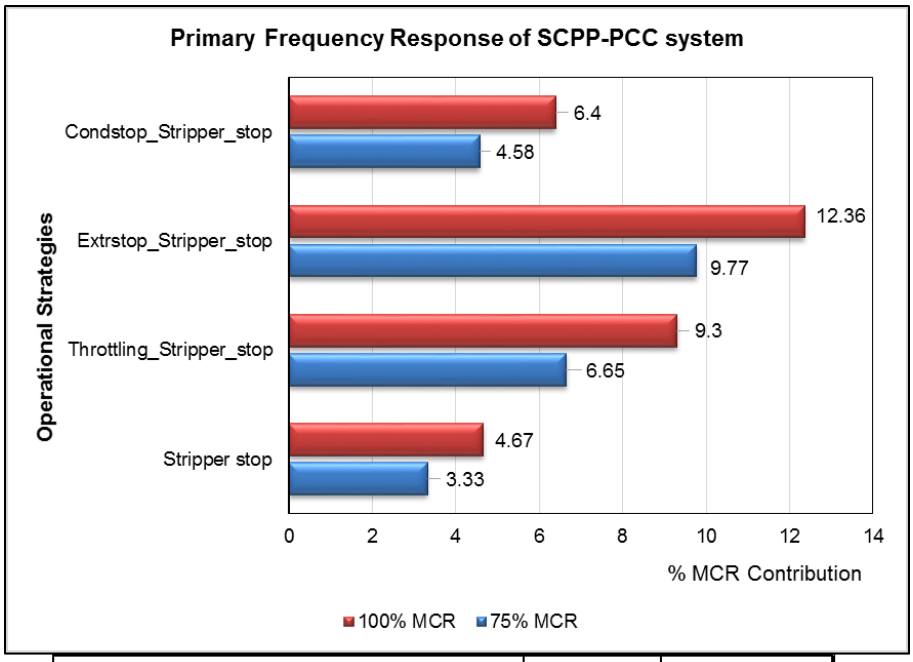


| Strategy | 75% MCR | 100% MCR |
|---|---|---|
| Throttling_Stripper_stop (%) | 6.65 | 9.3 |
| Throttling_Stripper_stop (MWe) | 39.9 | 55.83 |

Figure 7.14: Contribution of Main steam throttling and Stripper stop

The result (Figure 7.14) shows a very significant addition to the stripper stop-only mechanism to meeting the primary frequency response requirement. At 100% MCR and 75% MCR, a combined effect of the stripper stop and the main steam throttling contributed about 9.3% MCR and 6.7% MCR respectively. This shows that steam throttling and stripper stop mechanism can almost achieve the 10% MCR requirement only when operating at full load as shown in this study.

### 7.6.4 Combination of Stripper Stop and Extraction stop (IPT-LPT Extraction)

Combining the extraction stop mechanism described in Chapter six with the stripper stop mechanism is perhaps the most promising of the configurations described in this thesis

for the higher additional % MCR contribution for the frequency control. The simulation was performed based on 0.5 Hz frequency drop over 10 seconds as required by the UK grid. The configuration for extraction stop was simulated simultaneously with the stripper stop configuration. The result (Figure 7.15) show a significant increase of over 50% compared to the stripper stop-only mechanism and about 45% increase to the extraction stop-only configuration.

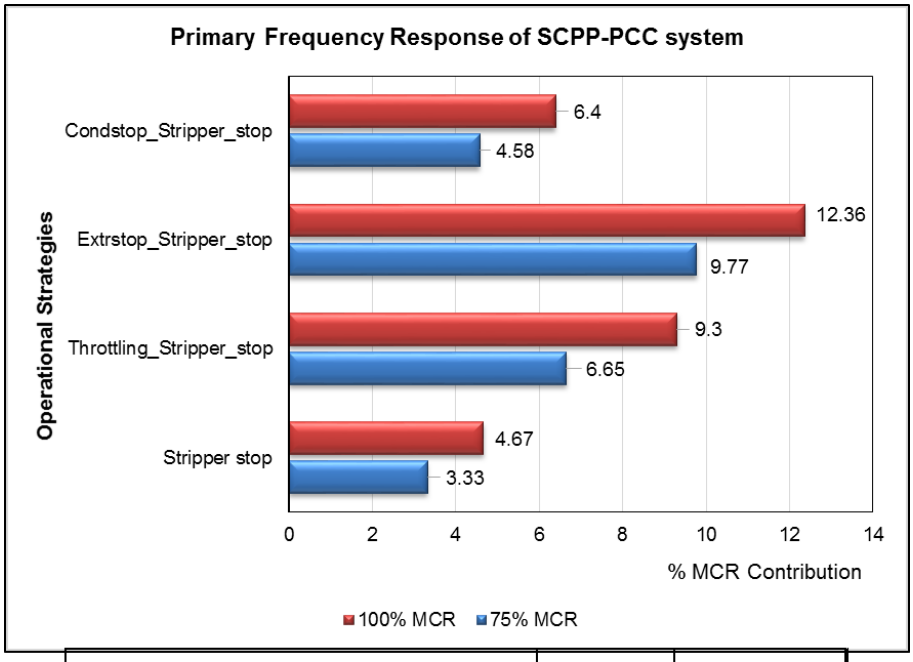


| Strategy | 75% MCR | 100% MCR |
|---|---|---|
| Extrstop_Stripper_stop(%) | 9.77 | 12.36 |
| Extrstop_Stripper_stop (MWe) | 58.61 | 74.16 |

Figure 7.15: Contribution of Extraction stop and Stripper stop

At 100% MCR and 75% MCR, a combined effect of the stripper stop and the extraction stop contributed about 12.4% MCR and 9.8% MCR as shown in Figure 7.15. This indicated that combination of extraction stop and stripper stop mechanisms can achieve the 10% MCR requirement when operating at above 75% MCR as shown in this study.

## 7.7 Summary

This chapter analysed the strategies for operating the SCPP integrated with PCC unit under the UK grid requirement as regards to primary frequency response. The integrated model was simulated to determine the contribution of the stripper stop approach to the primary frequency response. The result show that the stripper stop mechanism produces about 4.67% MCR (~28 MWe) increase in the SCPP at full load condition. This is however, not sufficient for the 10% MCR required for the primary response. A combination of the “stripper stop” mechanism with the SCPP’s steam throttling, condensate or extraction stops. The results show that the combination of stripper stop mechanism with extraction stop can meet the 10% MCR requirement for integrated plant operating at above 75% of its full capacity. The throttling and stripper stop configuration only barely meets the demand at full load capacity. The condensate stop combination with the stripper stop mechanism on the other hand could not meet the frequency response requirement at any load level.

# Chapter 8 Conclusions and Recommendation for Future Study

## 8.1 Conclusions

This thesis presents a model-based studies and operational analysis of a supercritical coal-fired power plant integrated with post-combustion $CO_2$ capture under UK grid code requirement. Steady state, dynamic modelling of SCPP and PCC were reviewed to identify current gaps in knowledge as detailed in Chapter 2 of this thesis. The review showed that there have been an enormous work done on the modelling of SCPP and PCC units (dynamic and steady state) individually. However, it was observed that there are very few dynamic model of a SCPP integrated with a dynamic model of PCC based on chemical absorption under stringent grid code operating conditions had been reported in open literature.

### 8.1.1 Steady state simulation of SCPP Integrated with PCC

Chapter 3 presents a steady state simulation of SCPP integrated with PCC in Aspen Plus®. The SCPP model was validated against design data from a Greenfield reference plant. The PCC model was validated at pilot-scale with experimental data. The model was scaled up and integrated with the SCPP model. The model is made up of different subsystems. Each subsystem bases its calculations on inputs from other subsystems, and constants set during the model. There were several stages in the development of the model, and validation checks were performed to ensure realistic results were achieved. Aspen Plus® was able to match the steady state operating conditions of the reference plant with a relative error of 1.65% in gross power output. It is concluded that the steady state model is fairly accurate when comparing the solutions from the model with design data from the reference SCPP. The model was verified by comparing the solutions from the model with design data at full load. The model output is consistent with the data from the reference plant at full load and that gives confidence on the future use of the model. The importance of this model is to familiarise with the steady state working condition of

the SCPP system integrated with PCC, to carry out further analyses and case studies on strategies for minimising energy penalties in the system (i.e. exergy analysis, efficiency etc.), and as a prerequisite to the dynamic model development process.

### 8.1.2 Conventional and Advanced Exergy Analysis of SCPP Integrated with PCC

Conventional and advanced exergetic analysis was performed in Chapter 4 to allow for a consistent and detailed evaluation of energy consumption in the SCPP-PCC integrated system from a thermodynamic point of view. The conventional exergy analysis evaluates the amount and location exergy destruction with the whole system. The advanced exergetic analysis estimates the sources (endogenous or exogenous) of the exergy destruction in individual component or the whole system and the potential for reducing it (unavoidable or avoidable). The boiler subsystem has the largest exergy destruction but also has a limited influence on fuel-saving potentials of the SCPP system. The turbine subsystem shows very small exergy destruction compared to the boiler subsystem, but more significance in reducing fuel consumption. This study show that a combination of improvement in turbine performance design and reduction of the driving forces responsible for the $CO_2$ capture (without compromising cost) can help improve the rational efficiency of the integrated system. Seven modifications to the conventional MEA-Based PCC were considered for reducing exergy destruction: AIC, SF, AIC+SF, SIH, SIH+AIC, LVR, and LVR+AIC. The LVR+AIC configuration shows the most significant reduction in exergy destruction, reboiler energy and efficiency penalties when compared to the conventional case. The results show that the energy/exergy consumption and the efficiency of the integrated system can be improved by recovering the avoidable exergy destruction in the system.

### 8.1.3 Dynamic Model of SCPP Once-through Boiler

Chapter 5 presents a dynamic model and comparison of the lumped parameter and distributed parameter modelling approaches for SCPP once-through boiler steam generation process. The models were developed from the mass, momentum, and energy conservation principles. The simulation results show that in the distributed parameter model, the relative errors in predicting the outlet steam temperature and pressure of the

evaporator waterwall were less than 1% and 5% respectively at 87% BMCR (boiler maximum continuous rating), 75% BMCR, and 50% BMCR. The lumped parameter model on the other hand, shows average relative error of 2% and 7% for steam temperature and pressures respectively at all the simulated cases. The study shows that a distributed parameter model gives a more accurate prediction of the SCPP boiler dynamics at different load levels and will be more reliable to investigate transient behaviour under very stringent scenarios. The lumped parameter however is also useful for model-based control studies due to its simplicity and reasonable accuracy. The distributed parameter model developed in this chapter will be used in investigating the response of the whole SCPP under varying load and frequency changes.

### 8.1.4 Dynamic Modelling and Operational analysis of SCPP under UK Grid Requirement

Dynamic modelling and analysis of the strategies for operating a SCPP under the UK grid code requirement as regards to primary frequency response was performed in Chapter 6. The SCPP model was used to simulate the flexibility of the SCPP for rapid load changes and variations in system frequency. The UK grid code stipulates that depending on the operating load as a percentage of the registered capacity (MCR), up to 10% of registered capacity has to be supplied within 10–30s of a 0.5Hz frequency drop occurring over a 10s period. The simulation results show that using turbine throttling approach (about 3.3% MCR), extraction stop (about 6.8% MCR) or condensate stop (about 1% MCR) individually was not sufficient to meet the grid requirement. On the other hand, the study shows that a combination of turbine throttling, extraction stop and/or condensate stop can achieve a 10% increase in generating capacity (MCR) of a SCPP within 10s to 30s of primary frequency change as required by the UK grid while operating at a load level of between 60–100% of its registered capacity.

### 8.1.5 Operational analysis of SCPP Integrated with PCC under UK Grid Requirement

Chapter 7 presents the Integration of dynamic model of the SCPP developed in Chapter 5 with dynamic model of a PCC unit developed by Lawal (2010). The integrated model

was used to analyses the strategies for operating the SCPP integrated with PCC unit under the UK grid code requirement as regards to primary frequency response. The integrated model was simulated to determine the contribution of the stripper stop approach to the primary frequency response. The result show that the stripper stop mechanism produces about 4.67% MCR (~28 MWe) increase in the SCPP at full load condition. This is however, not sufficient for the 10% MCR required for the primary response. A combination of the “stripper stop” mechanism with the SCPP’s steam throttling, condensate or extraction stops. The results show that the combination of stripper stop mechanism with extraction stop can meet the 10% MCR requirement for integrated plant operating at above 75% of its full capacity. The throttling and stripper stop configuration only barely meets the demand at full load capacity. The condensate stop combination with the stripper stop mechanism on the other hand could not meet the frequency response requirement at any load level.

## 8.2 Recommendation for Future Study

Further studies beyond the scope of this thesis; such as including $CO_2$ compression and transport systems as part of the primary response systems will also be useful to investigate different variants of the “stripper stop” mechanisms such as stripper pressure reduction and $CO_2$ venting, $CO_2$ compressor trip (if compression is added to the CCS chain), lean and rich amine storage etc. as described in Haines and Davison (2014).

A detailed model-based control studies of the standalone SCPP to investigate further the stability and controllability of the system under UK grid code requirement. The SCPP-PCC integration controllability issues under the same UK grid scenario should also be carried out with a view to analysing the control challenges under normal and emergency operations (i.e. primary frequency response) in the wake of continuous influx of renewables into an already stringent grid system and the carbon emission reduction targets.

Further analysis of the steady state simulation of the integrated SCPP-PCC system should also be carried out to investigate:

- The sensitivity of the integrated SCPP-PCC system to changes in coal composition should be investigated
- The steady state simulation of the SCPP should be performed using both gPROMS® and Aspen Plus® and the results compared with the reference plant.
- Analysis of using different packing type/material and different MEA solvent concentration on the performance of the integrated system

Further analysis of the dynamic model can also be investigated to improve the operational insight of the SCPP-PCC under the UK grid. In this case, the SCPP-PCC model can be integrated with $CO_2$ Compression, $CO_2$ transport, $CO_2$ storage and/or utilization models for a complete CCS network analysis under the UK grid code requirement. The analysis can consider issues such as:

- The primary and secondary response capability of the SCPP in a whole chain CCS network scenario using different configurations of the CCS network to recover extra power for the SCPP during a frequency drop.
- The sensitivity, energy penalties and operability of the PCC unit can be investigated by developing dynamic model of the PCC with the different configurations (e.g. dynamic model of absorber intercooling configuration) studied in Chapter 4 of this thesis. This dynamic models can then be integrated with the SCPP and the downstream $CO_2$ compression, transport and storage.
- The economics of the different PCC system can also be investigated to make appropriate design decision considering the trade-offs between the amount of energy penalties reduction and the additional costs of changing to a new configurations or system.

# REFERENCES


Aboudheir, A., Tontiwachwuthikul, P., Chakma, A. and Idem, R., (2003). Kinetics of the reactive absorption of carbon dioxide in high $CO_2$-loaded, concentrated aqueous monoethanolamine solutions. *Chemical Engineering Science*, Vol. 58, pp. 5195 – 5210.

Adams, J., Clark, D. R., Louis, J. R., and Spanbauer, J.P., (1965). Mathematical modelling of once-through boiler dynamics, IEEE Winter Power Meeting, New York, IEEE, pp. 146-156.

Amrollahi, Z., Ertesvag, I.S., Bolland, O., (2011). Optimized process configurations of post-combustion $CO_2$ capture for natural-gas-fired power plant—power plant -Exergy analysis, Int. J. Greenhouse Gas Control 5, pp. 1393-1405.

Aroonwilas A, Veawab A., (2007). Integration of $CO_2$ capture unit using single and blended-amines into supercritical coal-fired power plants: implications for emission and energy management. Int J Greenhouse Gas Contr. 1(2), pp. 143‑50.

Ashrafizadeh S.A., Amidpour M., Abolmashadi M. (2013) Exergy Analysis of Distillation Column Using Concept of Driving Forces. Journal of Chemical Engineering of Japan 46 (7), pp. 434–443.

AspenTech, (2013). Aspen physical property system: physical property methods. Burlington, MA, USA: Aspen Technology Inc.

Berry JE, Holland MR, Watkiss PR, Boyd R, Stephenson W., (1998). Power Generation and the Environment – a UK Perspective. Report number AEAT3776, ExternE Project, AEA Technology Environment, Abingdon, Oxfordshire.

Bhambare, K.S., Mitra, S.K., Gaitonde, U.N., (2007). Modelling of a coal-fired natural circulation boiler. Journal of Energy Resources Technology 129, pp. 159-167.

Biliyok, C., Lawal, A., Wang, M., Seibert, F., (2012). Dynamic modelling, validation and analysis of post-combustion chemical absorption $CO_2$ capture plant. International Journal of Greenhouse Gas Control 9, pp. 428-445.

Bishnoi, S. and Rochelle, G.T., (2002). Thermodynamics of Piperazine / Methyl diethanolamine / Water/ Carbon Dioxide. Ind*. Eng. Chem.* 41 (3), pp. 604–612.

Blokh, A.G. 1987. Heat transfer in steam boiler furnaces. Hemisphere publishing corporation, London. ISBN 0-89116-626-2.

Botsch, T.W., Stephan, K., Alcock, J.-L., Webb, D.R. (1997) Modelling and Simulation of the Dynamic Behaviour of a Shell and Tube Condenser, International Journal of Heat Transfer 40 (17), pp. 4137-4149.

Bravo J.L., Rocha J.A., Fair J.R. (1992), Comprehensive model for the performance of columns containing structured packings. Inst. Chem. Eng. Symp. Ser. 129, pp. A439-457.

Canepa R, Wang M, Biliyok C, Satta A., (2013). Thermodynamic analysis of combined cycle gas turbine power plant with post-combustion $CO_2$ capture and exhaust gas recirculation. Proc Inst Mech Eng Part E: J Process Mech Eng 227(2), pp. 89‑105.

Chaibakhsh, A. and Ghaffari, A., (2008). Steam turbine model. Simulation Modelling Practice and Theory 16 (9), pp. 1145-1162.

Chaibakhsh, A., Ghaffari, A. and Moosavian, S. A. A. (2007), "A simulated model for a once-through boiler by parameter adjustment based on genetic algorithms", Simulation Modelling Practice and Theory 15 (9), pp. 1029-1051.

Ciechanowicz, W., (1968). The Dynamics of a Vapour Condenser. Nuclear Engineering and Design 7, pp. 1-8.

Dawid H.P., Biliyok C., Yeung H., Bialecki R., (2014). Heat integration and exergy analysis for a supercritical high-ash coal-fired power plant integrated with a post-combustion carbon capture process, Fuel 134, pp. 126-139.

Diegel, D., Eckstein, S., Leuchs, U., Zaviska, O., (2006). Fulfilment of Grid Code Requirements in the area served by UCTE by Combined Cycle Power Plants. Siemens AG, Power Generation, Germany.

Dimian, A.C. (2003). Integrated Design and Simulation of Chemical Processes. Elsevier Science B.V., Amsterdam, Netherlands.

DOE/NETL, (2014). Quality Guidelines for Energy Systems Studies: Process Modelling Design Parameters. US Department of Energy.

Dong, Y. and Tingkuan C., (2001). HGSSP-A Computer Program for Simulation of Once-through Boiler Start-up Behaviour. Heat Transfer Engineering, 22(5), pp. 50-60.

Dugas, E. R., (2006). Pilot plant study of carbon dioxide capture by aqueous mono-ethanolamine, M.S.E thesis, University of Texas at Austin, USA.

Edali, M., Aboudheir, A. and Idem, R. Kinetics of carbon dioxide absorption into mixed aqueous solutions of MDEA and MEA using a laminar jet apparatus and a numerically solved 2D absorption rate/kinetics model. *International Journal of Greenhouse Gas Control*, Vol.3 (2009) 550–560.

El-Sayad, M. A. H., Eteiba, M. B. and Sheirah, M. A., (1989). Self-tuning control of thermal power plants. International Journal of Electrical Power & Energy Systems 11 (1), pp. 2-8.

Faber, R., Kopcke, M., Biede, O., Knudsen, J.N. and Andersen, J., (2011). Open-loop step responses for the MEA post-combustion capture process: Experimental results from the Esbjerg pilot plant. Energy Procedia 4, pp. 1427-34.

Fair J.R., Bravo J.L., (1987). Prediction of mass transfer efficiencies and pressure drop for structured tower packings in vapour/liquid service. Inst. Chem. Eng. Symp. Ser., 104, pp. A183-200.

Freund P., (2003). Making deep reductions in $CO_2$ emissions from coal-fired power plant using capture and storage of $CO_2$. Proc Inst. Mech Eng Part A: J Power Energy 217:18.

Gaspar, J; Cormos, A.M., (2011). Dynamic modeling and validation of absorber and desorber columns for post-combustion CO2 capture, Computer & Chemical Engineering 35, 2044-2052.

Geuzebroek, F.H., Schneiders, L.H.J.M., Kraaijveld, G.J.C., Feron, P.H.M., (2004). Exergy analysis of alkanolamine—based $CO_2$ removal unit with Aspen Plus. Energy 29 (9/10), pp. 1241–1248.

Goff, G. S. and Rochelle, G. T., (2004). Monoethanolamine degradation: $O_2$ mass transfer effects under $CO_2$ capture conditions. Ind. Eng. Chem. Res. 43, pp. 6400-6408.

Harkin T., Hoadley A., Hooper B., (2009). Process integration analysis of a brown coal fired power station with $CO_2$ capture and storage and lignite drying. Energy Procedia 1(1), pp. 3817–3825.

Haywood R.W. (1981), Equilibrium thermodynamics for engineers and students. Chichester, New York, Brisbane, Toronto: Wiley Interscience Publication, John Wiley and Sons Inc.

Harun, N., Douglas, P.L., Ricardez-Sandoval, L. and Croiset, E., (2011). Dynamic simulation of MEA absorption processes for $CO_2$ capture from fossil fuel power plant. *Energy Procedia* 4, pp. 1478–1485.

Hikita H, Asai S, Ishikawa H, Honda M. (1977), The kinetics of reactions of carbon dioxide with monoethanolamine, diethanolamine, and triethanolamine by a rapid mixing method, Chem. Eng. J., 13, pp. 7-12.

Horlock, J.H., Young, J.B., Manfrida, G., (2000), Exergy Analysis of Modern Fossil–Fuel Power Plants, J. Eng. Gas Turbines and Power 122, pp. 1-7.

Idem, R., Wilson, M., Tontiwachwuthikul, P., Chakma, A., Veawab, A., Aroonwilas, A. and Gelowitz, D., (2006). Pilot Plant Studies of the $CO_2$ Capture Performance of Aqueous MEA and Mixed MEA/MDEA Solvents at the University of Regina $CO_2$ Capture Technology Development Plant and the Boundary Dam $CO_2$ Capture Demonstration Plant. Ind. Eng. Chem. Res. 45 (8), pp. 2414–2420.

Inoue, S., Itakura, T., Nakagaki, T., Furukawa, Y., Sato, H., Yamanaka, Y., (2013). Experimental Study on $CO_2$ Solubility in Aqueous Piperazine/Alkanolamines Solutions at Stripper Conditions. Energy Procedia, GHGT-11, PP 1751-1759.

Jassim, M.S., Rochelle, G.T. (2006). Innovative Absorber/Stripper for CO2 capture by Aqueous Monoethanolamine, Industrial Engineering Chemistry Research 45, pp. 2465–2472.

Kalnitsky, K.C., Kwatny, H.G., (1981) A First Principles Model for Steam Turbine Control Analysis. J. Dyn. Sys. Meas. Control 103(1), pp. 61-68.

Kaushik S.C., Siva Reddy V., Tyagi S.K., (2011). Energy and exergy analysis of thermal power plants: a review. Renew Sustain Energy Rev 15, pp. 1857–1872.

Khan, F.M., Krishnamoorthi, V. And Mahmud, T., (2011). Modelling reactive absorption of $CO_2$ in packed columns for post-combustion carbon capture applications. Chemical Engineering Research and Design 89, (9), pp. 1600-1608.

Kitto, J.B., and Stultz, S.C., (2005). Steam: its Generation and Use, The Babcock and Wilcox Company, Barberton, Ohio, USA, 41st Edition.

Knudsen, J.N., Jensen, J.N., Vilhelmsen, P. and Biede, O., (2009). Experience with $CO_2$ capture from coal flue gas in pilot-scale: testing of different amine solvents. Energy Procedia 1 (1), pp. 783–790.

Kohl, A.L., Nielsen, R.B., (1997). Gas Purification, 5th Edition, Gulf Publishing Company, Houston, Texas, US.

Kotas T.J., (1995). The Exergy Method of Thermal Plant Analysis. Kriegler Publishing Company: Malabar, Florida, US.

Kucka, L., Richter, J., Kenig, E.Y., Gorak, A., (2003). Experimental Study on $CO_2$ Solubility in Aqueous Piperazine / Alkanolamines Solutions at Stripper Conditions. Sep. Purific. Tech 31, pp. 163 – 175.

Kvamsdal, H.M. and Rochelle, G.T., (2008). Effects of the temperature bulge in $CO_2$ absorption from flue gas by aqueous monoethanolamine. Ind. Eng. Chem. Res. *47* (3), pp. 867–875.

Kvamsdal, H.M., Jakobsen, J.P. and Hoff, K.A. (2009), Dynamic modelling and simulation of a $CO_2$ absorber column for post-combustion $CO_2$ capture. Chemical Engineering and Processing: Process Intensification 48 (1), pp. 135-144.

Lawal A., Wang M., Stephenson P., Obi O., (2012). Demonstrating full-scale post combustion $CO_2$ capture for coal-fired power plants through dynamic modelling and simulation. Fuel 101, pp. 115–28.

Lawal, A., Wang, M., Stephenson, P., Koumpouras, G. and Yeung, H., (2010). Dynamic modelling and analysis of post-combustion $CO_2$ chemical absorption process for coal-fired power plants. *Fuel*, 10 (10), pp. 2791-2801.

Lawal, A., Wang, M., Stephenson, P., Yeung, H., (2009a). Dynamic modelling of $CO_2$ absorption for post combustion capture in coal-fired power plants. Fuel 88(12), pp. 2455-2462.

Lawal, A., Wang, M., Stephenson, P., Yeung, H., (2009b). Dynamic modelling and simulation of $CO_2$ chemical absorption process for coal-fired power plants. Comp. Aided Chem. Eng. 27, pp. 1725-1730.

Leites, I.L., Sama, D.A., Lior, N., (2003). The theory and practice of energy saving in the chemical industry: some methods for reducing thermodynamic irreversibility in chemical technology processes. Energy 28, pp. 55–97.

Li, B., Chen, T. and Yang, D., (2005). DBSSP–A computer program for simulation of controlled circulation boiler and natural circulation boiler start up behaviour. Energy Conversion and Management 46(4), pp. 533-549.

Lu, H., Yang, D., Zhou, X., Xu, L., Bian, B., Shao, G. (2011). Calculation of Pressure Drop and Outlet Steam Temperature of Water wall Pipes for Supercritical Once-through Boiler (In Chinese). Journal of Xi'an Jiaotong University, Xi'an, China. 45(1), pp. 38–42.

Lu, S., (1999). Dynamic modelling and simulation of power plant systems. Proc Instn Mech Engrs, Part A, Journal of Power and Energy, 213, pp. 7-22.

Lundqvist R, Schrief A, Kinnunen P, Myohanen K, Seshamani M., (2003). A Major Step Forward-The Supercritical CFB Boiler. In: Power-Gen International Las Vegas, USA.

MacDowell, N. And Shah, N., (2014). Dynamic modelling and analysis of a coal-fired power plant integrated with a novel split-flow configuration post-combustion $CO_2$ capture process. International Journal of Greenhouse Gas Control 27, pp. 103-119.

Maffezzoni, C. (1992). Issues in modelling and simulation of power plants. In Proceedings of IFAC symposium on control of power plants and power systems 1, pp. 19-27, Munchen, Germany.

Mangalapally H.P., Hasse H., (2011). Pilot plant study of post-combustion carbon dioxide capture by reactive absorption: methodology, comparison of different structured packings, and comprehensive results for monoethanolamine. Chemical Engineering Research and Design, 89: pp. 1216-1228.

Masada, G.Y., (1979). Modelling and Control of Power Plant Boiler-Turbine—Generator Systems, Sc. D Thesis, Department of Mechanical Engineering, MIT.

Masada, Y., Wormley, D.N., (1982). Dynamic model of a 1400MW supercritical pressure steam plant. ASME Paper, 82-JPGC-Pwr-13, pp. 1 - 9.

Mercier J., Drenik O., (2013). Power Plant and Method of Operating a Power Plant, US Patent (WO2013005071A1), International Application No: PCT/IB2011/002321.

Morosuk T., Tsatsaronis G. (2009b). Advanced exergetic evaluation of refrigeration machines using different working fluids. Energy 34(12), pp. 2248–58.

Morosuk, T., Tsatsaronis, G. (2009a). Advanced exergy analysis for chemically reacting systems—application to a simple open gas-turbine system. Int. J. Thermodyn. 12(3), pp. 105 – 111.

Morosuk T., Tsatsaronis G., Schult M. (2013). Conventional and Advanced Exergy Analyses: Theory and Application, Arab J. Sci. Eng 38, pp. 395-404.

Moser, P., Schmidt, S., Sieder, G., Garcia, H., Stoffregen, T., Stematov, V., (2011). The post-combustion capture pilot plant Niederaussem – Results of the first half of the testing programme. Energy Procedia 4, pp. 1310–1316.

Muhammed, O., Wang, J., Guo, S., AlDuri, B. and Wei, J., (2010). Modelling study of supercritical power plant and parameter identification using genetic algorithm. Proceedings of the World Congress on Engineering, WCE 2010*,* II, London.

National Grid, (2012). The Grid Code. 4, (10). National Grid Electricity Transmission plc, London WC2N SEH, UK.

Nicholls, R.J., and Maxim, C., (2008). Supercritical coal-fired plant requirements and the Grid Code, E.ON UK.

Notz, R., Asprion, N., Clausen, I. and Hasse, H., (2007). Selection and pilot plant tests of new absorbents for post-combustion carbon dioxide capture. Chemical engineering research and design 85 (4), pp. 510-515.

O'Kelly, P., (2013). *Computer Simulation of Thermal plant Operations.* Springer, ISBN 978-1-4614-4255-4, London.

Ordys, A. W., Pike, A.W., Johnson, M. A., Katebi, R. M., and Grimble, M. J. (1994). *Modelling and simulation of power generation plants.* Springer Verlag. (Advances in Industrial Control), ISBN 9783540199076, London.

Oyenekan, B., Rochelle, G.T., (2007). Alternative stripper configurations for $CO_2$ capture by aqueous amines, AIChE Journal 53, pp. 3144-3154.

Paranjape, R. D., (1996). Modelling and control of a supercritical coal-fired boiler, PhD thesis, Texas Technical University, Lubbock, USA.

Park, S-E., Min, B-M., Lee, J-S., and Eum, H-M., (2004). A study about $CO_2$ absorption process design for thermal power plant flue gas. Studies in surface science and catalysis 153, pp. 539-542.

Peng, J., Edgar, T.F., Eldridge, R.B., (2003). Dynamic rate-based and equilibrium models for a packed reactive distillation column. Chem. Eng. Sci. 58, pp. 2671 – 2680.

Pfaff, I., Oexmann, J., Kather, A., (2010). Optimised integration of post-combustion $CO_2$ capture process in Greenfield power plants, Energy 35, pp. 4030–4041.

Pinsent B.R., Pearson L., Roughton F.J.W., (1956). The kinetics of combination of carbon dioxide with hydroxide ions, Trans. Faraday Soc., 52, pp. 1512-1520.

Posch, S. and Haider, M., (2013). Dynamic modelling of $CO_2$ absorption from coal-fired power plants into an aqueous monoethanolamine solution. *Chemical Engineering Research and Design* 91 (6), pp. 977–987.

Ray, A., (1980). Dynamic modelling of once-through subcritical steam generator for solar applications", Applied Mathematical Modelling 4, pp. 417-423.

Ray, A., Bowman, H.F., (1976). A Nonlinear Dynamic Model of a Once-Through Subcritical Steam Generator. J. Dyn. Sys. Meas. Control 98(3), pp. 332 – 339.

Reddy V.S., Kaushik S.C., Tyagi S.K., (2014). Exergetic analysis and evaluation of coal-fired supercritical thermal power plant and natural gas-fired combined cycle power plant, Clean Techn Environ Policy 16, pp. 489-499.

Sanpasertparnich, T. Aroonwilas, A. (2009), Simulation and optimization of coal-fired power plants, *Energy Procedia,* 1, (1), pp. 3851-3858.

Sanpasertparnich, T., Idem, R., Bolea, I., de Montigny, D., Tontiwachuwuthikul, P., (2010). Integration of post-combustion capture and storage into a pulverized coal-fired power plant. International Journal of Greenhouse Control 4, pp. 499-510.

Siamak F., Saffar-Avval M., Younessi-Sinaki M., (2008). Efficient design of feedwater heaters network in steam power plants using pinch technology and exergy analysis, Int. J. Energy Res., 32, pp. 1-11.

Shinohara, W. and Koditschek, D.E., (1996). A simplified model based supercritical power plant controller. Proceedings of the 35th Conference on Decision and Control, December 1996, Kobe, Japan, IEEE, pp. 4486-4491.

Shinohara, W. and Koditschek, D.E., (1995). A simplified model of a supercritical power plant, University of Michigan, Control Group reports CGR-95-08.

Shoureshi R., and Paynter H.M., (1983). Simple Model for Dynamics and Control of Heat Exchangers. American Control Conference, FP7- 2:30, pp. 1294-1298.

Sinnott R.K., Towler G.(2013), Chemical engineering design – principles, practice and economics of plant and process design. 2nd ed. Oxford, UK: Elsevier.

Sulzer, (2012). Structured packings for distillation, absorption and reactive distillation. Winterthur, Switzerland: Sulzer Chemtech Ltd.

Suzuki, Y., Pak, P.S., Uchida, Y., (1979). Simulation of a supercritical once-through boiler. Simulation 33 (6), pp. 181 – 193.

Szargut J., (2005). Exergy method: Technical and ecological applications. Southampton, UK.

Taylor R., Krishna R. (1993), *Multicomponent Mass Transfer*, New York: John Wiley & Sons, Inc.

Thompson, R.E., King, C.J., (1987). Energy Conservation in Regenerated Chemical Absorption Process, Chem. Eng. Process, 21, pp. 115 – 129.

Tobiesen, F.A., Svenden, H.F. and Juliussen, O., (2007). Experimental validation of a rigorous absorber model for $CO_2$ post-combustion capture AlChE J., 53, pp. 846–865.

Treybal, R.E., (1981). Mass Transfer Operations, 3rd Edition, McGraw-Hill International Editions.

Tsatsaronis G, Winhold M., (1984). Thermoeconomic analysis of power plants. In: Final Report EPRI AP-3651, RP 2029-8, Electric Power Research Institute (EPRI), Palo Alto, CA, USA.

Tsatsaronis, G.; Morosuk, T., (2008). A general exergy-based method for combining a cost analysis with an environmental impact analysis. In: Proceedings of the ASME International Mechanical Engineering Congress and Exposition, files IMECE2008-67218, IMECE2008-67219, Boston, Massachusetts, USA.

Van Wagener, D., Rochelle, G.T., (2011). Stripper configurations for CO2 capture by Aqueous monoethanolamine and piperazine, Energy Procedia, 4, pp. 1323-1330.

Wang L., Yang Y., Morosuk T., Tsatsaronis G.(2012) Advanced thermodynamic analysis and evaluation of a supercritical power plant. Energies 5(6), pp. 1850–63.

Wang M, Lawal A., Stephenson P., Sidders J., Ramshaw C. (2011), Post-combustion $CO_2$ capture with chemical absorption: A state-of-the-art review, Chemical Engineering Research and Design 89, pp.1609–1624.

Woods M.C., Capicotto P.J., Halsbeck J.L., Kuehn N.J., Matuszewski M., Pinkerton L.L., Rutkowski M.D., Schoff R.L., Vaysman V., (2007). Bituminous Coal and Natural Gas to Electricity. In: Cost and Performance Baseline for Fossil Energy Plants, Final Report DOE/NETL-2007/1281, National Energy Technology Laboratory (NETL), USA.

Yang Y., Wang L., Dong C., Xu G., Morosuk T., Tsatsaronis G., (2013). Comprehensive exergy-based evaluation and parametric study of a coal-fired ultra-supercritical power plant, Applied Energy 112, 1087-1099.

Zhang Y., Chen C-C., (2013). Modelling $CO_2$ absorption and desorption by aqueous monoethanolamine solution with Aspen rate-based model, *Energy Procedia* 37:1584-1596.

Zhang, D., Liu P., West, L., Li Z., Ni, W., (2011). Reducing Initial Barriers for CCS Deployment on Pulverized Coal-fired Power Plants in China by Optimizing the Capture

Ratio of Carbon dioxide, International Conference for Renewable Energy and Environment (ICMREE) 2, pp. pp. 1619-1623.

Zhang, Y., Chen, H., Chen, C., Plaza, J.M., Dugas, R., Rochelle, G.T., (2009). Rate-based process modelling study of $CO_2$ capture with aqueous Monoethanolamine solution. Ind. Eng. Chem. Res., 48, pp. 9233-9246.

Ziaii, S., Rochelle, G.T. and Edgar, T.F., (2009). Dynamic modelling to minimize energy use for $CO_2$ capture in power plants aqueous monoethanolamine. Ind. Eng. Chem. Res. 48, pp. 6105-6111.

Zindler, H., Walter, H., Hauschke, A., and Leithner, R (2008), Dynamic simulation of a 800MWe hard coal once-through supercritical power plant to fulfil the Great Britain grid code. 6th IASME/WSEAS International Conference on Heat Transfer, Thermal Engineering and Environment, pp. 184-192.

# APPENDIX

## Appendix A: Publications generated from this PhD

### A.1: Journal Papers

Olaleye, A.K., Wang, M., Kelsall, G. (2015), Steady state simulation and exergy analysis of supercritical coal-fired power plant with $CO_2$ capture, *Fuel*, Vol. 151, p57-72.

Oko, E., Wang, M., Olaleye, A.K. (2015), Simplification of Detailed Rate-based Model of Post-combustion $CO_2$ Capture for Full Chain CCS Integration Studies, ***Fuel***, Vol. 142, pp. 87-93.

Olaleye, A.K., Wang, M., Xu, C., Kelsall, G. (2015) Dynamic Modelling, Validation and Analysis of Supercritical Coal-fired Power Plant Operation under Stringent UK Grid Code Requirement – Planned for submission to the Journal of Applied Energy

Olaleye, A.K., Oko, E., Wang, M., Kelsall, G.(2015) Dynamic Modelling and Analysis of Supercritical Coal-fired Power Plant Integrated with Post-Combustion $CO_2$ Capture under Stringent UK grid Code Requirement – Planned for submission to International Journal of Greenhouse Gas Control

### A.2: Peer-Reviewed Conference Papers

Olaleye A.K., Wang M., Xu, C., Kelsall G., (2015) Dynamic Modelling, Validation and Analysis of Coal-fired Supercritical Once-through Boiler-Turbine Generator Systems under Stringent UK Grid Requirement, 8th International Symposium on Coal Combustion (8th ISCC), Beijing, China, July 19-22, 2015.

Olaleye A.K., Oko, E., Wang M., Kelsall G., (2015) Dynamic Modelling and Analysis of Coal-fired Supercritical Power Plant Integrated with CO2 Capture under UK Grid Requirement, 8th International Symposium on Coal Combustion (8th ISCC), Beijing, China, July 19-22, 2015.

Olaleye, A.K., Wang, M. (2015), Conventional and advanced exergy analysis of post-combustion $CO_2$ capture from supercritical coal fired power plant, *7th International Exergy, Energy and Environment Symposium, (IEEES7)*, Valenciennes, France.

Olaleye, A.K., Wang, M., Kelsall, G. (2015), Dynamic modelling of steam generation in once-through supercritical boiler: Distributed vs Lumped parameter approach, *10th European Conference on Industrial Furnaces and Boilers (INFUB-10)*, Porto, Portugal 7-10 April.

**A.3: Conference/Seminar Posters and Presentations**

Olaleye, A.K., Wang, M., Kelsall, G. (2015). Dynamic modelling of steam generation in once-through supercritical boiler: Distributed vs Lumped parameter approach, INFUB-10, Porto, Portugal 7-10 April. (Conference Poster).

Olaleye, A.K., Wang, M. (2015), Conventional and advanced exergy analysis of post-combustion $CO_2$ capture from supercritical coal fired power plant, *7th International Exergy, Energy and Environment Symposium, (IEEES7)*, Valenciennes, France. 27th – 29th April (Conference Presentation)

Olaleye, A.K., Wang, M., Kelsall, G. (2015), Steady state simulation and exergy analysis of supercritical coal-fired power plant with $CO_2$ capture, European Conference on Coal Research and its Application (10th ECCRIA), University of Hull, Hull, United Kingdom September, 2015 (Conference Presentation)

## Appendix B: Preliminary Calculations in Mathcad 14 for Steady State Simulation of SCPP

### B.1: Air Volumetric Composition

Assumptions: Dry Air is assumed to be made up of $N_2$ and $O_2$, since they make up to 99% of air on volumetric basis (i.e. 79% $N_2$, 21% $O_2$)

Hence, for:

$$1mole_{O2} = 3.76mole_{N2}$$

Therefore, in every mole of $O_2$

$$1mole_{O2} + 3.76mole_{N2} = 4.76mole_{dry.air}$$

$$mole_{dry.air} = 4.76mol$$

Ambient Air usually contains water vapour (determined via the relative humidity)

Assumption: air used is at 25ºC and 65% relative humidity (typical UK annual average). From steam table, saturation pressure of water at 25ºC, $P_{sat}$ = 0.0316975 bar

$$\phi = \frac{mass_{watervapour\_inair}}{mass_{max\_watervap\_air\_can\_hold}}$$

From ideal gas law,

$$\phi = \frac{\frac{P_{vap} \cdot Vol_{air}}{(R_{vap} \cdot T_{air})}}{\left[\frac{P_{satur} \cdot Vol_{air}}{(R_{vap} \cdot T_{air})}\right]} = \frac{P_{vap}}{P_{satur}}$$

$$P_{vap} = partial\_pressure\_of\_water\_vap\_in\_air \quad ,$$

$$P_{satur} = sat\_press\_at\_given\_temp$$

From ideal gas law, mole ratio of water vapour to dry air is the ratio of their partial pressures:

$P_{air} = partial\_press\_dry\_air$

$$\frac{N_{vap}}{N_{air}} = \frac{P_{vap}}{P_{air}}$$

Since $P_{vap} = \phi \cdot P_{satur}$

$$N_{vap} = N_{air} \cdot \left( \frac{\phi \cdot P_{satur}}{P - \phi \cdot P_{satur}} \right)$$

and $P = P_{vap} + P_{satur}$

$$N_{vap} := 1 \cdot \frac{(0.65 \times 0.0316975)}{(1.0 - 0.65 \times 0.0316975)} \qquad N_{vap} = 0.021$$

Hence, there is 0.021 moles of water vapour in 1 mole of the dry air. Therefore, in 4.76 mole of air, the moles of water vapour = 0.021*4.76 = 0.09996

Hence molar composition of air is written thus:

$$O_2 + 3.76N_2 + 0.09996H2O = 4.85996mol_{of\_combustion\_air}$$

Therefore.

$$\begin{pmatrix} Air \\ Nitrogen \\ Oxygen \\ water\_vapour \end{pmatrix} = \begin{pmatrix} vol\_Basis \\ 77.37 \\ 20.58 \\ 2.05 \end{pmatrix}$$

### B.2: Combustion Analysis of the UK Bituminous Coal

This appendix shows the estimation of the coal elemental composition and its combustion using a stoichiometric reaction used in the steady state simulation

As Received Ultimate Analysis (kg/100kg coal) Molecular Weight (kg/kmol)

$$\begin{pmatrix}\text{moisture}\\ \text{carbon}\\ \text{hydrogen}\\ \text{Nitrogen}\\ \text{Chlorine}\\ \text{sulphur}\\ \text{Ash}\\ \text{Oxygen}\end{pmatrix} = \begin{pmatrix}12.0\\ 60.0\\ 3.9\\ 1.3\\ 0.2\\ 1.6\\ 15.0\\ 6.0\end{pmatrix} \qquad \begin{pmatrix}\text{moisture}\\ \text{carbon}\\ \text{hydrogen}\\ \text{Nitrogen}\\ \text{Chlorine}\\ \text{sulphur}\\ \text{Ash}\\ \text{Oxygen}\end{pmatrix} = \begin{pmatrix}18.015\\ 12.010\\ 1.008\\ 14.006\\ 35.453\\ 32.062\\ 0\\ 15.999\end{pmatrix}$$

Ultanalysis (kg/kmol)

$$\text{ultanal} := \begin{pmatrix}12.0\\ 60.0\\ 3.9\\ 1.3\\ 0.2\\ 1.6\\ 6.0\end{pmatrix} \qquad \text{molcwt} := \begin{pmatrix}18.015\\ 12.010\\ 1.008\\ 14.006\\ 35.453\\ 32.062\\ 15.999\end{pmatrix}$$

Number of moles (kmol) in 100kg of the coal is estimated thus:

$$\text{mol\_coal} := \frac{\text{ultanal}}{\text{molcwt}} \qquad \text{mol\_coal} = \begin{pmatrix}0.666\\ 4.996\\ 3.869\\ 0.093\\ 5.641\times 10^{-3}\\ 0.05\\ 0.375\end{pmatrix} \quad \begin{pmatrix}\text{moisture}\\ \text{carbon}\\ \text{hydrogen}\\ \text{nitrogen}\\ \text{chlorine}\\ \text{sulphur}\\ \text{oxygen}\end{pmatrix}$$

Also, the coal formula can be expressed in moles/mole carbon thus:

$$\text{mol\_per\_mol}_{carbon} := \frac{\text{mol\_coal}}{\text{mol\_coal}_1}$$

$$\text{mol\_per\_mol}_{carbon} = \begin{pmatrix} 0.133 \\ 1 \\ 0.774 \\ 0.019 \\ 1.129 \times 10^{-3} \\ 9.989 \times 10^{-3} \\ 0.075 \end{pmatrix} \quad \begin{pmatrix} \text{moisture} \\ \text{carbon} \\ \text{hydrogen} \\ \text{nitrogen} \\ \text{chlorine} \\ \text{sulphur} \\ \text{oxygen} \end{pmatrix}$$

The formula of the coal based on the carbon atom used in the steady state simulation is thus: $[C_1 H_{0.774} N_{0.019} S_{0.00999} O_{0.075} Cl_{0.001129} + 0.0133(H_2O)]$

Hence, the stoichiometric equation for the complete combustion of the UK Bituminous Coal can be represented thus:

$$C_1 \cdot H_{0.774} N_{0.019} \cdot O_{0.075} S_{0.01} + 0.133 H2O + a \cdot \left(O_2 + 3.76 N_2 + 0.09996 H2O\right) = bCO_2 + c \cdot H2O + dSO_2 + e \cdot N_2$$

The coefficients a, b, c, d, and e is solved using a system of equations. From conservation of mass for the reaction, the equation is set up based on the moles of each element on each side of the equation

$$\begin{pmatrix} \text{carbon} \\ \text{hydrogen} \\ \text{nitrogen} \\ \text{sulphur} \\ \text{oxygen} \end{pmatrix} = \begin{pmatrix} 0 & 1 & 0 & 0 & 0 \\ -0.19992 & 0 & 2 & 0 & 0 \\ -7.52 & 0 & 0 & 0 & 2 \\ 0 & 0 & 0 & 1 & 0 \\ -2.09996 & 2 & 1 & 2 & 0 \end{pmatrix} \cdot \begin{pmatrix} a \\ b \\ c \\ d \\ e \end{pmatrix} = \begin{pmatrix} 1 \\ 1.04 \\ 0.019 \\ 0.01 \\ 0.208 \end{pmatrix}$$

$$\begin{pmatrix} a \\ b \\ c \\ d \\ e \end{pmatrix} := \begin{pmatrix} 0 & 1 & 0 & 0 & 0 \\ -0.19992 & 0 & 2 & 0 & 0 \\ -7.52 & 0 & 0 & 0 & 2 \\ 0 & 0 & 0 & 1 & 0 \\ -2.09996 & 2 & 1 & 2 & 0 \end{pmatrix}^{-1} \cdot \begin{pmatrix} 1 \\ 1.04 \\ 0.019 \\ 0.01 \\ 0.208 \end{pmatrix}$$

$$\begin{pmatrix} a \\ b \\ c \\ d \\ e \end{pmatrix} = \begin{pmatrix} 1.166 \\ 1 \\ 0.637 \\ 0.01 \\ 4.394 \end{pmatrix}$$

The stoichiometric equation of the combustion of UK bituminous coal is:

$$C_1 \cdot H_{0.774} N_{0.019} \cdot O_{0.075} S_{0.01} + 0.133 H2O + 1.166\left(O_2 + 3.76 N_2 + 0.09996 H2O\right) = 1 CO_2 + 0.637 \cdot H2O + 0.01 SO_2 + 4.394 \cdot N_2$$

Since it's impossible for a power plant boiler to achieve stoichiometric combustion, it's important to have excess air, so as to minimise the effect of unburned carbon and CO. Assume $O_2$ level at economiser exit, 3.5% by volume, the excess air was determined to be 23.1%

$$C_1 \cdot H_{0.774} N_{0.019} \cdot O_{0.075} S_{0.01} + 0.133 H2O + 1.166 (1.231)\left(O_2 + 3.76 N_2 + 0.09996 H2O\right) = f\ CO_2 + g \cdot H2O + h\ SO_2 + i \cdot N_2 + j \cdot O_2$$

$$\begin{pmatrix} \text{carbon} \\ \text{hydrogen} \\ \text{nitrogen} \\ \text{sulphur} \\ \text{oxygen} \end{pmatrix} \begin{pmatrix} 1 & 0 & 0 & 0 & 0 \\ 0 & 2 & 0 & 0 & 0 \\ 0 & 0 & 0 & 2 & 0 \\ 0 & 0 & 1 & 0 & 0 \\ 2 & 1 & 2 & 0 & 2 \end{pmatrix} \cdot \begin{pmatrix} f \\ g \\ h \\ i \\ j \end{pmatrix} = \begin{pmatrix} 1 \\ 1.327 \\ 10.813 \\ 0.01 \\ 3.079 \end{pmatrix}$$

$A =$

$$\begin{pmatrix} f \\ g \\ h \\ i \\ j \end{pmatrix} := \begin{pmatrix} 1 & 0 & 0 & 0 & 0 \\ 0 & 2 & 0 & 0 & 0 \\ 0 & 0 & 0 & 2 & 0 \\ 0 & 0 & 1 & 0 & 0 \\ 2 & 1 & 2 & 0 & 2 \end{pmatrix}^{-1} \cdot \begin{pmatrix} 1 \\ 1.327 \\ 10.813 \\ 0.01 \\ 3.079 \end{pmatrix}$$

Hence,

$$\begin{pmatrix} f \\ g \\ h \\ i \\ j \end{pmatrix} = \begin{pmatrix} 1 \\ 0.663 \\ 0.01 \\ 5.407 \\ 0.198 \end{pmatrix}$$

Hence combustion with (23.1%) excess air is thus:

$$C_1 \cdot H_{0.774} N_{0.019} \cdot O_{0.075} S_{0.01} + 0.133 H2O + 1.435\left(O_2 + 3.76 N_2 + 0.09996 H2O\right) = 1 CO_2 + 0.663 \cdot H2O + 0.01 SO_2 + 5.407 \cdot N_2 + 0.198 O_2$$

$$\begin{pmatrix} O2 \\ CO2 \\ H2O \\ SO2 \\ N2 \end{pmatrix} = \begin{pmatrix} 0.198 \\ 1 \\ 0.663 \\ 0.01 \\ 5.407 \end{pmatrix}$$

$$sum := \sum \begin{pmatrix} 0.198 \\ 1 \\ 0.663 \\ 0.01 \\ 5.407 \end{pmatrix} \qquad sum = 7.278 \qquad ind := \begin{pmatrix} 0.198 \\ 1 \\ 0.663 \\ 0.01 \\ 5.407 \end{pmatrix} \qquad comp_{vol} := \frac{ind}{sum}$$

$$comp_{vol} = \begin{pmatrix} 0.0272 \\ 0.1374 \\ 0.0911 \\ 1.374 \times 10^{-3} \\ 0.7429 \end{pmatrix} \begin{pmatrix} O2 \\ CO2 \\ H2O \\ SO2 \\ N2 \end{pmatrix}$$

Composition of the flue gas on Volume basis is thus:

$$\begin{pmatrix} component \\ CO2 \\ H2O \\ SO2 \\ N2 \\ O2 \end{pmatrix} = \begin{pmatrix} composition\_vol\% \\ 13.74 \\ 9.11 \\ 0.14 \\ 74.29 \\ 2.72 \end{pmatrix}$$

**B.3: Scale-Up of Pilot-Scale PCC Used for Steady State Simulation**

Reference Pilot Plant Parameters

Packing type: Sulzer BX 500 (Absorber / Stripper)

Total packing height Absorber $= 4.25m$

Total packing height Stripper$= 2.55m$

Absorber Temperature (Flue gas) $= 47℃$

Absorber Temperature Inlet (Solvent) $= 40℃$

$F - factor = 1.6Pa^{0.5}$ $(\max 2.1)$

$CO_2 removal\ rate = 90\%$

Absorber/ Stripper inner diameter = 0.125m

Series used: Series B (with partial pressure corresponding to coal-fired partial pressure)

$$partial\ pressure = 102mbar$$

$$[1mmH_2O = 9.80665 \times 10^{-5}bar]$$

$$102mbar = \frac{102 \times 10^{-3}bar \times 1mmH_2O}{9.80665 \times 10^{-5}}$$

$$= 1040.11mmH_2O$$

Packing type:

Sulzer type BX 500 (Metal gauze)

Structured Packing

Pressure drop per theoretical stage $\rightarrow 0.1 - 0.5\text{mbar}$

Load range:

$F - factor \rightarrow 1\ - 2.5\sqrt{Pa}$

Minimum load approximate $0.05m^3/m^2h$

Diameter and operating range: $40mm \rightarrow 6m\ (on\ type)$

$pressure \rightarrow 1mbar \rightarrow Atmospheric\ pressure$

$surface\ area = 500m^2/m^3$

F-factor (fluid dynamics load of the absorber): Is the vapour kinetic energy term defined as the product of gas velocity and square root of gas density

<u>19 Pilot Plant cases</u>:

Case Chosen $[A7 - A12]$

Flue gas flow rate $= 80Kg/hr$

Same diameter for absorber/stripper $= 0.125m$

Lean loading $(molMEA/mol\ CO_2 = 0.186)$

Rich loading $(mol\ CO_2/molmEA = 0.437)$

$P_{CO_2} = 102mbar$

Regeneration energy $= 4.09MJ/Kg\ CO_2$

$L/G\ ratio = 2.5$

$optimum\ L/G\ ratio\ from\ the\ expperimental\ study$

$CO_2$ Partial pressure in flue gases of different combustion system:

Coal fired boiler:

$CO_2\ concentration$: $12 - 14\ \%\ volume$

$CO_2$ Partial pressure : $0.012 - 0.014\ MP_a$

Pressure:

$Fuel\ gas$: $1.033bar\ (0.29\ psig)$

$Absorber\ pressure = 1\ atm$

$lean\ MEA\ in\ absorber = 1.703bar\ (10\ psig)$

Aspen Plus® value: Pressure drop

Total Pressure drop in column $= 1.66\ in\ H_2O$

Simmot & Towler recommended pressure drop: $15 - 50mmH_2O/\ meter\ of\ packing$

**Scale – up calculation**

At fill load, flue gas flow rate; $603.4Kg$ with $CO_2\ concentration$: $21.35\ wt\%$

$$CO_2\ in\ flue = 21.35\%\ (603.4)$$

$$= 128.8259Kg/s$$

In kmol/s,

$$= \frac{128.8259}{44}$$

$$= 2.9279Kmol/s$$

Amount of $CO_2$ captured based on 90% capture efficiency

$$0.9 \times 128.8259$$

$$= 115.9433Kg/s$$

Amount of MEA used based on 14 wt% absorption capacity

$$= \frac{115.9433\ Kg/s}{0.14}$$

$$= 828.1665\ Kg/s$$

Note:

Absorption capacity is the difference between rich and lean (MEA) solvent loading.

Based on 30.48 wt. % MEA solution,

$$total\ solvent\ flow\ rate\ (kg/s) = \frac{828.1665}{0.3048}$$

$$= 2717.0817$$

**For the Absorber diameter:**

$$F_{LV} = \frac{Lw^*}{Vw^*}\sqrt{\frac{P_V}{P_L}}$$

Where

$F_{LV}$= liquid/vapour flow factor

$Lw^*$= liquid mass flow rate/ $m^2$

$Vw^*$= vapour mass flow rate/$m^2$

$P_L = 1006.2\ Kg/\ m^3$

$P_v = 1.12246\ Kg/\ m^3$

$Lw^* = 2717.0817\ Kg/s\ m^2$

$Vw^* = 128.8259 Kg/s\ m^3$

$Lw^*/_{Vw^*}$= 2.41975

$$F_{LV} = \frac{2717.0817}{128.8259}\left(\frac{1.12246}{1006.2}\right)^{1/2}$$

$$F_{LV} = (21.0911)(0.0334)$$

$$= 0.7044$$

Assuming a pressure drop of $42mmH_2O/m$

From Chart:

$$K_4 \sim 2.0$$

At flooding; $K_4 = 3.0$

$$\text{Percentage flooding} = \sqrt{\frac{2}{3}} \times \frac{100}{1}$$

$$= 66.67\ \%$$

Hence;

From;

$$K_4 = \frac{13.1(Vw^*)^2 F_p \left(\frac{\mu_L}{P_L}\right)^{0.1}}{P_V(P_L - P_V)}$$

$F_p$ $= packaging\ factor\ based\ on\ size\ and\ type\ of\ packaging\ [see\ refence]$

$Vw^* = gas\ flow\ rate\ for\ unit\ column\ cros\ sectional\ area\ (Kg/m^2 s)$

$F_p$ $= 72.7 m^{-1}$

$\mu_L = 0.00355 P_a . s$

$$Vw^* = \sqrt{\frac{K_4 P_V (P_L - P_V)}{13.1\ F_p \left(\frac{\mu_L}{P_L}\right)^{0.1}}}$$

$$= \left[\frac{2.0(1.12246)(1006.2 - 1.2246)}{(13.1)(72.7)\left(\frac{0.00355}{1006.2}\right)^{0.1}}\right]^{1/2}$$

$$= \left[\frac{(2256.32)}{(13.1)(72.7)(0.2849406456)}\right]^{1/2}$$

$$Vw^* = 2.8835 Kg/m^2 s$$

Column area required:

$$A = \frac{603.4}{2.8835}$$

$$= 209.2594 m^2$$

$$d = \sqrt{\frac{4A}{\pi}}$$

$$= 16.323 m$$

Maximum available diameter for BX = 6m

| Stripper Diameter (m) | n (Number of columns) | Absorber Diameter (m) |
|---|---|---|
| 13.06 | 1 | 16.33 |
| 9.23 | 2 | 11.54 |
| **5.33** | **3** | 8.1615 |
| | **4** | **5.74** |

For the Stripper:

Rich solvent flow= $2788.74\ kg/s$

Stripper area = $133.98\ m^2, d = 13.06 m$

## Appendix C: Transport Properties Estimation

### C.1: SCPP Once-through Boiler – Lumped Parameter Model

The correlations for calculating the heat exchangers inside (water/steam side) and outside (i.e. flue gas side) convective heat transfer coefficients used in section 5.2 of Chapter 5 are presented in this appendix.

- *C.1.1: Inside Tube Convective Heat Transfer: Lumped Parameter Model*

The heat transfer coefficient was derived from dimensional analysis. The forced convective heat transfer coefficients are derived from correlations based on three dimensionless groups, the Nuselt number, Reynolds number, and the Prandtl number:

$$Nu = f(Re, Pr) \qquad \text{C.1.1}$$

For the inside tube convective heat transfer coefficient, assuming a fully developed turbulent flow, the correlation of McAdams (Masada, 1979) was used. McAdams correlation can be expressed thus:

$$\left(\frac{h_i D}{k_b}\right) = 0.023 \left(\frac{\rho_b V D}{\mu_b}\right)^{0.8} \left(\frac{\mu c_p}{\mu_b}\right)_b^{0.4} \qquad \text{C.1.2}$$

Where the subscript b refers to the bulk or mixed fluid temperature and is valid for $0.5 < Pr < 120$ and $2300 < Pr < 10^7$

Solving equation C1.2 for the inside tube transfer coefficient,

$$h_i = 0.023 \left(\frac{{k_b}^{0.6} {c_{pb}}^{0.4}}{D^{0.4} {\mu_b}^{0.4}}\right) (\rho_b V)^{0.8} \qquad \text{C.1.3}$$

The flowrate through each tube can be represented thus:

$$m_i = \frac{m}{n} = \rho_b V = \frac{m}{nA} \qquad \text{C.1.4}$$

Where $n$ is the number of tubes, $m$ is the total fluid mass flowrate, $m_i$ is the mass flowrate through individual tubes, and $A$ ($m^2$) is the cross sectional flow area of the tubes

Replacing the expression $\frac{m}{nA}$ in C1.4 into the expression for $\rho_b V$ in C1.3 gives:

$$h_i = 0.023\left(\frac{{k_b}^{0.6}{c_{pb}}^{0.4}}{D^{0.4}{\mu_b}^{0.4}}\right)\left(\frac{m}{nA}\right)^{0.8}$$

$$h_i = 0.023\left(\frac{{k_b}^{0.6}{c_{pb}}^{0.4}}{D^{0.4}{\mu_b}^{0.4}}\right)\left(\frac{4m}{n\pi D^2}\right)^{0.8}$$

Hence,

$$h_i = 0.0279\left(\frac{{k_b}^{0.6}{c_{pb}}^{0.4}}{D^{0.4}{\mu_b}^{0.4}}\right)\frac{m^{0.8}}{n^{0.8}D^{1.6}} \qquad \text{C.1.5}$$

Equation C1.5 shows that the heat transfer coefficient inside the tube (i.e. from metal to steam) is dependent on the properties of the fluid, the number and sizes of the tubes.

The implemented forms of the inside heat transfer coefficient assumes a time dependent base on the fluid mass flow only (Masada, 1979). The fluid properties were estimated at the rated load and held constant because there were no significant variation in the property expressions. The IAPWS steam tables for supercritical water/ steam was used in estimating the properties. The maximum error in the constant properties assumption was about 10%.

Hence,

$$h_C A \cong U_{kg}{m_g}^{0.6} \qquad \text{C.1.6}$$

*Where* $U_{kg}$ is the lumped properties estimated from the steam table and kept constant during the simulations

C.1.2: Outside Tube Convective Heat Transfer: Lumped Parameter Model

For the outside tube convective heat transfer coefficient (i.e. from gas to metal), the correlation of Colburn is used (Masada, 1979). Colburn correlation can be expressed thus:

$$\left(\frac{h_o D_o}{k_f}\right) = C\left(\frac{\rho_f V_{max} D_o}{\mu_f}\right)^{0.6}\left(\frac{\mu c_p}{k}\right)_f^{0.33} \qquad \text{C.1.7}$$

Where subscript *f* refers to the film temperature defined as the average temperature between the wall and bulk temperatures

Solving equation C1.6 for the outside tube transfer coefficient,

$$h_o = C\left(\frac{k^{0.667} {c_p}^{0.33}}{{D_o}^{0.4}\mu^{0.267}}\right)_f \left(\rho_f V_{max}\right)^{0.6} \qquad \text{C.1.8}$$

The maximum velocity can be obtained from the mass flow rate of gas and the minimum flow area, $A_{min}$ (obtained from the total passage area less the projected area of a typical row in the tube bank)

$$V_{max} = \frac{m_g}{\rho_f A_{min}} \qquad \text{C.1.9}$$

substituting $V_{max}$ into C1.8 gives:

$$h_o = C\left(\frac{k^{0.667} {c_p}^{0.33}}{\mu^{0.267}}\right)_f \left(\frac{m_g}{A_{min}}\right)^{0.6}$$

$$h_o = C\left(\frac{k^{0.667} {c_p}^{0.33}}{\mu^{0.267}}\right)_f \left(\frac{{m_g}^{0.6}}{{D_o}^{0.4}{A_{min}}^{0.6}}\right) \qquad \text{C.1.10}$$

Hence, the outside heat transfer coefficient from gas to metal depends on the gas properties, the size and configurations of the tubes, and the total flowrate of gas.

Similarly, the outside heat transfer coefficient can be expressed thus

$$h_C A \cong U_{kg} {m_g}^{0.6} \qquad \text{(C1.11)}$$

## Appendix D: The Evaporator loop – Distributed Parameter

The derivation is presented using a single tube approach (O'Kelly, 2013). The multiple tubes of the real evaporator are handled by grouping similar tubes into tube banks, within each of which all tubes can be regarded as identical. Individual banks differ from another. In each derivation all variables were considered spatially (along ordinate z) and time t. The flow is considered at single and two phase (liquid and vapour) conditions.

### D.1: Profile of Mass Flow from the Mass Balance

The mass balance equation for a two phase system is expressed thus:

$$\frac{1}{A}\frac{\partial m}{\partial z} = \frac{1}{v^2}\frac{\partial v}{\partial t} = \frac{1}{v^2}\left(\frac{\partial v}{\partial \rho}\frac{\partial \rho}{\partial t} + \frac{\partial v}{\partial x}\frac{\partial x}{\partial t}\right) \quad \text{(D.1.1)}$$

Since for water/steam, the steam fraction is expressed thus:

$$v = xv'' + (1-x)v' \quad \text{(D.1.2)}$$

Taking the derivative of (D1.2) gives:

$$\frac{\partial v}{\partial x} = v'' - v' \quad \text{(D.1.3)}$$

Putting (D1.3) into (D1.1) gives:

$$\frac{1}{A}\frac{\partial m}{\partial z} = \frac{1}{v^2}\frac{\partial v}{\partial t} = \frac{1}{v^2}\left(\frac{\partial v}{\partial \rho}\frac{\partial \rho}{\partial t} + (v'' - v')\frac{\partial x}{\partial t}\right) \quad \text{(D.1.4)}$$

Also, partial derivative of wet saturated steam properties from the definition of steam quality $x$ to reduce (D1.4) further:

$$x = \frac{h - h'}{h'' - h'} = \frac{v - v'}{v'' - v'} \quad \text{(D.1.5)}$$

Equation (D1.5) can be further expressed thus:

$$h = h' + \left(\frac{h'' - h'}{v'' - v'}\right)(v - v')$$

$$v = v' + \left(\frac{v'' - v'}{h'' - h'}\right)(h - h') \quad \text{(D.1.6)}$$

obtaining derivative of (D1.6) with respect to the specific enthalpy at constant pressure gives:

$$\left.\frac{dv}{dh}\right|_{p=const} = \frac{v'' - v'}{h'' - h'} \quad (for\ saturated\ vapour) \tag{D.1.7}$$

Differentiating equation (D1.6) with respect to pressure;

$$\left.\frac{dv}{dp}\right|_{h} = \frac{dv'}{dp} - (h - h')\frac{d}{dp}\left(\frac{v'' - v'}{h'' - h'}\right) + \left(\frac{v'' - v'}{h'' - h'}\right)\frac{d}{dp}(h - h')$$

Which can be reduced to the form:

$$\left.\frac{dv}{dp}\right|_{h} = h\frac{d}{dp}\left(\frac{v'' - v'}{h'' - h'}\right) + \frac{d}{dp}\left(\frac{v'' - v'}{h'' - h'}\right) \tag{D.1.8}$$

After further manipulation and simplification,

$$\left.\frac{dv}{dp}\right|_{h} \cong x\frac{dv''}{dp} \tag{D.1.9}$$

Hence, (D1.4) can be expressed thus:

$$\frac{1}{A}\frac{\partial m}{\partial z} = \frac{1}{v^2}\frac{\partial v}{\partial t} = \frac{1}{v^2}\left(x\frac{dv''}{dp}\frac{\partial p}{\partial t} + (v'' - v')\frac{\partial x}{\partial t}\right) \tag{D.1.10}$$

This equation shows the influence of both pressure and steam fraction changes on the local flow rate. Since $\partial v''/\partial p$ is negative, as increase in local pressure induces a decrease in local mass flow to a degree proportional to the local steam content and inversely proportional to the local pressure. The term $\partial x/\partial t$ can be eliminated as follows:

The evaporator fluid mass fraction is defined in terms of local fluid enthalpy thus (O'Kelly 2013)

$$h = xh'' + (1 - x)h' = h' + x\boldsymbol{r}, \tag{D.1.11}$$

Where the latent heat of evaporation $\mathbf{r} = h'' - h'$ is a function of local pressure. The partial differentials of h with respect to time $t$ and space $z$ are

$$\frac{\partial h}{\partial t} = \frac{\partial h'}{\partial t} + x\frac{\partial \boldsymbol{r}}{\partial t} + \boldsymbol{r}\frac{\partial x}{\partial t} \tag{D.1.12}$$

$$\frac{\partial h}{\partial z} = \frac{\partial h'}{\partial z} + x\frac{\partial \boldsymbol{r}}{\partial z} + \boldsymbol{r}\frac{\partial x}{\partial z} \tag{D.1.13}$$

The time derivative can be expressed thus:

$$\frac{\partial h}{\partial t} = \frac{\partial h'}{\partial t} + x\frac{\partial h''}{\partial t} - x\frac{\partial h'}{\partial t} + \boldsymbol{r}\frac{\partial x}{\partial t}$$

$$= (1-x)\frac{\partial h'}{\partial t} + x\frac{\partial h''}{\partial t} + \boldsymbol{r}\frac{\partial x}{\partial t}$$

$$= \left((1-x)\frac{\partial h'}{\partial p} + x\frac{\partial h''}{\partial p}\right)\frac{\partial p}{\partial t} + \boldsymbol{r}\frac{\partial x}{\partial t}$$

Hence,

$$\frac{\partial h}{\partial t} = \frac{\partial h}{\partial p}\frac{\partial p}{\partial t} + \boldsymbol{r}\frac{\partial x}{\partial t} \qquad or \qquad \text{(D.1.14)}$$

$$\frac{\partial x}{\partial t} = \frac{1}{\boldsymbol{r}}\frac{\partial h}{\partial t} - \frac{1}{\boldsymbol{r}}\frac{\partial h}{\partial p}\frac{\partial p}{\partial t} \qquad \text{(D.1.15)}$$

Hence, from equation (D1.10)

$$(v'' - v')\frac{\partial x}{\partial t} = \left(\frac{v'' - v'}{h'' - h'}\right)\frac{\partial h}{\partial t} - \left(\frac{v'' - v'}{h'' - h'}\right)\frac{\partial h}{\partial p}\frac{\partial p}{\partial t}$$

$$(v'' - v')\frac{\partial x}{\partial t} = \frac{\partial v}{\partial h}\frac{\partial h}{\partial t} - \frac{\partial v}{\partial h}\frac{\partial h}{\partial p}\frac{\partial p}{\partial t} \qquad \text{(D.1.16)}$$

Therefore, the mass conservation equation is obtained by replacing equation (D1.16) for $(v'' - v')\frac{\partial x}{\partial t}$ in (D1.10):

$$\frac{v^2}{A}\frac{\partial m}{\partial z} == \left(x\frac{dv''}{dp}\frac{\partial \rho}{\partial t} + \frac{\partial v}{\partial h}\frac{\partial h}{\partial t} - \frac{\partial v}{\partial h}\frac{\partial h}{\partial p}\frac{\partial p}{\partial t}\right)$$

$$\frac{v^2}{A}\frac{\partial m}{\partial z} = \left(x\frac{dv''}{dp} - \frac{\partial v}{\partial p}\right)\frac{\partial p}{\partial t} + \frac{\partial v}{\partial h}\frac{\partial h}{\partial t} \qquad \text{(D.1.17)}$$

Replacing $x\frac{dv''}{dp}$ in equation (D1.17) with the approximation in (D1.9), the mass balance equation becomes:

$$\frac{v^2}{A}\frac{\partial m}{\partial z} = \frac{\partial v}{\partial h}\frac{\partial h}{\partial t} \qquad \text{(D.1.18)}$$

### D.2: Profile of Pressure from Momentum Balance

Removing local compression effects, the momentum equation reduces to:

$$\frac{\partial p}{\partial z} = -\left(\frac{1}{A}\frac{\partial m}{\partial t} - \frac{m^2}{A^2}\frac{\partial v}{\partial h}\frac{\partial h}{\partial z} - \left.\frac{\partial p}{\partial z}\right|_{loss} - \rho\, g \sin\beta\right) \qquad \text{(D.1.19)}$$

Where $\frac{1}{A}\frac{\partial m}{\partial t}$ accounts for the flow inertia

At steady state, $\frac{1}{A}\frac{\partial m}{\partial t} = 0$, and the pressure is defined by head difference and flow losses.

The volume expansion term $\frac{m^2}{A^2}\frac{\partial v}{\partial h}\frac{\partial h}{\partial z}$ is generally small and can be neglected (O'Kelly, 2013) and equation (D1.19) reduces to:

$$\frac{\partial p}{\partial z} = \left.\frac{\partial p}{\partial z}\right|_{loss} + \rho\, g \sin\beta \qquad \text{(D.1.20)}$$

The expression $\left.\frac{\partial p}{\partial z}\right|_{loss}$ is the irreversible pressure loss due to energy dissipation.

### D.3: Profile of the Working Fluid Enthalpy from the Energy Balance

By neglecting kinetic and gravitational potential energy, the general energy conservation equation (5.35) can be restated thus:

$$\frac{v}{A}\frac{dq}{dz} = \left(\frac{\partial h}{\partial t} + v\frac{\partial h}{\partial z}\right) - v\frac{\partial p}{\partial t} + v\left(\frac{\partial v}{\partial t} + v\frac{\partial v}{\partial z} + g\sin\beta\right) \qquad \text{(D.1.21)}$$

Equation (D1.21) can be further reduced to:

$$v\frac{\partial h}{\partial z} = \frac{v}{A}\frac{dq}{dz} - \frac{\partial h}{\partial t} + v\frac{\partial p}{\partial t} \qquad \text{(D.1.22)}$$

The thermal inertia represented by $\partial h/\partial t$ . The energy balance in the evaporation loop is driven by heat transfer term $dq/dz$. In an open-flow system such as this, the compression energy term $v\,\partial p/\partial t$ is relatively negligible.

At steady state, $\partial h/\partial z = 0$ and $\partial h/\partial t = 0$ and mass flow $(m/A)$ will be uniform along the flow path $i.e.[1/A\,(\partial m/\partial z)] = 0$. Equation (D1.22) therefore shows that the spatial gradient of enthalpy $(\partial h/\partial z)$ is defined by the heat transferred to the flow $(dq/dz)$.

Hence, equation (D1.22) reduces to:

$$m\frac{dh}{dz} = \frac{dq}{dz} \qquad \text{(D.1.23)}$$

For two-phase flow process modelling, equation (D1.14), derived in terms of the local fluid specific volume and enthalpy is combined with the single-phase energy conservation equation (D1.21) to account for the state of the working fluid. Hence, combining equation (D1.14) and (D1.21), and re-arranging gives the two-phase energy conservation equation.

### D.4: Calculation of the Evaporator Tube Wall Temperature

Each evaporator tube wall is assumed to be a cell that can be adequately represented by a single metal temperature $T_m$ (O'Kelly, 2013). A simple heat balance on the *j*$^{th}$ cell gives:

$$\begin{aligned} c_m M_m \frac{dT_{m,j}}{dt} &= q_{frn,j} - q_{tf,j} + \lambda A_x (T_{m,j} - \frac{T_{m,(j+1)}}{dz} + \lambda A_x (T_{m,(j-1)} \\ &\quad - T_{m,j})/dz - \alpha_{hxf} A_{tf} (Tm_j - T_{f,j}) \\ &= q_{frnR,j} + \lambda_{frn} A_{frn} \left(T_{frn} - T_{m,j}\right) \quad + \lambda A_x (T_{m,j} \\ &\quad + T_{m,(j+1)} - 2T_{m,j})/dz \; - \alpha_{hxf} A_{tf} (Tm_j - T_{f,j}) \end{aligned} \qquad \text{(D.1.24)}$$

Where:

| | |
|---|---|
| $q_{frnR,j}$ | Radiant heat to the *jth* evaporator tube cells |
| $q_{tf,j}$ | Convective heat from furnace to the *jth* evaporator tube cell |
| $A_x$ | Longitudinal heat flow cross-sectional area |
| $A_{frn}$ | Outer tube area receiving convective heat from the furnace |
| $A_{tf}$ | inner tube area between tube and evaporator fluid |
| $T_{frn}$ | Furnace temperature used for convective heat transfer |
| $T_{f,j}$ | Temperature of the evaporator fluid in the *j*$^{th}$ cell |
| $\alpha_{frn}$ | Convective heat transfer coefficient furnace and evaporator tube |
| $\alpha_{hxf}$ | Convective heat transfer coefficient evaporator tube/fluid |
| λ | Coefficient of thermal conductivity of the evaporator tube |
| $C_m$ | Specific heat capacity of the tube metal |
| $M_m$ | mass of the tube metal per unit length |

## Appendix E: Degree of Freedom (DOF) in the gPROMS® Component Models

The DOF analysis is performed before any gPROMS simulation is initiated. It provides an information on the relationship between the model equations and the number of variables. In this section, the DOF analysis of the pulveriser, the turbine, the heat exchangers, and the electric generator is presented thus:

### E1: DOF Analysis of Coal Pulveriser

The gPROMS® structural analysis report shows a summary of the DOF analysis. The coal pulveriser model is made up of 47 variables (28 assigned and 19 unknown), 16 of the unknown variables are algebraic while the remaining 3 are differential variables. There are 22 equations, 19 of these are model equations, and 3 are initial conditions. The model equations are derived from conservation and constitutive equations as follows:

| Model Equations | | Remarks |
|---|---|---|
| $\frac{dM_c}{dt} = m_{in} - m_{out}$ | (E1.1) | Mass balance of coal pulveriser |
| $m_{out} = K_{out} M_c$ | (E1.2) | Mass flow of coal out of the pulveriser as a function of feeder stroke |
| $\frac{dX_{ci}}{dt} = \frac{1}{\rho_c V}(K_{out} M_c - m_{pf})$ | (E1.3) | Mass balance on volume fraction of coal in the exhauster and deflector |
| $m_{pf} = \frac{\rho_c}{\rho_{air}} m_{air} \frac{X_{ci}}{1 - X_{ci}}$ | (E1.4) | The flow of pulverised coal into the furnace |
| $Total.Mole = \sum (N_i \times MW_i)$ | (E1.5) | Convert mole composition of air to mass composition |
| $Masscomp_i = N_i \times \frac{MW_i}{Total.Mole}$ | (E1.6) | Convert mole composition of air to mass composition |
| $\rho_{air} = f(T_{air}, N_i, Masscomp_i)$ | (E1.7) | Computing density of air |

| | | |
|---|---|---|
| $M_{mill}C_{p.mill}\frac{dT_{mill}}{dt} = \dot{Q}_{coal} + \dot{Q}_{air} + \dot{Q}_{moist} - \dot{Q}_{airout} + \dot{Q}_{pf} - \dot{Q}_{moistout} + P_{motor}$ | (E1.8) | Energy balance of the pulveriser |
| $\dot{Q}_{coal} = (1 - w_{in}) \times m_{in}C_{pcoal}(T_{coal} - T_{ref})$ | (E1.9) | Heat flow from coal into the pulveriser |
| $\dot{Q}_{air} = m_{air}C_{pair}(T_{air} - T_{ref})$ | (E1.10) | Heat flow from air into the pulveriser |
| $\dot{Q}_{airout} = m_{air}C_{pair}(T_{mill} - T_{ref})$ | (E1.11) | Heat flow due to air out of the pulversier |
| $\dot{Q}_{pf} = m_{pf}C_{pcoal}(T_{mill} - T_{ref})$ | (E1.12) | Heat flow of the pulverised coal out of the pulveriser |
| $\dot{Q}_{moi} = w_{in} \times m_{in}C_{pmoi}(T_{coal} - T_{ref})$ | (E1.13) | Heat flow from moisture in the coal |
| $\dot{Q}_{moistout} = w_{out} \times m_{out}C_{pmoi}(T_{mill} - T_{ref}) + (w_{in} - w_{out}) \times m_{out}C_{pmoi}(T_{mill} - T_{ref})$ | (E1.14) | Heat flow due tochange in moisture content out of the pulveriser |
| $M_c = 0, at\ \frac{dM_c}{dt} = 0\ and\ t = 0$ | (E1.15) | Initial Condition |
| $\frac{dX_{ci}}{dt} = 0, at\ t = 0$ | (E1.16) | Initial condition |
| $T_{mill} = 298K, at\ \frac{dT_{mill}}{dt} = 0\ and\ t = 0$ | (E1.17) | Initial condition |
| $T_{mill}, P_{mill}, m_{pf} = (T_{out}, P_{out}, m_{out})$ | (E1.18) | Boundary Equation for pulverised coal port connection |
| $f(T_{in}, P_{in}, m_{in}) = (T_{coal}, P_{coal}, m_{coal})$ | (E1.19) | Boundary Equation for raw coal port connection |

## E2: DOF Analysis of Steam Turbines

A single turbine model is made up of 15 variables (3 assigned and 12 unknown), 11 of the unknown variables are algebraic while the remaining 1 is a differential variable. There are 13 equations, 12 of these are model equations, and 1 is an initial condition. The model equations are derived from the Stodola equations, the conservation and the constitutive.

## E3: DOF Analysis of Heat Exchangers

In the SCPP model there are basically two types of heaters/heat exchangers: the convectional heat exchangers and the radiant heat exchangers. A summary of a single heat exchanger model's DOF analysis is made up of 27 variables (12 assigned and 15 unknown), 10 of the unknown variables are algebraic while the remaining 5 are differential variable. There are 20 equations, 15 of these are model equations, and 1 is an initial condition. The model equations are derived from the conservation and the constitutive equations described in Chapter 5.

## E4: DOF Analysis of Electric Generator

The electric generator model is made up of 8 variables (6 assigned and 2 unknown), 2 of the unknown variables are differential while there are no is algebraic variables. There are 4 equations, 2 of these are model equations, and 2 are initial conditions. The model equations are derived from the torque-balance equation as described in Chapter 6.